

HD-A134 059

RESEARCH ON COMPOSITE MATERIALS FOR STRUCTURAL DESIGN
(U) TEXAS A AND M UNIV COLLEGE STATION MECHANICS AND
MATERIALS RE. D ALLEN ET AL. APR 83 MM-4665-83-4

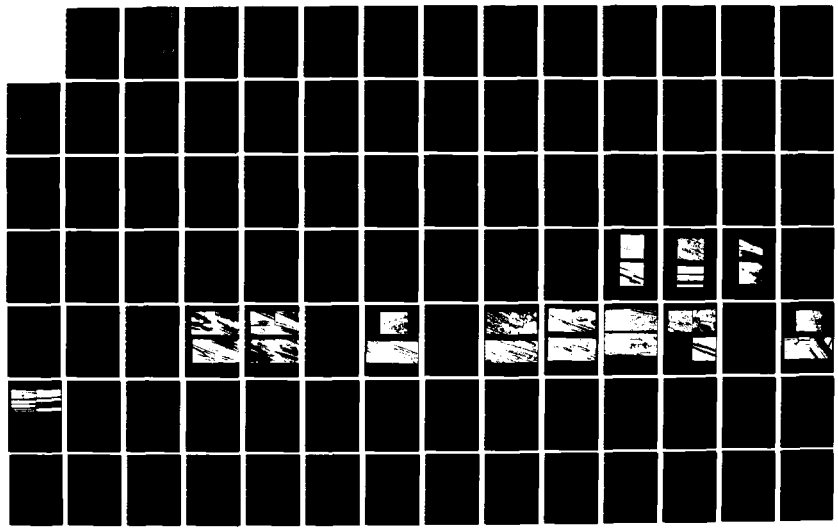
1/3

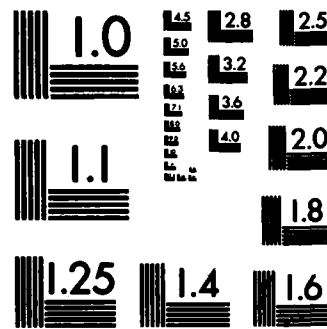
UNCLASSIFIED

AFOSR-TR-83-0861 F49620-82-C-0057

F/G 11/9

NL

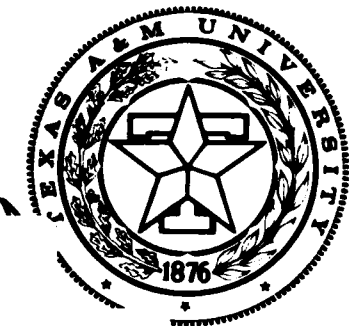




MICROCOPY RESOLUTION TEST CHART
NATIONAL BUREAU OF STANDARDS-1963-A

AFOSR-TR- 83-0861

Mechanics and Materials Center
TEXAS A&M UNIVERSITY
College Station, Texas



AD-A134 059

RESEARCH ON COMPOSITE MATERIALS FOR
STRUCTURAL DESIGN
ANNUAL TECHNICAL REPORT

DTIC
SELECTED
OCT 24 1983
S D

AIR FORCE OFFICE OF SCIENTIFIC RESEARCH
OFFICE OF AEROSPACE RESEARCH
UNITED STATES AIR FORCE
CONTRACT No. F49620-82-C-0057

DTIC FILE COPY

MM 4665-83-4

APRIL 1983

APPROVED FOR PUBLIC RELEASE; DISTRIBUTION UNLIMITED

UNCLASSIFIED

SECURITY CLASSIFICATION OF THIS PAGE (When Data Entered)

REPORT DOCUMENTATION PAGE		READ INSTRUCTIONS BEFORE COMPLETING FORM
1. AFOSR-TR- 83-0861		2. GOVT ACCESSION NO. 3. RECIPIENT'S CATALOG NUMBER <i>AD-A134 059</i>
4. TITLE (and Subtitle) RESEARCH ON COMPOSITE MATERIALS FOR STRUCTURAL DESIGN		5. TYPE OF REPORT & PERIOD COVERED ANNUAL 1 Jan 82 - 31 Dec 82
7. AUTHOR(s) D. Allen, W. Bradley, W. Haisler, J. Ham, B. Harbert, C. Hoeve, R. Schapery, Y. Weitsman		6. PERFORMING ORG. REPORT NUMBER MM 4665-83-4
9. PERFORMING ORGANIZATION NAME AND ADDRESS TEXAS A&M UNIVERSITY MECHANICS & MATERIALS CENTER COLLEGE STATION, TX 77843		10. PROGRAM ELEMENT, PROJECT, TASK AREA & WORK UNIT NUMBERS <i>61102F</i> <i>2307/B2</i>
11. CONTROLLING OFFICE NAME AND ADDRESS AIR FORCE OFFICE OF SCIENTIFIC RESEARCH/NA BLDG. 410 BOLLING AIR FORCE BASE, D.C. 20332		12. REPORT DATE April 1983
14. MONITORING AGENCY NAME & ADDRESS (if different from Controlling Office)		13. NUMBER OF PAGES 36 + Appendix
15. SECURITY CLASS. (of this report) UNCLASSIFIED		
15a. DECLASSIFICATION/DOWNGRADING SCHEDULE		
16. DISTRIBUTION STATEMENT (of this Report) Approved for public release; distribution unlimited		
17. DISTRIBUTION STATEMENT (of the abstract entered in Block 20, if different from Report)		
18. SUPPLEMENTARY NOTES		
19. KEY WORDS (Continue on reverse side if necessary and identify by block number) Composite Materials Delamination Fracture Resins Residual Stresses Damage Adhesives Viscoelasticity		
20. ABSTRACT (Continue on reverse side if necessary and identify by block number) → Summarized are research activities related to advanced fiber reinforced plastics in the areas of fracture, delamination, distributed damage, residual stresses, moisture effects, and toughening mechanisms in elastic and viscoelastic materials. Also included are nine papers and abstracts of three M.S. Theses describing recently completed work in these areas. ↗		

Accession For			
NTIS GRA&I	<input checked="" type="checkbox"/>		
DTIC TAB	<input type="checkbox"/>		
Unannounced	<input type="checkbox"/>		
Justification			
By			
Distribution/			
Availability Codes			
Dist	Avail and/or Special		
<table border="1"> <tr> <td>A</td> <td></td> </tr> </table>		A	
A			



RESEARCH ON COMPOSITE MATERIALS
FOR STRUCTURAL DESIGN

Annual Technical Report

by the
Professional Staff
of the
TEXAS A&M UNIVERSITY
MECHANICS AND MATERIALS CENTER

Submitted to the
Air Force Office of Scientific Research
Office of Aerospace Research
United States Air Force

MM 4665-83-4

Contract No. F49620-82-C-0057

AIR FORCE OFFICE OF SCIENTIFIC RESEARCH (AFSC) April 1983

NOTICE OF TRANSMITTAL TO DTIC
This technical report has been reviewed and is
approved for public release (AFWAFR 190-12).
Distribution is unlimited.

MATTHEW J. KERPER
Chief, Technical Information Division

TABLE OF CONTENTS

	Page
1. INTRODUCTION	
1.1 Summary	1
1.2 Statement of Work	1
2. MATRIX CONTROLLED FRACTURE BEHAVIOR OF GRAPHITE/EPOXY COMPOSITES	2
2.1 Delamination and Transverse Fracture in Graphite/Epoxy Composite Materials	2
2.2 In-Situ Fractographic Study of Graphite Epoxy Composite Materials	3
3. MATRIX CONTROLLED FRACTURE ANALYSIS OF FIBROUS COMPOSITES	5
3.1 Deformation and Fracture Theory for Visco- elastic Composites with Distributed Damage	5
3.2 Evaluation of Energy Release Rates in Uni- directional Split Laminate Specimens	5
3.3 Slow, Stable Delamination in Graphite/Epoxy Composites	6
3.4 Analysis of Effect of Matrix Degradation Due to Fatigue on Deformation and Strength	6
4. STUDIES RELATED TO RESIDUAL STRESSES IN COMPOSITE MATERIALS	10
4.1 Introduction	10
4.2 Residual Stresses Due to Moisture and Temperature	10
4.3 Chemical Cure-Shrinkage Stresses	13
4.4 Thermo-viscoelastic Characterization of Polymeric Resins	13
4.5 Moisture Diffusion in Hybrid Composites	15

5.	STRUCTURE AND BEHAVIOR OF WATER IN RESINS	16
5.1	General Studies	16
5.2	Glass Points of Epoxies	17
5.3	Studies on a Model Epoxy	17
6.	TOUGHNESS RELATED EFFECTS OF MOLECULAR CHAIN STIFFNESS	18
7.	DEVELOPMENT OF ELASTIC STRAIN RATIO TRANSLATOR (ESRT) GAGE	20
7.1	Introduction	20
7.2	Description	20
7.3	Results and Discussion	22
8.	GRADUATE RESEARCH ASSISTANT ACTIVITIES	25
8.1	Summary	25
8.2	Abstracts of M.S. Theses	25
9.	PROFESSIONAL PERSONNEL INFORMATION	29
9.1	Faculty Research Assignments	29
9.2	Additional Professional Staff	30
9.3	Spoken Papers and Lectures, Publications, and Other Composites-Related Professional Activities of the Faculty	30
10.	REFERENCES	35
	APPENDIX	36

1. INTRODUCTION

1.1 Summary

Primary activities during 1982 consisted of (i) conducting research in accordance with the Statement of Work given in Section 1.2; (ii) preparing eight technical papers, three M.S. theses, and one invention disclosure; (iii) various interactions of the faculty with the technical community through presentations of papers, participation as members of technical committees, etc.

Sections 2-8 summarize the research activities. The professional personnel associated with the project and the outside activities of the faculty related to composites are given in Section 9. The Appendix contains nine articles on work published or completed in 1982.

1.2 Statement of Work

Specific areas to be investigated are:

1. micro- and macro-mechanisms of fracture of resins and composites, with emphasis on processes involved in delamination growth
2. effects of transient temperatures and moisture content on deformation and fracture properties, including consideration of residual stresses and their effect on intraply and interply cracking (delamination)
3. behavior and structure of water in resins and model resin systems, and its effect on basic deformation and fracture properties
4. toughening mechanisms in high temperature resins, including study of the separate effects of energy absorption in crack-tip failure processes and far-field deformation and micro-damage processes
5. improved theoretical models for characterizing and predicting deformation and failure behavior of resins and composites

2. MATRIX CONTROLLED FRACTURE BEHAVIOR OF GRAPHITE/EPOXY COMPOSITES*

2.1 Delamination and Transverse Fracture in Graphite/Epoxy Composite Materials

The asymmetrically loaded split laminate specimen has been used to study mixed mode I/mode II fracture in several graphite/epoxy unidirectional systems with quite different neat resin toughnesses. For the very tough F185 resin of Hexcel Corporation ($G_{IC} \approx 6000 \text{ J/m}^2$), the critical energy release for the composite ranged from about 2500 J/m^2 for pure mode I delamination to 2000 J/m^2 for mixed mode where $G_{II}/(G_I + G_{II}) = 0.40$. For Hexcel 155 resin ($G_{IC} \approx 730 \text{ J/m}^2$) and Hercules 3502 resin ($G_{IC} \approx 70 \text{ J/m}^2$), the delamination critical energy release rate monotonically increased from approximately 600-850 J/m^2 and 225-475 J/m^2 respectively as $G_{II}/(G_I + G_{II})$ increased from 0.0 to 0.40.

The results indicate that the introduction of strong but brittle fibers into a tough resin decreases the energy dissipated in delamination fracture by decreasing the total volume of resin deforming ahead of the crack tip and possibly decreasing the strain due to the constraint provided by the fibers. By contrast, strong but brittle fibers introduced into a brittle resin system whose strength is less than the fibers' strength enhances the toughness of the system against delamination fracture. This is because the fracture process will include not only resin cracking but also some interaction of the crack tip with the strong, brittle fibers, thus increasing the resistance to crack propagation. Even for pure mode I opening on a

*Prepared by W.L. Bradley

macroscopic scale, crack tip interaction with the fibers occurs on a microscopic scale due to fiber misalignment, ply waviness, and other microscopic heterogeneities.

The effect of superposition of mode II loading onto mode I loading is to repeatedly redirect the crack tip into the fibers. In brittle resin systems, this increases the resistance to crack propagation, whereas in tough systems it can actually decrease the total energy dissipated in fracture, as was observed for the Hexcel F185 system.

Compact tension specimens were used to study transverse cracking in the same systems. A comparison of transverse cracking to delamination cracking suggested the same pattern. There is no resin rich region in transverse cracking which is comparable to that seen by the crack tip between plies during delamination cracking. Thus, a greater incidence of crack tip interaction with the fibers is expected than in delamination cracking. For a brittle resin, this would enhance toughness whereas for a more ductile resin, it would give a net decrease in toughness. These trends were noted in the systems studied.

A more detailed summary of this effort is contained in the M.S. thesis of Ron Cohen (cf. Section 8) and the paper "Delamination and Transverse Fracture in Graphite/Epoxy Materials" contained in the Appendix, publication No. 1.

2.2 In-Situ Fractographic Study of Graphite Epoxy Composite Materials

In-situ fracture in the scanning electron microscope was used to better understand the various micromechanisms of fracture. These

observations were subsequently compared with post mortem fractographic observations to guide in interpretation of the various artifacts observed in the fracture surface in delamination fracture.

The composite systems studied were found to be much more heterogeneous in their fracture behavior than expected. The particle toughened resins F155 and F185 were also found to be quite heterogeneous. In the tough resin systems, variation in thickness of the resin rich region along the crack path gave fracture behavior which varied from large scale deformation, with dimple like artifacts similar to ductile fracture in metals, to a "furrowed field" look similar to that observed in delamination fracture in brittle resin systems. The deformation and damage zone in the ductile systems was often observed four to five diameters removed from the plane of the crack and apparently accounts for the much higher G_{lc} values observed in these systems. Fiber breakage was almost always associated with fiber debond followed by stretching the fiber across the two surfaces behind the crack tip until the resultant bending loads gave fracture. The crack tip "meandered along" in a somewhat irregular way in the F155 and F185. The heterogeneous distribution of rubber particles added for toughening the system resulted in soft and hard spots in the resin ahead of the crack tip. Coalescence of the voids with the crack tip constituted crack tip advance.

The results of this investigation are presented in greater detail in an invited paper prepared for the 6th Annual Structural Composites Meeting in New Orleans, January, 1983, contained the in Appendix, publication No. 2.

3. MATRIX CONTROLLED FRACTURE ANALYSIS OF FIBROUS COMPOSITES

3.1 Deformation and Fracture Theory for Viscoelastic Composites with Distributed Damage*

Methods of quasi-static deformation and fracture analysis have been developed for nonlinear viscoelastic materials; they are described in the Appendix, publications Nos. 5 and 6. The correspondence principles which provide the basis for the viscoelastic analysis are not limited to crack growth; they apply to crack closing and healing as well as to other types of problems involving ablation and interfacial contact and separation. However, only crack growth examples are given. The theory, which allows for distributed, microscale damage, is not much more involved than that of nonlinear elasticity or special cases of linear viscoelasticity. This simplicity, compared to what one might expect, is a direct result of the particular constitutive equations and mechanical variables selected to characterize rheological behavior. We believe the theory provides a practical approach to the development of realistic damage and global fracture models for nonlinear elastic, viscous, and viscoelastic media. It is potentially applicable to the mathematical modeling of crack tip regions, such as the delamination tip in fibrous composites with rubber-toughened matrices (cf. Appendix, publication No. 1, Fig. 3).

3.2 Evaluation of Energy Release Rates in Unidirectional Split Laminate Specimens

An improved beam theory which accounts for rotation at the crack tip is described in the .S. thesis by J.R. Weatherby; see Section 8

*Sections 3.1-3.3 prepared by R.A. Schapery

for the Abstract. The primary findings are:

Deformation of the laminate ahead of the crack affects stiffness and energy release rate as a function of delamination length.

For mode I, a model consisting of a beam supported at the crack tip by a torsion spring (with a length-independent spring constant) can be used to predict stiffness and energy release rate as a function of length.

An approximate analytical prediction of the mode I spring constant agrees well with finite element solutions. In a limited analytical study of mode II delamination, the correction for beam deformation near the crack tip is estimated to be 1/3 that for mode I.

3.3 Slow, Stable Delamination in Graphite/Epoxy Composites

Using unidirectional, split laminates under fixed-grip conditions, the relation between delamination crack speed, \dot{a} , and energy release rate, G , was found for one tough composite (Hexcel F185) and one brittle composite (Hercules AS/3502). This study is reported in the M.S. thesis by H. Razi; its Abstract is in Section 8. The principal conclusions are:

The energy release rate during slow growth is approximately 15% less than the initiation value G_C for the brittle system (3502) and 30% less than G_C for the tough system (F185).

For the brittle system, $G \approx 204\dot{a}^{0.0045}$ (dry, RT) and $G \approx 195\dot{a}^{0.0046}$ (wet, RT) where G is J/m^2 and \dot{a} is cm/s .

For the tough system, $G \approx 1665\dot{a}^{0.022}$.

3.4 Analysis of Effect of Matrix Degradation Due to Fatigue on Deformation and Strength *

Results of R.T. Arenburg's M.S. thesis [1] indicated a strong correlation between matrix damage and ultimate failure of graphite/epoxy. The current effort involves a more detailed study of this phenomenon and quantification of the mechanisms involved.

*Prepared by D.H. Allen and W.E. Haisler

In order to better facilitate the research, the finite element code developed by Arenburg has been completely reconstructed and streamlined. The current code has the capability of predicting the strain energy release rate as a function of delamination crack growth in layered orthotropic elastic media with any user-specified layup. As shown in Fig. 1, the model has the capability of analyzing the behavior of uniaxial specimens with cracks propagating longitudinally between any user specified plies. Results have currently been obtained for $[0/90]_s$ and $[\pm 45/90]_s$ layups.

Future program development will involve the inclusion of residual (thermal and moisture expansion) strains which will be predicted via an already constructed and compatible heat conduction/diffusion computer code. In addition, the material model is being internally altered to include the effect of matrix degradation via a damage growth law.

A coexisting effort with the computer code development involves the construction of a growth law for the prediction of the global damage state. It is well known that in graphite/epoxy laminates the fatigue process causes multiple fracture events on different scales [2,3]. These events are primarily characterized by microvoid growth in the matrix, transverse cracking of the matrix, and fiber-matrix debonding, eventually leading to fiber fracture and delamination causing ultimate failure. Growth of this damage is strongly affected by geometry of the layup [2,3], so that the damage growth law is quite complex. Thermodynamic constraints have shown that a potential function for stress exists [4], and this framework is being studied along with the theory of Section 3.1 as a basis for development of a continuum model. It is anticipated that the thermodynamic formulation

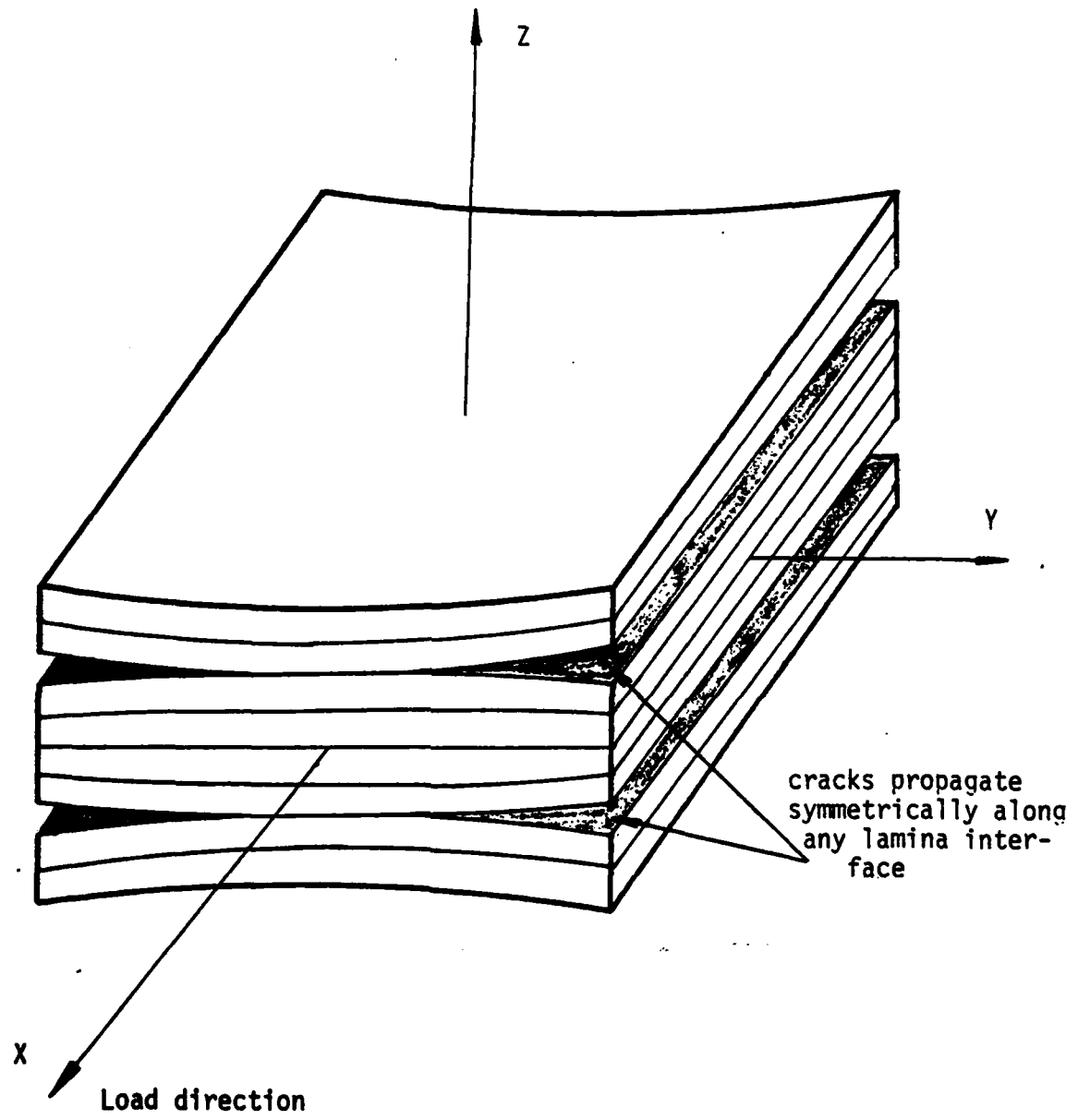


Figure 1: Computer Code Modelling Ability

will result in a model of the form

$$\sigma_{ij} = \partial\psi/\partial\epsilon_{ij}, \quad \psi = \psi(\epsilon_{ij}, T, W),$$

where ψ is the Helmholtz free energy, σ_{ij} is the stress tensor, ϵ_{ij} is the strain tensor, T is temperature, and W is a scalar-valued internal state variable modeling damage. The mechanisms of internal damage discussed above will be related to a global damage parameter using the following form:

$$W \equiv \int_V A_i \alpha_i dV,$$

where A_i are weighting parameters accounting for stacking sequence, and α_i are a set of coupled parameters modeling the growth of the various damage mechanisms, with growth laws of the form:

$$\dot{\alpha}_i = \dot{\alpha}_i(\epsilon_{ij}, T, \alpha_i).$$

This equation comprises the heart of the damage growth research in the context of thermodynamics. Growth law development will involve considerable coordination with experimental research currently underway.

4. STUDIES RELATED TO RESIDUAL STRESSES IN COMPOSITE MATERIALS*

4.1 Introduction

Much of the work summarized in Sections 4.2-4.4 will be detailed in the Ph.D. dissertation "On the Effects of Post Cure Cool Down and Environmental Conditioning on Residual Stresses in Composite Laminates", by B.D. Harper; completion is expected by August 1983. Portions of these studies on residual stresses are also covered in publications 7-9 in the Appendix to this Annual Report. An investigation of moisture diffusion in hybrid composites, Section 4.5, was recently initiated as an M.S. thesis project by D.L. Clark.

4.2 Residual Stresses Due to Moisture and Temperature

Effects of moisture and temperature on residual stresses in composites were investigated by measuring the curvatures of non-symmetric AS/3502 plates. The plates' dimensions (4" x 4") and lay-up [0/90/0₄/90₄/0/90]_T were selected so as to avoid premature cracking and achieve appreciable curvatures, while remaining within the range of linear plate theory. The plates were cured and postcured at 350 F, following the standard cure process, and cooled down to room temperature of 75F. Groups of specimens, three in each group, were then subjected to controlled levels of moisture and temperature, causing moisture to be absorbed in the plates. The various test conditions are listed in Table 1.

*Prepared by Y. Weitsman

RH \ T° (F)	73	130	150	163
Dry			X	X
13%	X	X	X	
75%	X	X	X	
95%	X	X	X	X

Table 1: Environmental Conditions Employed in Test Scheme

Upon saturation, the plates were placed in a dry environment, causing moisture desorption. Moisture content was measured by periodical weighings of the specimens and compared with moisture levels in uni-directional coupons that were exposed to identical environments. Plate curvatures were measured periodically and recorded. The distribution of moisture across the thickness of the plates was calculated from classical linear diffusion theory. Curvatures were then computed on the basis of linear elastic plate theory, accounting for the thermal and moisture-induced strains. Those calculations resulted in discrepancies of up to 50%, when compared with experimental measurements. Employing a viscoelastic characterization, which accounts for the effects on creep of both moisture and temperature, the plate deformations and curvatures were computed using linear theory, leading to much better agreement with experimental observations. See Figure 2.

Upon drying, the observed curvature was again found to be quite different from that predicted by elasticity theory. However, as shown in Figure 2, the experimentally observed curvature is shifted in the opposite direction to the curvature predicted by viscoelasticity. We thus conclude that the drying stage caused damage (microcracking or

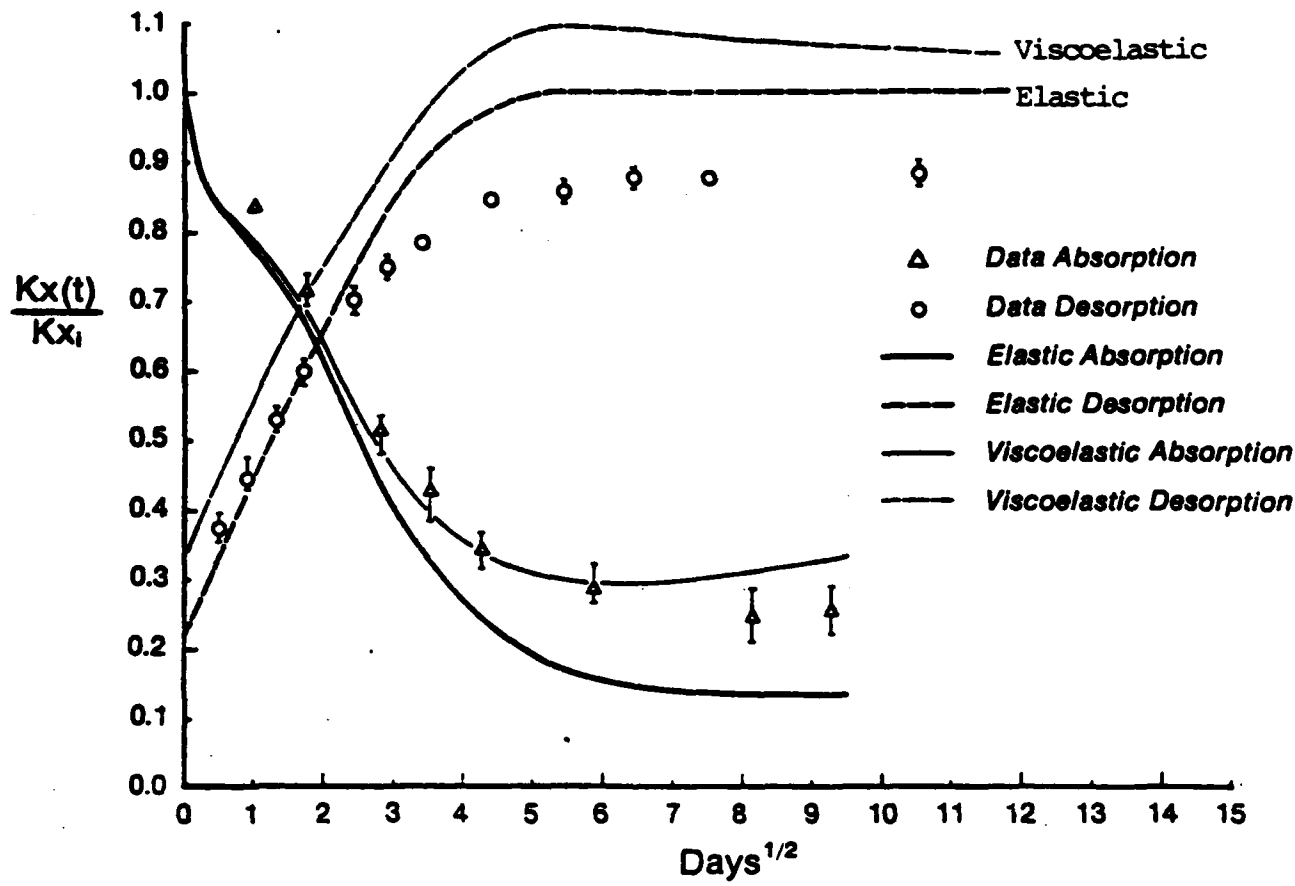


Figure 2. Curvatures of Plates Environmentally Conditioned at 163°F and 95% RH Relative to Initial Curvature K_{xi} (73°F, dry).

some other physical change) in the laminate.

It was concluded that although linear elasticity may suffice to analyze thermal effects in AS/3502 composites, the influence of moisture on material response is large enough to require viscoelastic as well as damage analysis. It was also noticed that moisture weight gains in the cross-ply plates exceeded consistently the moisture absorption in uni-directional plates. This phenomenon is likely due to stress effects (e.g. damage) on moisture sorption, in view of the tensile residual (thermal) lamination stresses which exist in an asymmetric plate, but which are absent in a unidirectional coupon.

4.3. Chemical Cure-Shrinkage Stresses

An assessment of residual stresses due to chemical cure-shrinkage in 3502 (Hercules) resin was obtained by measuring curvatures in laminated 3502/aluminum beams during cure and following cool-down. Strain-gages were attached at the resin/aluminum interface and at the outer surface of the aluminum and readings were recorded vs. time during cure, and vs. temperature during cool-down. The results were analyzed by means of a linear, elastic laminated-beam theory. It was concluded that residual stresses due to cure shrinkage accounted for about 30% of the total residual stresses after cool-down.

4.4 Thermo-viscoelastic Characterization of Polymeric Resins

The customary approach to correlating the effects of time and temperature on creep (or relaxation) is to employ the so-called "time-temperature" analogy. This analogy presupposes that when creep data at several levels of constant temperature are plotted vs. time on log scales, these data can be coalesced to form a continuous "master curve" by shifting isothermal curves parallel to the log t axis

(horizontal shift). This provides the "shift factor" function a_T which is then employed to cast the viscoelasticity formulation in terms of "reduced" time $\xi = t/a_T$.

There are, however, circumstances in which isothermal data cannot be shifted in the above manner, and vertical shifts are required in addition to horizontal translations. The reduction is ambiguous in the case of "power law" creep, where all isothermal data fall on straight, parallel lines on log-log plots.

It has been shown that all such ambiguities and uncertainties can be removed by conducting more generalized creep tests. These involve creep and recovery measurements, in which creep is recorded at some elevated temperature under constant load and recovery is recorded after an abrupt removal of the load accompanied by a simultaneous, sudden reduction of the temperature to a fixed, lower level. These "T-Drop" recovery data then serve to define the vertical and horizontal shift and determine the appropriate manner in which the vertical shift must be further split into two components to be employed in a superposition integral. At this time the characterization work is complete, both experimentally and analytically.

To examine the validity of this approach, several verification tests have been performed in which both temperature and stress were allowed to fluctuate. In these verification tests, the stress was increased linearly from 0 to 10 MPa at a rate ranging between .01 to .03 MPa/sec, and then either held constant or returned to zero at the same rate. The temperature was simultaneously increased in an approximately linear path from 70 C to 120 C at a rate of around .05 C/sec, and then lowered at a much faster rate (from .5 - 2.5 C/sec).

In all cases, the predictions based upon the aforementioned characterization agreed very well with the experimental data. A paper outlining the theoretical aspects of this scheme appeared recently in the Proceedings of the 4th International Congress on Composite Materials; see Appendix, publication No. 8.

4.5 Moisture Diffusion in Hybrid Composites

This investigation aims at developing a model for the diffusion of moisture into hybrid laminates. The hybrid consists of materials that can be co-cured simultaneously but each one possesses its own diffusivity coefficient and reaches a different saturation level.

Two materials, Hexcel F155 and F185, were selected for the experimental task. Laminated unidirectional coupons, some consisting of $[155_2/185_2]_S$, $[185_2/155_2]_S$, and others made of four plies of each of the above materials alone, were exposed to several levels of relative humidity and temperature. Moisture uptake was recorded during the past four months.

At the present time no analytical solution exists for moisture diffusion in hybrids. The major complication involved in modeling this case concerns the existence of discontinuities in moisture level at interfaces. In addition, a solution by means of Fourier analysis requires generalizations of such concepts as "inner product" and orthogonality. A generalized solution has been developed and a computational scheme is now in progress. The solution and computational scheme have the required flexibility to include the appropriate interface conditions based on thermodynamics.

5. STRUCTURE AND BEHAVIOR OF WATER IN RESINS*

5.1 General Studies

Water absorption in resins is often detrimental to the mechanical properties. Since under atmospheric conditions water absorption is slow, degradation may occur only after months or years, depending on the size of the body. It is our object to investigate the basic mechanism of water absorption, as well as the diffusion rate, and to develop reliable methods for predicting long-term usage. In order to do this successfully, more insight in the process of water absorption is required. Since epoxies absorb relatively small amounts of water (a few percent) basic studies are difficult with this commonly used resin. Therefore, we have first conducted experiments with other model resins capable of higher water absorption, so the results can more easily be interpreted. Of course, these studies are based on the premise that the behavior of water in different resins is similar.

Our previous studies have shown that, indeed, for quite different resins water absorption follows similar patterns [5]. The results of further studies by Mr. Kinard on methylcellulose (publication No. 4 in the Appendix) have been submitted to the Journal of Polymer Science. The results can be summarized as follows. Even in rigid resins diffusion of water is relatively rapid. Water molecules are not bound to specific groups, but diffuse as a diluent through the resin in liquid-like fashion. At low temperature no ice is formed, but diffusion slows until the temperature reaches 150 K. In this temperature range diffusion ceases.

*Prepared by C.A.J. Hoeve

5.2 Glass Points of Epoxy

Although water absorption in epoxies occurs only up to several percent, in view of the previous general conclusions we are in an excellent position to extend these studies to epoxies. The glass transition temperature T_g values of a resin is of paramount importance for its mechanical properties. Usually the modulus decreases more than a thousand fold in raising the temperature through T_g . Since only a few mg of sample is required for the calorimetric measurements (the Perkin Elmer DSC 2), we can absorb water in the sample rather quickly and measure the effect of water on T_g in a relatively short time. Preliminary measurements indicate that the T_g -values of epoxies can be depressed by 20 C by water absorption of only a few percent.

5.3 Studies on a Model Epoxy

The commercial samples tested so far have been highly crosslinked. In this the case the T_g value is above 100 C and the modulus is high under atmospheric conditions. High crosslink densities also lead, however, to brittle samples. In order to display toughness the sample should be more linear. In addition, for a better understanding of the mechanical properties in terms of the chemical structure, simpler linear resins are preferable. For this reason we have synthesized a linear model epoxy from the monomers Epon (Shell Co.) and butylamine. Although its T_g value is only 40 C, too low for a useful structural material, the glass transition is quite pronounced and is easily measurable. Furthermore, the effect of water absorption on T_g and on the mechanical properties should be relatively easy to observe and interpretation of the results should be facilitated.

6. TOUGHNESS RELATED EFFECTS OF MOLECULAR CHAIN STIFFNESS*

Some rheological property measurements have been made on a thermoplastic polysulfone, and the results are reported in a paper presented at the American Chemical Society national meeting in Kansas City in August 1982; see Appendix, publication No. 3. It has a molecular structure which is similar to the chains between crosslinks in a thermosetting material being developed by AFML as a candidate resin for high temperature composites. The candidate material suffers from brittleness at room temperature which will have to be reduced before this material can be accepted. The thermoplastic material has excellent toughness but cannot be processed with conventional technique and lacks the solvent resistance coming from crosslinking. This study is an attempt to find the molecular size between crosslinks sufficient for the material to have acceptable toughness and yet still be processed with thermoset technology. These studies indicate some unexpected behavior which is believed to be a consequence of chain stiffness at room temperature in solution.

A paper in preparation, "Chain Stiffness in a Polysulfone", is an elaboration of the included publication but also describes in greater detail the rheometric data on the neat resin at high temperatures and the solution measurements in moderately concentrated solutions at room temperature. The static and quasi-static measurements such as intrinsic viscosity and light scattering show beyond doubt that this molecule is in a random coil configuration in solution. On the other hand, an entanglement effect observed in moderately concentrated

*Prepared by J.S. Ham

solutions implies a stiffness exists within the molecule. The thermal shifts of the rheometric data show marked deviations from the WLF type shift with a tendency toward the Arrhenius behavior. This is in keeping with what one would expect if the energy barriers for shape changes depended to some extent upon the rotational barriers, which in turn would give rise to a Arrhenius behavior (rather than the three dimensional surroundings which give rise to the WLF behavior).

Another paper in preparation is on similar measurements on a polyphenylquinoxaline. This is a thermoplastic material, also related to a high temperature thermoset candidate, but the development on this resin has been postponed by AFML since the polysulfones appear to be more promising. This paper includes rheometric and moderate concentration solution data parallel to those in the polysulfone paper. The data have been collected and partially analyzed so that this paper can be completed shortly after the polysulfone paper.

A third study concerns the formation of thermosets with a glassy transition higher than the actual cure temperature. The view of curing of thermosets says that the curing reaction slows down drastically whenever the glassy transition rises to the actual curing temperature. There has recently appeared some cases in the literature where this rule is violated. This is a very interesting phenomenon since it could result in the curing of high temperature resins without the very high curing temperatures normally required. This work is at an early stage of development.

7. DEVELOPMENT OF ELASTIC STRAIN RATIO TRANSLATOR (ESRT) GAGE*

7.1 Introduction

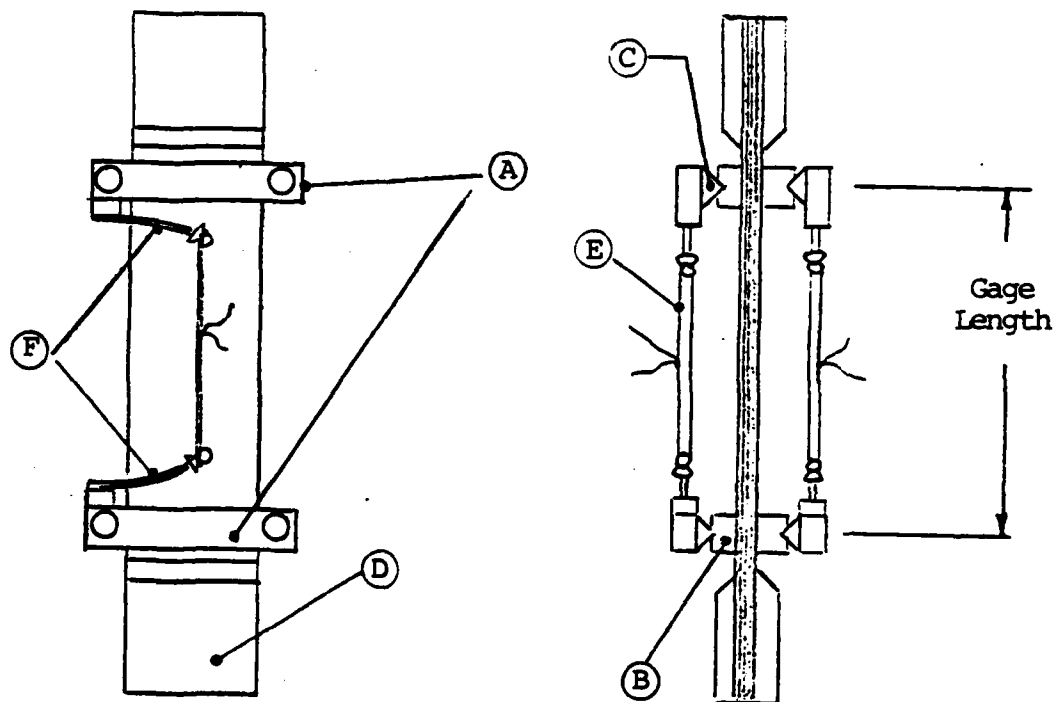
A device for measuring uniaxial strains was developed which is believed will greatly enhance experimental capabilities in the mechanical characterization of fibrous composites and other materials. Efforts culminated in the filing of a "Disclosure of Invention" through the Texas A&M University System, dated Oct. 22, 1982. We have complied with Air Force requirements regarding disclosure submittal and the completion of the Air Force Systems Command Abstracts of New Technology (ANT).

7.2 Description

Figure 3 is a schematic showing the basic elements of operation of the "ESRT" gage. Two stainless steel clamps, A, are secured to a uniaxial test specimen by pressure applied from the clamps through a pressure foot, B. Fixation of the position of the clamp to the pressure foot is accomplished by indentation indexing through an arrangement of steel balls or a knife edge.

Two such clamps are located on the test specimen, D, with the gage length being determined by the on-center spacing between the two clamps. The longitudinal strain sensing elements of the device are composed of two electrical resistive strain loops, E, which are made of very small diameter alloy wires coated with enamel. These loops are in turn placed in a condition of pre-tension through the cantilever springs, F. Subsequent axial straining of the test specimen produces

*Prepared by B.C. Harbert



- A. Stainless steel gage clamps secured to test specimen at two locations. Gage length determined by on-center distance between clamps.
- B. Pressure foot or raised surface.
- C. Recessed hardened steel ball or knife edge.
- D. Typical tabbed end uniaxial test specimen.
- E. Electrical resistive strain loop.
- F. Cantilever loading spring.

Figure 3. ESRT Gage Mounted on a Uniaxial Specimen

changes in the wire tension and the electrical resistance of the strain loops. The electrical changes can be treated in the usual manner as with standard bonded resistance strain gages, regarding electrical circuitry, signal conditioning, and analysis.

7.3 Results and Discussion

Operation of the ESRT gage on uniaxial test specimens has been performed to check out various gage characteristics such as accuracy, repeatability, sensitivity, calibration, linearity, fatigue limit and, to a lesser degree, gage sensitivity to temperature and humidity. Accuracy of the gage was established in part by comparing strains measured with the gage and two independent strain measuring techniques; a uniaxial graphite/epoxy composite test specimen subjected to a sinusoidal loading history was used. Figure 4 shows the comparison of mean cyclic strain measured by a conventional bonded resistance strain gage, an Instron type extensometer and the ESRT gage. Cyclic loading was performed on an Instron test machine at room temperature and humidity. Loading was essentially linear at 0.5 Hertz, with a typical cycle initially being a 300 lb. peak decreasing to 100 lb. The different steps on this curve reflect upward changes in the peak loading and corresponding changes in the low level during the cycle. The final cyclic load variation at the time of specimen failure was 750/200 lbs. The correlation between the ESRT gage and the clip gage extensometer is very good over the entire test range including the point of failure. Initially the agreement between the conventional bonded strain gage was good; however, disagreement between the strain gage and the other two devices increased with each increase in cyclic load level, until at a mean strain of 0.85% the

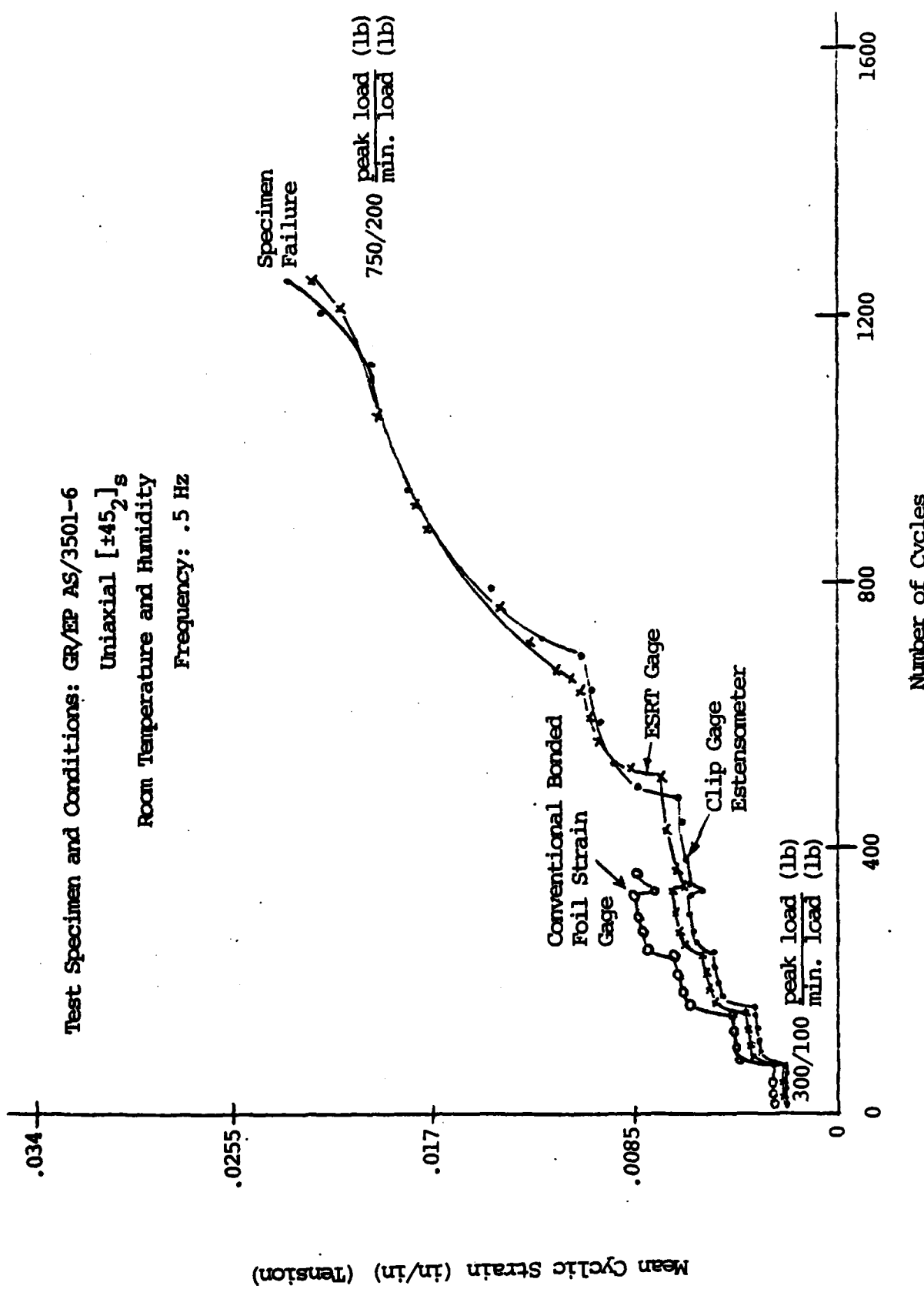


Figure 4. Performance of ERST Gage Compared to Conventional Bonded Strain Gage and Instron Extensometer on $[\pm 45]_2$ s Graphite/Epoxy Composite Material.

conventional strain gage failed. Typical of these bonded gages, a considerable zero shift occurs under cyclic loading above 0.2% strain, increasing exponentially as the strain level increases. Therefore, even though the conventional strain gage continued to provide data, it was greatly in error by virtue of the zero shift which increased with each increase of load at strains above 0.2%. In contrast, we have obtained excellent agreement between the ESRT gage and a conventional bonded strain gage on an aluminum specimen tested at a constant strain rate of $.01 \text{ min}^{-1}$.

With additional experience and refinements it is believed the ESRT gage will become a very valuable experimental tool because it offers certain advantages over conventional strain measuring techniques:

Large strains can be measured (in excess of 5% if desired) because of the translation ratio imparted by the springiness of the cantilevered beams (as opposed to a 1:1 relationship for a bonded strain gage).

Since the strain loops are coupled through elastic metallic elements, no adhesive bonding is required; thus performance of the gage is not degraded at the high temperatures and high humidities at which polymeric adhesives creep.

The "ESRT" has been demonstrated to function very reliably under conditions of fatigue loading, both at high and low strain levels, as illustrated in Figure 4, and observed during many other tests. The levels of strain measured under fatigue loadings greatly exceed the capabilities of conventional strain gages.

8. GRADUATE RESEARCH ASSISTANT ACTIVITIES

8.1 Summary

The fourth group of graduate engineering students to participate on the M.S. level in the AFOSR research project entered the program in September 1981. They have completed all of their requirements for a Master of Science degree, and the results of the research are reported in the following theses:

1. Cohen, R.N., "Effect of Resin Toughness on Fracture Behavior of Graphite/Epoxy Composites".
2. Razi, H., "Slow, Stable Delamination in Graphite/Epoxy Composites".
3. Weatherby, J.R., "Evaluation of Energy Release Rates in Unidirectional Double Cantilevered Beam Fracture Toughness Specimens".

The abstracts are in Section 8.2. Copies of the theses will be provided upon written request to the Principal Investigator (R.A. Schapery).

To date, twenty two M.S. students have participated in the project and graduated. Emphasis of the graduate program shifted from the M.S. level to the Ph.D. level in 1981. The current group consists of three M.S. and five Ph.D. students.

8.2 Abstracts of M.S. Theses

See pages 26-28.

ABSTRACT

Effect of Resin Toughness on Fracture Behavior
of Graphite/Epoxy Composites (December 1982)

Ronald Nelson Cohen, B.S., Purdue University

Chairman of Advisory Committee: Dr. Walter L. Bradley

Energy release rates for delamination and transverse fracture have been experimentally determined for three different graphite/epoxy systems. Various combinations of mode I (opening)/mode II (in-plane shear) load ratios for delamination fracture have been investigated to determine the effect of resin toughness on delamination fracture. The micromechanisms of fracture were determined using in-situ fracture in a scanning electron microscope along with subsequent fractography on fractured surfaces. The energy release rate for delamination fracture and transverse fracture is less than the energy release rate for the neat material for a tough resin system. For a brittle resin system, the delamination and transverse toughness is greater than for the neat material. The results have been interpreted in terms of the relative contributions of resin deformation and fiber pullout and breakage to the total energy dissipated during fracture.

ABSTRACT

Slow, Stable Delamination in
Graphite/Epoxy Composites (December 1982)
Hamid Razi, B.S. Mechanical Engineering
University of Washington

Chairman of Advisory Committee: Dr. R.A. Schapery

Split laminated beam specimens tested under a fixed-grip condition are used to obtain relationships between the opening-mode energy release rate and crack speed in one brittle and one tough unidirectional, graphite/epoxy composite with moisture contents corresponding to ambient humidity, 45% RH, and 95% RH. The analysis employs a linear elastic fracture mechanics approach coupled with nonlinear beam theory to account for large deflections and rotations produced during the delamination tests.

ABSTRACT

Evaluation of Energy Release Rates in
Unidirectional Double Cantilevered Beam
Fracture Toughness Specimens (December 1982)

Joe Randall Weatherby, B.S. Mechanical Engineering
Texas A&M University

Co-Chairmen of Advisory Committee: Dr. R.A. Schapery
Dr. M. Henriksen

An improved beam theory model is proposed for calculating energy release rates in symmetrically loaded unidirectional double cantilevered beam fracture toughness specimens having longitudinally oriented fibers. The proposed model consists of a beam supported at the crack front by a torsion spring. Here the spring is used to account for the strain energy in the region ahead of the crack front. Values for the spring constant are obtained from a two dimensional approximate analytical solution and from finite element models. Energy release rate calculations based on the beam and spring model are compared to those obtained by numerical evaluation of Irwin's crack closure integral. Comparisons are also made with results from techniques previously used in the analysis of isotropic double cantilevered beam specimens.

9. PROFESSIONAL PERSONNEL INFORMATION

9.1 Faculty Research Assignments

Each participating faculty member is responsible for the research conducted in at least one specific area of investigation, as shown below. In addition, most serve as chairmen of one or more of the graduate advisory committees for M.S. and Ph.D. students and, as such, direct their students' research projects. The faculty also contribute to other research activities on the project by serving on student advisory committees, through technical meetings, informal discussions, and, in some cases, through specific research.

The Principal Investigator (R.A. Schapery) has responsibility for overall technical direction and coordination and for project management. In addition he has direct responsibility for certain research work, as noted below. It should also be observed that there is considerable overlap between the areas in the Statement of Work, and therefore most of the faculty are strongly involved in more than one area.

<u>Faculty Member/Departmental Affiliation</u>	<u>Primary Research Responsibility</u>
Dr. David Allen/Aerospace Engineering	(5)* theoretical models/formulation and numerical solution methods
Dr. Walter Bradley/Mechanical Engineering	(1) delamination fracture properties and SEM studies
Dr. Walter Haisler/Aerospace Engineering	(5) theoretical models/numerical solution methods
Dr. Joe Ham/Physics	(4) toughening mechanisms (molecular aspects)
Dr. Cornelius Hoeve/Chemistry	(3) behavior and structure of water in polymers

*Number in parenthesis indicates area in Statement of Work (p. 1).

Dr. Richard Schapery/Aerospace and Civil Engineering (5) theoretical models/formulation and analysis

Dr. Jack Weitsman/Civil Engineering (2) temperature and moisture effects/residual stresses

9.2 Additional Professional Staff

Mechanics and Materials Center

Ms. Jennifer Casler - Systems Analyst

Mr. Carl Fredericksen - Electronics Technician

Mr. Bob Harbert - Assistant Research Engineer

Mr. Richard Tonda - Laboratory Manager

9.3 Spoken Papers and Lectures, Publications, and Other Composites-Related Professional Activities of the Faculty

D.H. Allen

Lectures and Conference Presentations:

"Characterization of the Material Behavior of Inelastic Metals at Elevated Temperature," Texas Institute for Computational Mechanics, University of Texas at Austin, November 1982.

"Experimental and Analytical Correlation of Several Rate Dependent Thermo-mechanical Constitutive Equations at Elevated Temperature," Society of Engineering Science 19th Annual Meeting, Rolla, Missouri, October 1982.

"Experimental and Analytical Correlation of Current Constitutive Models for Metals at Elevated Temperature," Symposium on Advances and Trends in Structural and Solid Mechanics, Washington, D.C., October 1982.

W.L. Bradley

Conference Presentations:

"Delamination and Transverse Fracture in Graphite/Epoxy Composite Materials," with R.N. Cohen, Gordon Research Conference on Composite Materials, Ventura, CA, January 1982.

"Mixed Mode Delamination Fracture in Graphite/Epoxy Composite Materials," Society of Engineering Science 19th Annual Meeting, Rolla, Missouri, October 1982.

Publications

"In-Situ Fractographic Study of Graphite/Epoxy Composite Materials," with R.N. Cohen, Proc. 6th Conference on Fibrous Composites in Structural Design, New Orleans, January 1983.

"Delamination and Transverse Fracture in Graphite/Epoxy Composite Materials," with R.N. Cohen, Proc. Fourth Int. Conf. on Mechanical Behavior of Materials, Sweden, August 1983.

"A New Method for Mixed Mode Delamination Fracture Studies," with P. Vanderkley, Experimental Mechanics, (in preparation).

"Transverse Fracture in Graphite/Epoxy Composite Materials," with D. Williams, J. of Engineering Materials and Technology, (in preparation).

"Delamination and Transverse Fracture in Several Graphite/Epoxy Composite Systems," with R.N. Cohen, J. of Composite Materials, (in preparation).

"Micromechanisms of Fracture in Graphite/Epoxy Systems Based on In-Situ Fracture Studies," with R. Cohen (in preparation).

Consulting:

Ashland Chemical, Columbus, Ohio, on mixed mode delamination fracture behavior.

W.E. Haisler

Conference Presentations:

"An Uncoupled Viscoplastic Constitutive Model for Metals at Elevated Temperature," with J. Cronenworth, presented at the AIAA/ASME/ASCE/AHS Structures, Structural Dynamics and Materials Conference, Paper No. 83-1016-CP, Lake Tahoe, May 1983.

"Experimental and Analytical Correlation of Current Constitutive Models for Metals at Elevated Temperature," with D.H. Allen and W.L. Bradley, presented at the Symposium on Advances and Trends in Structural and Solid Mechanics, Arlington, Virginia, October 1982.

"Experimental and Analytical Correlation of Several Rate Dependent Thermomechanical Constitutive Equations at Elevated Temperature," with D.H. Allen and W.L. Bradley, Society of Engineering Science 19th Annual Meeting, University of Missouri, Rolla, October 1982.

"Application of an Uncoupled Elastic-Plastic Creep Constitutive Model to Metals at High Temperature," with J. Cronenworth, Symposium on Nonlinear Constitutive Relations for High Temperature Applications, University of Akron, May 1982.

Consulting:

Finite element analysis of cord-rubber composite used in high pressure hoses. Investigation of the forming process for metal couplings on composite rubber hoses and prediction of optimum cord layup and coupling geometry. Work is for Dayco Corporation under Mr. Larry Oliver.

Development of material model and computer program for predicting response of nonlinear, orthotropic composite behavior used in rocket motor cases and nozzles. Classified work for the Navy.

J.S.Ham

Conference Presentations:

"Effects of Chain Stiffness in a Polysulfone," American Chemical Society Annual Meeting, Kansas City, September 1982; also poster session at American Physical Society Annual Meeting, Dallas, March 1982.

Papers in Progress:

"Stiffness in a Polysulfone Chain". (To be submitted to J. Polymer Science).

"Stiffness in a Polyphenoxyquinoxaline Chain". (To be submitted to Applied Physics Communications).

"Attainment of Glassy Transition Temperature Above the Actual Curing Temperature". (To be submitted to J. Polymer Science).

C.A.J. Hoeve

Publication:

"Heat Capacity of Water Absorbed in Methylcellulose," with D.A. Kinard, submitted to J. Polymer Science.

R.A. Schapery

Lectures and Conference Presentations:

"Time-Dependent Deformation and Failure Behavior of Composite Materials," 1982 Midwest Mechanics Lecture Series at Eight Universities: Michigan, Michigan State, Wisconsin, Minnesota, Notre Dame, Illinois Institute of Tech., Illinois, Purdue.

"Models for Damage Growth and Fracture in Nonlinear Viscoelastic Particulate Composites," Ninth U.S. National Congress of Applied Mechanics, Cornell University, June 1982.

"Characterization of Damage Growth and Fracture in Filled Elastomers," IUPAC International Symposium on Macromolecules, University of Mass., July 1982.

"Research on Composite Materials for Structural Design," Eight Annual Mechanics of Composites Review, Dayton, Ohio, October 1982.

"Micro-Damage Analysis for Composite Materials," University of Texas, Austin, December 1982.

Publications:

"Models for Damage Growth and Fracture in Nonlinear Viscoelastic Particulate Composites," Proc. Ninth U.S. National Congress of Applied Mechanics, 1982.

"Continuum Aspects of Crack Growth in Time Dependent Materials," to be published in Encyclopedia of Materials Science and Engineering, Pergamon Press.

"Correspondence Principles and a Generalized J Integral for Large Deformation and Fracture Analysis of Viscoelastic Media," submitted to Int. J. Fracture Mechanics.

Consulting:

United Technology Corp., Vought Corp., and Ashland Chemical Co. on deformation and fracture of composites. Air Force Materials Lab. (W.B. Jones) on fracture of resins.

Y. Weitsman

Lectures and Conference Presentations:

"On the Thermoviscoelastic Characterization of Adhesives and Composites," 4th International Conference on Composite Materials, Tokyo, October 1982.

"Optimal Cooling of Cross-Ply Composite Laminates and Adhesive Joints," Winter Annual Meeting of ASME, Phoenix, November 1982.

"The Modeling of Crazes in Polymers," Technion, Haifa, Israel, December 1982.

Publications:

"Optimal Cooling of Cross-Ply Composite Laminates and Adhesive Joints," with B.D. Harper, J. of Applied Mechanics ASME, Vol. 49, pp. 735-739, December 1982.

"On the Thermoviscoelastic Characterization of Adhesives and Composites," Proc. ICCM-IV, Tokyo, 1982.

"Assessment of Chemical Cure-Shrinkage Stresses in Two Technical Resins," with B.D. Harper and D. Peretz, Proc. 24th SDM Conference, Lake Tahoe, May 1983.

Consulting:

Israel Aircraft Industry, December 1982.

Technical Committee Membership:

ASME Committee on Composite Materials

AIAA Sub-committee on Composite Materials

In addition to the above activities some of the faculty attended other conferences, chaired technical sessions, and published papers and served as consultants in areas not related to composites.

10. REFERENCES

1. Arenburg, R.T., "Analysis of the Effect of Matrix Degradation on Fatigue Behavior of a Graphite/Epoxy Laminate," M.S. Thesis, Texas A&M University, May 1982.
2. Stinchcomb, W.W., Reifsnider, K.L., Yeung, P., and Masters, J., "Effect of Ply Constraint on Fatigue Damage Development in Composite Material Laminates," in Fatigue of Fibrous Composites, ASTM STP 723, pp. 65-84, 1981.
3. Reifsnider, K.L. and Jamison, R., "Fracture of Fatigue-Loaded Composite Laminates," Int. J. Fatigue, pp. 187-197, 1982.
4. Coleman, B.D. and Gurtin, M.E., "Thermodynamics with Internal State Variables," J. Chem. Phys., Vol. 47, No. 2, pp. 597-613, 1967.
5. Hoeve, C.A.J., "Structure of Water in Polymers", ACS Symposium Series, Vol. 127, pp. 135-146, 1980.

APPENDIX

Recent Publications
of Work on AFOSR Project

1. "Delamination and Transverse Fracture in Graphite/Epoxy Materials," by W.L. Bradley and R.N. Cohen.
2. "In-Situ Fractographic Study of Graphite/Epoxy Composite Materials," by W.L. Bradley and R.N. Cohen.
3. "Effects of Chain Stiffness in a Polysulfone," by J.S. Ham.
4. "Heat Capacity of Water Absorbed in Methylcellulose," by D.A. Kinard and C.A.J. Hoeve.
5. "Continuum Aspects of Crack Growth in Time Dependent Materials," by R.A. Schapery.
6. "Correspondence Principles and a Generalized J Integral for Large Deformation and Fracture Analysis of Viscoelastic Media," by R.A. Schapery.
7. "Assessment of Chemical Cure-Shrinkage Stresses in Two Technical Resins," by B.D. Harper, D. Peretz, and Y. Weitsman.
8. "On the Thermoviscoelastic Characterization of Adhesives and Composites," by Y. Weitsman.
9. "Optimal Cooling of Cross-Ply Composite Laminates and Adhesive Joints," by Y. Weitsman and B.D. Harper.

Delamination and Transverse Fracture

In Graphite/Epoxy Materials

W.L. Bradley* and R.N. Cohen*

*Mechanical Engineering, Texas A&M University

**General Dynamics Corporation, San Diego, USA

ABSTRACT

Four graphite/epoxy composite materials systems have been studied to determine the transverse and delamination fracture behavior. Measured energy release rates have been correlated with micromechanisms of fracture determined using in-situ fracture observations in a SEM in combination with post-mortem fractographic examinations.

KEYWORDS

Delamination fracture; transverse fracture; graphite/epoxy; fractography; in-situ fracture.

INTRODUCTION

Graphite/epoxy composite material systems have exciting potential in weight critical applications because of their exceptional strength to weight ratio when loaded in a direction parallel to the fibers. However, in many practical applications of fiber reinforced plastics, significant loads may arise in the component in directions not reinforced by fibers, leading to component failure at relatively low loads. Out-of-plane stresses resulting from local buckling or geometric irregularities can lead to delamination. Loading

Prepared for the 4th International Conference on Mech. Behavior of Materials, Stockholm, Sweden, August 1983.

perpendicular to the fiber direction in a to the fiber direction in a lamina or a unidirectional laminate can also produce matrix cracking parallel to fibers, and therefore as with delamination, result in failure at relatively low stress levels by transverse cracking.

The initial development of graphite/epoxy systems emphasized composite stiffness and high glass transition temperature, T_g , to allow higher service temperatures. The resins which optimize these properties, however, are generally quite brittle, making the composite very vulnerable to transverse and/or delamination cracking. More recent development work has sought to replace these brittle resins with somewhat tougher ones that still have a reasonably high stiffness and glass transition temperature. In this research program, we have studied the delamination and transverse fracture behavior of four graphite/epoxy systems. Our approach has been to characterize the macroscopic fracture behavior using a fracture mechanics approach, and then, relate this behavior to micromechanisms of fracture determined using in-situ fracture in a scanning electron microscope and correlated with the post-mortem fractography of the fracture mechanics test coupons.

TRANSVERSE AND DELAMINATION FRACTURE

This study of the fracture behavior of graphite/epoxy composite materials emphasized the macroscopic measurement of energy release rate which was correlated with the microscopic observation of various energy dissipative process.

Macroscopic Fracture Toughness Measurements Using Fracture Mechanics Approach

Four different graphite/epoxy systems were chosen for this study: Hercules AS1/3502 and AS4/3502 and Hexcel T6T145/F185 and T6C190/F155.

The comparison of the behavior of the two Hercules systems allowed us to determine how much effect the fiber toughness and interfacial strength have on transverse and delamination fracture toughness since the AS4 fiber is significantly tougher than the AS1 fiber (higher strength and strain to failure) but less adherent to resin because of its smooth finish. The Hexcel F185 and F155 are rubber toughened epoxies with neat specimen critical energy release rates of 6000 J/m^2 and 730 J/m^2 (Moulton, 1982), respectively, compared to the Hercules 3502 whose G_{1C} is 70 J/m^2 (Williams, 1981).

Transverse cracking was studied using compact tension specimens with $W = 5\text{cm}$. and $B = 0.5\text{cm}$. These were tested in a 20Kip MTS machine equipped with a 100 lb. load cell. LVDT's were attached to the ends of specimens and were used to measure crack opening displacement. They were also used to control the closed loop system, allowing testing to be done under crack tip opening displacement control rather than simply actuator displacement control. This arrangement permitted very stable crack growth completely across the width of the specimen. Crack size was measured directly using resistance gages (Kraak gages) and unloading compliances were measured at intervals of crack growth of about 0.1 cm. Energy release rates were determined in the usual way using measured changes in compliance with crack size (dC/da) and the loads required at each crack length to continue crack extension. Corrections were made in the analysis to account for the fact that displacement was measured at the edge of the specimen rather than along the load line.

Delamination cracking was studied using a split laminate (double cantilevered beam) arrangement. Crack growth was stable throughout

the test. Mode I fracture was produced using symmetric loading while a mixed mode I/mode II fracture was produced using asymmetric loading of the split ends of the laminate while supporting the uncracked end of the specimen. The ratio of $G_{II}/(G_I + G_{II})$ varied from 0.0 to 0.40 in this study. Cracking in these tests was continuous (no interruption for unloading compliance measurements) with the energy release rate calculated using an analysis previously developed by Devitt, Schapery, and Bradley (1980). This analysis involved the measurement of load, displacement and beam stiffness EI, allowing the calculation of the crack length and energy release rate using linear beam theory.

The results of the mode I delamination and transverse fracture testing are summarized in Table I. In the very brittle 3502 resin, the introduction of fibers is seen to increase the energy absorbed in transverse and delamination fracture while in the more ductile F155 and F185, the introduction of fibers decreased the transverse and delamination fracture toughness. These results may be interpreted to imply that introduction of strong brittle fibers into a weaker, brittle resin enhances the energy absorbed in fracture. This enhancement is a result of the fact that the resin rich region between plies is very thin and minor fiber misalignment or waviness will result in some interaction of the crack tip with the fibers. The details of this interaction will be discussed further in the fractography section. The introduction of fibers into a more ductile resin decreases the energy absorbed in fracture by decreasing the volume of material ahead of the crack tip capable of significant deformation and constraining the deformation of the available resin. The result is a net decrease in energy absorbed in fracture, the

increase in energy dissipation via crack tip/fiber interaction being less than the decrease in energy dissipation resulting from the reduced resin deformation.

TABLE 1 Transverse and Delamination Fracture Toughness

Material	Type of Fracture	Ave. a (m/s)	G_C (J/m ²)
Neat 3502 Resin			69 [10]
AS1/3502	Delamination		155
AS1/3502	Transverse		225
AS4/3502	Delamination	2.8×10^{-5}	225
AS4/3502	Transverse	1.74×10^{-5}	120
Neat F155 Resin			730
T6C190/F155	Delamination	3.5×10^{-5}	600
T6C190/F155	Transverse	3.85×10^{-5}	410
Neat F185 Resin			6040
T6T145/F185	Delamination	4.5×10^{-5}	2600
T6T145/F185	Transverse	1.39×10^{-5}	1525

It is further worth noting that the transverse fracture toughness is less than the delamination fracture toughness in the tougher resin systems. If these systems derive their toughness principally from resin deformation, then one would expect delamination fracture to be more difficult than transverse fracture. This is because the crack tip extension in delamination occurs through a thicker resin rich region in delamination than in transverse cracking. The AS1/3502 system shows increasing resistance to crack propagation comparing delamination to transverse cracking, as one might expect in a system where crack tip interaction with the fibers enhances resistance to crack propagation. That this trend is not noted in the AS4/3502 may be a result of the weaker interfacial bonding in AS4 than in AS1 due

to the much smoother fiber surface finish.

The energy release rate versus degree of mode II loading is summarized in Fig. 1. The toughest resin (F185) shows a monotonically decreasing G_C with increasing degree of mode II loading, while the 3502 systems showed an increased energy absorbed with increasing mode II shear. The change for T6C190/F155 at various ratios of mode II shear was not very significant.

Fractographic results to be presented presently seem to suggest that mode II shear simply rotates the microscopic plane of fracture which continually redirects the crack tip into the fibers. Thus, the mixed mode loading results in a series of mini mode I cracks joined by tear ridges, giving a scalloped appearance to the fracture surface. As previously explained, interaction of the crack tip with the fibers enhances the energy absorbed in fracture in a system in which the resin is brittle. Thus, the increasing mode II loading would be expected to give an increasing total energy release rate for the 3502, and it does. The very tough F185, which derives its toughness from matrix deformation decreases, in toughness with increasing crack tip interaction with the fibers, since this probably reduces the matrix deformation locally.

A history effect has also been observed, particularly in the systems with the brittle 3502 resin. When a high fraction of mode II shear is followed by pure mode I loading, the observed energy release is greater than it would be for a history of only mode I, as seen in Fig. 2. This appears to be associated with fiber and bundle pullout or even occasional local ply jumping which gives a significant roughening of the slip plane which is not reversible when pure mode I

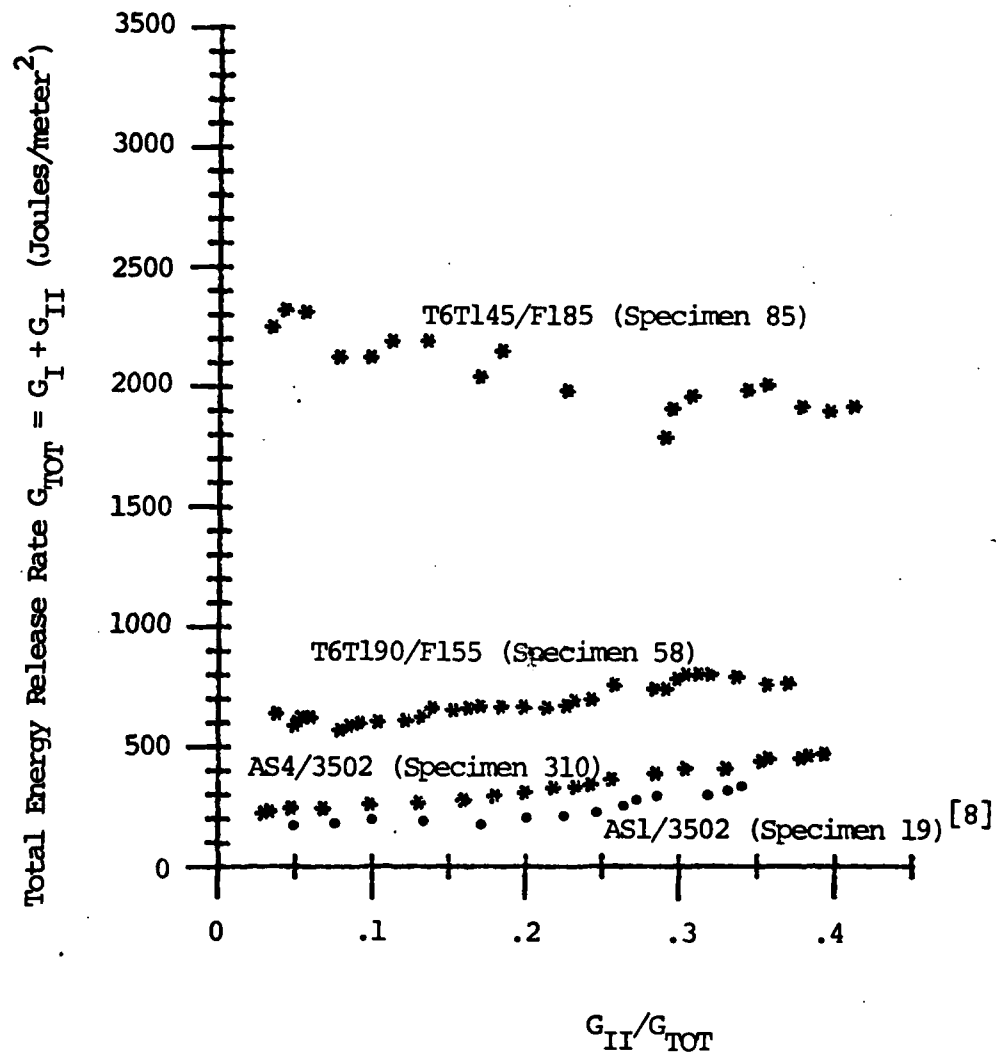


Fig. 1. Total energy release rate for mixed mode delamination for increasing fraction of mode II shear as indicated by the ratio mode II energy release rate to total energy release rate.

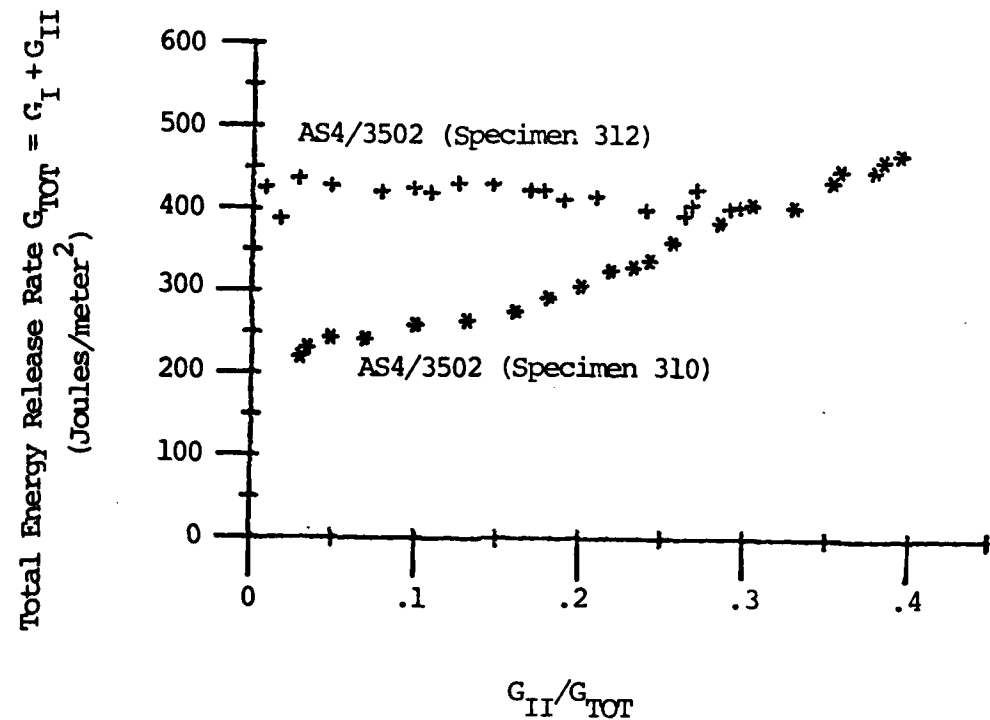


Fig. 2. Total energy release rate for delamination fracture for increasing fraction of mode II shear (specimen 310) and decreasing fraction of mode II shear (specimen 312) for AS4/3502.

loading is resumed subsequently. This rougher fracture plane increases the actual surface area being created in fracture (as distinct from the nominal projected area). The bundle pullout can also lead to tie zone formation which does dissipate additional energy.

Micromechanisms of Fracture Using In-situ Fracture in SEM

In-situ delamination fracture results are seen in Fig. 3 for the tough Fl85 and the brittle 3502. Deformation and microcracking in the Fl85 resin is seen to occur over 4-5 fiber diameters on either side of the primary crack, while in the 3502 the deformation and resultant energy dissipation is limited to the resin rich region between fibers bounding the primary crack.

Fractographic results on the Fl85 and 3502 are seen in Fig. 4 for mode I delamination fracture. Gross matrix deformation around the rubber particles in the local resin rich regions is seen in the Fl85 system. The fractured surface of the 3502 is seen to be brittle and fairly featureless with the only interesting artifact being the scalloping in the resin rich regions which results from crack tip interaction with the fibers. This interaction occasionally results in fiber breakage, beginning with decohesion at the fiber/matrix interface as shown in Fig. 5A. More typically it results in initiation of a series of microcracks in the matrix just ahead of the crack tip as seen in Fig. 3. Small tear ridges then join the new microcracks to the primary crack producing a series of scallops. This repeated scalloping pattern is clearly seen in Fig. 4.

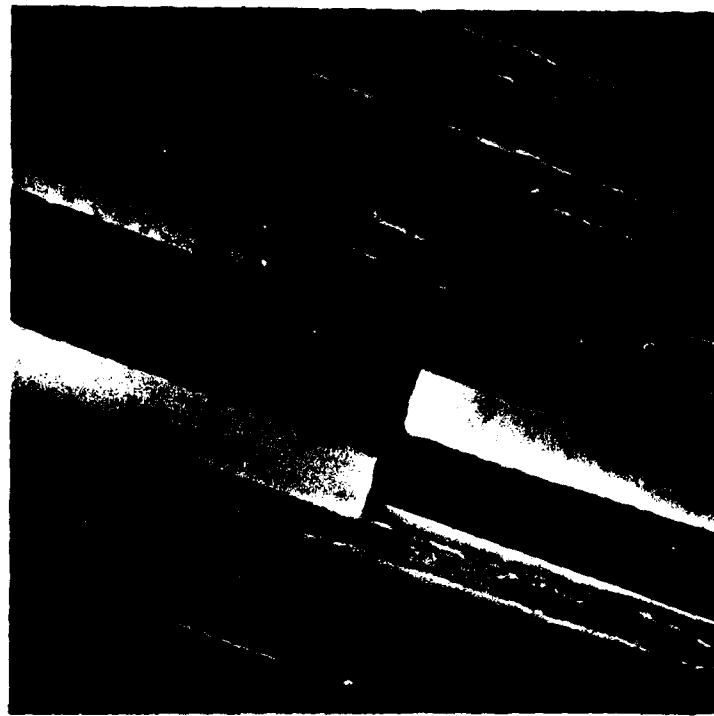
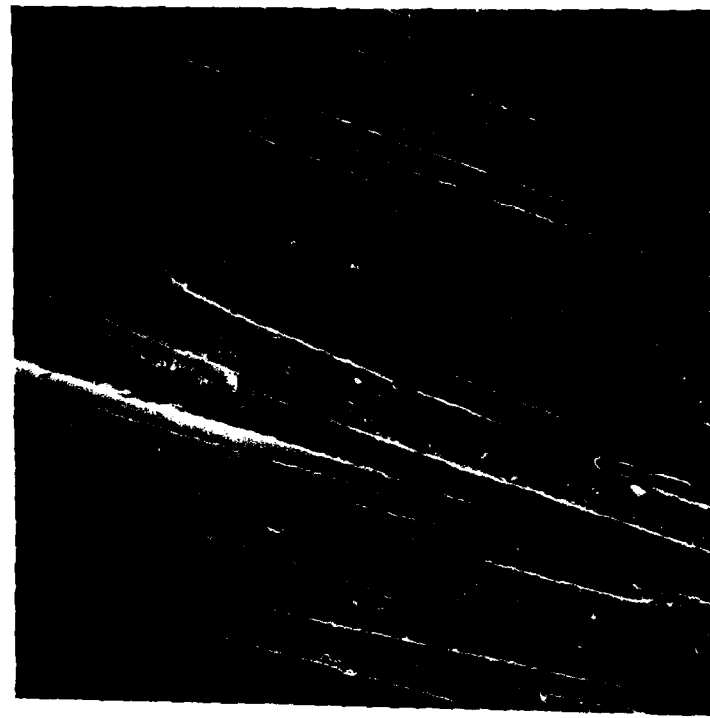


Fig. 3. In-situ fracture of T6T145/F185 (top, 500X) and AS4/3502 (bottom, 1300X).

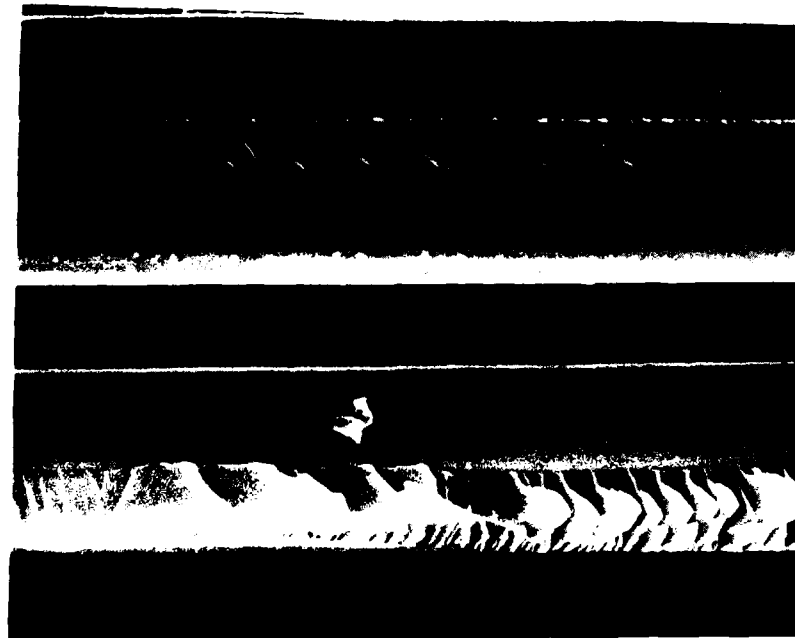
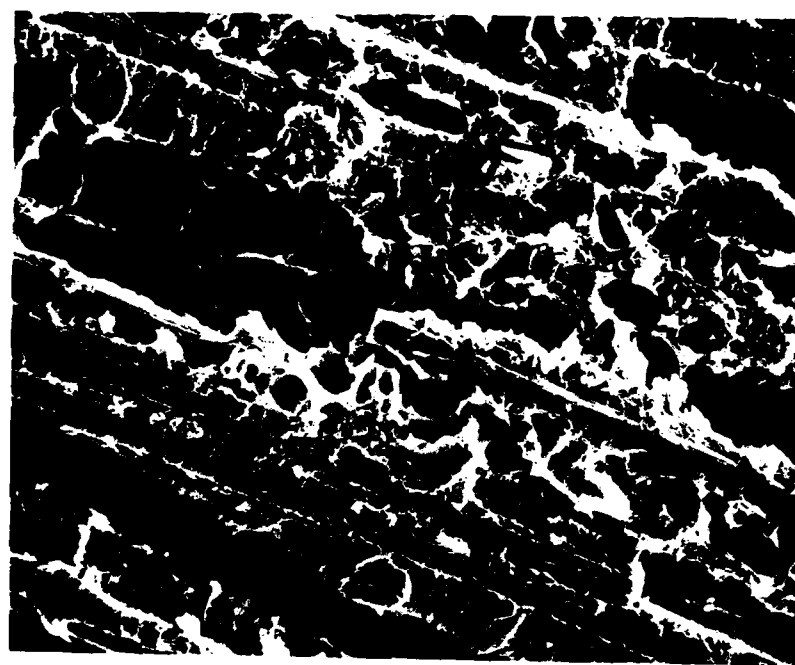


Fig. 4. Post-mortem fractography of T6T145/F185 (top, 700X) and AS4/3502 (bottom, 2000X).

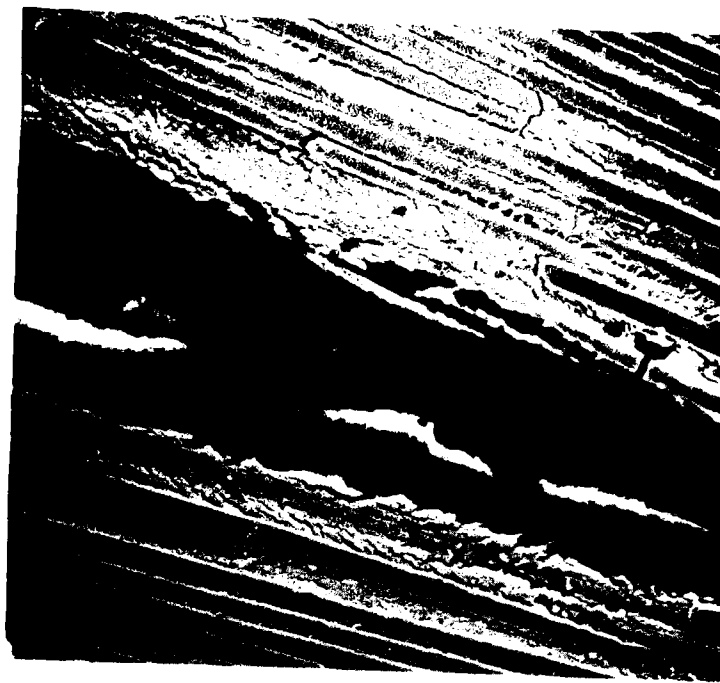


Fig. 5A and 5B. In-situ fracture showing decohesion at interface leading to fiber breakage in T6T145/F185 (top, 500X); T6C190/F155 showing heterogeneity of resin ahead of crack tip (bottom, 600X).

The distribution of rubber particles as well as the cross-link density in the F155 resin is apparently somewhat heterogeneous as suggested by the in-situ fractography shown in Fig. 5B. The resin ahead of the primary crack tip is brittle in some areas but quite soft and ductile in others.

SUMMARY

The transverse and delamination fracture have been observed to depend on the matrix ductility, and in more brittle systems, to the incidence of crack tip interaction with the fiber. In such systems, mixed mode loading increases the total energy dissipated in fracture. History effects have been noted. In-situ fracture clearly shows the large volume of matrix which may deform during delamination fracture, including material 3-4 fiber diameters removed from the primary fracture plane.

ACKNOWLEDGEMENTS

The generous support of the Air Force Office of Scientific Research (contract F49620-82-C-0057) is gratefully acknowledged.

REFERENCES

Devitt, D.F., R.A. Schapery and W.L. Bradley (1980). A method for determining the mode I delamination fracture toughness of elastic and viscoelastic composite materials. Report MM 3824-80-6, Texas A&M University.

Moulton, R.J. (1982). Personal communication and customer bulletins from Hexcel Corporation.

Williams, D. (1981). Mode I cracking in an epoxy and a graphite fiber reinforced epoxy. Master's thesis, Texas A&M University, August, 1981.

IN-SITU FRACTOGRAPHIC STUDY OF
GRAPHITE/EPOXY COMPOSITE MATERIALS

WALTER L. BRADLEY
Professor of Mechanical Engineering
Texas A&M University
College Station, Texas 77843

RONALD COHEN
Engineer
General Dynamics
San Diego, California

ABSTRACT

Fractography may be used to better understand the micromechanisms of fracture in composite materials as a guide to improving the fracture strength and toughness. However, the fracture behavior of composite materials is quite complicated and post-mortem interpretation of the artifacts on the fracture surface is not straightforward. In-situ fracture of composite materials specimens in the SEM has been used to observe directly the fracture processes and the formation of the various artifacts usually observed in post-mortem fractography. These results have clarified the significance of many of the features commonly observed on the fracture surface of composite materials.

INTRODUCTION

The utilization of graphite/epoxy composite materials for structural components requires a better understanding of the fracture behavior of these complex materials system. Various approaches to the characterization of the fracture toughness of such systems have been developed in recent years. Using fracture mechanics analysis in conjunction with mechanical testing of split laminates (or double cantilevered beams) and compact tension specimens, the fracture behavior has been characterized using the critical energy release rate G_{lc} or critical stress intensity K_{lc} . Fractographic examination of the fracture surface after test coupon failure has been used to identify the various dissipative mechanisms responsible for the observed critical energy release rate. Because the failure process in composite materials is quite complicated, this post-mortem fractographic examination often reveals surface artifacts that are difficult to interpret.

Our objective in this research program has been to fracture graphite/epoxy composite material specimens in a pure mode I delamination mode in the scanning electron microscope, allowing direct observation of the fracture process as viewed from the edge of the specimen. Subsequent examinations of the fractured surface and interpretation of the artifacts observed thereon has been guided by the prior direct observation of the fracture process.

EXPERIMENTAL PROCEDURE

Four graphite/epoxy composite materials were selected for this study: Hercules AS1/3502 and AS4/3502, and Hexcel T6T145/F185 and T6C190/F155. The AS1 and AS4 fibers differ principally in smoothness with the AS4 being much smoother than the AS1. This smoother surface gives a higher strain to fracture as well as a higher strength. The Hexcel resins F155 and F185 are rubber particle toughened epoxy systems differing principally in the volume fracture of second phase present. The neat F185 resin has approximately 6% rubber particles and a $G_{lc} = 6000 \text{ J/m}^2$. The F155 with only 1% rubber particles has a G_{lc} of 750 J/m^2 . These systems were selected because they give a wide variety of resin toughness, fiber toughness and interfacial bond strength.

Specimens were fractured in-situ in a JEOL JSM-35 scanning electron microscope using a special tensile stage (JEOL 35-TS2). These specimens were cut to size (3.0 cm by 1.3 cm) from a 30 cm by 30 cm panels that were 8 or 10 plies thick. The delamination forces are applied by a wedge introduced between the center plies. For the F185 and F155 epoxy systems, the initial centerline crack into which the wedge was introduced was created during fabrication of the panels by placement of a small teflon strip on one edge between the center plies. A significant portion of the cracking occurs with the wedge traversing newly fractured surface beyond the teflon. Thus some frictional forces are present in addition to the pure mode I opening forces.

The initial crack in the 3502 systems was introduced along one edge using a razor blade, nominally along the centerline. The SEM photographs of the crack path do not indicate a resin rich region, which implies that the delamination of these specimens may not have occurred between the plies at the centerline but rather in one of them.

The crack growth parallel to the fiber direction was viewed along the edge of the specimen. Each specimen was ground on the edge to be observed using emery paper, polished using diamond paste and then coated with a 100-200Å thick gold/palladium alloy by vapor deposition using a Technics Hummer. Several specimens were viewed without the coating to verify that the artifacts being observed were generally associated with the fracture of the specimen rather than the fracture of the coating. The microcracks observed appear to develop in the coating prior to actual microcracking of the specimen. However, the larger microcracks were found to be the results of cracking in specimen and coating. The uncoated specimens could be observed in the SEM though charging significantly reduced the quality of the photographs that could be taken. Thus, most of the photographs were taken for specimens coated with the gold/palladium alloy.

EXPERIMENTAL RESULTS AND DISCUSSION

T6T145/F185 SYSTEM

In-situ fracture of T6T145/F185 specimens coated with gold/palladium

and another uncoated specimen of the same material are seen in Figure 1. The general features are seen to be quite similar. The microcracking in the coated specimen is much more distinct than that observed in the uncoated specimen. Because the coating is only 100-200A thick, a small amount of strain may result in fracture of the coating. Since the F185 resin is quite ductile, the coating fracture probably preceded fracture of the resin. Thus, the fine microcracks in the coated material may represent regions of resin deformation greater than some threshold strain required to fracture the coating. Therefore, the extensive microcracking observed in the coated F185 specimens should be interpreted at this time as defining the volume of material around the crack tip that has been deformed to a strain greater than some critical value for coating rupture. Some of the microcracks do represent actual microcracking in the resin as well as the coating but further study will be required to determine which these are. The coating effectively enhances our ability to see the microcracks, but may exaggerate somewhat their size and total number.

Figure 2 shows fiber breakage in progress, again in an uncoated and coated specimen. The bright appearance of the uncoated fiber is a result of charging. Though the graphite fiber is quite conductive, the coating, or skin, is not. The fibers at the surface had their skin removed during the polishing of the edge to be observed prior to fracture in the microscope. This fiber was beneath the surface; thus, its skin was wholly intact. The coated specimen shows breakage of a small bundle of fibers in progress. Both the uncoated and the coated specimens show significant microcracking, though the microcracking is much more distinct in the coated specimen. Since the coating rupture precedes resin rupture, coating rupture will have a more significant crack open displacement by the time resin rupture occurs. Furthermore, the imaging characteristics of the gold/palladium are much better than the resin or graphite fibers. Thus, the microcracking is much easier to see in the coated specimens, though the coating will tend to exaggerate the extent of the effect, as previously noted.

Figure 3 shows a sequel to the fiber bundle pullout prior to bundle breakage shown in the coated specimen in Figure 2. The fibers are seen to have debonded from the matrix (left), and final fracture (right) indicates the bundle had five fibers. Fiber breakage in this investigation was always preceded by debonding causing the fiber to be stretched across the crack opening until rupture occurred. Where the matrix is fairly compliant, the fiber breakage occurs only after the crack tip has progressed a considerable distance ahead of the fiber spanning the fractured surfaces. This phenomena of fiber debonding leading to many fibers or bundles of fibers spanning the fracture surfaces gives rise to tie zones, which may significantly increase the energy dissipated in fracture. It is clear that tie zone formation is facilitated by a compliant resin and interfacial bonding that is not too strong.

Figure 4 shows the deformation/damage zone extends 4-5 fiber diameters from the primary fracture plane. The apparent heterogeneity in fiber spacing in these pictures is a result in part of the fact that the plane of observation at the surface after polishing is a random plane in the composite,

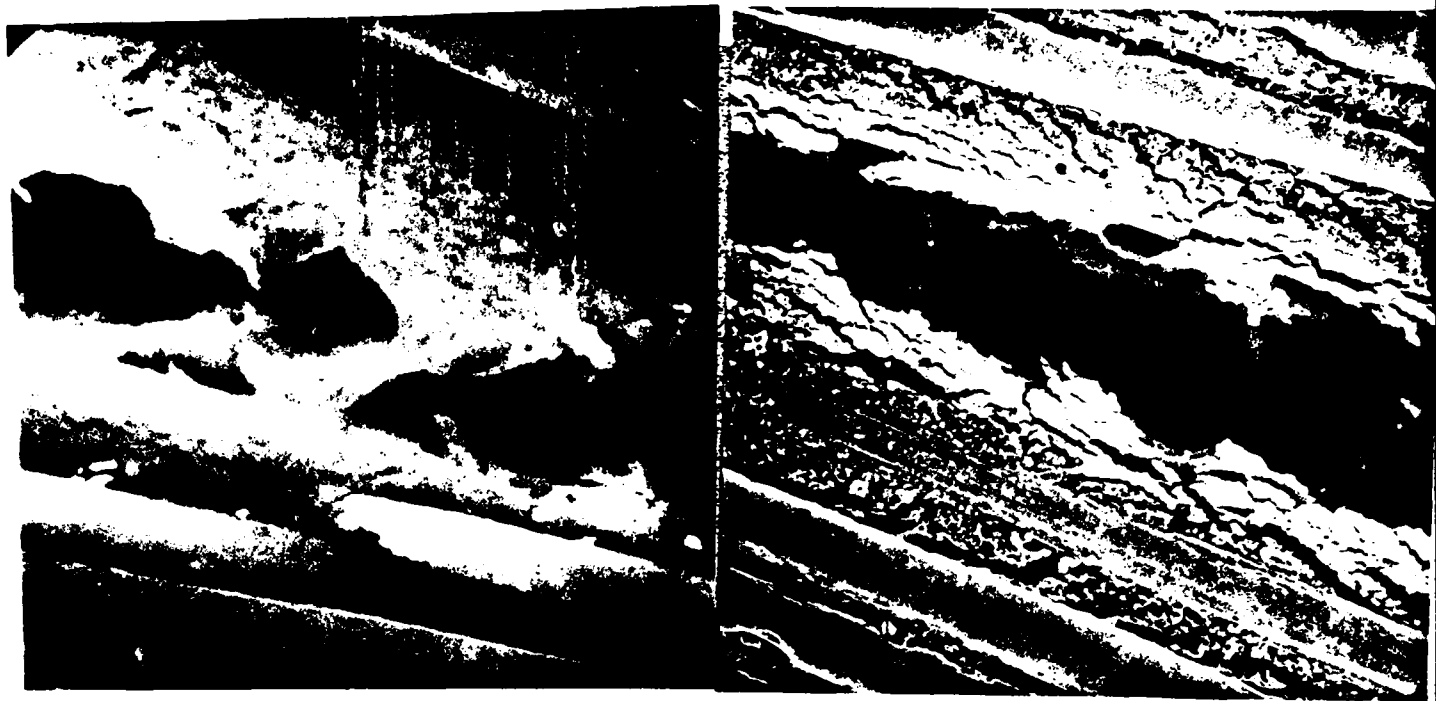


Figure 1. T6T145/F185 specimens photographed during in-situ fracture in the scanning electron microscope at 1500X, uncoated (left) and coated with gold/palladium alloy (right).

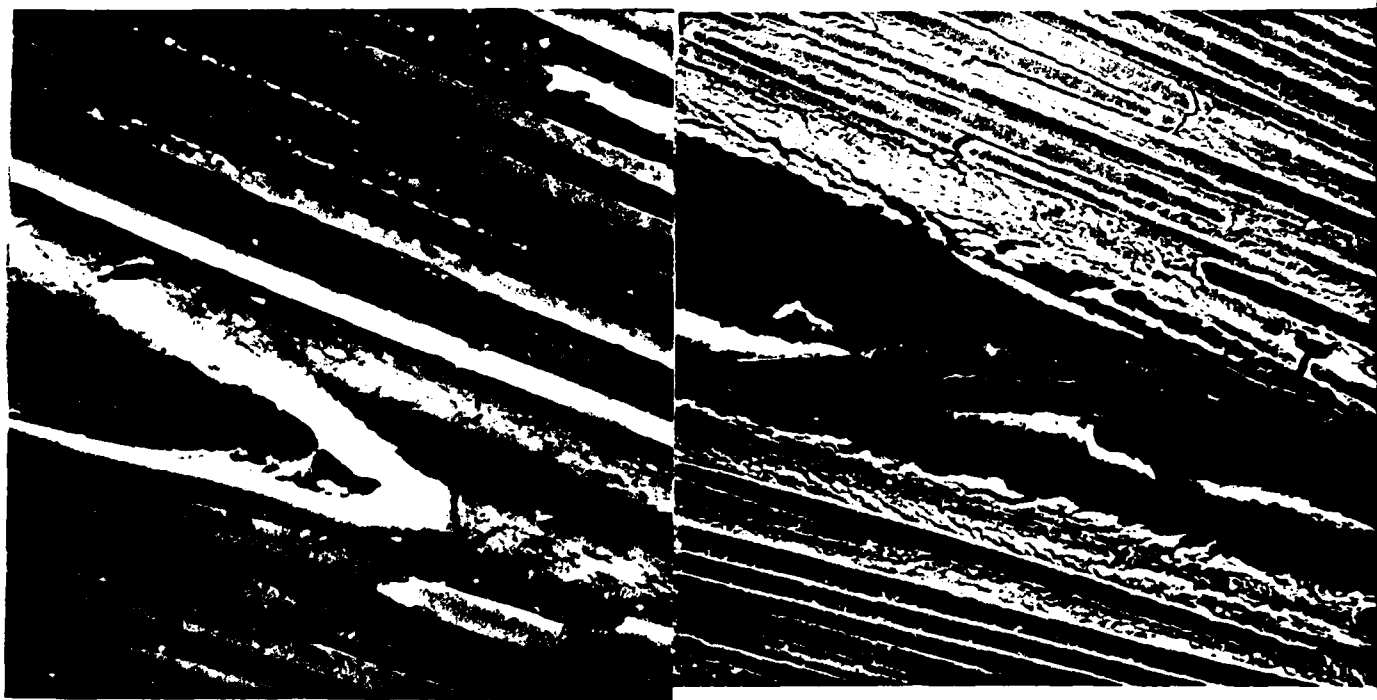


Figure 2. T6T145/F185 specimens photographed during in-situ fracture in the scanning electron microscope. Left, uncoated at 650X; right, coated at 500X.



Figure 3. T6T145/F185 specimen (coated) fractured in-situ in SEM showing clearly that fiber debond preceded fiber pullout (left, 1300X) and that the pullout in this case involved at least five fibers (right, 500X).

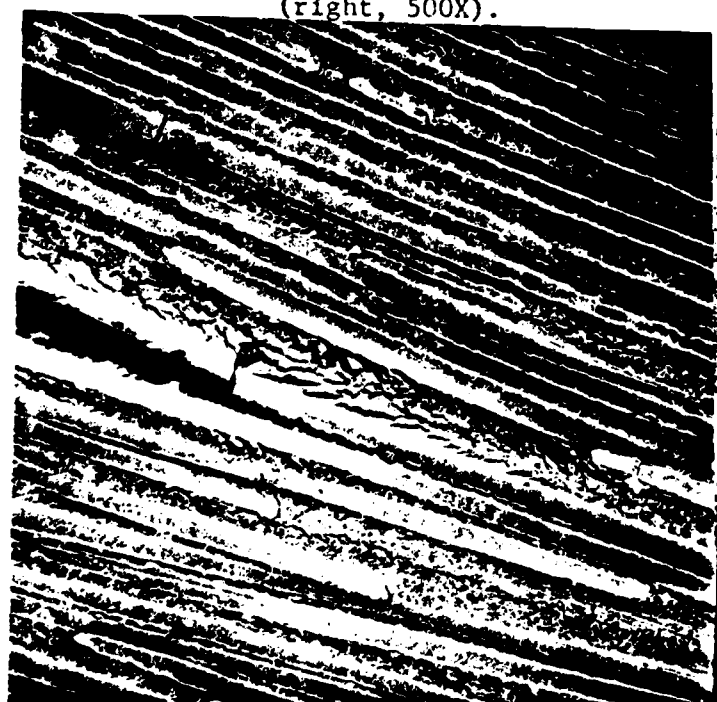


Figure 4. T6T145/F185 specimen (coated) fractured in-situ in SEM (left, 500X; right, 2000X) showing deformation/damage zone that extends four to five fiber diameters from the plane of the primary crack.

cutting some fibers along their axes and others parallel to their axes, but near the edge of the fiber. The former case is seen as fibers whose observed width corresponds to the actual fiber diameter and whose spacing is quite close when several adjacent fibers are sectioned approximately through their axes. Equally closely spaced fibers sectioned near their edges parallel to their axes will appear to be thin and more widely spaced. Thus, along the crack front a mixture of more tightly packed and loosely packed fibers are encountered, even in the absence of manufacturing heterogeneities such as those seen in Figure 5.

Figure 5 shows a unidirectional (0°) split laminate after fracture that has been sectioned perpendicular to the fiber direction, mounted in bakelite ground with emery cloth, and polished with diamond paste on a lapping wheel. The various ply interfaces are seen to be wavy rather than flat as is the fracture surface (top) which resulted when delamination between the two center plies occurred. Additional manufacturing irregularities are also noted, particularly a few resin rich regions.

Figure 6 is the fractured surface of a split laminate of T6T145/F185 that was fractured in a materials testing system under pure mode I delamination loading. The duplex appearance of the microstructure is apparently the result of the crack path traversing resin rich regions, as seen in Figure 1, and resin lean regions, as seen in Figure 4. The relative roughness of the two areas of the fractured surface seen in Figure 6 at 700X are quite consistent with the roughness of the primary crack surfaces pictured in Figures 1 and 4 if one properly allows for differences in magnification. The interfacial strength relative to the resin strength appears to be quite good in this system as evidenced by the fact that even in resin lean regions, continuous cracking along the interface is not observed. The fractured surfaces for these regions is still rough on a scale commensurate with the thickness of the resin layer between fibers. Fiber breakage which results from debond at weak interfaces is also a relatively unusual artifact on the fractured surfaces of specimens of T6T145/F185. A low interfacial strength relative to resin strength will be seen in the AS4/3502 system to give a much smoother fractured surface than is seen in the T6T145/F185.

The fracture of an even thicker resin rich region is seen in Figure 7. In this region the effect of the rubber particles introduced to enhance toughness is more evident. The voids on the fracture surface are enlargements of spaces previously occupied by the rubber particles. The resin deformation adjacent to these particles is significantly greater than in other regions. The appearance of the fracture surface in this area is reminiscent of ductile fracture in metals which occurs by void formation at second phase particles followed by void growth and coalescence.

Considerable microcracking ahead of the crack tip was often observed in regions where the resin thickness was sufficiently great. This microcracking is similar to that observed adjacent to the primary crack in Figures 1-4. The resultant fracture surface formed as these microcracks coalesce, advancing the macrocrack, is seen in Figure 8. We had previously thought that the hackles, or scallops developed one by one as the crack tip locally

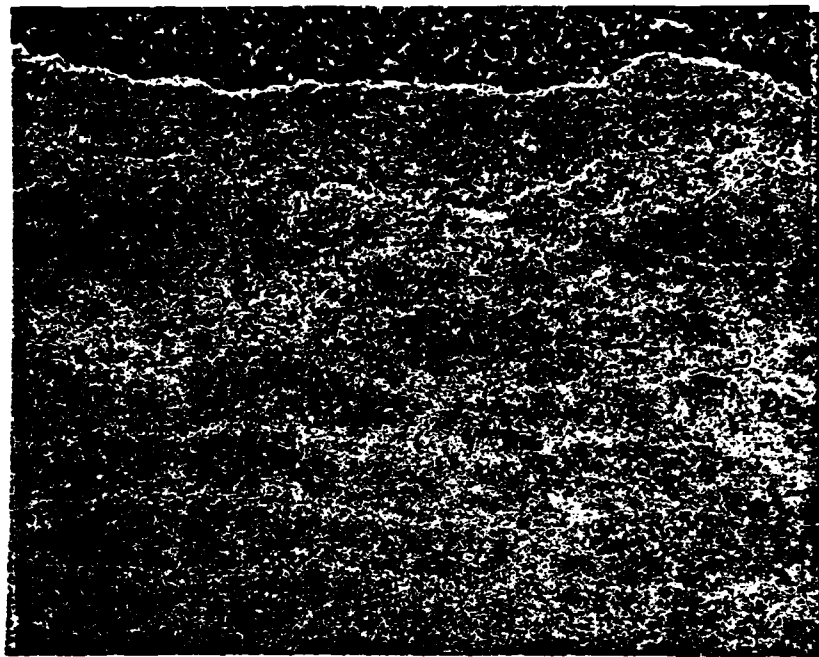


Figure 5. T6T145/F185 microstructure as revealed by sectioning perpendicular to the fiber direction and preparing metallographically for examination one arm of a split laminate after delamination fracture. Fractured surface at 45X is seen as top edge.



Figure 6. T6T145/F185 photographed in SEM after fracture in MTS using pure mode I delamination loading. Note duplex appearance of micro-structure on fractured surface. (left, 45X; right, 700X)

repeatedly contacted a misaligned fiber or was directed into it by some mode II loading. The in-situ SEM suggests in this very tough system, a series of hackles is the result of the coalescing of a series of microcracks which may form some distance ahead of the macroscopic crack tip.

T6C190/F155 SPECIMENS

In-situ delamination fracture of a T6C190/F155 specimen is seen in Figures 8 and 9. In Figure 8, the crack is propagating from left to right with a rather extensive damage zone seen ahead of the macroscopic crack tip. Rubber particles and gross deformation are evident in the damage zone (lower right) ahead of the macroscopic crack tip (upper left) of Figure 9A. Fiber debonding and a more brittle microcracking is noted in Figure 9B, which is an enlargement of Figure 8A. The rubber particles introduced to enhance toughness may not be uniformly distributed, as suggested by the great variety of damage preceding the crack tip.

Figure 10 shows additional in-situ delamination in the same T6C190/F155 specimen seen in Figure 9. The resin again appears to have soft, ductile regions in which cracking occurs ahead of the crack tip more easily. Macroscopic crack extension results when these areas of significant damage ahead of the crack tip coalesce with the crack tip. The ductile damage zone ahead of the crack tip on the right side of Figure 10A has become the macroscopic crack tip in Figure 10B (center). Ahead of this new crack tip note the more brittle cracking and debonding as the next segment of crack advance is developing. The light regions of Figures 9 and 10 are the result of specimen charging after coating rupture has occurred.

The appearance of the fracture surface is quite varied, showing regions of fiber debond and brittle fracture and regions of much more ductile fracture, which were always associated with the presence of rubber particles, as seen in Figures 11 and 12. The shapes of the voids previously occupied by rubber particles as well as the observation of a few rubber particles on the fracture surface indicates that the particles are usually oblong and relatively thin. The regions of high rubber particle density apparently deform more easily and to a much greater degree than those regions of the resin where the rubber particle density is much lower. The very ductile and brittle damage ahead of the crack tip in Figures 9 and 10 surely correlate with these areas on the fracture surface.

In regions where the fracture is more brittle and the fraction of mode II shear loading is increased, a much greater incidence of hackles, or scallops are noted on the fracture surface, as seen at high magnification in Figure 11D. These may be the result of repeated interactions of crack tip in a region containing some modest amount of resin, but no local rubber particle toughening.

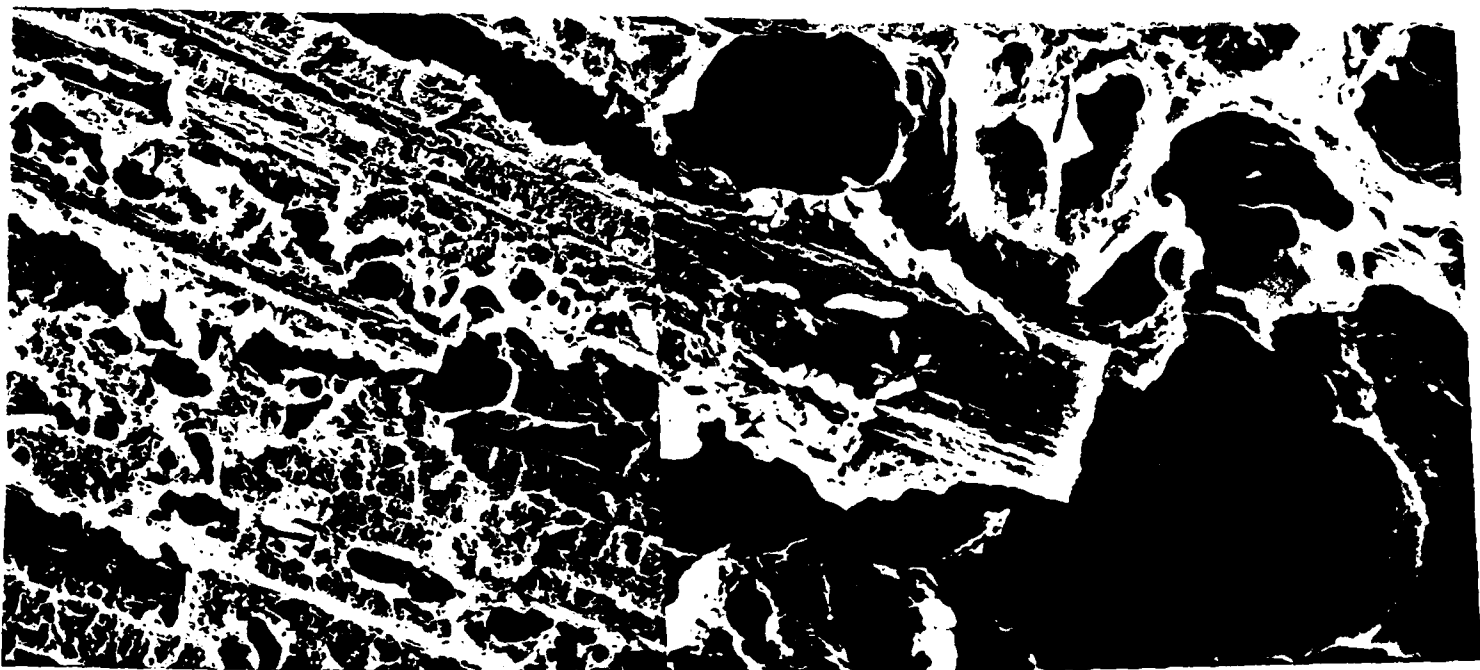


Figure 7. T6T145/F185 specimen photographed in SEM after being fractured in MTS using pure mode I delamination loading. A resin rich region shows significant resin deformation. Voids are enlargements of sites previously occupied by rubber particles introduced to enhance toughness. (left, 700X; right, 3000X)

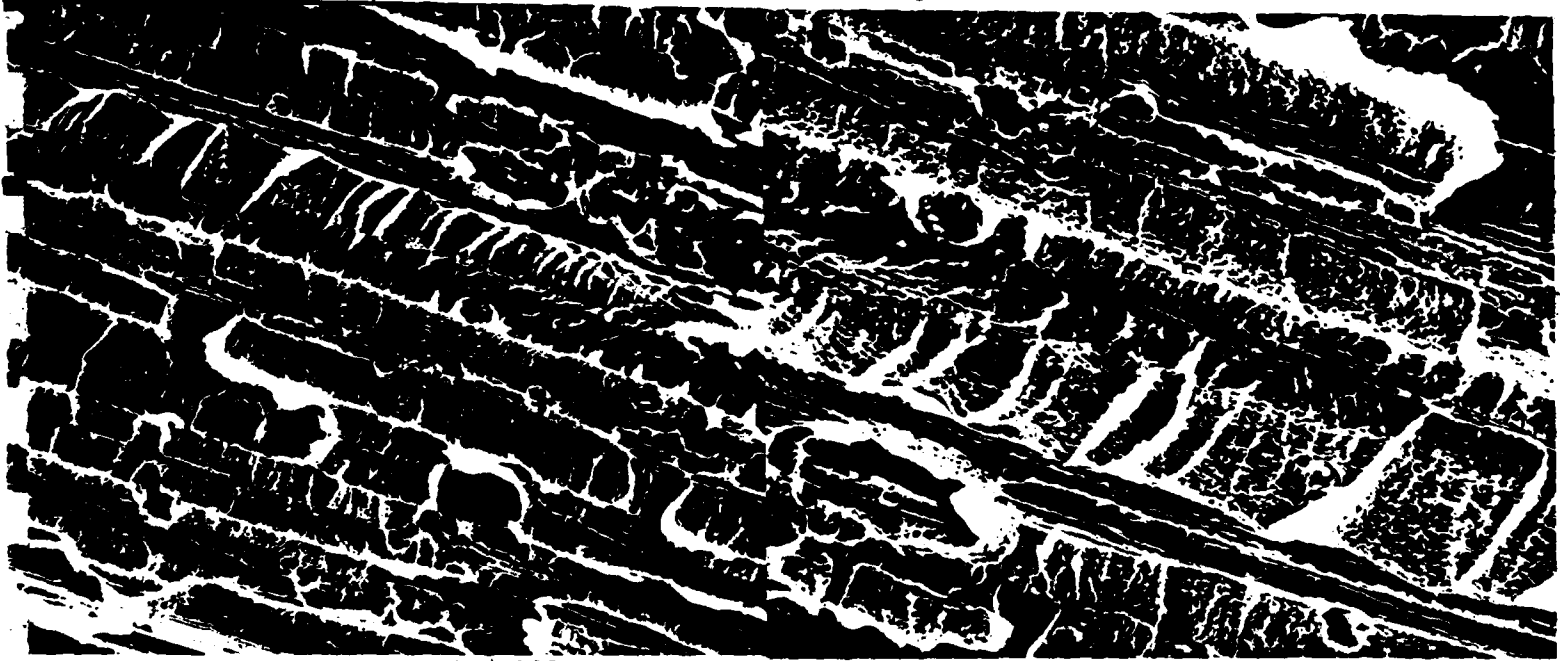


Figure 8. T6T145/F185 specimen photographed in the SEM after being fractured in the MTS using pure mode I delamination loading. Scalloping, or hackle marks are the result of coalescence of microcracks similar to those seen in Figures 1-4 adjacent to the primary crack, but in this case ahead of the macroscopic crack tip. (left, 1000X; right, 2000X)

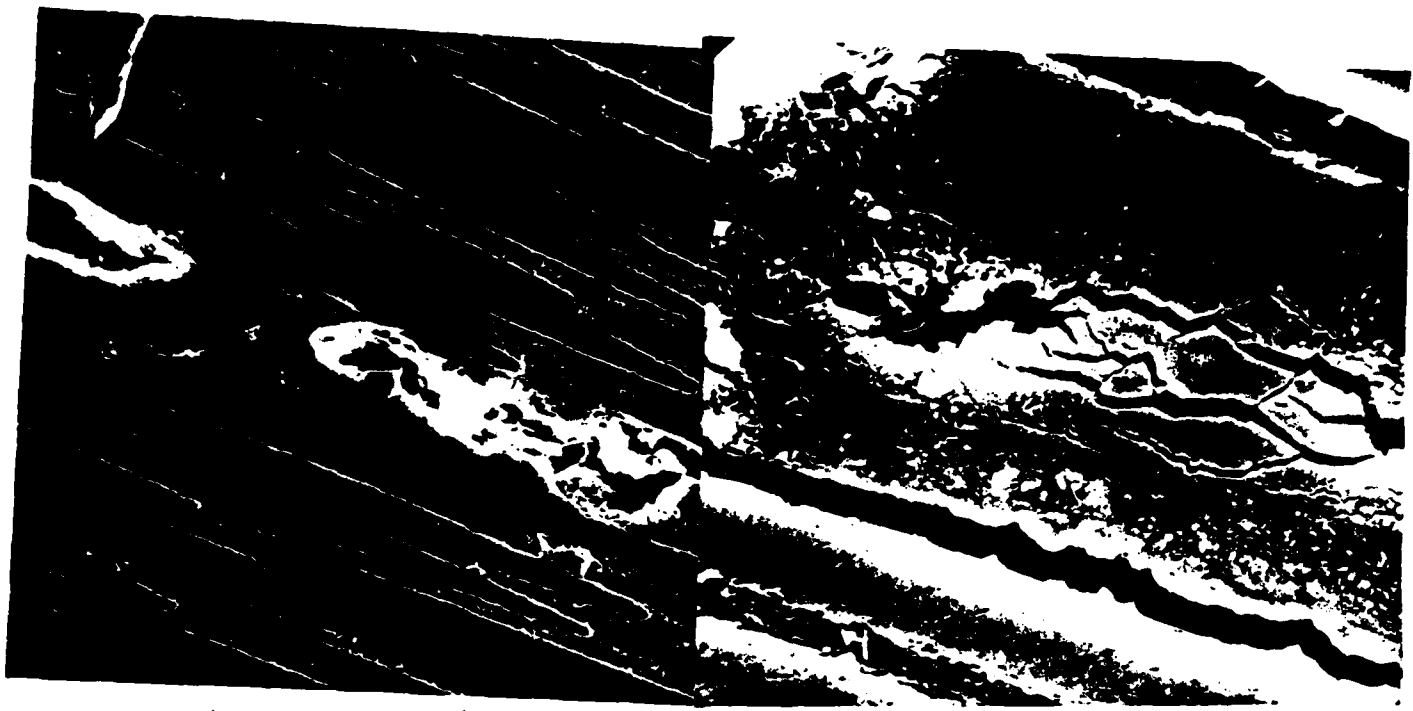


Figure 9. In-situ delamination fracture of T6C190/F155 showing both very ductile and relatively brittle matrix cracking, fiber debonding and a few rubber particles. (left, Figure 9A, 600X; right, Figure 9B, 2200X)

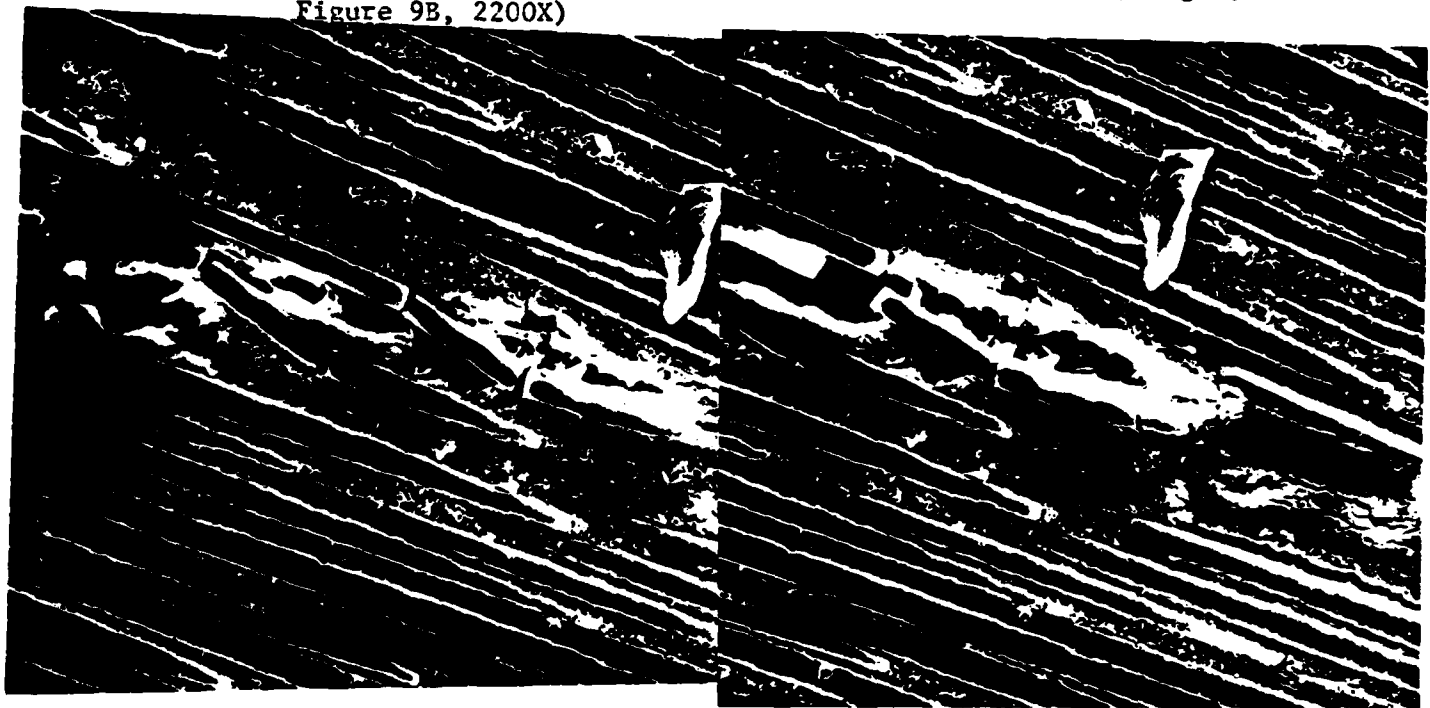


Figure 10. In-situ delamination fracture of T6C190/F155 showing crack extension following damage zone development ahead of crack tip. (left, Figure 10A, 650X; right, Figure 10B, 650X)

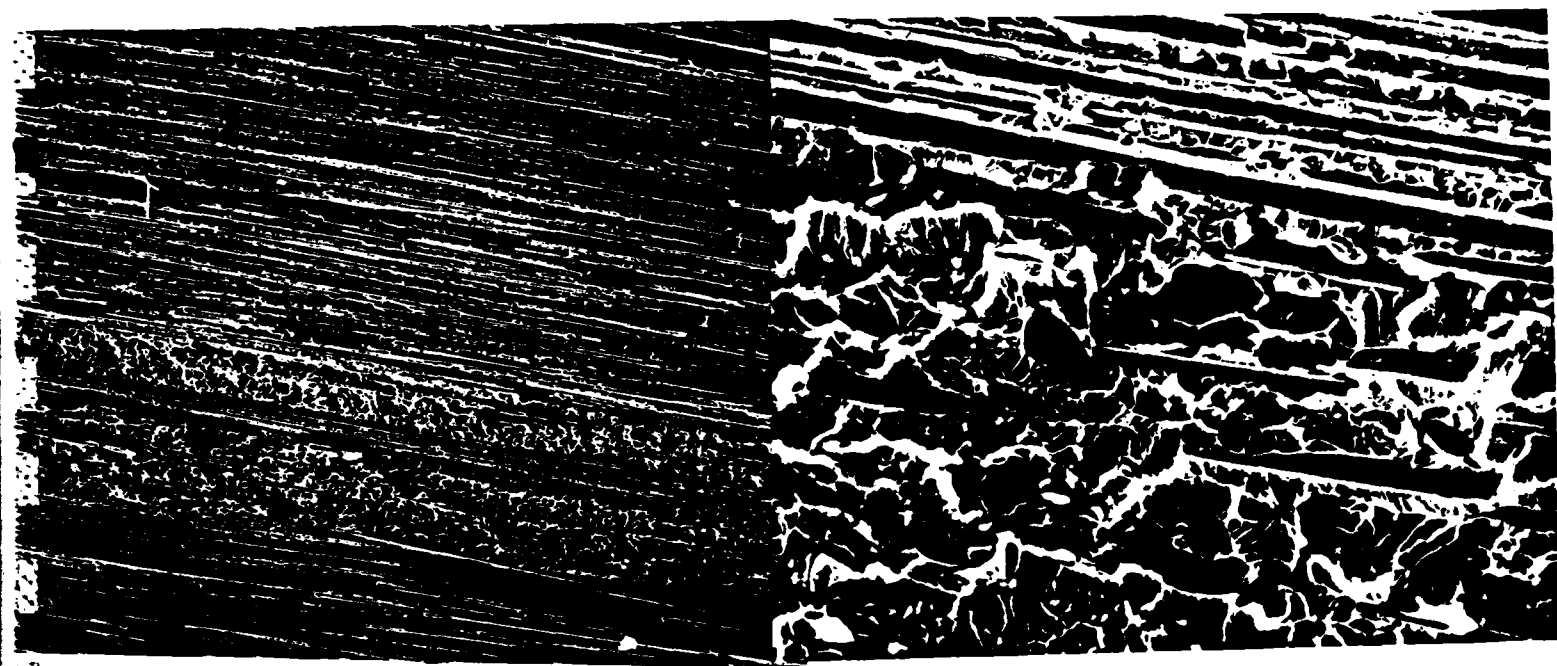


Figure 11A

Figure 11B



Figure 11C

Figure 11D

Figure 11. Fracture surface of delamination specimen of T6C190/F155 showing fractured regions of quite ductile fracture and regions of brittle fracture due to fiber debonding or local absence of rubber particles responsible for toughening resin. Specimens A-C were fractured with pure mode I loading, whereas D was fractured with $G_{II}/(G_I + G_{II}) = 0.37$. (A, 45X; B, 450X; C, 700X; D, 3000X)

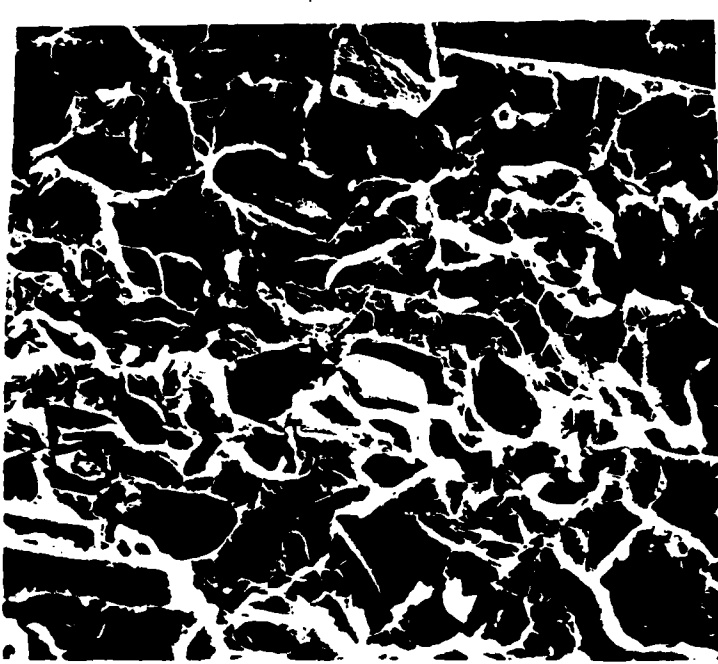


Figure 12. Fracture surface of delaminated specimen of T6C190/F155 showing ductile fracture region containing originally a high density of rubber particles. (left, 700X; right, 3000X)

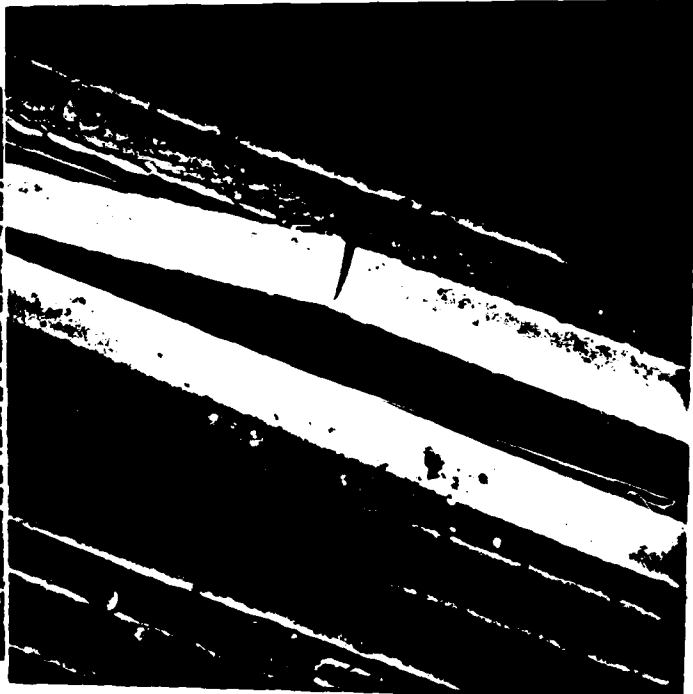
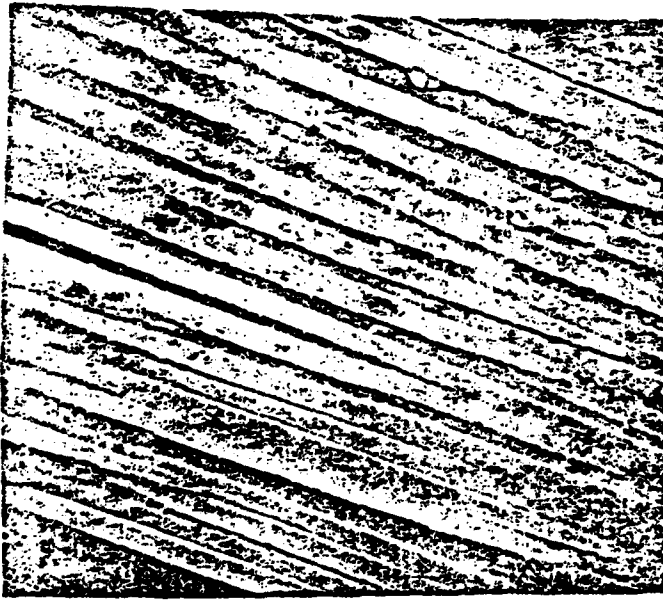


Figure 13. In-situ mode I delamination of AS4/3502 specimen showing no matrix deformation. Fiber breakage due to fiber debond is seen occasionally. (left, 500X; right, 3000X)

AS4/3502 SPECIMENS

The crack tip region of the AS4/3502 specimens was quite different from that observed in the F185 and F155 composite systems. There was no indication of deformation at the crack tip, no damage zone of any kind preceding the crack tip. In fact, the exact location of the crack tip was difficult to define it was so sharp, as shown in Figure 13. Occasional fiber breakage was noted and always associated with fiber debond. The debonds observed in this AS4/3502 showed no indication of resin adhesion, suggesting a very weak interface. In fact loose fibers were often found on the fracture surface, as shown in Figure 14. Previous work at this laboratory on AS1/3502 indicated a much stronger interface, with cracking usually occurring adjacent to the interface, no loose fibers on the fractured surfaces and rather infrequent fiber breakage associated with debonding. This may be due to a difference in surface roughness of the AS1 and AS4 graphite fibers, the AS4 being much smoother. The skin is essentially the same in both fibers but the AS1 fiber is rougher, which implies that the interfacial adhesion in the AS1/3502 has a significant mechanical component in addition to the chemical component.

AS4/3502 specimens fractured in mode I loading and mixed mode I/mode II [$G_{II}/(G_I + G_{II}) = 0.39$] and then examined in the SEM are shown in Figures 15 and 16. The fracture surface shows considerable debonding with the resin fracture between adjacent fiber debonds showing hackle marks. The origin of these hackle, or scallop marks is still uncertain since they were not observed in the in-situ fracture. This is probably because our in-situ fracture for this system did not occur in the resin rich region between plies. The formation of these artifacts may be unique to fracture in the resin rich region.

Comparison of the results for pure mode I fracture (Figure 15) with the results for mixed mode I/mode II (Figure 16) clearly indicates that the hackles frequency increases with increasing mode II shear. One possible explanation for hackles in this brittle system is that they represent a brittle crack extension that is interrupted by a misaligned fiber or by the crack movement toward the fiber on a principal normal plane no longer parallel to the fiber due to the mode II shear. The strength of the fiber forces re nucleate the crack in an adjacent, highly stressed region of the matrix and coalescence of this new crack with the original one through formation of a tear ridge producing a scallop. Repeated interaction of the crack tip with the fiber produces many such scallops. The increasing frequency with increasing mode II shear is consistent with this hypothesis.

SUMMARY

Many practical implications of these observations could be drawn. However, we will limit our summary to noting that in-situ fracture studies do indeed give significant insight into the micromechanisms of fracture in composite materials and the many varied artifacts that result from these fracture processes. A better interpretation of these fracture processes will guide further development of new composite materials with even better properties.

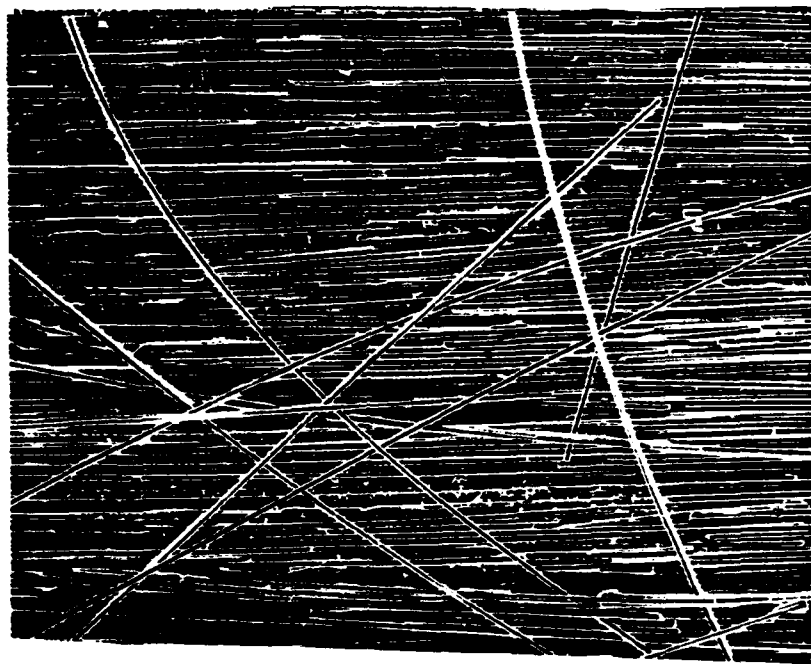


Figure 14. Fracture surface of AS4/3502 after mode I delamination fracture. Note large number of broken and loose fibers. 100X

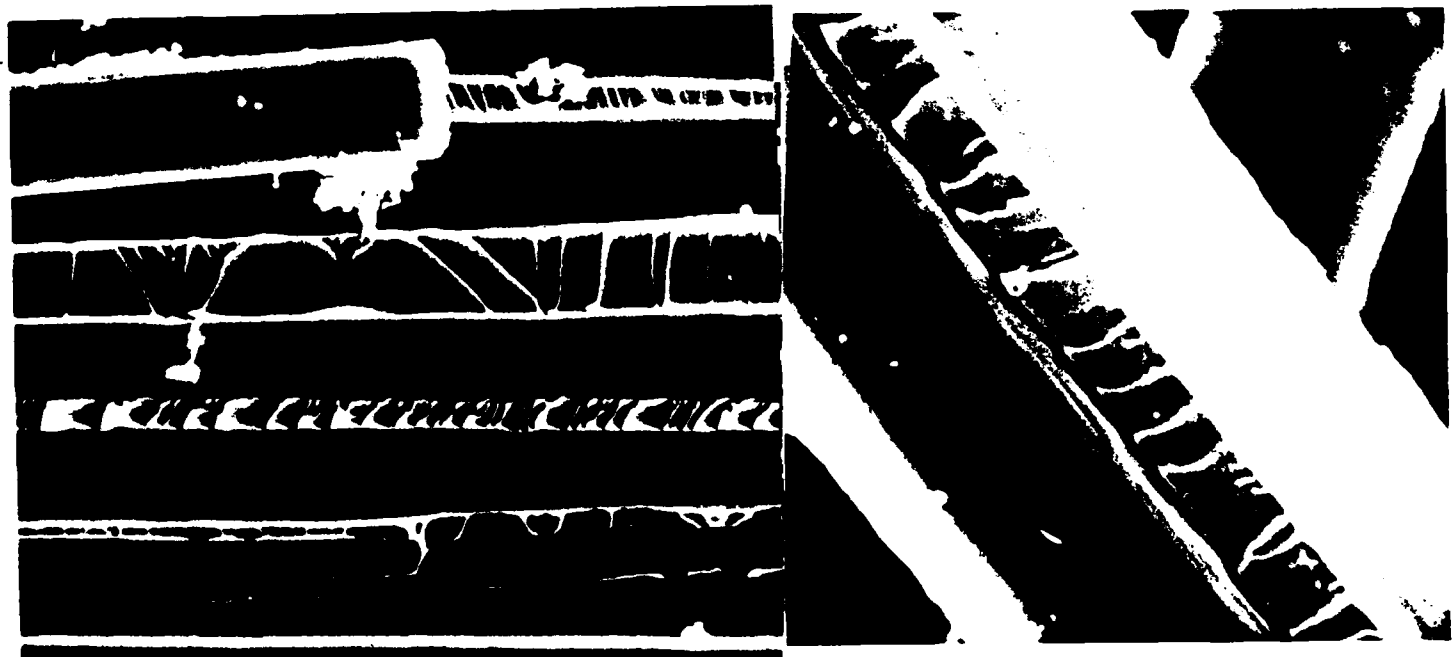


Figure 15. Mode I delamination of AS4/3502 specimens indicating a very brittle fracture. Consistent with the in-situ fractography, no resin deformation is noted and fiber debond is indicated. (left, 2000X; right, 4500X)

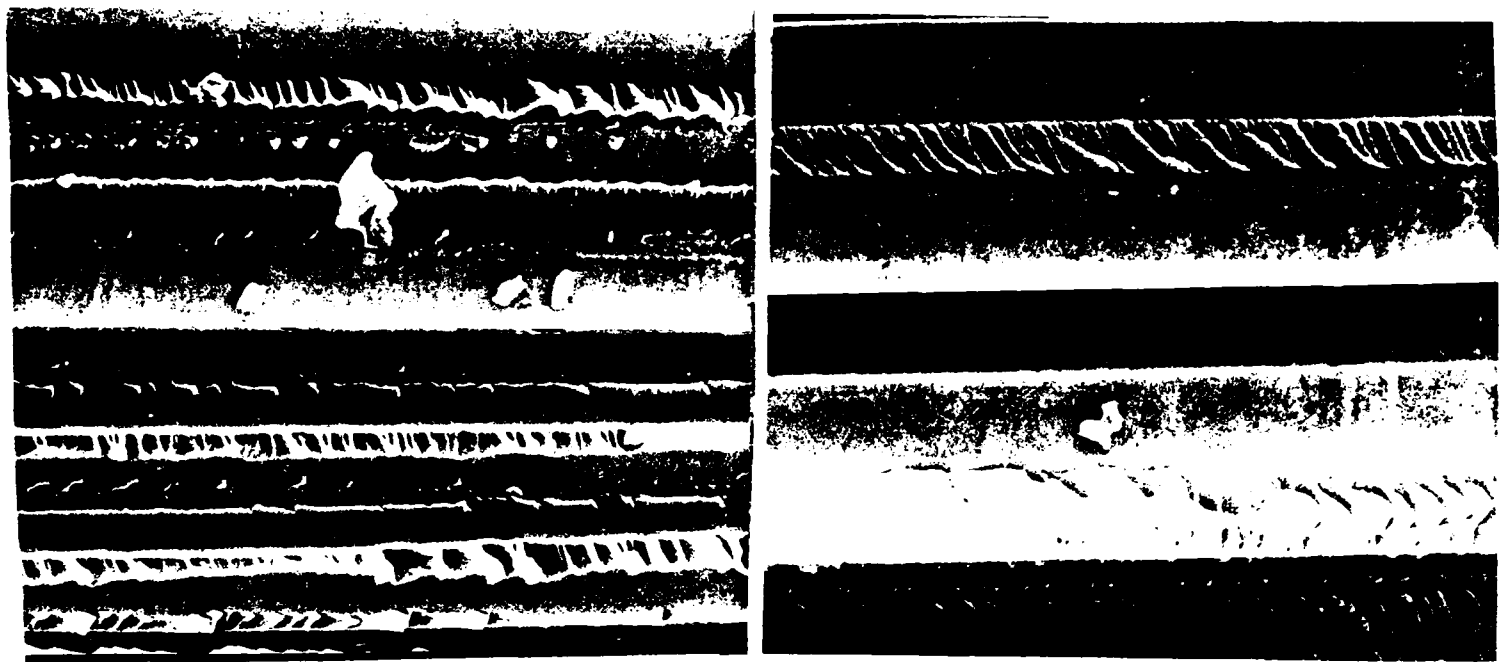


Figure 16. AS4/3502 photographed in SEM after mixed mode delamination fracture with $G_{II}/(G_I + G_{II}) = 0.39$. 2000X

EFFECTS OF CHAIN STIFFNESS IN A POLYSULFONE

by

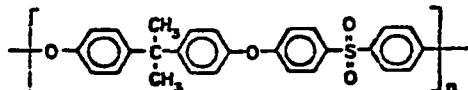
Joe S. Ham

Department of Physics

Texas A&M University, College Station, TX 77841

It is credible that short molecular chains between crosslinks in a tightly crosslinked thermosetting material will produce only a short elongation at break. However, whether longer chains between the crosslinks will permit greater elongation at break is not clear. In thermosets, as in elastomers, a greater length between crosslinks will possibly increase the elongation at break until entanglements replace the crosslinks as load bearing. Therefore, a study of entanglements in a polysulfone was part of an Air Force program to develop a family of acetylene-terminated sulfones. The polysulfone was selected to correspond to the molecular chain in the thermoset.

A sample of the commercial polyether, P-1800 Union



Carbide), was crudely fractionated into five fractions. Dilute and concentrated solution viscosities were measured in a series of capillary viscometers using standard methods. High temperature measurements in a Rheometric Mechanical Spectrometer, using parallel plate geometry and small strains, determined the melt viscosity.

The expression $[n] = 1.03 \times 10^{-3} M^{0.55}$ found by Allen and coworkers for this polysulfone in dimethylformamide solvent determined the molecular weights from the intrinsic viscosity. They used light scattering to standardize this expression. Lenner used osmotic measurements to standardize the expression $[n] = 1.22 \times 10^{-3} M^{0.55}$ in the same solvent. If the difference between the number and weight average molecular weights is considered, these expressions are consistent. Allen and coworkers found $M_w/M_n = 1.6$ for samples fractionated in a fashion similar to that used here. The molecular weights of the five fractions studied are shown in Table I. In addition, an unfractionated sample of low molecular weight is listed. The molecular weight listed for this sample should be considered only as indicative since it is beyond the calibration range of the equation.

Measurements of the real and imaginary parts of the complex modulus were made for each molecular weight sample over a temperature range from 280 to 380 °C. A master curve was obtained by standard shifting techniques. Measurements of fractions 3, 4 and 5 were in a spectral region where the imaginary part of the complex modulus was proportional to the frequency and the real part was proportional to the square of the frequency. This implies that the frequencies are low compared to the inverse relaxation times. Measurements at lower temperatures and thus at higher reduced frequencies involved stresses that were too large to be measured with our geometry and load cell.

Fraction 1 shows a clear deviation from the above frequency behavior in both the real and imaginary parts of the complex modulus, indicating that our range of measurements included some relaxation times in this fraction. Fraction 2 shows only a slight deviation from the frequency dependence of fractions 3, 4 and 5.

The melt viscosity involved no corrections to low frequencies in fractions 3, 4 and 5 and only a small correction in fraction 2. The melt viscosity is consistent with the often observed law $\eta = M^{3.5}$. Only fraction 1 deviated from this law with a larger viscosity due either to imprecise extrapolation to low frequencies or to the presence of a high molecular weight tail.

None of the fractions showed evidence of a viscosity

characteristic of the molecular weight range where entanglements are not important. Nor were measurements obtained that indicate a plateau region in the relaxation spectrum. Within a plateau region the steady state shear compliance determines a molecular weight between entanglements.

Ferry established that the entanglement length can be determined from the viscosity of concentrated solutions in samples that have a molecular weight larger than that between entanglements. Gressley has criticized this approach and he and others have proposed theoretical models.

According to Ferry, the critical concentration multiplied by the molecular weight should be a constant. In other words, each part of a chain can give rise to an entanglement so that the onset of entanglements occurs when the product of the contour length of the chain and the polymer concentration is a critical value. This implies $cM = \text{constant}$.

The viscosity of each fraction was measured at various concentrations. A change in the form of the concentration dependence occurred in the solutions between the concentration of 2 and 7 g/dl. To determine the concentration at which this change occurred, the logarithm of the viscosity was plotted against the logarithm of the concentration and shifted along the concentration axis until the curves for each molecular weight would fall upon the same master curve. The concentration at which the change in dependence occurred is listed in Table I.

Table I shows that cM is not a constant but $cM^{1/2}$ is much closer to a constant. If the volume occupied by the chains in a random walk conformation determine the critical concentration, then the total volume in the chains is proportional to $cM^{1/2}$. The low critical concentrations show that the chains entangle at a low polymer concentration.

Mills⁶ described the strong forces between the sulfone groups as a possible contribution to entanglements. This is separate from the entanglements of chains wrapped around their neighbors. However, little thermodynamic interaction seems to occur between the sulfone groups in solution. Allen found the exponents in the Mark-Houwink equation almost 0.50 for three solvents. Only in chloroform does the exponent (0.72) deviate appreciably from the theoretical 0.5. The values of the second virial coefficient estimated from the concentration dependence of the dilute solution viscosity indicate little nonideality in all of the solvents. In chloroform the Flory interaction parameter is 0.37 compared to the value of 0.5 under 0 conditions. Although these thermodynamic quantities are the result of an average over all the forces between the molecules and are the differences between the solvent-polymer and the polymer-polymer forces, they show nothing unusual in the forces between the chains in several different solvents. One would not expect strong forces to cancel out in such varied solvents. Therefore, the entanglements do not appear to be due to strong forces between the sulfone groups within the polymer.

Allen has shown conclusively that the polysulfone has a random walk conformation in dilute solution. He found from the measurements of the intrinsic viscosity and from calculations assuming reasonable bond lengths and angles that $\langle r^2 \rangle / M^{1/2} = 602 \pm 20 \times 10^{-11} \text{ cm}$. The rigid aromatic groups spread out the chain so it is unlikely to curl back upon itself, creating steric effects which limit bond angles. This produces a very low value of 2 for $C_e = \langle r^2 \rangle / M^{1/2}$.

Mills⁶ estimated from the steady state compliance the entanglement molecular weight in the melt to lie between 2500 and 5000. Other mechanical properties supported this short entanglement length. The compressive yield stress

reached a plateau value at relatively small molecular weights and the fracture toughness showed little molecular weight dependence with only the sample of molecular weight about 5000 showing an absence of plastic deformation. Bersted lists $M_w = 6300$ and Aharoni lists $N_c = 320$ which corresponds to $M_w^c = 8600$. These values are all high compared to the concentrated solution entanglements in this paper.

The ability of this polysulfone to entangle so readily is attributed to its stiffness. A chain may have a random walk conformation but if the rotation about the bonds is slow, it will then sluggishly change its shape. Two such chains will entangle more readily if each chain is so stiff that it cannot readily change its conformation. If a chain is completely stiff, it will entangle severely at a concentration where the chains first begin to overlap. In an undiluted polymer very little flow could occur.

Changes in conformation must occur in this polysulfone during viscous flow because the volume of the hydrodynamic spheres at the critical concentrations found in Table I show the molecules must overlap. In addition, the viscous flows in the undiluted state require changes in conformation. Yet, if these chains have some stiffness, they can entangle at low concentrations without equilibrium measurements showing strong interaction between the chains.

In contrast to this hypothesis of stiffness, Aharoni classifies polymers as flexible or rigid, using two parameters: the number of backbone chain atoms between entanglements (N_c) and C_m . The values of $N_c = 320$ and $C_m = 2$ definitely classifies polysulfone with the flexible polymers. Even though a much smaller value of N_c is predicted from entanglements in concentrated solution, he would continue to classify polysulfone as a flexible polymer since $N_c = 320$ is already high compared to his best correlation for flexible polymers of N_c versus C_m . A definite value for N_c is not deduced from the data in Table I since the solutions do not follow the dependence of $cM^2 = \text{constant}$.

The presence of sulfone groups in a polymer promotes a high glassy transition temperature. This high value can result from either strong forces between chains or from stiffness within a single chain so that any motion will require simultaneous movement of many atoms. If the strong intermolecular forces are excluded because of the small second virial coefficients in solution, then a stiffness of the chain could be the source of the high glassy transition temperature.

Inelastic scattering of light or neutrons should be capable of detecting stiffness within the chains. The dependence of viscosity upon shear rate should also depend upon this assumed stiffness, but the interpretation of such data is not as direct as for inelastic scattering.

Acknowledgements: Thanks are due Tim Heinricks for taking much of the data and to T. Helminiak, C. L. Fenner, and W. E. Jones for their advice and encouragement. The experimental data were collected during two summers at the Air Force Materials Laboratory-Wright-Patterson Air Force Base and the analysis was supported in part by grant F49620-82-C-0057 from the Air Force Office of Scientific Research to Texas A&M University.

REFERENCES

1. G. Allen, J. McAinsh, and C. Strazielle, *Europ. Polymer J.* 5, 319 (1969).
2. C. L. Fenner, unpublished results.
3. G. C. Berry and T. G. Fox, *Adv. Polymer Sci.* 5, 261 (1967).
4. W. W. Graessley, *Adv. Polymer Sci.* 16, 1 (1974); *Polymer* 21, 258 (1980); W. W. Graessley and S. F. Edwards, *Polymer* 22, 1329 (1981).

5. P. G. deGennes, *J. Chem. Phys.* 55, 572 (1971).
6. N. J. Mills, *Rheol. Acta* 13, 185 (1974).
7. B. H. Bersted, *J. Appl. Polymer Sci.* 24, 37 (1979).
8. S. H. Aharoni, *Polymer Preprints* 23, 273 (1982).

Table I

Fractions	$[\eta]$ in dl/gm.	M_w	c in gm/dl.	$cM^{1/2}$ $\times 10^{-2}$	cM $\times 10^{-5}$	η_{sp}
1	0.628	116,000	2.63	8.96	3.05	11.9
2	0.512	80,000	3.31	9.36	2.65	10.3
3	0.480	71,000	3.63	9.67	2.58	9.7
4	0.396	50,000	4.07	9.10	2.04	9.7*
5	0.24	20,000	6.91	9.77	1.38	
Low	0.15	8,600	10.7	9.92	0.92	

The viscosity is reduced to 138 °C. Sample 4 shifted differently from the higher molecular weight samples.

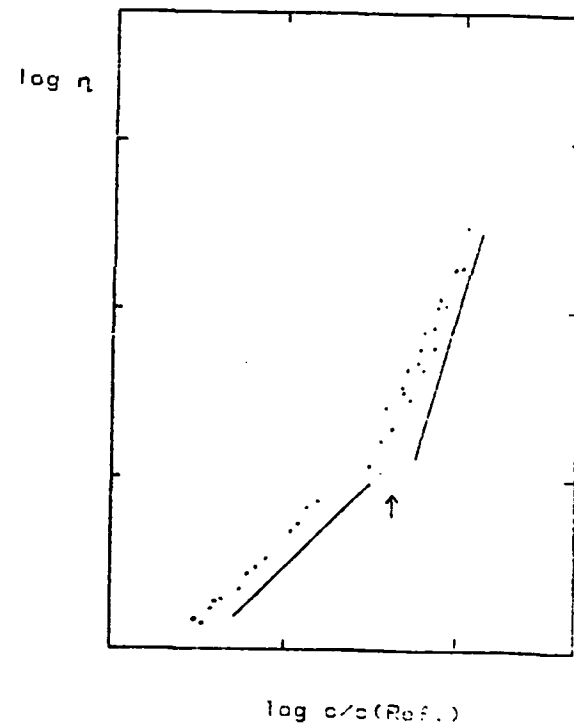


FIGURE 1. REDUCED VISCOSITY CURVES FOR DILUTE SOLUTIONS OF P-1000 IN THF. THE LINE WAS FITTED AND SHIFTED ONLY FROM THE LOWER TO THE HIGHER CONCENTRATION. THE LINES INDICATE SERIES OF 1 AND 3.

Heat Capacity of Water Absorbed in
Methylcellulose

D. A. Kinard and C. A. J. Hoeve, Department of Chemistry,
Texas A&M University, College Station, Texas 77843

Synopsis

The heat capacity of methylcellulose is determined at various water contents over a wide range of temperatures, down to 125K. From the data the partial specific heat capacity of water has been obtained. The results show that water should be considered as a single, mobile phase. No evidence exists for bound water. Near 130K water becomes immobilized in a glassy state.

Introduction

Mechanical properties of polymers are strongly affected by water absorption. Even small amounts of water can significantly change the modulus^{1,2} and crack propagation³ before rupture occurs. Often this large effect of water is surmised to be resulting from specific interactions with the polymer matrix. Usually diffusion of water through the matrix is exceedingly slow, giving rise to the suspicion that water may be bound to some of the polar groups. Furthermore, considerable amounts of water fail to freeze, even at liquid nitrogen temperatures, reenforcing the notion that this water is strongly bound. Wideline NMR results of hydrated proteins⁴⁻⁸ have indeed been interpreted on the basis of two fractions of water, one of which is bound and the other being liquidlike. Other than as a convenient assumption for interpretation of the NMR results, however, direct evidence for binding is lacking. *A priori* these assumptions are difficult to understand on the basis of the available forces. Hydrogen bonds between water and the matrix are prime candidates for strong forces. Surely in bulk liquid water strong hydrogen bonds occur; in this case, however, they are not strong enough to prevent rapid diffusion. It is then difficult to see why the hydrogen bonds between water and the matrix would lead to stronger binding.

A more direct way to study possible binding is to perform heat capacity measurements of water absorbed over a range of concentrations. If a small number of water molecules are so strongly bound as to become immobilized then the heat capacity should be close to that of ice, $0.5 \text{ cal deg}^{-1} \text{ g}^{-1}$. This value has indeed been found for several crystalline salt hydrates.⁹ Larger amounts of water, if unbound, should have a heat

capacity of twice this value, comparable to $1 \text{ cal deg}^{-1} \text{ g}^{-1}$ for liquid water. Thus if water is absorbed in excess of the bound fraction the heat capacity of water should increase significantly. On the basis of this analysis no evidence was found for bound water in the proteins collagen^{9,10} and elastin^{11,12} and in poly[2-(2-hydroxyethoxy)ethylmethacrylate].¹³

It is important to establish if this conclusion is generally valid and can be extended to other polymers. To this end we report the results for water absorbed in methylcellulose. This polymer is relatively simple in that it contains only hydroxyl groups as potential binding sites. Although cellulose is less suitable since its complex crystalline morphology might obstruct interpretation, methylcellulose is devoid of any crystallinity as shown by our heat capacity data. All measurements reported in this article were carried out in the glassy state of methylcellulose. Thus we know that the polymer matrix is amorphous and immobile.

Experimental

Methylcellulose (Methocel) was obtained from Dow Chemical Company. The number average molecular weight is given as 91,000. The degree of substitution of hydroxyl groups by methyl groups is between 1.8 and 2.2 (out of a maximum of 3). The average of two combustion analyses yielded carbon 50.8% and hydrogen 7.33% (the theoretical values for the degree of substitution 2 are 53 and 7, respectively). These samples were purified by extraction with water, as follows. Fifty times the amount of hot water was added to the polymer during stirring. After the powder was thoroughly wetted an equal amount of cold water was added and the mixture was stirred in an ice bath until the sample dissolved. This solution was then filtered through a sintered glass funnel and cast into plastic petri dishes. These films were then dried at 310K for two days and stored in desiccators.

For the heat capacity measurements 5 to 10 mg of sample was placed in small aluminum pans. After the sample was weighed on a microbalance a suitable amount of water was added with a microsyringe and an aluminum cover was placed on the pan and crimped tight. The amount of water was determined by another weighing. Additional weighings were performed before and after the heat capacity measurements to determine any leakage. If leaking had occurred the sample was discarded. To check the water contents after the measurement the pans were punctured, placed in the oven at 373K and weighed.

Heat capacity measurements were carried out with a Perkin-Elmer Differential Scanning Calorimeter DSC2. Measurements at low temperature were conducted using the cold finger immersed in liquid nitrogen. Heating rates were at 20K per minute. Temperature calibrations were performed

using the melting points of water (273K), mercury (234K), and methylcyclohexane (146K). Corrections were made for differences in aluminum pan weights.

Results and Discussion

The results of the heat capacity measurements are given in Fig. 1 for the temperatures 269, 226, 162, and 125 K. The heat capacity is expressed in cal K^{-1} for 1g of methylcellulose and yg of water. The horizontal axis y denotes the amount of water in g per g of methylcellulose. For each temperature the least-square linear line was drawn through the experimental points. As can be seen, within experimental error, the straight lines represent the data quite well. The plots are given in this somewhat unusual manner since the partial specific heat capacity of water (the partial molar heat capacity divided by the molecular weight of water) can be directly obtained from the slope of these lines. Table 1 gives the values of the slope, intercept and standard deviation of each line. Fig. 2 represents a plot of the partial specific heat capacity of water at different temperatures.

It is noteworthy (Fig. 1) that for each temperature the partial specific heat capacity of water is independent of its concentration between 0 and 30 percent based on the dry polymer weight. Since the value at 269 K, $1.2 \text{ cal K}^{-1} \text{ g}^{-1}$, is close to that of bulk water, no immobile water is present at this temperature. It should be noted that this value need not be exactly equal to 1.0, since the structure of these small amounts of water in the matrix is surely different from that of bulk water. The importance of the high value is that it is considerably above that for ice. We conclude that extensive hydrogen bond rearrangements occur with temperature, in contrast to the behavior expected for bound water. Although binding does not occur at 269 K, it is more likely to occur at lower temperatures. However, as shown in Fig. 1, at lower temperatures, even down to 125K no evidence exists for two fractions of water, since at all temperatures straight lines are obtained. The partial specific heat capacities of water are given in Table 1 and Fig. 2. It is to be noted that ice formation is ruled out, since our

heat capacity data would have revealed even traces of ice on heating the samples through 273K. Although no ice is formed, the partial specific heat capacity of water decreases gradually from the high value of 1.2 to the value of $0.205 \text{ cal K}^{-1} \text{ g}^{-1}$ at 125K, close to the value of ice at that temperature. We conclude that the low value results from the immobility of water molecules at 125K. Although at first glance unbound water is expected to freeze, in retrospect the failure to form ice is not surprising since the space available for water molecules in the rigid polymer matrix does not permit formation of large three-dimensional ice crystals. The alternative, diffusion of water molecules out of the sample, followed by ice formation, would rupture hydrogen bonds with the polymer matrix. Restoring hydrogen bonds between the hydroxyl groups of the matrix would be too slow in the glassy matrix. If water remains absorbed in the matrix, it can provide complete hydrogen binding by virtue of its mobility.

The low heat capacity of water at 125K can be interpreted to represent a glasslike structure of water. This proposal is consistent with the known glass transition of bulk water at 135K.¹⁴ We would expect the mobility of water absorbed in a glassy matrix to be less than in bulk. It is, therefore, surprising that the transition from glasslike water to a more mobile state does not occur at a considerably higher temperature in the matrix than in bulk. Apparently, the mobility of water is not seriously impaired by the glassy polymer matrix.

These results are similar to those observed for collagen^{9,10} and elastin^{11,12}. It is significant that the glassy state of water absorbed both in the proteins and in methylcellulose occurs in the same region. In view of the similar results obtained for dissimilar matrices, we conclude that contrary to widespread opinion, water appears not to be specifically bound to polymer matrices.

Acknowledgment

**This work was supported by the Air Force Office of Scientific Research,
number F49620-82-C-0057.**

References

1. H.W. Starkweather, Jr., "Water in Polymers", ACS Symposium Series 127, S.P. Rowland, Ed. American Chemical Society, Washington D.C., 1980, p. 433.
2. P. Moy and F.E. Karasz, *ibid.*, p. 505.
3. P.E. Bretz, R.W. Hertzberg, J.A. Manson, and A. Ramirez, *ibid.*, p. 531.
4. G.E. Chapman, K.A. McLauchlan, *Proc. Roy. Soc.*, B173, 223 (1969).
5. G.E. Chapman, S.S. Danyluk, and K.A. McLauchlan, *ibid.* B178, 465 (1971).
6. B.M. Fung and P. Trautmann, *Biopolymers*, 10, 391 (1971).
7. B.M. Fung and S.C. Wei, *ibid.* 12, 1053 (1973).
8. C. Migchelsen and H.J.C. Berendsen, *J. Chem. Phys.*, 59, 296 (1973).
9. C.A.J. Hoeve and S.R. Kakivaya, *J. Phys. Chem.*, 80 745 (1976).
10. C.A.J. Hoeve and A.S. Tata, *J. Phys. Chem.*, 82, 1660 (1978).
11. S.R. Kakivaya and C.A.J. Hoeve, *Proc. Nat'l. Acad. Sci., U.S.*, 72, 3505 (1975).
12. C.A.J. Hoeve, "Water in Polymers", ACS Symposium Series 127, S.P. Rowland, Ed. American Chemical Society, Washington D.C., 1980, p. 135.
13. J. Pouchlý, J. Biros and S. Beneš, *Makromol. Chem.*, 180, 745 (1979).
14. M. Sugisaki, H. Suga and S. Seki, *Bull. Chem. Soc. Japan*, 41, 2591 (1968).

Table I

Least-square lines for the heat capacity of methylcellulose with absorbed water

Temperature, K	Slope cal K ⁻¹ g ⁻¹	Intercept cal K ⁻¹ g ⁻¹	Standard deviation cal K ⁻¹ g ⁻¹
269	.1.20	.321	0.013
226	.81	.264	.011
162	.298	.216	.011
125	.205	.163	.005

Fig. 1. Heat capacity in cal K^{-1} for 1g of methylcellulose and $y\text{g}$ of water.
Squares: 269 K; open circles: 226 K; filled circles: 162 K; triangles:
125 K.

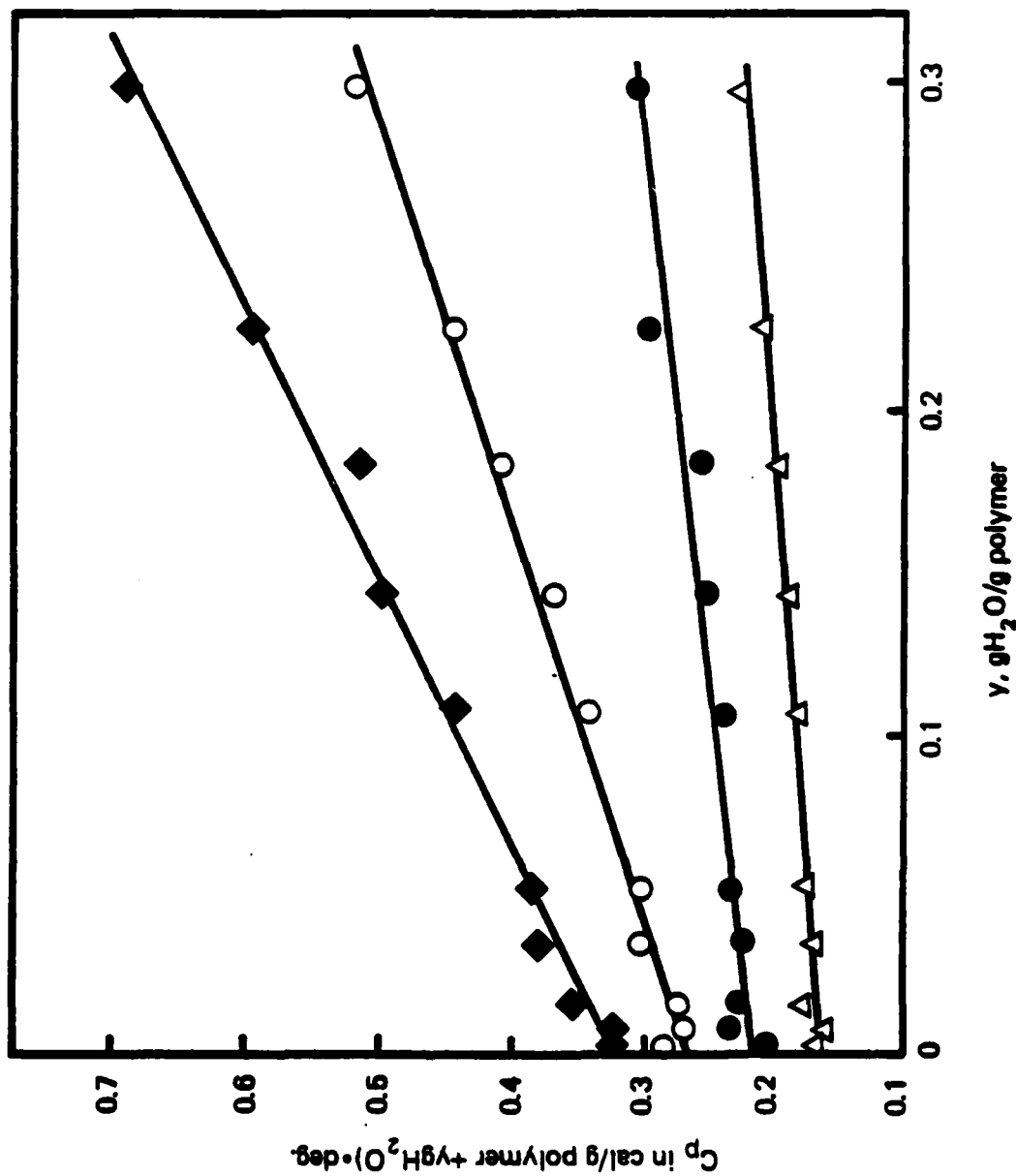
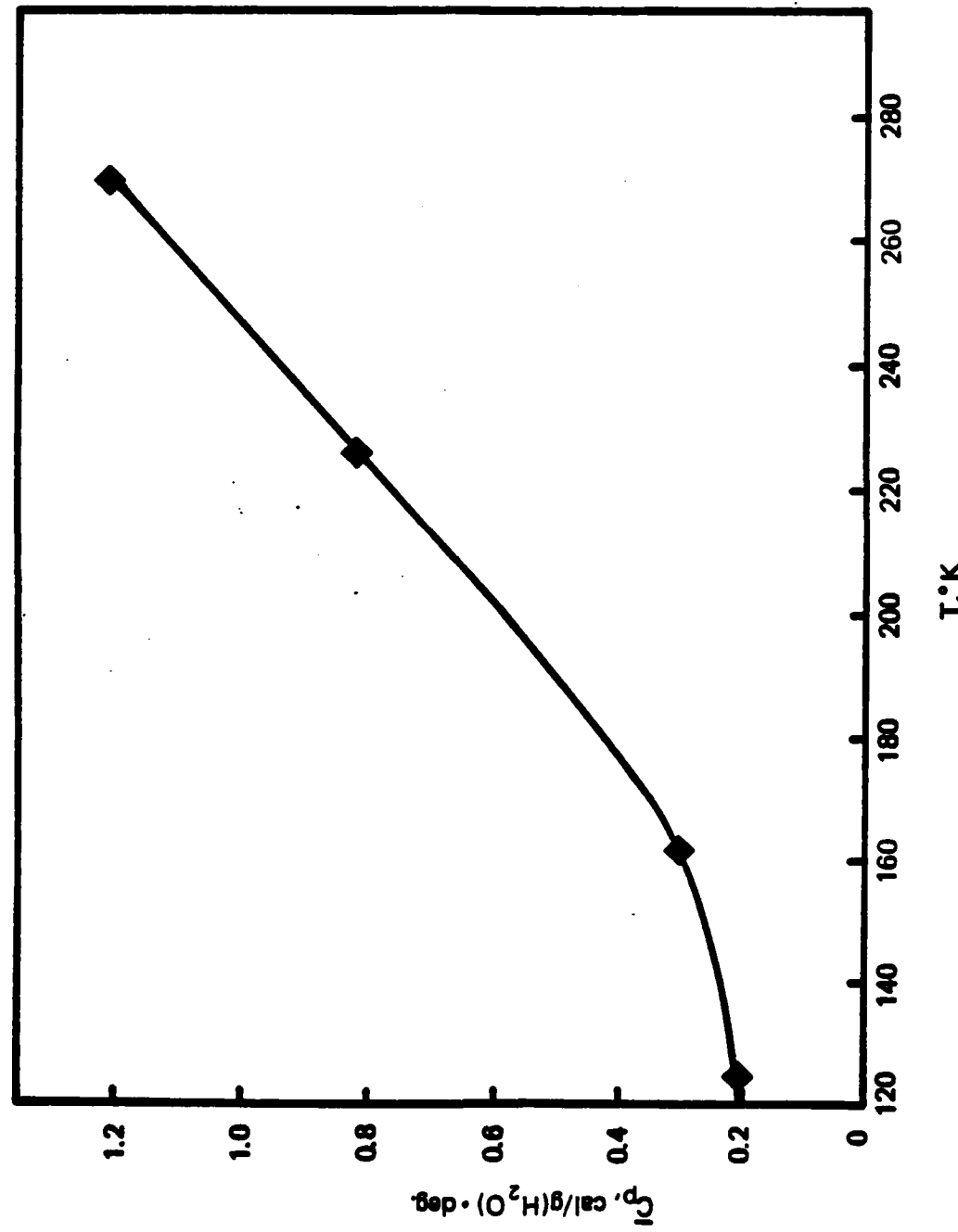


Fig. 2. Partial specific heat capacity in $\text{cal K}^{-1} \text{ g}^{-1}$ of water in methyl-cellulose.



CONTINUUM ASPECTS OF CRACK GROWTH IN
TIME DEPENDENT MATERIALS*

by

R.A. Schapery

Mechanics and Materials Center
Civil Engineering Department
Texas A&M University, College Station, TX 77843

ABSTRACT

The effect of time dependent rheological properties on crack growth in a class of nonlinear continua is studied. Starting with a single-integral, nonlinear viscoelastic constitutive equation for a monolithic or composite material, an elastic-viscoelastic correspondence principle is introduced, which leads to crack growth criteria expressed in terms of a generalized J integral. Rheological properties of the continuum are reflected in the value of the J integral and a creep compliance, both of which appear explicitly in the equations for time of initiation of growth and speed of continuous growth. Concluding discussions include comparison of the present results with some existing fracture models for materials which exhibit linear viscoelasticity or nonlinear transient and steady-state creep. A generalization of the theory to materials whose rheological properties account for certain types of distributed damage is given in the Appendix.

*Prepared for Encyclopedia of Materials Science and Engineering,
Pergamon Press.

1. INTRODUCTION

The growth of microcracks and macrocracks is affected by time-dependent material behavior, whether it is limited to the crack tip neighborhood or exists throughout the body. This article is concerned with specific ways in which rheological properties of continua affect both initiation and continuation of crack growth under quasi-static conditions (i.e. when inertia effects due to straining can be neglected). The highly damaged and failing material at the tip of growing cracks is not explicitly modelled; rather, emphasis is on the use of mechanics and properties of the surrounding continuum to predict local crack tip deformations and the mechanical work available for extending cracks.

Equations are developed which relate initiation time and instantaneous speed to a generalized J integral as the driving force for crack growth. This is done by combining methods and results from existing theories of crack growth in linear viscoelastic and nonlinear viscous media with a J integral theory previously developed for fracture initiation in nonlinear time-independent materials. The unified analytical framework is achieved by starting with a single-integral nonlinear viscoelastic constitutive equation to represent rheological behavior. A correspondence principle is then introduced which provides a simple relationship between the mechanical states of elastic and viscoelastic media. Deformation fields based on bounded rather than infinite strains at the crack tip are used in order to retain important local rheological effects. However, the analysis is simplified by using small strain theory for the continuum, while allowing for large strains in the failing material at crack tips. Certain generalizations, including large strain effects, are discussed in the Conclusions.

2. CONSTITUTIVE EQUATIONS

Outside of the highly damaged and failing material in the neighborhood of crack tips, the deformation behavior is assumed to be characterized by a nonlinear viscoelastic constitutive equation in the form of a single hereditary integral for the strains,

$$\epsilon_{ij}^e = E_R \int_0^t D(t - \tau, t) \frac{\partial \epsilon_{ij}^e}{\partial \tau} d\tau \quad (1)$$

The quantities ϵ_{ij}^e are second order tensor components which depend on material properties and, in general, are functions of stresses σ_{ij} , spacial coordinates x_i , and time t ,

$$\epsilon_{ij}^e = \epsilon_{ij}^e(\sigma_{kl}, x_m, t) \quad (2)$$

in which $\sigma_{kl} = \sigma_{kl}(x_i, t)$, with all indices taking the values 1, 2, 3. The coefficient E_R is a free constant which will be termed the reference modulus; it is helpful in discussing special material behavior and introducing dimensionless variables.

When ϵ_{ij}^e is used in Eqn. (1), the time argument is specified as the variable of integration; viz., t should be replaced by τ where explicitly shown in Eqn. (2) and in the argument of stress. Normally, to simplify notation, the arguments of stress and strain will not be written out unless required for clarity. For all cases it will be assumed that $\epsilon_{ij} = \epsilon_{ij}^e = \sigma_{ij} = 0$ when $t < 0$ and $D(t - \tau, t) = 0$ when $t < \tau$. In order to allow for the possibility of a discontinuous change in ϵ_{ij}^e with time at $t = 0$, the lower integration limit in Eqn. (1) and succeeding hereditary integrals should be interpreted as 0^- unless indicated otherwise.

The quantities ϵ_{ij}^e will be called pseudo strains. Their

explicit dependence on x_m in Eqn. (2) accounts when necessary for material nonhomogeneity, while t is introduced to allow for aging and time-dependent residual strains (such as those due to thermal expansion (Schapery, 1981)). The function $D(t - \tau, t)$ is a creep compliance; it provides creep under constant stress as well as other hereditary effects under time varying stress in both aging and non-aging materials. The significance of ϵ_{ij}^e and D will be brought out by considering some special cases.

First, however, it will be useful to rewrite Eqns. (1) and (2) by expressing stress in terms of strain history. Supposing that the inverses exist, Eqn. (2) becomes

$$\sigma_{ij} = \sigma_{ij}(\epsilon_{kl}^e, x_m, t) \quad (3)$$

where the ϵ_{ij}^e are related to the physical strains through the inverse of Eqn. (1),

$$\epsilon_{ij}^e = E_R^{-1} \int_0^t E(t - \tau, t) \frac{\partial \epsilon_{ij}}{\partial \tau} d\tau \quad (4)$$

in which E is a relaxation modulus; its relationship to D is given by

$$\int_{\tau_0^-}^t D(t - \tau, t) \frac{\partial}{\partial \tau} E(\tau - \tau_0, \tau) d\tau = H(t - \tau_0) \quad (5)$$

where $\tau_0 \geq 0$ and $H(t - \tau_0)$ is the Heaviside step function (i.e., $H(t - \tau_0) = 0$ and 1 for $t < \tau_0$ and for $t > \tau_0$, respectively).

A linear viscoelastic material without residual stresses which is isotropic, homogeneous, and has a constant Poisson's ratio ν , is characterized by Eqn. (1) if we use

$$\epsilon_{ij}^e = E_R^{-1} [(1+\nu)\sigma_{ij} - \nu\sigma_{kk}\delta_{ij}] \quad (6)$$

where δ_{ij} is the Kronecker delta, and the standard summation convention is followed in which repeated indices imply summation over their range. For a uniaxial stress state, $\sigma_{11} \neq 0$ and all other $\sigma_{ij} = 0$, Eqn. (1) for ϵ_{11} becomes

$$\epsilon_{11} = \int_0^t D(t - \tau, t) \frac{\partial \sigma_{11}}{\partial \tau} d\tau \quad (7)$$

If $\sigma_{11} = \sigma_0 H(\tau - t_0)$, where $t_0 \geq 0$ and σ_0 is constant, Eqn. (7) reduces to $\epsilon_{11} = D(t - t_0, t) \sigma_0$. Inasmuch as ϵ_{11}/σ_0 is customarily termed the creep compliance, we shall use this name for D throughout this article. Similarly, if $\epsilon_{11} = \epsilon_0 H(\tau - t_0)$ for a uniaxial stress state, where ϵ_0 is constant, one finds that the relaxation modulus, σ_{11}/ϵ_0 , is equal to $E(t - t_0, t)$. When the second argument in E and D in Eqns. (1) and (4) is dropped, so that $D(t - \tau)$ and $E(t - \tau)$ appear in Eqns. (1) and (4), respectively, linear viscoelastic behavior for a nonaging material is recovered.

The mechanisms which may require the aging form to be used for E and D (e.g. $D = D(t - \tau, t)$) are not limited to chemical processes. For example, this form accounts for the effect of transient temperatures on the creep compliance and relaxation modulus and includes the familiar thermorheologically simple behavior of polymers as a special case. It should be noted that the expression $D(t, \tau)$ is sometimes used instead of $D(t - \tau, t)$ in characterizing viscoelastic behavior of an aging material. Although both forms are equally general, the latter is used here as it is a more convenient notation in equations which govern crack growth.

Allowing now for nonlinear, anisotropic, and nonhomogeneous media, observe that for the special case of a constant relaxation

modulus, $E = E_R$, Eqn. (4) reduces to $\epsilon_{ij}^e = \epsilon_{ij}$. Thus, Eqn. (3) becomes the constitutive equation for an elastic material (in that the current stress state depends on the current strain state but not past values of strain). Obviously, an equivalent result is found by using $D = E_R^{-1}$ in Eqn. (1). Viscous behavior results by using $E = t_v E_R \delta(t - \tau)$ in Eqn. (4) (where $\delta(t - \tau)$ is the Dirac delta function and t_v is a time constant), or by setting $D = (t_v E_R)^{-1}(t - \tau)$ in Eqn. (1). In this case the pseudo strains are found to be proportional to the strain rates, i.e. $\epsilon_{ij}^e = t_v \partial \epsilon_{ij} / \partial t$, and thus the current stress state becomes a function of the current strain rates; Eqn. (1) takes this form after integrating it by parts and then differentiating and inverting the result.

Hereditary integrals will be used throughout this article, and consequently it is desirable to introduce an abbreviated notation for them. Specifically, for any function f of time,

$$\{Ddf\} \equiv E_R \int_0^t D(t-\tau, t) \frac{\partial f}{\partial \tau} d\tau, \quad \{Edf\} \equiv E_R^{-1} \int_0^t E(t-\tau, t) \frac{\partial f}{\partial \tau} d\tau \quad (8)$$

Thus, Eqns. (1) and (4) are, respectively,

$$\epsilon_{ij} = \{Dd\epsilon_{ij}^e\}, \quad \epsilon_{ij}^e = \{Ed\epsilon_{ij}\} \quad (9)$$

3. CORRESPONDENCE PRINCIPLE

The close relation between mechanical states of nonlinear elastic and viscoelastic media with stationary or growing cracks will be given in this section. It will be stated in the form of a so-called correspondence principle, and will serve as the basis for the development of crack growth theory. First, let us introduce a reference elastic solution $\sigma_{ij}^R, \epsilon_{ij}^R, u_i^R$ corresponding to the case

in which $D^{-1} = E = E_R$. This solution is defined to satisfy the field equations,

$$\frac{\partial \sigma_{ij}^R}{\partial x_j} = 0 \quad (10)$$

$$\epsilon_{ij}^R = \frac{1}{2} \left(\frac{\partial u_i^R}{\partial x_j} + \frac{\partial u_j^R}{\partial x_i} \right) \quad (11)$$

$$\epsilon_{ij}^R = \epsilon_{ij}^e (\sigma_{kl}^R, x_m, t) \quad (12)$$

The following correspondence principle will be proved, in which the instantaneous geometry (including cracks) is the same for both elastic and viscoelastic problems:

Let surface tractions $T_i = \sigma_{ij} n_j$ be specified functions of time and position (which vanish when $t < 0$) on all surfaces S and throughout the volume V , respectively. Then the nonlinear viscoelastic solution based on Eqn. (1) is

$$\sigma_{ij} = \sigma_{ij}^R, \quad \epsilon_{ij} = \{D \epsilon_{ij}^R\}, \quad u_i = \{D u_i^R\} \quad (13)$$

where the variables with superscript R are defined to satisfy Eqns. (10)-(12) and the traction boundary condition $T_i = \sigma_{ij}^R n_j$ on all surfaces.

As proof, first observe that the viscoelastic stresses in Eqn. (13) meet the condition $T_i = \sigma_{ij} n_j$ on S (which includes the instantaneous crack faces) and satisfy equilibrium Eqn. (10). The pseudo strains ϵ_{ij}^R obey Eqn. (11) (compatibility conditions), and clearly the viscoelastic strains in Eqn. (13) satisfy the same equations without the superscript R (since D is independent of x_i and the hereditary integral is a linear operator). Thus, except for

consideration of displacements due to crack growth, the proposed viscoelastic solution is seen to meet compatibility requirements. With or without crack growth, relative displacement between crack faces, Δu_i , is the difference of the displacements in Eqn. (13) evaluated on adjacent faces,

$$\Delta u_i = \{Dd\Delta u_i^R\}, \quad (14)$$

where Δu_i^R is the displacement difference in the reference elastic problem. Since we specify the instantaneous geometry of all cracks in the reference problem to be the same as in the actual viscoelastic body, Δu_i is correctly predicted to vanish until the time t_c , say, a crack tip reaches any given physical location; this follows from the fact that $\Delta u_i^R = 0$ at this same location when $t < t_c$ (assuming prior cracking and rejoining of crack faces has not occurred) which in turn implies the hereditary integral in Eqn. (14) vanishes when $t < t_c$.

The correspondence principle may be generalized to allow for specification of displacements U_i on some or all surfaces (Schapery 1981). In this case, the specified surface displacements in the elastic problem are $U_i^R = \{Edu_i\}$ and, as in Eqn. (13), elastic and viscoelastic stresses throughout the continuum are equal with stationary and growing cracks.

4. GENERALIZED J INTEGRAL AND THE CRACK TIP MODEL

The widely used J integral for fracture analysis of time independent materials will be generalized in this section for subsequent use with the nonlinear viscoelastic materials described by Eqn. (1). In the elastic problem the important path-independence

of the J integral follows from the thermodynamically-based result that a potential W exists with the property that $\sigma_{ij} = \partial W / \partial \epsilon_{ij}^e$. The classical deformation theory of plasticity for loading of metals may be expressed in terms of a potential analogous to the strain energy density W , and therefore the J integral is often useful even if large scale plastic deformation exists as long as there is not significant unloading from the plastic state. Without excluding unloading, equations for crack growth in nonlinear viscoelastic media may be developed and expressed in terms of a J integral in many cases if σ_{ij} in Eqn. (3) can be written as

$$\sigma_{ij} = \partial \Phi / \partial \epsilon_{ij}^e \quad (15)$$

It has been shown that the potential Φ exists for materials under general loading histories if they are at least elastic at short times under sudden straining (Schapery, 1981). For linear viscous media one may invoke Onsager's principle to establish Eqn. (15). Although thermodynamic arguments apparently cannot be used to justify Eqn. (15) for nonlinear viscous behavior, the standard equations used for secondary creep of metals may be written in this form (e.g. Leckie and Hayhurst 1974). In analogy with elasticity theory, Φ is called the pseudo strain energy density.

Before developing a fracture theory which uses Eqn. (15), certain simplifications concerning the crack tip will be introduced. The idealized crack tip geometry and a local orthogonal set of Cartesian axes (x_i) are shown in Fig. 1. In the unstrained state the crack surfaces in the neighborhood of the tip are assumed to be planar and to coincide with the local $x_1 - x_3$ plane, where x_3 is

perpendicular to the plane of the page; the x_2 axis is embedded in the continuum at any convenient horizontal location. The crack tip or edge is a straight or curved line in space whose intersection with the plane of the page (the $x_1 - x_2$ plane) is indicated by the point P. It is assumed the tip is essentially straight and parallel to x_3 in the neighborhood of P. (By definition, the neighborhood of P refers here to the material contained in a sphere which is centered at P and has a radius on the order of ten times the failure zone length α .)

The region designated as the failure zone in Fig. 1 is where intense damage and material separation occurs. Outside of this zone it is assumed that Eqn. (15) applies. We prefer to use this term over other common names, such as process zone and damage zone, because the material outside may be damaged and the effects taken into account in more general theories. Also, for analysis purposes it is more convenient to define P as the crack tip location, instead of the left end of the failure zone. The latter position is called the apparent crack tip.

Consider now the line integral,

$$\mathcal{L} \equiv \oint (\phi dx_2 - T_i \frac{\partial u_i}{\partial x_1} ds) \quad (16)$$

where the path of integration is in the $x_1 - x_2$ plane and is any closed contour on and inside of which ϕ exists and which does not enclose cracks; one such path is that designated as C_T in Fig. 1. This integral vanishes if i) $\partial u_i / \partial x_3 = 0$ and ii) $\partial \phi / \partial x_1 = \partial \phi / \partial x_3 = 0$ on and inside C_T . The first condition implies the depth of the body in the x_3 direction near the tip must be large compared to α (the

usual case) or else much smaller than α . According to the second condition, the most general admissible form of Φ is $\Phi = \Phi(\epsilon_{ij}^e, x_2, t)$; dependence of ϵ_{ij}^e on x_1 is permitted, but any material nonhomogeneity is restricted to variations normal to the local crack plane. Note that $\mathcal{L} = 0$ follows directly from elasticity theory for the continuum within the contour C_T (Rice 1968) since \mathcal{L} is expressed in terms of mechanical state variables for the reference elastic problem and the potential Φ is defined by Eqn. (15); recall that $\sigma_{ij}^R = \sigma_{ij}$ and $\epsilon_{ij}^R = \epsilon_{ij}^e$ according to the correspondence principle.

A generalized J integral, denoted by J_v , is now introduced,

$$J_v = \int_{C_1} (\Phi dx_2 - T_i \frac{\partial u_i^R}{\partial x_1} ds) \quad (17)$$

where C_1 is the portion of C_T indicated in Fig. 1; integration starts at point 1 and is taken counterclockwise to point 2. In contrast to the early elastic theory (Rice 1968), we do not assume the crack faces are traction-free, and thus that part of C_1 which is adjacent to the surfaces is retained. (A later study by Palmer and Rice (1973) included body forces and crack surface tractions in analyzing slip surfaces in clay without time dependence.) The condition $\mathcal{L} = 0$ may be written as

$$J_v = J_f \quad (18)$$

where

$$J_f = \int_{C_2} (\Phi dx_2 - T_i \frac{\partial u_i^R}{\partial x_1} ds) \quad (19)$$

and integration starts at point 1 and proceeds counterclockwise along the edge of the failure zone to point 2. The path C_1 for J_v is arbitrary except that it starts and ends at the apparent crack tip (points 1 and 2). It is not necessary to use a contour having

segments parallel to the crack faces; but if the tractions T_i vanish on such segments to the left of the failure zone, there is no contribution to J_V (since $dx_2 = T_i = 0$) and therefore C_1 could start and end anywhere along the lower and upper crack faces.

Equation (18) provides a basic relationship between the mechanical state of the continuum through J_V and the characteristics of the failing material at the crack tip through J_f . Given that real stresses and strains (including those at P) are not infinite, in many cases one can neglect the contribution to J_f from ϕdx_2 and assume the tractions T_i are equal (with opposite signs) across the upper and lower parts of C_2 ; such simplicity obviously exists if the failure zone is thin (in the x_2 direction) relative to a . Then, Eqn. (19) becomes

$$J_f = \int_0^a (\tau_{f1} \frac{\partial \Delta u_1^R}{\partial \xi} + \sigma_f \frac{\partial \Delta u_2^R}{\partial \xi} + \tau_{f3} \frac{\partial \Delta u_3^R}{\partial \xi}) d\xi \quad (20)$$

where σ_f is the normal stress and τ_{f1} and τ_{f3} are the shearing stresses in the x_1 and x_3 directions, respectively, along the interface between the failure zone and continuum; the Δu_i^R are the components of the relative displacement vector between initially adjacent material points on the crack plane. The normal stress and displacement and the local coordinate $\xi = a - x_1$ are indicated in Fig. 2.

5. CRACK GROWTH

Essential features of criteria for predicting the time at which crack growth initiates, t_i , and subsequent crack propagation speed \dot{a} , will be illustrated by assuming a slender failure zone (cf. Eqn. (20)) and the opening mode of crack tip displacement. In this case, shearing stresses and sliding displacements along the crack plane are zero in the neighborhood of the tip.

Initiation of Growth

In order to avoid excessive mathematical complexity in predicting t_i , the failure stress distribution σ_f will be assumed independent of ξ , and denoted by σ_m . Equation (20) becomes $J_f = \sigma_m \Delta u_{2\alpha}^R$, where $\Delta u_{2\alpha}^R$ is the elastic opening displacement at $\xi = \alpha$. Using $J_v = J_f$, the displacement is $\Delta u_{2\alpha}^R = J_v / \sigma_m$, and the correspondence principle, Eqn. (13), yields the time-dependent displacement,

$$\Delta u_{2\alpha} = \{Dd(J_v / \sigma_m)\} \quad (21)$$

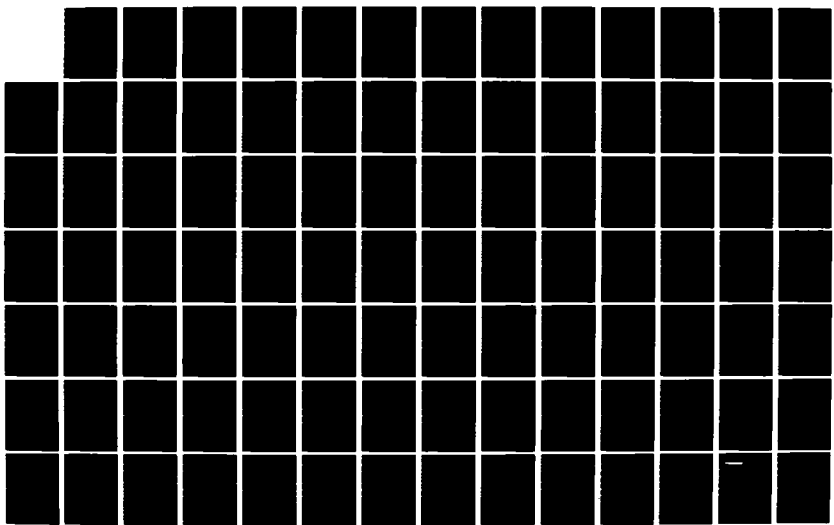
where σ_m is not necessarily constant in time. If the criterion for initiation is based on a critical value of opening displacement, Δu_c , one would determine the time for which $\Delta u_{2\alpha}$ in Eqn. (21) is equal to Δu_c . An alternative, commonly used criterion is based on mechanical work,

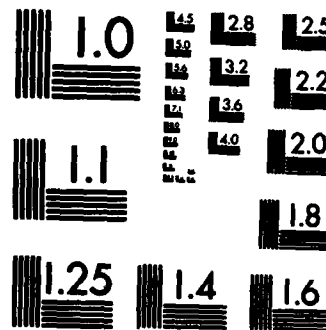
$$\int_0^{t_i} \sigma_{f\alpha} \frac{\partial \Delta u_{2\alpha}}{\partial t} dt = 2\Gamma_i \quad (22)$$

where Γ_i is the mechanical work per unit surface area required to break a fixed material column at the left end of the failure zone, $\xi = \alpha$; the factor of 2 is used to account for the two units of surface formed for each unit of cross sectional area of the column. The so-called fracture initiation energy, Γ_i , may be affected by the history of $\Delta u_{2\alpha}$, depending on the characteristics of the failure zone. For the case in which $\sigma_f = \sigma_m$, Eqn. (22) becomes

$$\int_0^{t_i} \sigma_m \{Dd(J_v / \sigma_m)\} / \partial t dt = 2\Gamma_i \quad (23)$$

AD-A134 059 RESEARCH ON COMPOSITE MATERIALS FOR STRUCTURAL DESIGN 2/3
(U) TEXAS A AND M UNIV COLLEGE STATION MECHANICS AND
MATERIALS RE. D ALLEN ET AL. APR 83 MM-4665-83-4
UNCLASSIFIED AFOSR-TR-83-0861 F49620-82-C-0057 F/G 11/9 NL





MICROCOPY RESOLUTION TEST CHART
NATIONAL BUREAU OF STANDARDS-1963-A

If σ_m is independent of time and the explicit representation for the hereditary integral is used (cf. Eqn. (8)), the criterion becomes

$$E_R \int_0^{t_i} D(t_i - \tau, t_i) \frac{dJ_v}{d\tau} d\tau = 2r_i \quad (24)$$

For an elastic continuum, $D = E_R^{-1}$, the criterion reduces to $J_v = 2r_i$; the failure zone may be viscoelastic, and therefore $2r_i$ is not necessarily constant. If the continuum is a linear or non-linear viscous material, $D = (t_v E_R)^{-1}(t - \tau)$ where t_v is a time constant, as noted previously. After integrating Eqn. (24) by parts it becomes

$$\frac{1}{t_v} \int_0^{t_i} J_v dt = 2r_i \quad (25)$$

Finally, it should be observed that the failure zone length α has not been assumed small in deriving Eqns. (21)-(25).

Propagation Speed

The failure criterion based on mechanical work may be written in the form

$$\int_0^\alpha \sigma_f \frac{\partial \Delta u_2}{\partial \xi} d\xi = 2r \quad (26)$$

where the fracture energy r , just as r_i , is the work required to rupture a fixed column of material in the failure zone. In contrast to the initiation problem, this column is not initially at the apparent (free surface) crack tip; instead, the column is initially within or ahead of the current failure zone, and its rupture is coincident with the arrival of the apparent tip. The left side of Eqn. (26) is the total work input to the column, starting with the time the tip P (cf. Fig. 1) first arrives. For convenience in analyzing continuous growth, the variable of integration has been changed from

t (cf. Eqn. (22)) to ξ , where $\xi = a - x_1$, and the differentiation and integration in Eqn. (26) are made with x_1 held constant. The time-dependent opening displacement at any point in the failure zone is $\Delta u_2 = \{Dd\Delta u_2^R\}$, which is to be substituted into Eqn. (26). The result is rather complex, as it requires two integrations and prediction of the elastic displacement Δu_2^R . Also, σ_f may be dependent on Δu_2 .

The problem can be greatly simplified if i) α is small enough that the neighborhood of the crack tip (say 10α) is free of other features involving characteristic dimensions (e.g. another crack tip), ii) σ_f , \dot{a} , and α are essentially constant in time during the time interval α/\dot{a} when the crack propagates a distance α , and iii) aging changes in the creep compliance during this same interval are negligible. With these conditions and the observation that the relation between Δu_2 and Δu_2^R is the same as for a linear viscoelastic material, an approximate evaluation of the hereditary integral may be employed (Schapery 1975 II) to find

$$\Delta u_2 = E_R D(\tilde{t}, t) \Delta u_2^R \quad (27)$$

where $\tilde{t} \equiv k\xi/\dot{a}$ and k is a factor which is a very weak function of the slope $n \equiv \partial \log D / \partial \log \tilde{t}$; this factor is practically 1/3 for the entire range of slopes ($0 \leq n \leq 1$) encountered in practice, and stems from the cusp-shaped opening displacement predicted for linear materials. Assuming the strains are continuous at the tip P, the local deformations will be close to those for a linear prestressed body (Brockway and Schapery 1978). Thus, although more careful study of this behavior is needed for highly nonlinear materials, the cusp

shape is expected to exist in many cases, permitting the use of $k = 1/3$. Substituting Eqn. (27) into Eqn. (26) and using the same type of approximation as in the linear theory (Schapery 1975 II), which does not require σ_f to be spacewise uniform, there results

$$E_R D(k\alpha/\dot{a}, t) \int_0^\alpha \sigma_f \frac{\partial \Delta u_2^R}{\partial \xi} d\xi = 2\Gamma \quad (28)$$

In view of Eqns. (18) and (20), the integral in Eqn. (28) may be replaced by J_V to derive the very simple result

$$E_R D(k\alpha/\dot{a}, t) J_V = 2\Gamma \quad (29)$$

The integration and differentiation in Eqn. (28) is for x_1 fixed, while that in Eqn. (20) is for t fixed (i.e., fixed crack tip location); however, as $\Delta u_2^R = \Delta u_2^R(\xi)$ for the steady-state propagation assumed during the time α/\dot{a} , these integrals are equal. Recall also that t in the second argument of D accounts for aging in the creep compliance, and the aging is assumed small during the time interval α/\dot{a} . In spite of the assumed constancy of \dot{a} and aging during α/\dot{a} , they may vary appreciably during the total time of crack propagation. Likewise, the size α is not necessarily constant, as it is related to other variables, such as J_V , through Eqn. (18); its prediction is illustrated in Sect. 6 for a nonlinear power law material.

The similarity of the formulas for initiation, Eqn. (24), and continuous growth, Eqn. (29), is noteworthy. As a special case, suppose J_V is constant for $t > 0$. Then Eqn. (24) reduces to

$$E_R D(t_i, t_i) J_V = 2\Gamma_i \quad (30)$$

This result and Eqn. (29) yield $t_i = k\alpha/\dot{a}$ if $\Gamma = \Gamma_i$. Thus, with

$k = 1/3$, the time required for initiation is only one-third of that required for subsequent growth of an amount α . On this basis, it can be expected in some problems that t_i will be negligible compared to the total time required for failure of a structure.

Whether or not Γ equals Γ_i depends on the hereditary and multi-axial stress characteristics of the failure zone, the physical environment (since the left edge, $\xi = \alpha$, is at the surface during $0 < t < t_i$) and on the state of the initial crack tip. In any event, one should not assume these energies are equal without adequate support from experimental data.

Energy Release Rate

The J_V integral is equal to the energy release rate for self-similar crack growth in the reference elastic problem, which is useful for experimental and theoretical determination of J_V . Namely,

$$J_V = -\partial P^R / \partial A \quad (31)$$

where dP^R is the change in potential energy of the reference elastic continuum and applied forces; dA is the increase in crack-plane area. This relationship can be derived by considering the work done by a general three-dimensional elastic continuum on a failure zone of width $x_3 \gg \alpha$ which is advanced an amount da without change; such self-similar growth does not have to exist during actual fracture tests for Eqn. (31) to apply if the length α is very small.

6. POWER LAW NONLINEARITY

Specific effects of nonlinearity on the opening mode of crack growth will be illustrated using a power law nonlinear material. By definition, the pseudo strain energy density for isotropic or anisotropic materials is a homogeneous function of degree $N+1$,

$$\phi(c\epsilon_{ij}^e) = |c|^{N+1} \phi(\epsilon_{ij}^e) \quad (32)$$

where N and c are constants and $|\cdot|$ denotes absolute value. For notational simplicity, the superscripts " e " and " R " will be omitted in succeeding equations until specific results are applied to viscoelastic crack growth analysis. With the definitions,

$$\epsilon_{ij}' \equiv c\epsilon_{ij}, \quad \phi' \equiv \phi(\epsilon_{ij}'), \quad \text{sgn}(c) \equiv \text{sign of } c \quad (33)$$

it follows that

$$\frac{\partial \phi'}{\partial \epsilon_{ij}'} = \text{sgn}(c)|c|^N \frac{\partial \phi}{\partial \epsilon_{ij}}, \quad \sigma_{ij}' = \text{sgn}(c)|c|^N \sigma_{ij} \quad (34)$$

For a uniaxial stress or strain state these relations imply $\sigma_{11} \sim \text{sgn}(\epsilon_{11})|\epsilon_{11}|^N$. Equation (32) contains as a special case the power law strain energy function commonly used for isotropic elastic materials (Rice and Rosengren 1968).

Let us introduce a set of dimensionless coordinates and mechanical state variables,

$$\hat{x}_i \equiv x_i/\alpha, \quad \hat{\sigma}_{ij} \equiv \sigma_{ij}/\sigma_m, \quad (35)$$

$$\hat{\epsilon}_{ij} = \text{sgn}(\sigma_m)|\sigma_0/\sigma_m|^{1/N} \epsilon_{ij}, \quad \hat{u}_i \equiv \text{sgn}(\sigma_m)|\sigma_0/\sigma_m|^{1/N} u_i/\alpha$$

The quantities σ_m and σ_0 are parameters with dimensions of stress, which are introduced for the purpose of using a dimensionless failure stress distribution f and strain energy density ϕ_N ,

$$f \equiv \sigma_f/\sigma_m, \quad \phi_N \equiv \phi/\sigma_0 \quad (36)$$

When these definitions are substituted into Eqns. (10), (11), and (15)

the field equations become

$$\frac{\partial \hat{\sigma}_{ij}}{\partial \hat{x}_j} = 0, \quad \hat{\epsilon}_{ij} = \frac{1}{2} \left(\frac{\partial \hat{u}_i}{\partial \hat{x}_j} + \frac{\partial \hat{u}_j}{\partial \hat{x}_i} \right), \quad \hat{\sigma}_{ij} = \frac{\partial \hat{\phi}_N}{\partial \hat{\epsilon}_{ij}} \quad (37)$$

where $\hat{\phi}_N \equiv \phi_N(\hat{\epsilon}_{ij})$. Observe that allowance is made for negative values of σ_f through the factor σ_m ; for unloading of a viscoelastic material this stress could be negative in limited periods of time without crack face contact.

Locate the origin of the coordinates at the crack tip P ($a = 0$ in Fig. 2), and assume the crack faces are traction free outside of the failure zone. Then, with the additional definition $n \equiv \xi/a = -\hat{x}_1$, the solutions to Eqn. (37) must satisfy the traction boundary condition $\hat{\sigma}_{22} = f(n)H(1-n)$ for $n > 0$ as well as meet the symmetry conditions associated with the opening mode. These solutions will depend at most on the dimensionless coordinates \hat{x}_i , apart from parameters in ϕ_N and those arising from conditions that would be applied on the continuum surrounding the failure zone. For example, the solution for dimensionless crack opening displacement is simply $\Delta\hat{u}_2 = g(n)$, where $n = -\hat{x}_1$. From Eqn. (35),

$$\Delta u_2 = \text{sgn}(\sigma_m) \alpha |\sigma_m/\sigma_o|^{1/N} g(n) \quad (38)$$

Equations (18), (20), (35), and (38) yield

$$\alpha = \left| \frac{\sigma_o}{\sigma_m} \right|^{1/N} \frac{J_v}{|\sigma_m I_f|} \quad \text{where} \quad I_f = \int_0^1 f(n) \frac{dg}{dn} dn \quad (39)$$

From Eqns. (38) and (39),

$$\Delta u_2 = (J_v/\sigma_m I_f) g(n) \quad (40)$$

The results in Eqns. (38)-(40) are not limited to a small-scale failure zone and are valid for materials which are and are physically nonhomogeneous with respect to x_2 ; dependence of ϕ on x_2 and t and related material parameters has been suppressed to simplify the notation. The dimensionless displacement g and stress f in Eqn. (38) and the integral I_f in Eqn. (39) could in general depend on all dimensionless parameters associated with phenomena that influence continuum deformation in the neighborhood of the crack tip. Considerable simplification in this dependency results if the continuum is physically homogeneous (at least locally) and if α is small enough that the failure zone is isolated from other geometrical features. The immediate continuum surrounding the crack tip neighborhood can then be analyzed by using a method similar to that in Rice and Rosengren (1968) for an isotropic power law material. With a polar coordinate system (r, θ) centered at P (cf. Fig. 2) it is found that for $r \gg \alpha$,

$$\hat{u}_i = \hat{r}(I_f/\hat{r})^{1/(N+1)}h_i(\theta), \quad \hat{\epsilon}_{ij} = (I_f/\hat{r})^{1/(N+1)}f_{ij}(\theta)$$

$$\hat{\sigma}_{ij} = (I_f/\hat{r})^{N/(N+1)}g_{ij}(\theta) \quad (41)$$

where $\hat{r} = r/\alpha$. The integral I_f is related to J_V through Eqn. (39), and the functions of θ are determined from the solution of Eqn. (37) and the condition of traction-free crack surfaces for $\hat{r} > 0$. The failure zone traction on the crack plane is neglected in solving this boundary-value problem; its effect enters the solution in the form of I_f after path-independence of J_V is taken into account through Eqn. (18). The dependence of Eqn. (41) solutions on r is the same as

found by Rice and Rosengren (1968), but the θ -dependence is not necessarily the same because the strain energy density used here is more general. Such detailed information is not needed for our purposes. Rather, it is sufficient to know that the entire influence of external loads and other far-field parameters and geometry (such as other cracks) on the dimensionless mechanical state variables in Eqn. (35) is accounted for by I_f .

For the small-scale failure zone, given the shape-function $f(n)$ of the failure stress distribution, we conclude that the predicted shape-function $g(n)$ of the crack-opening displacement can depend at most on I_f and parameters which enter ϕ_N (other than $\hat{\epsilon}_{ij}$) such as N . The integral in Eqn. (39) is thus an implicit relationship for predicting I_f . Its significance may be clarified by imagining the problem in which f is the only applied loading is solved first, not using Eqn. (39). External loading is then increased from zero by means of I_f in Eqn. (41) until infinite stresses and strains at P are removed. For the linear problem, $N=1$, it can be verified that the removal occurs when I_f is equal to the integral in Eqn. (39); this result becomes identical to a dimensionless form of the Barenblatt (1962) condition for finite crack tip stress after a familiar relationship, based on Eqn. (31) for the far field,

$$J_v = (1 - v^2) K_I^2 / E_R \quad (42)$$

is employed (where K_I is the opening-mode stress intensity factor, E_R is Young's modulus, and v is Poisson's ratio). Recall that Eqn. (39) comes from Eqns. (18) and (19) (through the special case Eqn. (20)) in which the portion of the contour C_2 around the tip P

vanishes on account of the physical requirement of finite stresses and strains. Thus, it appears that Eqns. (18) and (19), with the contour around P omitted, can be interpreted as a generalization of Barenblatt's condition to nonlinear, anisotropic, viscoelastic media with an arbitrarily large failure zone. For such a general situation, these equations may not assure that the crack faces do not overlap, and thus additional analysis involving contact phenomena could be needed.

Crack Growth

The analysis in Sect. 6 so far has been limited to a study of the reference elastic problem. With the addition of the superscript "R" to strains and displacements, we may use them with the results in Sect. 5. Recall that Eqns. (23) and (24) for fracture initiation were derived assuming σ_f does not vary with ξ , represented here by $f=1$ since $\sigma_m = \sigma_f$. In this case the criteria for initiation time t_i are very simple, and are not limited to a small-scale failure zone; indeed, there is no need to use the results for a power-law material. However, if $df/dn \neq 0$ one could predict t_i by using the original criterion, Eqn. (22), after substituting Eqn. (40) and the relation between pseudoelastic and viscoelastic displacements (with $g(1) \equiv g_1$),

$$\Delta u_{2\alpha}^R = J_v g_1 / \sigma_m I_f, \quad \Delta u_{2\alpha} = \{ Dd \Delta u_{2\alpha}^R \} \quad (43)$$

and recognizing that σ_m can be defined as σ_f at $\xi = \alpha$ without loss of generality of the analysis. Observe that if g_1/I_f is constant, the resulting criterion becomes identical to Eqn. (23) except r_i is modified by the factor I_f/g_1 .

Equation (29) for crack speed depends on the size of the failure

zone α . This size, assumed small, is related to J_V by Eqns. (18) and (20), and for the power law material α is given by Eqn. (39). Let us consider the physical significance of this result. First, we observe that the parameter σ_0 may be interpreted as a yield stress for the continuum when N is small. Namely, using $\Phi = \sigma_0 \Phi_N$ together with Eqn. (32) and one-dimensional or proportional loading through a stress σ , one finds $\epsilon \sim |\sigma/\sigma_0|^{1/N}$; hence, the strain is small when $\sigma < \sigma_0$ and large when $\sigma > \sigma_0$ if $N \ll 1$. Also, σ_m may be considered the intrinsic strength if it is taken to be the maximum value (with respect to location ξ) of the failure zone stress. Thus, the size α , Eqn. (39), increases with increasing yield stress and is sensitive to the ratio of yield stress-to-intrinsic strength, given J_V . In elasto-plastic fracture mechanics it is common practice to assume σ_m is the yield stress and $f=1$; in this case, the standard result $\alpha \sim J_V/\sigma_0$ is recovered since I_f is a constant.

The results so far have been expressed in terms of material functions for the failure zone, σ_f and r . These quantities may depend on \dot{a} , α and other variables such as temperature and moisture, especially if the zone is viscoelastic. One could explicitly incorporate specific physical models of the failure zone in order to complete the formulation of the theory. If we assume the failure process for material elements on the crack plane is unaffected by stresses prior to the arrival or near arrival of the crack tip, such an analysis for a small-scale failure zone would yield a function $\dot{a} = \dot{a}(J_V)$, with possible dependence on physical parameters and material constants such as temperature, age, nonlinear exponent N , etc; that the instantaneous J_V (but not past values) determines the

instantaneous \dot{a} follows from the fact that the crack tip neighborhood is surrounded by a stress field which is defined solely by the current value of J_V (i.e., Eqn. (41) in terms of the dimensional physical variables). Thus, when the dependence of \dot{a} on basic material parameters is not of direct interest, for many cases one could characterize fracture behavior with the function $\dot{a} = \dot{a}(J_V)$ found directly from experimental data. If theoretical investigations indicate a range exists for which $d\dot{a}/dJ_V < 0$, unstable crack growth (possibly in steps of stop-start behavior) may result and the intrinsic $\dot{a} - J_V$ function for slow, continuous growth could not be found experimentally. Indeed, for this case a more appropriate analysis may involve initiation and dynamic arrest phenomena.

Power Law Viscoelasticity

The creep compliance for viscoelastic materials can often be expressed as a power law in time. Thus, as an important special case, let us consider nonaging material behavior for which $D(t - \tau) = D_1(t - \tau)^n$ (where D_1 and n are positive constants) in order to predict the form of the equation $\dot{a} = \dot{a}(J_V)$ using certain specified failure zone characteristics. A small-scale failure zone with a shape factor, $f \equiv \sigma_f/\sigma_m$, that depends at most on $n = \xi/\alpha$ is assumed. In general, σ_m and Γ may depend on crack speed. If, however, σ_m and Γ are constant (so that this zone exhibits elastic-like behavior) Eqns. (29) and (39) yield

$$\dot{a} \sim J_V^p \quad (44)$$

where $p = 1 + (1/n)$. If Γ and α (instead of σ_m) are constant, Eqn. (29) predicts $p = 1/n$. The failure zone dimensions are defined by α and crack opening displacement Δu_2 at $\xi = \alpha$; if these two quantities

are constant, one may use Eqn. (27) for Δu_2 and Eqn. (38) for Δu_2^R at $n \equiv \xi/\alpha = 1$ to find that $p = [n(1+N)]^{-1}$. Notice that only in this last case does the nonlinearity exponent appear in the equation for p .

Experimentally determined values of p , when compared with the results for these and other cases, may be helpful in determining failure-zone characteristics and guiding theoretical model development. The values of $p = 3$ and $n = 0.5$ were obtained from experimental data on a globally linear elastomer; this is consistent with the assumption of constant Γ and σ_m (Schapery 1975 III). Some studies of crack growth in metals undergoing secondary creep, $n = 1$, provide values of $p \approx 1$ (Landes and Begley 1976, Nikbin et al. 1976); inasmuch as $N \ll 1$ typically, the data are consistent with the last two cases for constant values of Γ and α or $\Delta u_{2\alpha}$ and α . It should be added that the exponent N used here pertains to nonlinear behavior of the continuum in the neighborhood of the crack tip. The relationships are valid even if nonlinearity of material far from the tip (relative to α) does not obey a power law, or is linear ($N = 1$) while its local behavior is described using $N \neq 1$. The effect of the remote nonlinear behavior does not enter the $\dot{a} - J_V$ equation, but it does affect the functional dependence of J_V on the externally applied loads.

7. CONCLUSIONS

Through the use of a nonlinear single-integral constitutive equation, generalized J integral theory, and certain approximations, it has been possible to derive relatively simple crack growth equations (based on mechanical work) for time of initiation, Eqn. (24),

and speed, Eqn. (29). Only the opening mode of growth has been analyzed in detail; but the basic relationships in Sects. 2-4 could be used for shearing and mixed-mode conditions. All rheological properties of the continuum are reflected in the creep compliance D and the generalized integral J_v . The length α of the zone of failing material at the crack tip appears in the equation for speed; it provides a scale which determines, in effect, the magnitude of local strain rates resulting from crack growth. In general α is not constant; instead, it is related to J_v through Eqns. (18) and (20), which reduce to Eqn. (39) with power law nonlinearity.

All of these results come from an analysis of the continuum in the vicinity of the crack tip and its wake. Thus, for limited crack growth it is not necessary for the entire body to be represented by Eqn. (1) and the local creep compliance D . However, if it is, Eqn. (31) may be employed to predict J_v with an arbitrary amount of crack growth by using theoretical and experimental methods similar to those already developed for time-independent materials. In this expression P^R and J_v are defined just as for elastic materials, but displacements and strains are pseudo quantities $u_i^R = \{Edu_i\}$ and $\epsilon_{ij}^R = \epsilon_{ij}^e = \{Ede_{ij}\}$, respectively. Stresses and loads are the actual physical quantities. For example, experimentally measured displacements u_i would be converted to pseudo displacements u_i^R through Eqn. (8) before evaluating J_v from test data. The coefficient E_R is a free constant, and could be taken as the modulus or reciprocal of compliance at some specified time.

The Bibliography includes publications which describe various models for characterizing and predicting crack growth in different

types of materials. Several models are special cases of the theory presented here. For secondary creep (i.e. nonlinear viscous behavior), experimental data on crack speed have been successfully correlated in terms of a C^* parameter by many investigators (e.g. Landes and Begley 1976); the function $\dot{a} = \dot{a}(C^*)$ typically obeys a power law. This characterization is obtained from the present theory by using the relaxation modulus $E = E_R^\delta(t - \tau)$ in Eqn. (8) which reduces the pseudo variables to strain rates ($\dot{\epsilon}_{ij}^R = \dot{\epsilon}_{ij}$) and velocities ($\dot{u}_i^R = \dot{u}_i$); in turn, J_V becomes identical to C^* . The use here of non-singular strains at the crack tip, in contrast to earlier work on secondary creep, leads to a simple physical interpretation of J_V for viscous media. Specifically, from Eqn. (29) with $k = 1/3$ and $D = E_R^{-1}(t - \tau)$, corresponding to the aforesaid modulus, we find $J_V = 3(2\Gamma\dot{a}/\alpha) = 3 \times$ (average mechanical power input to the failure zone). For viscoelastic materials, J_V has a simple physical meaning if the continuum is essentially elastic except for a small amount of material around the crack tip. In this case J_V is approximately the energy release rate, $-\partial P/\partial A$, since $u_i^R \approx u_i$; also, $\Gamma/E_R D$ in Eqn. (29) may be properly called an effective fracture energy.

Crack growth in homogeneous linear viscoelastic media has been characterized traditionally in terms of stress intensity factors because of the many situations in which viscoelastic stresses are the same as in elastic materials. With isotropy, linearity, a constant Poisson's ratio, homogeneity, and locally plane strain, Eqn. (31) yields Eqn. (42). Substitution of Eqn. (42) into Eqns. (24) and (29) results in the same crack growth relations derived earlier (Schapery 1975). Similar results in terms of stress intensity factors for linear behavior exist without the restrictions of constant Poisson's ratio,

isotropy, and homogeneity (Brockway and Schapery 1978, Schapery 1975, 1978). This observation includes cracks between dissimilar media (i.e. adhesive fracture) if both materials are incompressible or one is rigid and the other is incompressible; without the incompressible behavior, tensile and shearing stresses act simultaneously on the crack plane, and a complex mixed-mode condition generally exists at the crack tip. The nonlinear theory in Sect. 5 is applicable to adhesive fracture if the mixed-mode state does not exist and D is the same for both materials (or one is relatively rigid); Γ_i and Γ in Eqns. (24) and (29) obviously have to be interpreted as the fracture energies for the particular material combinations involved.

Primary creep of metals and ceramics is customarily represented by using a nonlinear power law model of viscous flow with strain hardening. When crack growth exists this behavior is not described by Eqn. (1), and the correspondence principle, Eqn. (13), does not apply. However, with proportional loading and a stationary crack the constitutive equation becomes identical to that of a nonlinear, aging elastic body (e.g. Riedel 1981). Equation (1) takes the appropriate form by using $E_R D = h(t)$. A suitable choice of $h(t)$ and a power law potential $\Phi(\epsilon_{ij}^e)$, where the only time dependence is through $\epsilon_{ij}^e = \epsilon_{ij}/h$, yields the desired primary creep behavior as well as a singular stress field parameter C_h^* (Riedel 1981) which is identical to J_V . For a small scale failure zone, the early stages of crack growth are determined by the stress field surrounding a stationary crack tip and therefore by J_V . However, a theory does not appear to be available for characterizing crack speed, whether continuous or discontinuous, when the amount of growth becomes comparable to the scale

of the initial singular stress field.

It should be observed that a different type of primary creep, such as that used to characterize polymers, is contained in Eqn. (1) through the dependence of creep compliance D on $t - \tau$. Also, through the use of aging time in $\phi = \phi(\epsilon_{ij}^e, t)$, one may characterize different types of nonlinear behavior at short and long times even though the creep compliance itself is not a function of stress. Thus, in spite of the apparent simplicity of Eqn. (1) compared to other available nonlinear viscoelastic constitutive equations, it is really quite general and yet permits the use of the correspondence principle with large amounts of crack growth. Nevertheless, the accuracy of Eqn. (1) for different types of materials under various stress histories is not yet established.

The deformation and fracture analysis has been formulated using small-strain theory for the continuum. This restriction is needed because the correspondence principle is not rigorously valid with nonlinear strain-displacement relations. If large strains exist only where behavior is essentially elastic or at least if the quasi-elastic approximation is applicable, $\epsilon_{ij}^R \approx E_R^{-1} E(t, t) \epsilon_{ij}$ (which is often true for nondecreasing strains) the present theory is approximately correct. For example, the current practice of expressing crack speed in rubber at large strains using a function $\dot{a} = \dot{a}(-\partial P/\partial A)$ is consistent with the present theory since $J_y = -\partial P/\partial A$ for globally elastic behavior. Another possible complication not explicitly treated here is crack tip heating, which can be very significant in polymers because of their typically low thermal conductivity and high ultimate strains. If this heating is sufficiently localized, it could be included in the characteristics of the failure zone, and thus not complicate the

continuum analysis.

The idealization of a slender failure zone is quite realistic for crack tips in many materials, as well as for craze tips in plastics. Even without this slenderness, the form of the crack growth equations may not be different, but this has not been investigated. In considering the zone size, it should be recalled that only the part of the body which does not obey Eqn. (15) has to be included in the failure zone. In some cases it is helpful to represent part of the failing material (such as craze) as a surface loading, consequently accounting for it in J_V . Furthermore, it is shown in the Appendix that important aspects of the theory remain valid even if there is distributed damage, such as microcracks in the neighborhood of a much larger crack.

Considerable progress has been achieved in the last ten to twenty years in understanding effects of time dependent rheological properties on crack growth. However, most basic experimental and theoretical investigations have been for the opening mode of cohesive fracture in essentially homogeneous materials. In this same time period, use of fiber-reinforced materials, especially plastics, in load bearing structures has increased dramatically. Thus, considering the complex interactions which may occur at various scales and the importance of interfaces in fibrous lamina and laminates and in other multi-phase materials, there is an especially important need for more basic studies on mixed mode crack growth, adhesive cracking, and the effect of non-homogeneous time-dependent properties on all types of crack growth.

Acknowledgment

This work was sponsored by the U.S. Air Force Office of Scientific Research, Office of Aerospace Research.

BIBLIOGRAPHY

Andrews E H 1974 A generalized theory of fracture mechanics J. Mater. Sci. 9: 887-94

Barenblatt G I 1962 The mathematical theory of equilibrium cracks in brittle fracture. In: Advances in Applied Mechanics, Vol. VII. Academic Press, New York, pp 55-129

Brockway G S, Schapery R A 1978 Some viscoelastic crack growth relations for orthotropic and restrained media. Eng. Fracture Mechanics 10: 453-68

Christensen R M 1982 Theory of Viscoelasticity, An Introduction. Second Ed. Academic Press, New York.

Evans A G 1982 The high temperature failure of ceramics. In: Wilshire B, Owen D R J (eds.) Recent Advances in Creep and Fracture of Engineering Materials and Structures Pineridge Press, Swansea, pp. 53-133

Findley W N 1981 Creep of 2618 aluminum under side-steps of tension and torsion and stress reversal predicted by a viscous-viscoelastic model. J. Appl. Mech. 48: 47-54

Greenwood J A, Johnson K L 1981 The mechanics of adhesion of viscoelastic solids. Philos. Mag. A 43: 697-711

Kaminskii A A 1980 Investigations in the field of the mechanics of the fracture of viscoelastic bodies. Prikladnaya Mekhanika 16: 3-26 (English translation 1981, Plenum)

Kinloch A J 1980 Micromechanisms of crack extension in polymers. Metal Sci.: 305-18

Landes J D, Begley J A 1976 A fracture mechanics approach to creep crack growth. In: Mechanics of Crack Growth, ASTM STP 590. American Society for Testing and Materials, New York, pp. 128-148

Leckie F A, Hayhurst D R 1974 Creep rupture of structures. Proc. R. Soc. London, Ser. A 340: 323-47

McClintock F A, Bassani J L 1981 Problems in environmentally-affected creep crack growth. In: Nemat-Nasser S (ed.) Three-Dimensional Constitutive Relations and Ductile Fracture North-Holland, pp. 123-145

Morland L W, Spring U 1982 Single integral representations for non-linear viscoelastic solids. Mechanics of Materials 1: 161-170

Nikbin K M, Webster G A, Turner C E 1976 Relevance of nonlinear fracture mechanics to creep cracking. In: Cracks and Fracture, ASTM STP 601. American Society for Testing and Materials, New York, pp. 47-62

Palmer A C, Rice J R 1973 The growth of slip surfaces in the progressive failure of over-consolidated clay. Proc. R. Soc. London, Ser. A 332: 527-48

Passaglia E 1982 Relaxation of stresses in crazes at crack tips and rate of craze extension. Polymer 23: 754-60

Ponter A R S, Hayhurst D R (Eds.) 1981 Creep in Structures. Springer-Verlag, Berlin

Rice J R 1968 A path independent integral and the approximate analysis of strain concentration by notches and cracks. J. Appl. Mech. 35: 379-86

Rice J R, Rosengren G F 1968 Plane strain deformation near a crack tip in a power law hardening material. J. Mech. Phys. Solids 16: 1-12

Riedel H 1981 Creep deformation at crack tips in elastic-viscoplastic solids. J. Mech. Phys. Solids 29: 35-49

Schapery R A 1975 A theory of crack initiation and growth in visco-elastic media. Int. J. Fracture 11: Part I, Theoretical development pp. 141-59; Part II, Approximate methods of analysis pp. 369-88; Part III, Analysis of continuous growth pp. 549-62

Schapery R A 1978 A method for predicting crack growth in nonhomogeneous viscoelastic media. Int. J. Fracture 14: 293-309

Schapery R A 1981 On viscoelastic deformation and failure behavior of composite materials with distributed flaws. In: Wang S S, Renton W J (eds.) 1981 Advances in Aerospace Structures and Materials The American Society of Mechanical Engineers, New York, pp. 5-20

Shield R T 1977 Conservation Laws in Finite Elasticity. In: Rivlin R S (ed.) Finite Elasticity The American Society of Mechanical Engineers, New York, pp. 1-10

Taira S, Ohtani R, Komatsu T 1979 Application of J-integral to high-temperature crack propagation, Part II - Fatigue crack propagation. J. Eng. Mat. Techn. Trans ASME 101: 162-67

APPENDIX

The J_V Integral with Time Varying Distributed Damage

Consider the one dimensional stress-strain behavior illustrated in Fig. 3. The material is loaded to the strain ϵ_m and then unloaded. The curve for unloading may differ from that for loading because of the viscoelastic and aging effects already discussed and/or micro-structural changes. Depending on the material, these changes may consist of microcracking, dislocation density increases, hole growth, breaking of entanglement points along chains in polymers, etc. There is no need in the present analysis to identify the particular physical mechanisms involved, and therefore we shall use the term damage in accounting for them in a continuum model (whether or not they are beneficial or deleterious to structural performance). It will be assumed the form of Eqn. (1) is the same with damage, where only the material function Eqn. (2) or, equivalently, Eqn. (3), is affected by damage; this has been shown for microcracking (Schapery 1981). Additionally, to simplify the discussion, aging effects in the $\sigma - \epsilon^e$ relationship will be omitted. Thus, if the abscissa in Fig. 3 is pseudo strain ϵ^e instead of strain ϵ , the difference between loading and unloading curves is due entirely to damage. Although it is not necessary to assume the damage increases during loading and is otherwise constant, it may be helpful to think in these terms.

Throughout this Appendix, the superscripts R and e which identify pseudo variables will be omitted for notational simplicity; but it should be understood that the mechanical state variables are those for the reference elastic problem. (The correspondence principle, Eqn. (13), is applicable if the elastic problem includes the effect of

damage.) First, it will be argued that the potential ϕ in Eqn. (15) exists with realistic types of damage. Then, the validity of the fracture theory in Sects. 4 and 5 will be demonstrated. It is physically reasonable to assume a potential ϕ^C exists with constant damage. Examples are an elastic material with a fixed microcrack state (in the absence of significant interfacial frictional losses) and a ductile metal with constant plastic strain during unloading. For reasons to be given, the potential for a three-dimensional state of strain with constant damage is taken in the form

$$\phi^C = \phi_0(\epsilon_i) + \sum_{\alpha=1}^M \phi_\alpha [D_\alpha(\epsilon_i), D_{\alpha M}] \quad (45)$$

where $\phi_0, \phi_1, \dots \phi_M$ are continuous functions of strains ϵ_i ($i = 1, 2, \dots 6$); single index notation is used for convenience. With exception of ϕ_0 , the strains enter through functions of strain D_α (assumed continuous); as a special case, D_α may be the strain ϵ_α or a strain invariant. By definition, quantities $D_{\alpha M}$ (which will be called damage parameters) are constant during a constant damage process; for this case Eqns. (15) and (45) yield

$$\sigma_i = \frac{\partial \phi_0}{\partial \epsilon_i} + \sum_{\alpha=1}^M \frac{\partial \phi_\alpha}{\partial D_\alpha} \frac{\partial D_\alpha}{\partial \epsilon_i} \quad (46)$$

In the context of Eqn. (45), a damaging process is defined temporarily to be one in which $D_{\alpha M} = D_\alpha$ for all of these parameters. (Observe that this condition is analogous to $\epsilon_m = \epsilon$ on the loading curve in Fig. 3, where ϵ_m is the current maximum strain.) Suppose now that a material element undergoes a damaging process for the time period $t_1 < t < t_2$, and that all damage is constant for $t_2 \leq t < t_3$. Because the damage is

constant at $t = t_2$, Eqn. (46) applies. Assuming the stresses vary continuously with strains at all times including $t = t_2$, where t_2 is an arbitrarily selected time, Eqn. (46) also serves to define the stresses during the damaging process. (Referring to Fig. 3, this is simply the statement that a point on the loading curve is also the first point on an unloading curve.) A potential $\phi^D = \phi^D(\epsilon_i)$ exists during the damaging process, where

$$\sigma_i = \partial\phi^D / \partial\epsilon_i \quad (47)$$

if and only if

$$\partial\sigma_i / \partial\epsilon_j = \partial\sigma_j / \partial\epsilon_i \quad (48)$$

The variation of D_{am} with strain is to be considered in using Eqn. (48) and when integrating Eqn. (47) to obtain ϕ^D . We find that Eqn. (48) is indeed satisfied without imposing any further restrictions; however, it is also found that if at least one of the functions ϕ_α were to depend on more than one damage parameter (in a non-additive form), Eqn. (48) would not generally hold. In order to define fully the stresses by Eqn. (15), we assume $\phi = \phi^C$ when the damage is constant, $\phi = \phi^D$ otherwise, and $\phi = \phi^C = \phi^D$ at the transition $t = t_2$.

Not only does the particular form of Eqn. (45) guarantee the existence of ϕ^D , it appears to be general enough to account for some real damage processes. As one example, it is well-known that the deformation theory of isotropic metal plasticity may be written in the form of Eqn. (47). Given ϕ^D , one may construct a potential ϕ^C for linear elastic unloading, which is found to have the form of Eqn. (45); here, ϕ_0 contains the dilatational component of strain energy density. Another example is a special case of the constitutive theory with microcracking (Schapery 1981). The potentials are

$$\phi^D = \int_0^{D_{1m}} \psi(D_1) dD_1, \quad \phi^C = \psi(D_{1m})(D_1 - D_{1m}) + \phi^D \quad (49)$$

Without damage, $\psi = 1$ and $D_1 = D_1(\epsilon_i)$ is the pseudo strain energy density; D_{1m} is the maximum value of D_1 with respect to the entire straining history. The function $\psi = \psi(D_1)$ represents the direct softening effect of microcracks. The stress with constant or varying damage is

$$\sigma_i = \psi(D_{1m}) \frac{\partial D_1}{\partial \epsilon_i} \quad (50)$$

This result may be easily extended to allow for more general forms of damage parameters, such as a Lebesgue norm of D_1 (Schapery 1981) instead of the maximum value. In this case, approximate representations of ϕ^C and ϕ^D appear as potentials for an aging elastic material with damage; the strength of the time dependence decreases with increasing order of the norm.

The next question concerns the vanishing of the line integral \mathcal{L} , Eqn. (16). From the analysis of Rice (1968, Eqn. (3)), $\mathcal{L} = 0$ if

$$\int_A \left(\frac{\partial \phi}{\partial x_1} \right)_{x_2} dA = \int_A \sigma_{ij} \frac{\partial \epsilon_{ij}}{\partial x_1} dA \quad (51)$$

where A is the area within the contour used in Eqn. (16). Write $\phi = \phi(\epsilon_{ij}, x_1, x_2)$, allowing for nonhomogeneous material variations in both x_1 and x_2 ; expand the left side of Eqn. (51) and use Eqn. (15),

$$\int_A \left(\frac{\partial \phi}{\partial x_1} \right)_{x_2} dA = \int_A \sigma_{ij} \frac{\partial \epsilon_{ij}}{\partial x_1} dA + \int_A \left(\frac{\partial \phi}{\partial x_1} \right)_\epsilon dA \quad (52)$$

For the damage model based on Eqn. (45), ϕ consists of a sum of terms ϕ_α in both constant and varying damage regions, each corresponding to one of the pairs $D_\alpha, D_{\alpha m}$. Assuming the crack tip neighborhood

is homogeneous in x_1 apart from damage, whenever $D_{\alpha m} = D_\alpha$ the contribution of each ϕ_α is a function of only ϵ_i , and thus $(\partial\phi/\partial x_1)_\epsilon = 0$. Where $D_\alpha \neq D_{\alpha m}$, the contribution of ϕ_α is a function of $D_\alpha(\epsilon_i)$ and $D_{\alpha m}$; if $\partial D_{\alpha m}/\partial x_1 = 0$, the contribution to $(\partial\phi/\partial x_1)_\epsilon$ vanishes. Thus, if $\partial D_{\alpha m}/\partial x_1 = 0$ for all damage parameters in the constant damage part of A (for which $D_\alpha \neq D_{\alpha m}$) the last integral in Eqn. (52) will vanish, and consequently $\mathcal{L} = 0$. Observe that there is no contribution from this last integral along the interfaces between ϕ^C and ϕ^D because ϕ is continuous across them.

Consider the material elements along a continuous segment of a line $x_2 = \text{constant}$. Using, for example, the damage model Eqn. (49), the requirement is $\partial D_{1m}/\partial x_1 = 0$ where $D_1 < D_{1m}$; namely, all of the elements on this segment must have the same amount of damage, as defined by the maximum value of strain energy density experienced over the loading history. The damage does not have to be independent of x_1 where $D_1 = D_{1m}$. It is likely that a state of local homogeneous damage in x_1 (where $D_1 < D_{1m}$) will be met in many cases, such as when the damage is due to a crack propagating at constant or slowly changing speed.

Recall that the damaging process was defined previously to be one in which $D_{\alpha m} = D_\alpha$ for all parameters. This restriction, however, was introduced only to simplify the discussion and can be removed. It is easily shown that the arguments above remain valid if additional groups of terms are added to Eqn. (45), with each group representing a different damage process. The regions or zones of constant and varying damage for one group need not be the same physical locations as those for another group.

Finally, it is of interest to consider the interpretation of J_V as an energy release rate. Equation (31) may be established by dividing

the body into zones of constant and varying damage (corresponding to each group of damage parameters in Φ), recognizing that Φ is continuous throughout the continuum (including the interfaces between these zones), and then employing the same method of proof as without damage while allowing for propagation of the interfaces. This equation enables one to determine J_V for elastic and visco-elastic materials with damage by the same type of experimental and theoretical methods as employed for nonlinear, completely elastic materials.

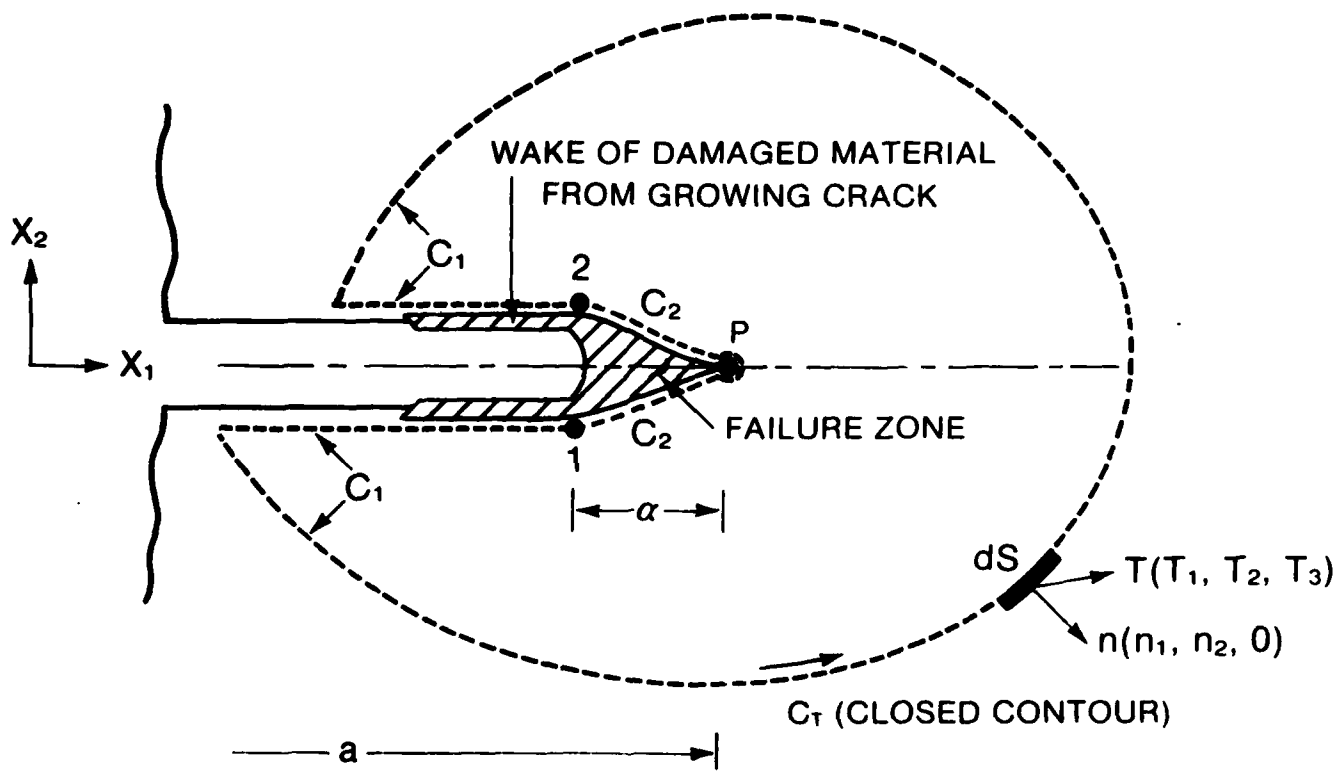


Figure 1. Cross-Section of Crack in Nonlinear Viscoelastic Material Showing Contours (---) Used in Line Integrals. Only the opening mode of displacement is drawn, although the basic formulation allows for shearing deformation and unsymmetric damage.

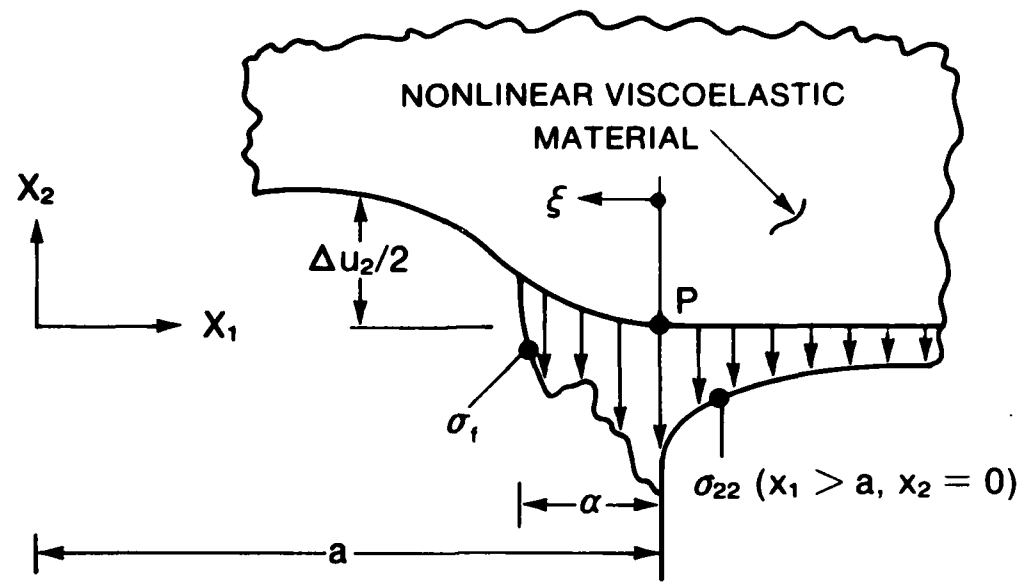


Figure 2. Normal Stress and Displacement Along Crack Plane

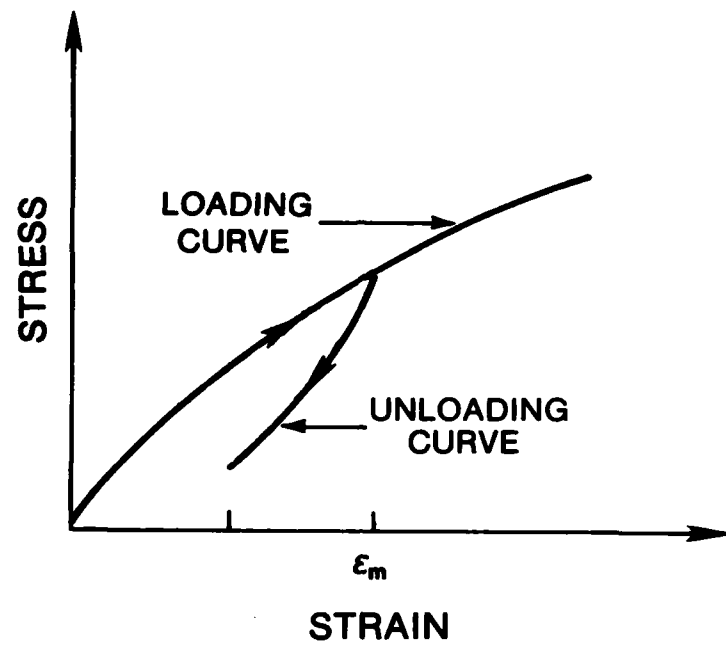


Figure 3. Stress-Strain Behavior of Material With Microscale Damage.

CORRESPONDENCE PRINCIPLES AND A GENERALIZED J INTEGRAL FOR LARGE
DEFORMATION AND FRACTURE ANALYSIS OF VISCOELASTIC MEDIA

by

R.A. Schapery

Mechanics & Materials Center
Civil Engineering Department
Texas A&M University, College Station, TX 77843

ABSTRACT

Methods of quasi-static deformation and fracture analysis are developed for a class of nonlinear viscoelastic media and sample applications are given. Selection of the class of media is guided by actual rheological behavior of monolithic and composite materials as well as the need for simplicity to be able to understand the effect of primary material and continuum parameters on crack growth behavior. First, pertinent aspects of J integral and energy release rate theory for nonlinear elastic media are discussed. Nonlinear viscoelastic constitutive equations are then given, and correspondence principles which establish a simple relationship between mechanical states of elastic and viscoelastic media are developed. These principles provide the basis for the subsequent extension of J integral theory to crack growth in viscoelastic materials. Emphasis is on predicting mechanical work available at the crack tip for initiation and continuation of growth; some examples show how viscoelastic properties and the J integral affect growth behavior. Included is the problem of a crack in a thin layer having different viscoelastic properties than the surrounding continuum. The Appendix gives an apparently new constitutive theory for elastic and viscoelastic materials with changing microstructure (e.g. distributed damage) and indicates the conditions under which the fracture theory in the body of the report is applicable.

1. Introduction

Methods for characterizing and predicting crack growth in materials which are elastic (except for the small-scale inelastic zone at crack tips) are well-established theoretically, and considerable experimental confirmation exists [1,2]. The methods for linear media now commonly use criteria for initiation and continuation of crack growth which are expressed in terms of stress intensity factors or energy release rate. For nonlinear media, especially rubber [2], energy release rate is often employed.

Fracture theory for materials exhibiting large scale inelastic behavior is considerably more limited. The J integral theory [1,3] has been successfully applied to initiation of crack growth in time-independent (elastoplastic) isotropic, homogeneous media under small strains. An analogous parameter, the C^* integral [4], has served in a similar manner to define crack speed in nonlinear viscous bodies. Analytical methods and their verification for crack growth in viscoelastic media are mainly limited to linear isotropic, homogeneous materials, although some theoretical results exist for linear orthotropic and nonhomogeneous materials [e.g., 5-9]; stress intensity factor is the primary characterizing parameter for fracture initiation time and crack speed.

The objective of much of the work on elastic and inelastic materials has been to identify a basic crack-growth controlling parameter, such as stress intensity factor or the J integral, which accounts entirely for the geometry of a body (including crack geometry) and the applied loads. Values of the parameter which produce crack initiation and various crack speeds are then found for a

given material, usually experimentally. This information may be used to predict crack growth in different geometries and aid the selection and design of fracture-resistant materials and structures. It is, of course, very important that the characterizing parameter account fully for the effect of geometry and loading conditions on crack growth if empirical corrections for each application are to be avoided.

In this paper we show that parameters analogous to the J integral and energy release rate may be used for quasi-static crack growth in a class of nonlinear viscoelastic materials under finite strain. In Section 2, results on the J integral and energy release rate for three-dimensional deformation of nonlinear elastic media are collected. Included is a simple (and apparently new) derivation of the relationship between the J integral and energy release rate. The J integral formulation is guided by Chen and Shield's work [10,11], and interpretations are given which are used for subsequent application of the theory to viscoelastic fracture.

Viscoelastic constitutive equations and methods of quasi-static deformation analysis using elastic solutions (correspondence principles) are discussed in Sections 3 and 4, respectively. Correspondence principles are given for a broader class of problems than considered in the fracture analysis; for example, they represent a new approach to analyzing crack closing and healing phenomena and ablation effects.

Sections 3 and 4 provide the basis for using the J integral and energy release rate in nonlinear viscoelasticity problems. This generalization, along with results in Section 5 for mechanical work input to the crack tip, is applied in Section 6 to relate fracture initiation time and crack speed to the J integral and viscoelastic

properties of the continuum and failing material at the crack tip; these relationships represent extensions of the author's earlier work [12] based on a two-dimensional J integral and small strains. Then, as another application of the theory, in Section 6 we also predict the effect on crack speed of the rheological properties of a zone of damaged or otherwise special material surrounding the crack tip. In practice, viscoelastic behavior of this zone is often significantly different from that of the far field as a result of high local stresses, dissipative heating, or the particular physical situation; the craze zone near crack tips in glassy polymers [13] and an adhesive interlayer are important examples. Surface or path-independence of the J integral exists for materials with certain types of distributed damage as shown in [12] and generalized in the Appendix; we use this important property here in accounting for behavior of the material surrounding the crack tip.

The deformation and crack growth theory in this paper is not much more involved than that of nonlinear elasticity or special cases of linear viscoelasticity. This simplicity, compared to what one would expect for nonlinear viscoelasticity, is a direct result of the particular constitutive equations and mechanical variables selected to characterize rheological behavior. We believe the theory provides a practical approach to the development of realistic damage and global fracture models for nonlinear elastic, viscous, and viscoelastic media, as illustrated by the author for a particulate composite material and polycrystalline metal [14,15].

2. The Reference Elastic Problem

Certain basic equations for elastic materials under large strains are summarized in this section. They are expressed in terms of stresses σ_{ij}^R ($i, j = 1, 2, 3$) and displacements u_i^R referred to an orthogonal set of Cartesian coordinates x_i which define the location of material points in the undeformed state of the body, B_0 . (Although B_0 is called the "undeformed state", it could be any fixed reference configuration, such as that existing at one time during the actual deformation history, without necessitating a change in the basic theory.) The instantaneous Cartesian coordinates y_i^R of material points in the deformed body B^R are referred to the same fixed axes as used for B_0 , and therefore $y_i^R = u_i^R + x_i$. In some cases σ_{ij}^R or u_i^R will be equal to the stresses or displacements in a viscoelastic body; but in general they are different, and therefore the superscript R is used to make this distinction. Section 4 is concerned with the correspondence between states of elastic and viscoelastic bodies. For now we shall just list and discuss relevant equations for elastic media.

The stresses σ_{ij}^R are taken to be the components of the so-called Piola stress field [16]. The components of the Lagrangian stress tensor T_{ij}^R [17] are given by the transpose of σ_{ij}^R ; viz., $T_{ij}^R = \sigma_{ji}^R$. Although σ_{ij}^R is not in general symmetric, these components are very convenient for our purposes because the equilibrium equations,

$$\frac{\partial \sigma_{ij}^R}{\partial x_j} + F_i^R = 0 \quad (1)$$

and the relation between surface tractions T_i^R and stresses,

$$T_i^R = \sigma_{ij}^R n_j \quad (2)$$

are identical in form to those in the linear theory. (Throughout this paper the summation convention is followed wherein repeated indices imply summation over their range unless stated otherwise.) All quantities are referred to B_0 , in which x_i are the independent variables. Namely, F_i^R is body force per unit undeformed volume, T_i^R is the surface force per unit undeformed area, and n_j is the outer unit normal of an area element defined in the undeformed state; force quantities are defined as the vectors existing at the current time t , but referred to the undeformed geometry, B_0 .

A potential ϕ is assumed to exist with the property that

$$\sigma_{ij}^R = \partial\phi/\partial(u_{i,j}^R) \quad (3)$$

where, by definition,

$$u_{i,j}^R = \partial u_i^R / \partial x_j \quad (4)$$

For an elastic material ϕ is the strain energy per unit undeformed volume [17]. If we invoke the physical requirement that ϕ is unaffected by rigid body rotation (and recall that we are using the coordinates x_i as the independent spacial variables) the dependence of ϕ on the displacement derivatives can enter only through the symmetric Green's strain tensor [17],

$$E_{ij}^R = (1/2) [u_{i,j}^R + u_{j,i}^R + u_{k,i}^R u_{k,j}^R] \quad (5)$$

However, considering the association between the present elastic problem and the actual (viscoelastic) problem introduced later, we shall not restrict ϕ by this usual physical condition. Instead, unless stated otherwise, we suppose only that

$$\phi = \phi(u_{i,j}^R, x_2, x_3, t) \quad (6)$$

implying possible dependence on the nine displacement derivatives, spacial variables x_2 , x_3 (allowing for nonhomogeneity with respect to x_2 and x_3) and time t (allowing for "aging" changes). The body is assumed to be homogeneous with respect to x_1 for now to achieve surface-independence of an integral that is useful in fracture analysis. With the same objective in mind, we assume a body force potential $\Phi_F = \Phi_F(u_i^R, x_2, x_3, t)$ exists, in which

$$F_i^R = -\partial\Phi_F/\partial u_i^R \quad (7)$$

Consider a generic volume V throughout which Φ and Φ_F exist with properties defined by Eqs. (3) and (7). Denote the bounding surface of this generic volume by S and let T_i^R be the surface tractions and n_j the components of the outer unit normal. Multiply Eqn.(1) by $-\partial u_i^R/\partial x_1$, integrate over the volume V , and then use the divergence theorem [18] to convert the integral to an integral over the surface S . The result is

$$\oint_S [(\Phi + \Phi_F)n_1 - T_i^R \partial u_i^R / \partial x_1] ds = 0 \quad (8)$$

where ds is an area element in the undeformed body. When $\Phi_F = 0$ and the body is homogeneous, the integral \oint becomes identical to the x_1 component of the integral vector derived by Knowles and Sternberg [16]; however, we have followed Chen and Shield [10] and not limited Φ to dependence on strains. By considering only the x_1 component, material nonhomogeneity with respect to x_2 and x_3 may be taken into account while retaining the property that $\oint = 0$. Only this component is needed in the fracture analysis to follow.

The J integral and crack tip model: Suppose the body contains one or more cracks. Figure 1 shows as an idealization the intersection of

a crack tip region and local crack faces with the plane of the page. The dashed line is the intersection of a representative surface S with the same plane. In order to meet the conditions which lead to $\delta = 0$, no crack can exist inside or on S .

The region designated as the failure zone in Fig. 1 is where material separation or at least intense damage occurs. The material comprising this zone in the undeformed state is of length α (not necessarily small) and is assumed to exist in a layer which is thin (in the x_2 direction) relative to α . Outside of the failure zone it is assumed there exists at least a small neighborhood around the crack tip for which $\delta = 0$. A useful definition of the crack tip P , and one that we employ, is that it is the leading edge of the material for which the conditions used in deriving $\delta = 0$ are not met.

It should be noted that tractions may exist along the crack faces to the left of the failure zone; for example, these may be due to a pressurized fluid, interfacial friction and contact pressure, or damaged material connecting the faces of the intact continuum (as in a craze zone in some plastics). In these cases, especially the last one, location of the left end of the failure zone (points 1 and 2) is somewhat arbitrary and its selection may depend on the particular application of interest. However, normally one would choose it so that α extends at least over the part of the surface $x_2 = 0$ for which crack tip material behavior is too complex to be able to predict the detailed traction distribution.

Next, we introduce the integral J_f :

$$J_f \equiv \int_0^\alpha \tau_i^R \frac{\partial \Delta u_i^R}{\partial \xi} d\xi \quad (9)$$

where τ_2^R is the normal stress and τ_1^R and τ_3^R are the shearing stresses in the x_1 and x_3 directions, respectively, along the interface between the failure zone and continuum; these are Piola stresses, as defined previously. It is assumed that the failure zone is sufficiently thin that the stresses in Eqn. (9) are the same along both top and bottom portions of the interface. The Δu_i^R are the components of the relative displacement vector between initially adjacent interface points across the local crack plane $x_2 = 0$. The viscoelastic normal stresses, τ_2 and σ_{22} , and displacement, $\Delta u_2/2$, along the upper surface of the continuum are indicated in Fig. 2.

For later use we shall suppose that the crack tip or edge P is essentially straight and parallel to the x_3 axis over at least a short distance ℓ_3 from the plane of the page ($x_3 = 0$). Over this same distance it is assumed the failure zone integral J_f does not vary. Since $n_1 = 0$ along the top and bottom interfaces it is readily shown that the contribution to α , Eqn. (8), from the portion of S along the top and bottom boundaries of the failure zone over the crack edge of length ℓ_3 is equal to $-J_f \ell_3$, assuming the integral over the small curved surface at the tip P can be neglected; this latter assumption is reasonable as long as the undeformed failure zone layer is thin relative to α and we impose the physical requirement of finite stresses (including those at P). Thus, from the condition $\alpha = 0$,

$$J_v = J_f \quad (10)$$

where

$$J_v = (1/\ell_3) \int_{S_1} [(\phi + \phi_F) n_1 - T_i^R \frac{\partial u_i^R}{\partial x_1}] ds \quad (11)$$

and S_1 is the portion of S not included in the integration along the

failure zone over the length ℓ_3 .

Notice that J_V is a surface-independent integral in that its value is the same (i.e. J_F) regardless of the choice of S_1 except for the conditions stated above. It can be reduced to Rice's path-independent J integral [3] by omitting the body force and assuming two-dimensional deformations. Specifically, let S be a cylinder (having the cross-section in Fig. 1) with generators and with normals to the end areas which are parallel to x_3 . At the ends $n_1 = 0$, and therefore the contribution to J_V from the cylinder ends vanishes if $T_i^R \partial u_i^R / \partial x_1 = 0$; this condition exists on the ends when $T_i^R = 0$ (e.g. plane stress) or $T_1^R = T_2^R = \partial u_3^R / \partial x_1 = 0$ (e.g. plane strain) or $T_3^R = \partial u_1^R / \partial x_1 = \partial u_2^R / \partial x_1 = 0$ (e.g. antiplane strain). With the integrand in Eqn. (11) further assumed to be independent of x_3 ,

$$J_V = \int_{C_1} [(\phi + \phi_F) dx_2 - T_i^R \frac{\partial u_i^R}{\partial x_1} dL] \quad (12)$$

where the integration path C_1 starts at point 1 in Fig. 1 and proceeds counterclockwise to point 2. Assuming $\phi_F = 0$, crack faces parallel to x_1 and traction-free, small strains and rotations, and further that ϕ is a function of $u_{i,j}^R$ through the strains, Eqn. (12) reduces to the original form of Rice's J integral.

Suppose S_1 in the three-dimensional version of J_V , Eqn. (11), is chosen so as to not include any portion of the failure zone-continuum interface (outside of ℓ_3). We may then consider Eqn. (10) to give a basic relationship between the mechanical state of the continuum through J_V and the characteristics of the failing material along a segment of the crack edge. In some cases one may want to use a failure zone integral in which ℓ_3 includes the entire crack edge (or a

large segment of it). If the integral, Eqn. (9)., is not constant or the edge is not straight along the length of interest, one would return to Eqn. (8) to derive the desired form, accounting as necessary for curvature of the edge.

Finally, it should be noted that Eqns. (10) and (11) do not depend on crack faces being parallel to the $x_1 - x_3$ plane. Rather, this condition is imposed only on the layer of material comprising the undeformed failure zone.

Energy release rate: Up to now we have not considered crack growth. By introducing a virtual crack extension, the value of J_v can be related to a global change in energy. This relationship may be useful for the experimental or theoretical determination of J_v for elastic and viscoelastic materials, as an alternative to evaluating it directly from the integral, Eqn. (11). The desired equation may be derived by first multiplying Eqn. (1) by a change in displacement δu_i^R , integrating over the volume V of B_0 , and using Eqns. (2), (3), (4), and (7) along with the divergence theorem. There results, finally, the familiar equation for virtual work,

$$\int_S T_i^R \delta u_i^R ds = \delta \int_V (\Phi + \Phi_F) dv \quad (13)$$

Both S and V have been assumed constant in deriving this result; e.g., there is no explicit change in crack tip location or phenomena such as material removal through melting. Crack growth will be simulated through a suitable choice of δu_i , as in [14], thus permitting the use of Eqn. (13). An edge segment of length l_3 (in the

x_3 direction) of only one of possibly many cracks in the body is to be advanced an amount δa , as illustrated in Fig. 3; this advancement is assumed independent of x_3 . The interface between the failure zone material and continuum of undeformed planar dimensions $(a + \delta a)$ by ℓ_3 is denoted as S_f and considered to be a portion of S in Eqn. (13). As before, we denote by Δu_i^R the current relative displacement components between originally adjacent material points across the local crack plane (which are specifically the displacements between the portions of S_f above and below the crack plane). Self-similar crack growth is now imposed: $\Delta u_i^R = \Delta u_i^R(\xi)$ along the failure zone; i.e., the relative displacement is a function of only ξ , where from Fig. 3

$$\xi = \lambda - \delta a - a_0 + a \quad (14)$$

is the distance between a material point and the advancing crack tip. The location of a material point referred to a fixed axis is defined by λ . Also, the crack tip location is given by a , with the initial value being a_0 and final value $a_0 + \delta a$ (at the end of the virtual displacement process).

Let δW^R be the virtual work of the failure zone on the continuum. Then, if $\delta a \ll a$,

$$\delta W^R = \int_{S_f} T_i^R \delta u_i^R ds = \int_{S_f} T_i^R \frac{\partial u_i^R}{\partial a} \delta a ds = \int_{S_f} T_i^R \frac{du_i^R}{d\xi} \frac{\partial \xi}{\partial a} \delta a ds \quad (15)$$

From Eq. (14) $\partial \xi / \partial a = 1$. Using the previously introduced notation for interface tractions and relative displacements (cf. Eqn. (9)), Eqn. (15) becomes

$$\delta W^R = -\ell_3 \delta a \int_0^{a+\delta a} \tau_i^R \frac{d \Delta u_i^R}{d \xi} d\lambda \quad (16)$$

Observe that $\partial \Delta u_i^R / \partial \lambda = d \Delta u_i^R / d \xi$ since $\partial \xi / \partial \lambda = 1$ from Eqn. (14).

Moreover, when we let $\delta a \rightarrow 0$ the integral in Eq. (16) becomes J_f , Eq. (9), because ξ in the latter equation is equal to λ . This result, together with Eqn. (13), yields,

$$J_f = -\partial P_v / \partial A \quad (17)$$

where $\partial P_v / \partial A \equiv \delta P_v / \ell_3 \delta a$ and

$$P_v \equiv \int_V (\phi + \phi_F) dv + \int_{S_T} \phi_T ds \quad (18)$$

where we have introduced a surface traction potential, $\phi_T = \phi_T(u_i^R, x_j, t)$, with the property that

$$T_i^R = -\partial \phi_T / \partial u_i^R \quad (19)$$

for the portion of the surface S_T . It is assumed that over the remaining surface, $S_U = S - S_f - S_T$, the displacements are given; i.e. $\delta u_i^R = 0$ in the virtual crack growth process. Although it will not be done here, Eqn. (18) can be easily generalized to the case of mixed traction-displacement conditions, in which different components of traction and displacement vectors are specified over the same surface.

Equations (10) and (17) provide the familiar result for the J integral,

$$J_v = -\partial P_v / \partial A \quad (20)$$

Recall that Eqn. (10) is dependent on the assumption that the material is physically homogeneous in the x_1 direction for the portion of the continuum bounded by the failure zone and the surface S_1 used in Eqn. (11). In contrast, this assumption is not needed to derive Eqn. (17), in that ϕ , ϕ_F , and ϕ_T in Eqn. (18) may depend explicitly on all coordinates x_i (as well as on displacement derivatives or displacements, as previously indicated).

Finally, it is to be observed that when surface tractions on S_T or body forces are specified functions of x_i (or treated as such), the potentials are

$$\Phi_F = -F_i^R u_i^R, \quad \Phi_T = -T_i^R u_i^R \quad (21)$$

Equation (18) then takes the familiar form,

$$P_V = \int_V (\Phi - F_i^R u_i^R) dv - \int_{S_T} T_i^R u_i^R ds \quad (22)$$

For elastic materials, the quantity P_V is the potential energy. Its physical significance is somewhat different for the class of viscoelastic materials discussed in the next section.

3. Viscoelastic Constitutive Equations

The constitutive equations which will be used are based on Eqn. (3), but the displacements u_i^R and stresses σ_{ij}^R are not necessarily physical quantities in the viscoelastic body. Instead, they are related to the physical displacements $u_i(x_k, t)$ and stresses $\sigma_{ij}(x_k, t)$ through hereditary integrals.

Specifically, considering displacements first, and assuming they vanish for $t < 0$,

$$u_i^R = E_R^{-1} \int_0^t E(t - \tau, t) \frac{\partial u_i}{\partial \tau} d\tau \quad (23)$$

where $u_i = u_i(x_j, \tau)$ is the physical displacement in terms of the time variable of integration, τ , and, as before, the coordinates x_i of the undeformed body. The quantity $E = E(t - \tau, t)$ is called a relaxation modulus, which imparts hereditary characteristics to the deformation behavior. The coefficient E_R is a free constant which will be termed the reference modulus; it is helpful in discussing special material

behavior and introducing dimensionless variables. In order to allow for the possibility of a discontinuous change in u_i with time at $t=0$, the lower integration limit in Eqn. (23) and succeeding hereditary integrals should be interpreted as 0^- unless indicated otherwise. The inverse of Eq. (23) is

$$u_i^R = E_R \int_0^t D(t-\tau, t) \frac{\partial u_i^R}{\partial \tau} d\tau \quad (24)$$

where $D = D(t-\tau, t)$ is termed a creep compliance. It is readily shown that E and D satisfy

$$\int_{t_0^-}^t D(t-\tau, t) \frac{\partial}{\partial \tau} E(\tau - t_0, \tau) d\tau = H(t - t_0) \quad (25)$$

where $t_0 \geq 0$ and $H(t - t_0)$ is the Heaviside step function: $H(t - t_0) = 0$ and 1 for $t < t_0$ and $t > t_0$, respectively.

It will be helpful to use abbreviated notation for the hereditary integrals. For any function of time, f ,

$$\{Edf\} \equiv E_R^{-1} \int_0^t E(t-\tau, t) \frac{\partial f}{\partial \tau} d\tau, \quad (26a)$$

$$\{Ddf\} \equiv E_R \int_0^t D(t-\tau, t) \frac{\partial f}{\partial \tau} d\tau \quad (26b)$$

Also, in view of Eqns. (23) and (24),

$$f = \{Ed\{Ddf\}\} = \{Dd\{Edf\}\} \quad (26c)$$

Equations (23) and (24) become, respectively,

$$u_i^R = \{Edu_i\}, \quad u_i = \{Ddu_i^R\} \quad (27)$$

Similar hereditary integrals are assumed to relate σ_{ij}^R and σ_{ij} , but modulus and compliance are interchanged,

$$\sigma_{ij}^R = \{D_1 d\sigma_{ij}\}, \quad \sigma_{ij} = \{E_1 d\sigma_{ij}^R\} \quad (28)$$

where the subscript 1 is used to indicate that the relaxation modulus and creep compliance (as well as another reference modulus E_{R1}) are not necessarily the same quantities as in Eqn. (27). Inasmuch as σ_{ij}^R and u_i^R are not in general the physical variables, we shall call them pseudo stresses and pseudo displacements, respectively. Similarly, the adjective pseudo will be used when referring to the potentials Φ , Eqn. (3), Φ_F , Eqn. (7), and Φ_T , Eqn. (19) in the context of viscoelastic analysis.

The hereditary integrals used here are linear functionals with relaxation and creep functions which are independent of x_i . This behavior provides the useful property that differentiation with respect to x_i and hereditary integration may be interchanged; e.g.,

$$\frac{\partial u_i^R}{\partial x_j} = \{Ed(\partial u_i/\partial x_j)\}, \quad \partial u_i/\partial x_j = \{Dd(\partial u_i^R/\partial x_j)\} \quad (29)$$

The choice of constitutive Eqn. (3), with pseudo and physical variables related in accordance with Eqns. (27) and (28), is motivated by the fact that this constitutive theory approximates well the deformation behavior of various materials, and leads to relatively simple equations for viscoelastic deformation and fracture analysis. The latter point will be brought out in this paper. The validity of the constitutive theory has been discussed in [12,14,15] for the case in which $\sigma_{ij}^R = \sigma_{ij}$. Observe that it reflects the commonly reported behavior in which stress-independent relaxation or creep functions in single integrals serve to characterize hereditary phenomena exhibited by many nonlinear materials. Also, some important special cases may be readily recovered through an appropriate choice of the material functions. Specifically, if $E = E_1 = D^{-1} = D_1^{-1} = E_R = E_{R1}$, Eqns.

(27) and (28) reduce to $u_i^R = u_i$ and $\sigma_{ij}^R = \sigma_{ij}$; consequently, Eqn. (3) reduces to that for nonlinear elasticity. If $D_1^{-1} = E_1 = E_{R1}$ and

$$D = (t_v E_R)^{-1} (t - \tau) \quad (30)$$

(where t_v is a time constant) we find $\sigma_{ij}^R = \sigma_{ij}$ and

$$u_i^R = t_v \partial u_i / \partial t \quad (31)$$

which, together with Eqn. (3), yields linear or nonlinear viscous behavior. The general creep compliance $D = D(t - \tau, t)$, together with $\sigma_{ij}^R = \sigma_{ij}$ (corresponding to $E_1 = E_{R1}$) and a pseudo strain energy density which is proportional to that for a linear elastic, isotropic material in terms of $u_{i,j}^R$, yields the standard constitutive theory for an aging linear viscoelastic material with constant Poisson's ratio; nonaging behavior results if $D = D(t - \tau)$. The generalization provided by Eq. (28) in which pseudo and actual stresses are not equal is useful for crack closing and healing analysis, as discussed later.

It should be mentioned that the notation $D = D(t, \tau)$ is employed in [14] instead of $D = D(t - \tau, t)$. These forms are equivalent, but the latter is more convenient in the study of crack growth. The pseudo energy Φ may also depend explicitly on time to account for effects of aging in the nonlinear behavior. "Aging" is not limited to intrinsic material changes, but may be due to direct physical causes such as transient temperatures and residual stresses [14].

4. Correspondence Principles

Correspondence principles in linear viscoelasticity theory usually refer to elastic-viscoelastic relationships involving Laplace transformed stresses and displacements. Instead, here we shall give three correspondence principles for time-dependent, quasi-static

solutions to nonlinear elastic and viscoelastic boundary value problems; they enable a viscoelastic solution to be easily constructed from an elastic solution. In terms of Piola stresses and coordinates x_i of B_0 the equilibrium equations are

$$\partial \sigma_{ij} / \partial x_j + F_i = 0 \quad (32)$$

The stress-pseudo displacement derivative equations,

$$\sigma_{ij} = \{E_1 d[\partial \Phi / \partial (u_i^R, j)]\} \quad (33)$$

and body forces

$$F_i = -\{E_1 d(\partial \Phi_F / \partial u_i^R)\} \quad (34)$$

in which

$$u_{i,j}^R \equiv \{E d(\partial u_i / \partial x_j)\}, \quad u_i^R \equiv \{E d u_i\} \quad (35)$$

lead to three integro-differential field equations for the three displacements u_i when substituted into Eqn. (32). The functions $\Phi = \Phi(u_{i,j}^R, x_k, t)$ and $\Phi_F = \Phi_F(u_i^R, x_k, t)$ are considered to be known; until Section 6, where the J_V integral is used, we allow for explicit dependence on all three coordinates x_k .

As boundary conditions we assume the traction potential $\Phi_T = \Phi_T(u_i^R, x_k, t)$ is specified on a portion S_T of the surface; viz.,

$$\sigma_{ij} n_j = T_i \equiv -\{E_1 d(\partial \Phi_T / \partial u_i^R)\} \quad \text{on } S_T \quad (36)$$

Elsewhere, displacements $u_i = U_i(x_j, t)$ are given,

$$u_i = U_i \quad \text{on } S_U \quad (37)$$

The total surface is $S = S_T + S_U$. Although not treated

here, generalization of the analysis is easily made for mixed conditions in which different traction and displacement components are specified over the same part of the surface.

In all three correspondence principles the reference configurations B_0 of the elastic and viscoelastic bodies are specified to be identical (with identical cracks, if any). The first correspondence principle is restricted to time-independent surfaces:

CP - I. The viscoelastic solution (i.e., the stresses and displacements in the viscoelastic body which satisfy Eqns. (32) - (37)) is

$$\sigma_{ij}^R = \{E_1 d\sigma_{ij}^R\}, \quad u_i^R = \{Ddu_i^R\} \quad (38)$$

where σ_{ij}^R and u_i^R satisfy equations of the reference elastic problem, Eqns. (1), (3), (4), and (7), together with the boundary conditions,

$$\sigma_{ij}^R n_j = T_i^R \equiv -\partial \Phi_T / \partial u_i^R \quad \text{on } S_T, \quad (39a)$$

$$u_i^R = U_i^R \equiv \{Edu_i\} \quad \text{on } S_U \quad (39b)$$

It is seen from Eqn. (39b) that we first transform the given displacements U_i (if any) using the hereditary integral and obtain those needed in the elasticity problem. The governing equations of elasticity for the variables σ_{ij}^R and u_i^R are then solved. This solution is used in Eqn. (38) to obtain the viscoelastic solution. That Eqn. (38) is correct is easily established by substituting it into Eqns. (32) - (37). If the body forces F_i or surface tractions T_i are specified in the viscoelasticity problem, then one transforms them to obtain $F_i^R \equiv \{D_1 dF_i\}$ or $T_i^R \equiv \{D_1 dT_i\}$, after which the elasticity

problem is solved using the potentials in Eqn. (21).

When S_T and S_U vary with time certain difficulties arise. If $\partial n_j / \partial t \neq 0$ on S_T , then Eqn. (39) does not result in the correct condition, Eqn. (36). This problem may be seen by observing that for the solution in Eqn. (38),

$$\sigma_{ij}n_j = \{E_1 d\sigma_{ij}^R\}n_j \neq \{E_1 d\sigma_{ij}^R n_j\} \text{ on } S_T \quad (40)$$

and therefore $\sigma_{ij}n_j \neq T_i$. Other difficulties are due to the effect of past values of T_i and U_i on current values of T_i^R and U_i^R . For example, consider $dS_T/dt > 0$ and Φ_T in Eqn. (21). (By this shorthand notation we mean at least a portion of S_U becomes in time a surface on which T_i is given.) Then the traction T_i^R cannot be predicted for all $t > 0$ from the given boundary conditions on the part of S where the change from a displacement to traction condition occurs.

The next correspondence principle is for this type of boundary value problem, but we assume $E_1 = E_{R1}$. Hence, $\{E_1 df\} = f$ for all functions f , and therefore the constitutive equations and body forces are, respectively,

$$\sigma_{ij} = \partial \Phi / \partial (u_{i,j}^R), \quad F_i = -\partial \Phi_F / \partial u_i^R \quad (41)$$

Also,

$$\sigma_{ij}n_j = T_i \equiv -\partial \Phi_T / \partial u_i^R \text{ on } S_T, \quad u_i = U_i \text{ on } S_U \quad (42)$$

CP - II. If $dS_T/dt \geq 0$, the solution of viscoelastic Eqns. (32), (35), (41), and (42) is

$$\sigma_{ij} = \sigma_{ij}^R, \quad u_i = \{D u_i^R\} \quad (43)$$

where σ_{ij}^R and u_i^R satisfy the equations of the reference elastic

problem, Eqns. (1), (3), (4), and (7), together with the boundary conditions in Eqn. (39) in which $T_i^R \equiv T_i$.

Verification of Eqn. (43) is readily accomplished as before by substituting this solution into the governing viscoelasticity equations. Inasmuch as the elastic and viscoelastic stresses are the same throughout V and on S at all times, no basic difficulties arise in verifying the solution if $\partial n_i / \partial t \neq 0$ on S_T and in determining T_i^R when Eqn. (21) is used for Φ_T . However, the present class of problems obviously allows for crack growth, and certain physical questions of material continuity and interference have to be addressed. Pursuing this point, we observe that the relative displacement between crack faces, Δu_i , in the viscoelastic body is the difference of displacements in Eqn. (43) evaluated on adjacent crack faces,

$$\Delta u_i = \{Dd\Delta u_i^R\} \quad (44)$$

where Δu_i^R is the displacement difference in the reference elastic problem. Since we have specified the instantaneous geometry of all cracks in the elastic problem to be the same as in the actual viscoelastic body, Δu_i is correctly predicted to vanish until the time t_1 , say, when a crack tip reaches any particular physical location; this follows from the fact that $\Delta u_i^R = 0$ at this same location when $t < t_1$ (assuming prior cracking and rejoining of the crack faces has not occurred) which in turn implies the hereditary integral in Eqn. (44) vanishes when $t < t_1$.

The present solution, Eqn. (43), does not account for contact or rejoining of crack faces. Rather, it would predict that adjacent crack faces pass through one another if in the actual situation they rejoin and interfacial compression exists. Following such rejoining,

the stresses in Eqn. (43) are not valid, and the solution may become much more involved. We shall not consider the general problem here; rather, only the case in which cracks are initially open and then close or shorten through a healing process is discussed. The third correspondence principle is concerned with the problem $dS_T/dt \leq 0$, and it is limited to the case $E = E_R$; Eqns. (32)-(37) still apply except $u_i^R = u_i$ and $u_{i,j}^R = u_{i,j}$ are now used.

CP - III. If $dS_T/dt \leq 0$ and if $\partial n_j/\partial t = 0$ on S_T , the viscoelastic solution for the case $E = E_R$ is

$$\sigma_{ij} = \{E_1 d\sigma_{ij}^R\}, \quad u_i = u_i^R \quad (45)$$

where σ_{ij}^R and u_i^R satisfy the equations of the reference elastic problem, Eqns. (1), (3), (4), and (7), together with the traction boundary conditions in Eqn. (39) and

$$u_i^R = U_i \quad \text{on } S_U \quad (46)$$

Verification of Eqn. (45) is made as before. Observe that elastic and viscoelastic displacements are now equal, while the stresses depend on the relaxation modulus E_1 . Also, it is of interest to observe that if tractions T_i are specified on crack surfaces (such as in the failure zone) the tractions T_i^R in the elastic problem are different from the actual values since $T_i^R = \{D_1 dT_i\}$.

The Correspondence Principles II and III are not limited to crack problems. For instance, they may be applied to problems involving contact between different continua or ablation. Furthermore, even though they are based on apparently different constitutive equations they may in some cases be used for the same material, at least as an

approximation. Indeed, for linear viscoelastic behavior in which the only effect of aging is in the relaxation moduli E and E_1 (i.e. $\dot{\epsilon}$ does not depend on time other than through the displacement derivatives), the two constitutive equations are easily shown to be equivalent if $E_1 = E$.

The remainder of this paper is concerned with crack growth analysis for materials obeying Eqns. (41) and (42). The Correspondence Principle II (CP-II) and J_V integral theory will be used in the development of criteria for predicting growth initiation time and crack speed.

5. Work Input To The Crack Tip

An important quantity in crack growth analysis is the mechanical work available from the viscoelastic continuum for producing the separation (or at least a significant change of state) of material in the failure zone. This work, W_f , will be defined using an idealized model of the crack tip, and subsequently expressed in terms of the parameters J_f and J_V of the reference elastic problem.

Consider as before a slender failure zone (in which α is large compared to the initial thickness of the failure zone in the x_2 direction) and locally two-dimensional deformations plus antiplane shearing. Before discussing W_f , let us recall that J_f for the elastic problem was defined through a line integral taken along the instantaneous interface between the continuum and failure zone. Furthermore, the surrounding material was assumed to obey Eqn. (3), while no such restriction was imposed on the zone itself. For the present purposes of discussion, let us suppose this zone consists of the thinnest material layer for which Eqn. (3) provides an adequate representation of the surrounding material. Figure 4 depicts the

deformed failure zone (in the opening mode for simplicity) using a solid line to indicate the interface.

For the viscoelasticity problem, the work per unit undeformed area (in the $x_1 - x_3$ plane) input by the continuum to a given material element (of width dx_1) in the failure zone from the time the crack tip arrives at the element, t_a , to the time the left end of the failure zone arrives, t_a , is

$$W_f = \int_{t_a}^{t_a} \tau_i \frac{\partial \Delta u_i}{\partial t} dt \quad (47)$$

The quantities τ_i and Δu_i ($i = 1, 2, 3$) are Piola stresses and relative displacements, respectively, along the interface, and therefore they have the same significance as their counterparts in J_f , Eqn. (9). Notice, however, that differentiation and integration in Eqn. (47) is for a fixed value of x_1 , whereas that in Eqn. (9) is for a fixed time; thus, J_f does not in general reflect the deformation of a given material element. As a result, quite apart from the distinction between elastic and viscoelastic solutions, W_f is believed to be a more basic parameter than J_f for defining material failure.

There is an additional important difference between W_f and J_f as they have been introduced. Since W_f is the work input to one material element, the continuum-failure zone interface has to consist of the same continuum material points at $\xi = 0$ as at $\xi = a$. The dashed line in Fig. 4 is intended to represent this interface. The height of the material element at $\xi = 0$ is indicated by h_0 , which defines the thickness of the layer that ultimately becomes part of the failure zone; depending on the material behavior, the two interfaces may essentially coincide along a partial width or entire width $0 < \xi$

$\leq \alpha$, or may not coincide until $\xi = \alpha$ ($t = t_\alpha$). Considering the analysis to follow, in which Δu_i^R and Δu_i are to be related through CP-II, we should use the same material interface in the elastic and viscoelastic problems; the outer interface (the dashed line in Fig. 4) may be used if the undeformed value of h_0 is small enough to not invalidate Eqn. (10). We shall assume that this is indeed the case.

According to CP-II, the relative displacements in the elastic and viscoelastic problems satisfy Eqn. (44) if the tractions acting on the elastic and viscoelastic continua are the same. (Recall that a traction potential Φ_T was used in the boundary conditions of CP-II (cf. Eqn. (42)); but it is clearly sufficient to use the same tractions, regardless of whether or not they are actually known or are expressed in terms of a potential.) Noting that stresses τ_i and τ_i^R are tractions along the continuum surface (apart from a sign change due to n_i), we specify $\tau_i^R = \tau_i$ in order to be able to use Eqn. (44) in the next section. Criteria for the time t_i at which crack growth initiates and for the speed of propagation \dot{a} will be studied.

6. Analysis of Crack Growth

Initiation of growth: For initiation we consider a material element which is at the left end of the failure zone $\xi = \alpha$ from $t = 0$ to t_i . As the body is loaded (beginning at $t = 0$) the crack tip P moves to the right but the element at $\xi = \alpha$ does not necessarily break immediately. Rather, it breaks at $t = t_i$, the so-called initiation time. We are interested in expressing the work input to this end element in terms of the far-field parameter J_V . In order to simplify the analysis so that viscoelastic effects may be shown clearly, behavior of the material in the failure zone will be idealized to that of a time-independent, rigid-plastic body; viz., we assume the τ_i are

independent of t and ξ . Thus, from Eqns. (9), (44), and (47),

$$J_f = \tau_i \Delta u_{i\alpha}^R \quad (48)$$

and

$$W_f = \tau_i \Delta u_{i\alpha} = \tau_i \{D \Delta u_{i\alpha}^R\} = \{D \Delta J_f\} \quad (49)$$

where $\Delta u_{i\alpha}^R$ and $\Delta u_{i\alpha}$ are the relative displacements at $\xi = \alpha$. The last result together with $J_v = J_f$, Eqn. (10), and the notation in Eqn. (26b), yields an explicit formula for work input at $t = t_i$:

$$W_f = E_R \int_0^{t_i} D(t_i - \tau, t_i) \frac{dJ_v}{d\tau} d\tau \quad (50)$$

This result is the crack tip work per unit undeformed area in terms of two continuum-related parameters, J_v (which accounts for the geometry of B_0 and applied loads) and D , the creep compliance of the continuum. The J_v integral is the same as J for an elastic material when expressed in terms of the surface tractions. Thus, just as for an elastic material, if the failure zone size α is small compared to all other geometric features, J_v is essentially independent of failure zone size and properties. Recall that E_R is a free constant, and may be selected as desired. (Its value does not actually affect W_f because J_v turns out to be inversely proportional to E_R .) Thus, if the continuum is elastic with a constant compliance D , we may use $E_R = D^{-1}$ and obtain the familiar result $W_f = J_v$.

An equation for predicting t_i is obtained by introducing the work $2\Gamma_i$ required to fail the element at $\xi = \alpha$. Thus, Eqn. (50) becomes

$$2\Gamma_i = \{D \Delta J_v\} \quad (51)$$

The factor of 2 is used because the "fracture initiation energy," Γ_i , is defined like a surface energy, counting the cross-sectional area of each side of the failed element at $\xi = a$ as one unit of area. This energy is not necessarily a constant, even when the physical state of the crack tip is the same for all conditions of interest; if the failure zone is viscoelastic, Γ_i may depend on t_i . Whether Γ_i is a given constant or a given function $\Gamma_i(t_i)$ Eqn. (51) is an implicit equation for predicting t_i in terms of the history of J_v . On the other hand, one could use Eqn. (51) to obtain Γ_i from tests of laboratory specimens by determining the value of the right hand side of Eqn. (51) when the crack starts to grow under various test conditions.

Finally, we observe that for the opening mode of crack tip deformation in a locally isotropic, linear viscoelastic material in plane strain,

$$J_v = (1 - \nu^2) K_I^2 / E_R \quad (52)$$

where K_I is the stress intensity factor and ν is the Poisson's ratio, assumed constant. (This familiar expression for elastic materials may be derived from Eqn. (10), for bounded crack tip stresses, by using [5, Part I, Eqn. (22)] for the displacement.) Substitution of Eqn. (52) into Eqn. (51) to express the initiation criterion in terms of K_I yields the author's earlier result for linear viscoelasticity [5, Part II, Eqn. (64)].

Crack speed: Predictions of W_f for the next case with $\dot{a} > 0$ is facilitated by using ξ rather than t as the independent variable. Thus, Eqn. (47) becomes

$$W_f = \int_0^\alpha \tau_i \frac{\partial \Delta u_i}{\partial \xi} d\xi \quad (53)$$

where $\Delta u_i = \Delta u_i(x_1, \xi)$. Equation (53) will be expressed in terms of J_v for short-term steady state conditions. Namely, the speed \dot{a} , interface stresses τ_i , and failure zone length α are assumed to be essentially independent of time during a generic time interval α/\dot{a} for which the crack tip moves a distance α ; during this same interval it is further assumed that Δu_i is essentially independent of x_1 and t (although it depends on ξ), α is small compared to the distance to other geometric features, and that there is no significant change in $D(t - \tau, t)$ due to aging (through the second argument, t).

These conditions, together with the observation from Eqn. (44) that Δu_i and Δu_i^R are related in the same way as for a linear viscoelastic nonaging material, lead to the approximation [5, Part II],

$$\Delta u_i = E_R D(\tilde{\tau}, t) \Delta u_i^R \quad (54)$$

where $\tilde{\tau} \equiv k\xi/\dot{a}$. The factor k is a very weak function of slope $n \equiv \partial \log D / \partial \log \tilde{\tau}$, and is practically $1/3$ for the entire range of slopes ($0 \leq n \leq 1$) encountered in practice. Equation (54) and the value of k stem from the smooth, cusp-shaped relative displacement $\Delta u_i^R(\xi)$ predicted for a linear continuum (with bounded crack tip stresses), such as that illustrated in Fig. 2 for the opening displacement. Although further study of the accuracy of Eqn. (54) seems warranted for nonlinear continua, it is likely to be a good approximation in many cases in view of the insensitivity of $\Delta u_i/\Delta u_i^R$ to the detailed behavior of $\Delta u_i^R(\xi)$ [5, Part II]; indeed, Eqn. (54) may not require α to be small.

Substituting Eqn. (54) into (53) and using the same type of approximation as in the linear theory [5, Part II], which does not

require τ_i to be spacewise constant, we find

$$W_f = E_R D(\tilde{t}_\alpha, t) \int_0^\alpha \tau_i \frac{\partial \Delta u_i^R}{\partial \xi} d\xi \quad (55)$$

where

$$\tilde{t}_\alpha \equiv ka/a \quad (56)$$

The integration and differentiation in Eqn. (55) is for x_1 fixed, while that in Eqn. (9) is for t fixed (i.e., fixed crack tip location); however, because Δu_i^R is independent of x_1 and t for short-term steady-state growth, these integrals are equal. Equation (55) thus reduces to

$$W_f = E_R D(\tilde{t}_\alpha, t) J_f \quad (57)$$

Upon equating W_f to the work required for failure of a material element, 2Γ , and using Eqn. (10) we obtain the desired result for \dot{a} ,

$$2\Gamma = E_R D(\tilde{t}_\alpha, t) J_v \quad (58)$$

It should be recalled that the crack speed has been assumed constant for only the generic period a/\dot{a} . Consequently, \dot{a} as well as the other relevant parameters may vary over much longer periods without invalidating Eqn. (58). Similar to the initiation problem, the linear theory [5, Part II] is recovered from Eqn. (58) by using Eqn. (52) for J_v .

The failure zone may be viscoelastic, and therefore Γ could depend on \dot{a} as well as other local parameters. After allowing also for possible dependence of a on J_v and \dot{a} , Eqn. (58) provides implicitly the functional relationship $\dot{a} = \dot{a}(J_v)$, as discussed in [12] and in the next subsection using two zones. The effect on \dot{a} of the geometry of the undeformed body B_0 (in which crack lengths vary with time) and applied loads is entirely accounted for by the instantaneous

value of J_V . In principle, a detailed model of the failure zone could provide this function; but if the effect of fundamental material parameters is not of concern, one would normally determine $\dot{a}(J_V)$ experimentally.

Effect of a process zone or interlayer on crack speed: Figure 5 shows a failure zone within a "process zone" of length β . The latter zone is introduced in part to account explicitly for the fact that with some materials, especially plastics, there is a zone around the crack tip which has different viscoelastic properties than the surrounding continuum [e.g., 13]. Also, Fig. 5 can be interpreted as a model for crack growth in an adhesive layer, in which the adjacent continuum represents the two elastic or viscoelastic adherends. Besides these uses, we may consider the process zone to be a failure zone as previously defined (but now with some limitations on its constitutive properties), and thereby obtain detailed information on Γ from the subsequent analysis.

For the class of damageable materials introduced in [12], and discussed further in the Appendix to the present paper, a pseudo strain energy density ϕ exists for the response to both loading and unloading. Additionally, J_V is independent of path under many conditions. We shall assume one path-independent integral exists for the process zone, and another exists for the surrounding continuum. The creep compliances and ϕ for the two regions may be different, and therefore these integrals are not necessarily equal.

Local two-dimensional deformations, appropriate to the use of Eqn. (12) for the process zone, are assumed. Furthermore, C_1 , is now taken to be the dashed line in Fig. 5, which is adjacent to the continuum-process zone interface. Subscripts "a" and "b" will be used

when necessary to distinguish between quantities for the failure zone and process zone, respectively. A letter subscript will not be used with parameters of the continuum.

The process zone is assumed to be thin in the x_2 direction (relative to β) so that arguments similar to those given previously for the failure zone may be employed; this slenderness greatly simplifies the analysis while the essential physical features are retained. Thus, Eqn. (10) is used,

$$J_v = J_{fb} \quad (59)$$

where J_v is in Eqn. (11) and (cf. Fig. 5),

$$J_{fb} = \int_0^\beta \tau_i \frac{\partial \Delta u_i^R}{\partial n} dn \quad (60)$$

Similarly, for the J integral in the process zone,

$$J_{vb} = J_{fa} \quad (61)$$

where

$$J_{fa} = \int_0^\alpha \tau_{ib} \frac{\partial \Delta u_{ib}^R}{\partial \xi} d\xi \quad (62)$$

It is important to recognize that in using Eqns. (59)-(62) we are, in effect, neglecting the contribution of the vertical segments at P and Q, Fig. 5, to the integral in Eqn. (8) for each contour. The other simplification employed is that the Piola stresses along the top horizontal line of each contour equal those along the bottom. The same simplifying features are assumed to apply to J_{vb} when evaluated on C_1 ; thus, Eqn. (12) yields

$$J_{vb} = \int_0^\beta \tau_{ib} \frac{\partial \Delta u_{ib}^R}{\partial n} dn + I_\alpha \quad (63)$$

where I_α is the integral along the vertical segment below point 1 and above point 2 in Fig. 5. This contribution is retained even though the integral along the vertical path at Q (within the process zone) is neglected. The difference is due to the value of ϕ_b at $\xi = \alpha$, which may be very large as a result of damage in the process zone (cf. Appendix), while ϕ_b at $n = 0$ will be small if $|\partial u_{ib}^R / \partial x_j|$ is small; the contribution of the integral of $T_i \partial u_{ib}^R / \partial x_1$ on the vertical lines is considered to be negligible due to, for example, smallness of $|\partial u_{ib}^R / \partial x_1|$ at $n = 0$ and $|T_{ib}|$ at $\xi = \alpha$ or the slenderness of the process zone. Considering the fact that the vertical paths at Q in the process zone and the continuum have been neglected and recalling conditions for which $\phi = 0$, we are, in effect, defining Q to be close to or ahead of the leading edge of major damage processes and to straddle the location where the creep compliance D and function ϕ (for the continuum) change to D_b and ϕ_b , respectively (for the process zone); of course, if $D = D_b$ and $\phi = \phi_b$, the latter constraint is not involved. The distance over which the change in functions occurs should be small compared to β or at least be such that the result of interest, Eqn. (73), is not sensitive to the physical location selected or calculated for Q.

Approximations like that in Eqn. (54) will be used to evaluate the viscoelastic displacement. Thus, for the continuum just outside the process zone,

$$\Delta u_i = E_R D(\tilde{t}, t) \Delta u_i^R, \quad \tilde{t} \equiv kn/\dot{a} \quad (64)$$

the process zone just inside the continuum,

$$\Delta u_{ib} = E_R D_b(\tilde{t}_b, t) \Delta u_{ib}^R, \quad \tilde{t}_b \equiv k_b n/\dot{a} \quad (65)$$

and the process zone just outside the failure zone,

$$\Delta u_{ib} = E_R D_b(\tilde{t}_a, t) \Delta u_{ib}^R, \quad \tilde{t}_a \equiv k_a \xi / \dot{a} \quad (66)$$

In view of the local steady-state assumption implicit in these approximations, $\dot{a} = \dot{b}$; also, because E_{Rb} and E_R are free constants, we have used $E_{Rb} = E_R$.

Let us next relate J_{vb} to J_v . This may be done by using the continuity of displacements and normal and shearing stresses across the continuum-process zone interface: $\Delta u_i = \Delta u_{ib}$ and $\tau_i = \tau_{ib}$. The first condition together with Eqns. (64) and (65) yields

$$\Delta u_{ib}^R = \frac{D(\tilde{t}, t)}{D_b(\tilde{t}_b, t)} \Delta u_i^R \quad (67)$$

Substitute this result into Eqn. (63), use the same type of approximation that lead from Eqn. (53) to Eqn. (55) (but now with the D-ratio in Eqn. (67) entering in place of D in Eqn. (54)), and then employ Eqns. (59) and (60). There results, finally,

$$J_{vb} = \frac{D(\tilde{t}_\beta, t)}{D_b(\tilde{t}_{b\beta}, t)} J_v + I_\alpha \quad (68)$$

where

$$\tilde{t}_\beta \equiv k_\beta / \dot{a}, \quad \tilde{t}_{b\beta} \equiv k_b \beta / \dot{a} \quad (69)$$

and approximately $k \approx k_b \approx 1/3$. Additionally (cf. Appendix),

$$I_\alpha \equiv - \int_a \phi_b dx_2 \quad (70)$$

where the integral is taken upward along the vertical lines at $\xi = \alpha$; on the basis of the physical significance of ϕ_b we have $I_\alpha \leq 0$, where

$I_a = 0$ when there is no damage in the process zone. It should be observed that we have neglected the contribution from the body force potential because of the slenderness of the process zone.

The work input to the failure zone is given by Eqn. (57) after replacing D by D_b , J_f by J_{fa} , Eqn. (62), and then using Eqns. (61) and (68),

$$W_f = E_R D_b(\tilde{t}_a, t) \left[\frac{D(\tilde{t}_\beta, t)}{D_b(\tilde{t}_{b\beta}, t)} J_V - \int_a \phi_b dx_2 \right] \quad (71)$$

where

$$\tilde{t}_a \equiv k_a a / \dot{a}, \quad k_a \approx 1/3 \quad (72)$$

Equating W_f to the work required for rupture of an element of unit area in the failure zone, 2Γ , we find the implicit equation for \dot{a} ,

$$2\Gamma_b = E_R D(\tilde{t}_\beta, t) J_V \quad (73)$$

where

$$2\Gamma_b \equiv \left[\frac{2\Gamma}{E_R D_b(\tilde{t}_a, t)} + \int_a \phi_b dx_2 \right] E_R D_b(\tilde{t}_{b\beta}, t) \quad (74)$$

The quantity Γ_b is the "fracture energy" of the process zone; it is introduced in order to write the crack speed relation, Eqn. (73), in the same form as Eqn. (58) for the failure zone alone; Γ_b consists of the failure zone energy Γ , the work of damage (given by the integral in Eqn. (74)), and the "local" creep compliance D_b in terms of two local times, \tilde{t}_a and $\tilde{t}_{b\beta}$.

As a result of damage in the process zone, the fracture energy Γ may be negligible (or, equivalently, the failure zone may not exist). Equation (74) then reduces to

$$2\Gamma_b = E_R D_b(\tilde{t}_{b\beta}, t) \int_a \phi_b dx_2 \quad (75)$$

which is to be substituted into Eqn. (73) to obtain the equation for $\dot{b}(\equiv \dot{a})$. This result corresponds to using $J_{vb} = 0$ in Eqn. (68).

If W_f in Eqn. (71) is negative, i.e.,

$$J_v < \frac{D_b(\tilde{t}_{b\beta}, t)}{D(\tilde{t}_\beta, t)} \int_a \phi_b dx_2 \quad (76)$$

there is insufficient mechanical work available to break material elements in the process zone. In this case, the crack will not propagate or, at least, quasi-static steady-state propagation cannot exist. Even if $W_f > 0$, steady-state propagation may not exist when Eqn. (73) predicts $dJ_v/d\dot{a} < 0$. An examination of Eqn. (73) indicates this situation is a physical possibility without having to consider dependence of a , β , Γ , and ϕ_b on \dot{a} . For example, suppose $\int \phi_b = 0$, $DE_R = 1$ and that a , β , and Γ are independent of \dot{a} . Also, let $k = k_a = k_b$ so that $\tilde{t}_\beta = \tilde{t}_{b\beta} = k\beta/\dot{a}$ and $\tilde{t}_a = k_a/\dot{a}$. Equations (73) and (74) yield

$$\frac{2\Gamma D_b(\tilde{t}_\beta, t)}{D_b(a\tilde{t}_\beta/\beta, t)} = J_v \quad (77)$$

It is helpful to express the derivative of J_v using logarithms,

$$-n_b + n_a = d \log J_v / d \log \dot{a} \quad (78)$$

where

$$n_b \equiv \frac{\partial \log D_b(s, t)}{\partial \log s} \quad \text{at } s = \tilde{t}_\beta \quad (79)$$

and

$$n_a \equiv \frac{\partial \log D_b(s, t)}{\partial \log s} \quad \text{at } s = a\tilde{t}_\beta/\beta \quad (80)$$

are logarithmic slopes of the creep compliance curve (for a fixed age t) at a creep time of $s = \tilde{t}_\beta$ and the shorter creep time $s = a\tilde{t}_\beta/\beta$. For real materials $(n_a, n_b) \geq 0$ and $n_a < n_b$ if s is sufficiently small; in this case, $dJ_v/d\dot{a} < 0$. For many materials $n_a > n_b$ at long creep

times s , and thus $dJ_v/d\dot{a} > 0$; the function $J_v(\dot{a})$ is therefore predicted to have a maximum at an intermediate crack speed.

Prediction of process and failure zone sizes: The lengths β and α which appear in the argument of creep compliance in the equations for crack speed are not necessarily constant. In fact they are related through Eqns. (59) and (61), respectively, to the J_v integrals and to a measure of the stress in the two zones. In [12] it was noted that for the failure zone alone the condition $J_v = J_f$ leads to such a relationship, which in turn reduces to that derived earlier for a small-scale failure zone in linear viscoelastic media using Barenblatt's condition for finite crack tip stresses [5, Part I]. Equations (59) and (61) are for slender zones, but β and α may be large and the material may be nonlinear, viscoelastic, and anisotropic.

Mechanical state solutions, including zone size, were derived in [12] for a failure zone in a power law material. Here, we use the same approach to derive β and α . Consider, for example, the use of Eqn. (59) and the power law potential (a so-called homogeneous function of degree $M + 1$),

$$\phi(cu_i^R, j) = |c|^{M+1} \phi(u_i^R, j) \quad (81)$$

to obtain an expression for β . The result is (cf. derivation of Eqn. (39) in [12]),

$$\beta = \left| \frac{\sigma_o}{\sigma_b} \right|^{1/M} \frac{J_v}{|\sigma_b I_f|} \quad (82)$$

where σ_b and σ_o have dimensions of stress and are independent of x_i , but may vary with t , \dot{a} , etc.; they are introduced to express the interface stresses τ_i and potential ϕ in terms of dimensionless functions f_i and ϕ_M ,

$$\tau_i = \sigma_b f_i , \quad \Phi = \sigma_0 \Phi_M \quad (83)$$

Also, $| |$ denotes absolute value and

$$I_f \equiv \int_0^1 (\partial g_i / \partial z) f_i dz \quad (84)$$

where $z \equiv \eta/\beta$, and g_i are dimensionless interface displacements,

$$g_i \equiv \text{sign} (\sigma_b) |\sigma_0 / \sigma_b|^{1/M} \Delta u_i^R / \beta \quad (85)$$

As in [12], it can be shown that under certain conditions I_f is a constant (apart from parameters which appear in Φ_M , such as M and aging time t); although linear strain-displacement relations were used previously, the form of the mechanical state solutions and the conditions are unaffected by the magnitude of the strains if the power law, Eqn. (81), is applicable. These conditions are: (i) the "shape factor" for interface tractions is given as $f_i = f_i(z)$ where $z \equiv \eta/\beta$; (ii) the continuum is locally homogeneous (i.e. Φ_M is independent of x_i , other than through $\partial u_i^R / \partial x_i$); (iii) the process zone size β is small compared to the distance to geometric features outside of the zone; (iv) the crack faces are locally traction free, apart from the interface tractions τ_i . Without further analysis one cannot quantify "local" and say how small β must be. However, it may be necessary for there to be a neighborhood of the crack tip on the order of $10 - 100\beta$ in which conditions (ii)-(iv) are met. The process zone must be small enough that the remote stress field is essentially the singular solution $\sigma_{ij}^R \sim r^{-M/(M+1)}$, where r is the distance (in the $x_1 - x_2$ plane) to the crack tip. Condition (iv) may be relaxed to allow for spacewise uniform tractions on a linear continuum and spacewise uniform normal tractions on an incompressible, nonlinear continuum;

the extension is achieved through superposition of a uniform stress field. Also, if $f_i = f_i(z, \dot{a}, J_v, \alpha)$ in condition (i), then $I_f = I_f(\dot{a}, J_v, \alpha)$.

For uniaxial stress σ_{11}^R -strain ϵ_{11}^R behavior, Eqn. (81) implies $|\epsilon_{11}^R| \sim |\sigma_{11}^R/\sigma_0|^{1/M}$. Thus, if $M \ll 1$, σ_0 may be interpreted as a yield stress; if $M = 1$, σ_0 is a modulus. Equation (82) in turn provides the relation between σ_0 , a measure of the intrinsic strength of the process zone σ_b , and a measure of the external loading J_v . If the process zone is also a power law material (in the neighborhood of the failure zone) with nonlinear exponent \hat{M} , a similar analysis yields

$$\alpha = \left| \frac{\sigma_{ob}}{\sigma_a} \right|^{1/\hat{M}} \frac{J_{vb}}{\left| \sigma_a^{I_{fa}} \right|} \quad (86)$$

where the parameters are analogous to those in Eqn. (82). If, however, there is considerable nonuniformly distributed damage surrounding the failure zone, it is not likely that a power law nonlinearity with a single exponent \hat{M} will be a good representation.

J_v as a characterizing parameter: Consider again a power law nonlinear material with a small scale process zone, in which the damage and failure behavior of material elements is unaffected by stresses and deformations prior to the arrival of the tip Q, Fig. 5. Further, assume J_v and b ($\equiv a$) are essentially constant during the time β/a required for the process zone to propagate its length. The state of stress in the remote continuum where the aforementioned singular solution applies is determined solely by the current value of J_v [12], just as for an elastic material. This dependence implies J_v is the only remote field parameter which affects Δu_i^R ; the process zone characteristics of course affect Δu_i^R . From Eqn. (64) we see that the same conclusion applies to the viscoelastic displacement, Δu_i , except crack speed now appears. The damage and failure parameters α , β , Γ ,

and $\int \Phi_b$ in Eqns. (73) and (74) may not be constant, but any variation will be due to J_v and \dot{a} (e.g. Eqn. (82)), apart from aging or environmental parameters such as the external temperature. (Local temperature changes due to mechanical deformation are determined similarly by J_v and \dot{a} .) Equation (73) therefore serves to define the function $\dot{a} = \dot{a}(J_v)$, indicating that J_v is the "characterizing parameter" for crack speed. In principle, this function could be obtained experimentally through measurements of speed. However, by introducing specific models for behavior of the process and failure zones, one could use Eqn. (73) to relate crack speed to material parameters as well as J_v . Elementary examples are given in [12] for a failure zone in a continuum obeying a power law with respect to both time (through the creep compliance) and strain; the relation $\dot{a} \sim J^{k'}$ is derived, where k' is a simple function of both exponents which depends on characteristics of the failure zone. The assumption of an "elastic-like" failure zone for opening mode propagation (Γ and τ_2 independent of speed) was shown in [5, Part III] to provide a function $\dot{a} = \dot{a}(J_v)$ which agreed well with experimental data on a crosslinked rubber; in this study there was no process zone and the continuum was linearly viscoelastic (cf. Eqn. (52)). See also [7, 20, 21] for linear behavior.

The J_v integral may serve as the characterizing parameter for initiation time or crack speed when some of the previously stated conditions (e.g. small-scale crack-tip zone) are not met, depending on characteristics of the process and failure zones. An example was given earlier for initiation time, Eqn. (51), in which a was not restricted in size. However, further experimental and theoretical studies are needed to establish the necessary conditions.

7. Concluding Remarks

Methods of quasi-static deformation and fracture analysis have been developed for nonlinear viscoelastic media. The correspondence principles which provide the basis for the analysis are not limited to crack growth; they apply to crack closing and healing as well as to other types of problems involving ablation and interfacial contact and separation. However, only crack growth examples are given.

Constitutive equations: Nonlinear effects in Eqn. (41) for stresses are characterized by a potential Φ which is analogous to strain energy density. This pseudo energy is expressed in terms of the history of displacement derivatives through Eqn. (23), rather than the history of Green's strains, and therefore material objectivity may not be satisfied when large deformations exist; i.e., depending on the deformation history and material type, Φ could be affected by rigid rotations. Material objectivity can always be satisfied when linear strain-displacement equations are applicable. In this case, one would express Φ as a function of displacement derivative history through the strain history [12].

A single hereditary integral, Eqn. (23), is used in Eqn. (41) to account for viscoelastic effects, and therefore some details of the complex stress-deformation behavior of many materials may not be followed. However, the theory does contain general material-objective representations of the important cases of nonlinear elastic and viscous media under small or large deformations and the common type of linear viscoelastic material which is characterized by one independent relaxation or creep function. In certain problems of crack growth in linear viscoelastic orthotropic materials, the several independent creep functions combine into just one function for predicting load-

displacement response of the crack plane [8]. This feature enables us to generalize Eqns. (58) and (73) for crack tip work by simply replacing D with this group of creep compliances.

For large deformations of viscous materials, the current geometry would be considered the "undeformed" state B_0 in order to recover the classical constitutive equations [17]; the basic expression for relating crack tip and far-field behavior, Eqn. (10), is not invalidated in this case if the opening displacement Δu_2 along the failure zone, Fig. 1, or process zone, Fig. 5., is small compared to the length α or β , respectively. On the other hand, this condition of a slender crack-tip zone in the current geometry is not needed for an elastic material.

As discussed in earlier work [12, 14], the nonlinear viscoelastic constitutive equations used here in the fracture theory may be written in the form of a special type of a so-called modified superposition principle employed successfully with polymers and metals [e.g. 15, 19]. We have introduced effects of aging and microstructural changes (e.g. damage) in the standard modified superposition principle. This "aging" is not limited to independent physical or chemical processes, and may be used to account for differences in nonlinear behavior at short and long times and, as shown in the Appendix, to account for damage characterized by Lebesgue norms of deformation-related parameters.

In view of these extensions of the standard single-integral representation for hereditary behavior, and the important limiting cases contained in the theory (including deformation theory of plasticity with elastic unloading), it is believed the constitutive

equations are sufficiently general to account for the primary features if not all details of actual deformation behavior of a wide variety of materials. Nevertheless, considerable additional study is needed to establish the range of validity of the equations for different materials and conditions. For example, it would be interesting to determine for rubber the accuracy of the stress-deformation relation in Eqn. (41), which is similar to the theory developed and successfully applied to rubber by Tschoegl and coworkers [22].

The "pseudo displacements", u_j^R , which appear in Eqns. (41) and (43), are related to the physical displacements u_j through the hereditary integral, Eqn. (23). If the constitutive theory is valid for global response, the material behaves overall as an elastic body when loads or stresses are expressed in terms of pseudo displacements; as illustrated in [15], this type of behavior for nonaging materials with constant damage may be easily checked by converting experimentally measured displacements to pseudo displacements through Eqn. (23) and then examining measured load-pseudo displacement diagrams.

Crack growth: Considering the complex states of deformation and damage around real crack tips, indirect determination of specific constitutive equations using specimens with stationary and propagating cracks may be an important complement to studies of specimens under homogeneous deformation histories. This determination would be aided by the simple relation between elastic and viscoelastic displacements, Eqn. (43), and the fact that Eqn. (41) for stresses, including the generalization in the Appendix, leads to relatively simple equations for crack growth, Eqns. (51), (58), and (73).

The quantity J_V in these equations has a very simple meaning in

certain cases. If hereditary behavior of the entire continuum outside of the process and failure zones can be represented by the one creep compliance D (or relaxation modulus E), then J_V is the same as the familiar J integral for nonlinear elastic materials and C^* for viscous materials when expressed in terms of externally applied loads (rather than displacements). The pseudo potential energy P_V , Eqn. (18), is related similarly to the potential energy for elastic media. If $u_i \approx u_i^R$, except possibly for a small neighborhood of crack tips, J_V and P_V are essentially the elastic J integral and energy release rate, respectively. The ratio $2\Gamma/E_R D$ from Eqn. (58), or $2\Gamma_b/E_R D$, Eqn. (73), then appears as the fracture energy for an elastic material if $J_V = P_V$; this "apparent fracture energy" may depend on crack speed through D , Γ , or Γ_b . For the rubber studied in [5, Part III], all effects of speed come through the nonaging form of compliance, $D = D(\tilde{t}_a)$. For a viscous body, C^* is approximately three times the length-averaged power input per unit area to the failure zone during short-term steady state propagation if we use $\tau_v = 1$ in Eqn. (30) [12]; it can be shown that the factor is exactly three for a linear viscous material.

Direction of crack growth: Prediction of the direction of crack growth has not yet been discussed in this paper. Many of the relationships hold whether or not the direction changes, but the problem is too complex to treat here in any detail. We would only suggest a possible approach. Referring to Fig. 3, suppose for purposes of discussion the local coordinate axis is fixed and various relative orientations θ for the continuum are considered. The actual θ 's for initiation and continuation of growth may correspond to the

predicted directions for which t_i is a minimum and \dot{a} is a maximum, respectively. These criteria automatically account for local and global material anisotropy through the variation of values of the material and loading parameters (such as Γ , a , and J_v in Eqn. (58)) with respect to θ . Also, these proposed criteria reduce to the well-established one of maximum energy release rate for crack growth in an elastic isotropic body. The equations for crack speed have been derived under the simplifying condition of short-term steady state behavior; with crack tip reorientation it is likely that the equations will remain valid if θ is small in magnitude and essentially constant for an amount of growth equal to the length α or β of the crack tip zone.

Crack tip models: Emphasis of the fracture analysis in this paper has been on predicting the mechanical work available at the crack tip for initiation and continuation of growth. The right-hand side of Eqns. (58) and (73) is this work at the failure zone (without a process zone) and process zone edges, respectively. By assuming the theory in the Appendix is valid for the process zone, we have obtained some information on how the creep compliance D_b and pseudo energy Φ_b of the process zone affect the required work $2\Gamma_b$, Eqn. (74). Viscoelastic behavior of the embedded failure zone in Fig. 5 is reflected in the value of Γ , and it may be different from that of the process zone and continuum. Because the process zone is slender, we were able to obtain a relatively simple relationship, Eqn. (68), between its J_v integral, J_{vb} , and J_v for the surrounding continuum (or the adherends, in the case the process zone is actually a thin adhesive interlayer). Also, it should be observed that Equation (73) for available work allows for distributed damage outside of the

process zone as long as the theory in the Appendix applies. This feature is important for many materials, especially composites.

With the dual crack tip zones, Fig. 5, one can account for a distinct, complex material separation zone (α) within a relatively well-defined layer of damaged material (β). This geometry may be a realistic model of the delamination tip region in fibrous composites with rubber-toughened matrices [23, Fig. 3] and a cracked craze layer in plastics. As a special case the failure zone could be omitted; one may interpret this situation as the original one in which only a failure zone exists, Eqn. (58), but with an explicit viscoelastic representation for the fracture energy. As shown in [5, Part III] this energy for rubber may be independent of crack speed. When this is true, the molecular theory for fracture energy of rubber in its elastic range [2] serves to relate Γ_b to molecular parameters, and Eqn. (73) brings in the only viscoelastic effects through D ; the notch-tip diameter ($\approx 50 \text{ \AA}$) used in [2] is to be associated with the process zone height in the undeformed state.

It is believed the theory in this paper will be helpful in developing detailed crack tip models which relate growth behavior directly to local physical, chemical, and mechanical processes; a possible general approach would consist of using the available crack tip work, Eqn. (73), in a local nonequilibrium thermodynamic formulation for the process and failure zones. Much of the published work on crack tip models employs the classical singular solutions for the local mechanical state. However, whether propagation is continuous or occurs in steps [e.g. 24, 25], use of continuum mechanics and thermodynamics with bounded stresses should lead to more direct

relationships between basic material parameters and crack growth, as illustrated here.

Acknowledgment

The author is grateful to the U.S. Air Force Office of Scientific Research, Office of Aerospace Research (with Major David Glasgow as Program Manager) for sponsoring this research, and to Mr. J.R. Weatherby, graduate research assistant, for his review of the manuscript and helpful comments.

REFERENCES

- [1] D. Broek, Elementary Engineering Fracture Mechanics, Third revised ed., Martinus Nijhoff Publishers (1982).
- [2] G.J. Lake, "Aspects of Fatigue and Fracture of Rubber", in Progress of Rubber Technology, Applied Science Publishers Ltd. (1983) 89-143.
- [3] J.R. Rice, "A Path Independent Integral and the Approximate Analysis of Strain Concentration by Notches and Cracks", J. Applied Mechanics, 35 (1968) 379-386.
- [4] J.D. Landes and J.A. Begley, "A Fracture Mechanics Approach to Creep Crack Growth", in Mechanics of Crack Growth, ASTM STP 590, American Society for Testing and Materials (1976) 128-148.
- [5] R.A. Schapery, "A Theory of Crack Initiation and Growth in Viscoelastic Media", Int. J. Fracture, 11 (1975): Part I, "Theoretical Development", 141-159; Part II, "Approximate Methods of Analysis", 369-388; Part III, "Analysis of Continuous Growth", 549-562.
- [6] A.A. Kaminskii, "Investigations in the Field of the Mechanics of the Fracture of Viscoelastic Bodies", Prikladnaya Mekhanika, 16 (1980) (English translation (1981) Plenum) 3-26.
- [7] R.M. Christensen, Theory of Viscoelasticity, An Introduction, Second Ed., Academic Press (1982).
- [8] G.S. Brockway and R.A. Schapery, "Some Viscoelastic Crack Growth Relations for Orthotropic and Prestrained Media", Eng. Fracture Mechanics, 10 (1978) 453-468.
- [9] R.A. Schapery, "A Method for Predicting Crack Growth in Non-homogenous Viscoelastic Media", Int. J. Fracture, 14 (1978) 293-309.
- [10] F.H.K. Chen and R.T. Shield, "Conservation Laws in Elasticity of the J-Integral Type", J. Applied Mathematics and Physics ZAMP, 28 (1977) 1-22.
- [11] R.T. Shield, "Conservation Laws in Finite Elasticity", in Finite Elasticity, R.S. Rivlin Ed., The American Society of Mechanical Engineers (1977) 1-10.
- [12] R.A. Schapery, "Continuum Aspects of Crack Growth in Time Dependent Materials", Texas A&M Univ. Report No. MM 4665-83-2 (Feb. 1983).
- [13] E. Passaglia, "Relaxation of Stresses in Crazes at Crack Tips and Rate of Craze Extension", Polymer, 23 (1982) 754-760.

- [14] R.A. Schapery, "On Viscoelastic Deformation and Failure Behavior of Composite Materials with Distributed Flaws", in 1981 Advances in Aerospace Structures and Materials, S.S. Wang and W.J. Renton, Eds., The American Society of Mechanical Engineers (1981) 5-20.
- [15] R.A. Schapery, "Models for Damage Growth and Fracture in Nonlinear Viscoelastic Particulate Composites", in Proc. Ninth U.S. National Congress of Applied Mechanics, The American Society of Mechanical Engineers (1982) 237-245.
- [16] J.K. Knowles and E. Sternberg, "On a Class of Conservation Laws in Linearized and Finite Elastostatics", Arch. Rat. Mech. Anal., 44 (1972) 187-211.
- [17] Y.C. Fung, Foundations of Solid Mechanics, Prentice-Hall, Inc. (1965).
- [18] M.D. Greenberg, Foundations of Applied Mathematics, Prentice-Hall, Inc. (1978).
- [19] W.N. Findley, "Creep of 2618 Aluminum Under Side Steps of Tension and Torsion and Stress Reversal Predicted by a Viscous-Viscoelastic Model", J. Applied Mechanics, 48 (1981) 47-54.
- [20] W.G. Knauss, "On the Steady Propagation of a Crack in a Viscoelastic Sheet: Experiments and Analysis", in Deformation and Fracture of High Polymers, H. Henning Kausch, John A. Hassell and Robert I. Jaffee, Eds., Plenum Press (1974) 501-541.
- [21] L.N. McCartney, "Crack Growth Laws for a Variety of Viscoelastic Solids Using Energy and COD Fracture Criteria", Int. J. Fracture, 15 (1979) 31-40.
- [22] N.W. Tschoegl, "Phenomenological Aspects of the Deformation of Elastomeric Networks", Polymer, 20 (1979) 1365-1370.
- [23] W.L. Bradley and R.N. Cohen, "Delamination and Transverse Fracture in Graphite/Epoxy Materials", Texas A&M Univ. Report MM 4665-83-5, April 1983. (To appear in Proc. 4th Int'l Conf. on Mech. Behavior of Materials, Stockholm, 1983.)
- [24] R.W. Hertzberg and J.A. Manson, Fatigue of Engineering Plastics, Academic Press (1980) 160.
- [25] A.J. Kinloch, "Micromechanisms of Crack Extension in Polymers", Metal Science, (1980) 305-318.

APPENDIX

Effect of Time-Varying Microstructural Changes

In earlier work on small deformation behavior [12] it was shown that certain important inelastic effects, besides those represented by the creep compliance, could be taken into account in the J_V integral theory. These additional effects were associated with "distributed damage" or, what may be a better term, "microstructural changes". Special cases are microcracking and dislocation motion and generation. Here, we review the damage theory in the broader context of large deformations and a three-dimensional J_V integral and discuss some additional features. The formulation is in terms of the reference problem, which is the reference elastic problem with damage; the viscoelastic variables are still related to those for the reference problem through Eqns. (27) and (28). For lack of a better short name, we are using "damage" when referring to changes in the microstructure or fabric of a material. However, the specific "damaging process" does not have to be identified; it could include healing (decrease in damage) as well as other changes which are beneficial to structural performance.

Constitutive theory: It is assumed on physical grounds that a strain energy potential exists when the damage is constant (for instance, during unloading without significant interfacial friction following development of microcracking in a composite or following plastic deformation in a metal). Denoting this potential by ϕ^C , for reasons to be given we assume it has the form

$$\phi^C = \phi_0^R(u_{i,j}^R, x_k, t) + \sum_{n=1}^N \phi_n(F_n, F_{cn}, x_k, t) \quad (A.1)$$

The u_i^R enter Φ_n through the functions $F_n = F_n(u_i^R)$; as a special case, F_n may be a strain or a strain invariant. We further assume that all of the functions are smooth enough to permit the various mathematical operations which are performed. The Φ 's may depend on x_i and t , as indicated, but this material nonhomogeneity and aging will not be explicitly shown in subsequent work unless needed for clarity. Also, throughout the Appendix summation over n is not intended unless Σ is used.

By definition, all quantities F_{cn} (which will be called damage parameters) are constant during a constant damage process. In this case Eqns. (3) and (A.1) yield the Piola stresses,

$$\sigma_{ij}^R = \frac{\partial \Phi_0}{\partial (u_{i,j}^R)} + \sum_{n=1}^N \frac{\partial \Phi_n}{\partial F_n} \frac{\partial F_n}{\partial (u_{i,j}^R)} \quad (A.2)$$

By further definition, the only other process which can occur is called a damaging process and is such that $F_{cn} = F_n$ for all parameters F_{cn} ; at the end of this Appendix a simple generalization will be made in which $F_{cn} \neq F_n$ for some of the damage parameters. It is assumed that the stresses are continuous in the displacement derivatives, and therefore Eqn. (A.2) defines the stresses with constant or varying damage.

This formulation for constant damage may be visualized very easily by considering a uniaxial stress $\sigma (\equiv \sigma_{11}^R)$ -strain $\epsilon (\equiv \partial u_1^R / \partial x_1)$ equation written in the form $\sigma = \sigma(\epsilon, \epsilon_C)$ for unloading from a maximum strain ϵ_C . The first-time loading curve with changing damage is $\sigma = \sigma(\epsilon, \epsilon)$, where $\epsilon_C = \epsilon$ is both the maximum strain and the current strain. A point on the stress-strain curve for loading $\sigma = \sigma(\epsilon, \epsilon)$ is also an end point on an unloading or reloading curve, $\sigma = \sigma(\epsilon, \epsilon_C)$ at $\epsilon = \epsilon_C$.

A potential ϕ^D exists during a damaging process, where

$$\sigma_{ij}^R = \partial\phi^D/\partial(u_{i,j}^R) \quad (A.3)$$

because

$$\partial\sigma_{ij}^R/\partial(u_{k,\ell}^R) = \partial\sigma_{k\ell}/\partial(u_{i,j}^R) \quad (A.4)$$

Equation (A.4) is easily verified for the stresses in Eqn. (A.2); in evaluating the derivatives of stress, one must first set $F_{cn} = F_n$ and then differentiate both arguments of each ϕ_n . It can also be shown that if at least one of the functions ϕ_n were to depend on more than one damage parameter, Eqn. (A.4) would not necessarily hold. In order to fully define the stresses by Eqn. (3), we write $\phi = \phi^C$ when the damage is constant, $\phi = \phi^D$ for a damaging process, and $\phi = \phi^C = \phi^D$ at the transition between the two types of processes.

As an aid in constructing ϕ^D from Eqns. (A.2) and (A.3) and the transition continuity condition, and in providing a physical interpretation of this damage theory, let us rewrite ϕ^C in a different but equally general form. Specifically, eliminate ϕ_n ($n = 1, \dots, N$) from Eqn. (A.1) in favor of new functions P_n and h_n , where

$$\phi_n = P_n(F_n, F_{cn}) + \int_0^{F_{cn}} h_n(F_n) dF_n \quad (A.5)$$

and

$$P_n(F_n, F_n) = 0 \quad (A.6)$$

Notice that Eqn. (A.6) implies $P_n(F_{cn}, F_{cn}) = 0$, and thus the integral in Eqn. (A.5) is equal to ϕ_n at the transition, $F_n = F_{cn}$. The potential for the constant damage process may be written in the form,

$$\phi^C = \phi_C^D + \sum_{n=1}^N P_n(F_n, F_{cn}) \quad (A.7)$$

where

$$\phi_C^D \equiv \phi_0 + \sum_{n=1}^N \int_0^{F_{cn}} h_n(F_n) dF_n \quad (A.8)$$

The stresses for constant damage are

$$\sigma_{ij}^R = \frac{\partial \phi_0}{\partial (u_{ij}^R)} + \sum_{n=1}^N \frac{\partial P_n}{\partial F_n} \frac{\partial F_n}{\partial (u_{ij}^R)} \quad (A.9)$$

Requirements of stress and potential continuity at the transition, $F_n = F_{cn}$, together with Eqn. (A.3), yield for the damaging process,

$$\phi^D = \phi_0 + \sum_{n=1}^N \int_0^{F_n} h_n(F'_n) dF'_n \quad (A.10)$$

and

$$\sigma_{ij}^R = \frac{\partial \phi_0}{\partial (u_{ij}^R)} + \sum_{n=1}^N h_n(F_n) \frac{\partial F_n}{\partial (u_{ij}^R)} \quad (A.11)$$

where

$$h_n(F_n) = \partial P_n(F_n, F_{cn}) / \partial F_n \quad \text{when } F_{cn} = F_n \quad (A.12)$$

Observe that $\phi_C^D = \phi^D$ at $F_n = F_{cn}$. Equations (A.6)–(A.12) constitute the damage theory which will be used in the remainder of the Appendix. In using Eqn. (3) with the damage theory, it should be kept in mind that $\phi = \phi^C$ for constant damage, $\phi = \phi^D$ for a damaging process, and that stresses are given explicitly by Eqns. (A.9) and (A.11).

Let us next consider the relationship of ϕ^D and ϕ^C to mechanical work and dissipation. Without body forces, the mechanical work input per unit initial volume for the reference problem in any given time interval $t_a \leq t \leq t_b$ is

$$W_{in}^R(t_a, t_b) = \int_{t_a}^{t_b} [\sigma_{ij}^R \partial (u_{ij}^R) / \partial t] dt \quad (A.13)$$

which may be readily established by means of the divergence theorem. Take $t_a = 0$ and assume the material is initially in its undeformed

state ($u_{i,j}^R = 0$) and that it does not age during the period 0 to t_b (i.e. ϕ depends on time only through $u_{i,j}^R$). Without loss in physical generality, we may set $\phi_0 = \phi^D = 0$ at $t = 0$. Consider next an arbitrary number of intervals of damaging and constant damage processes, starting with a damaging process. Substituting Eqn. (3) into Eqn. (A.13) and using continuity in ϕ at the transition between each process,

$$W_{in}^R(0, t_b) = \phi^D(t_b) \quad (A.14)$$

when t_b falls within a damaging process, and

$$W_{in}^R(0, t_b) = \phi^C(t_b) \quad (A.15)$$

when t_b falls within a constant damage process. Thus, for nonaging elastic materials with damage, ϕ^D and ϕ^C have a very simple physical meaning. Notice that if $\sigma_{ij}^R(t_b) = 0$ and the damage is constant at t_b , Eqn. (A.9) gives implicitly the residual values of $u_{i,j}^R$; also, $\phi^C(t_b)$ is the mechanical work "dissipated" as a result of damage. (If healing occurs during "damaging processes", the work input could be negative.) For uniaxial stress-strain behavior, one can think of $\phi^D(t_b)$ as the area under a stress-strain curve for loading, and $\phi^C(t_b)$ as this area less that under the curve for unloading.

It is believed the damage theory, Eqns. (A.6)-(A.12), is sufficiently general to provide a good approximation to the behavior of many real materials under many deformation histories. For example, one can show that the classical deformation theory of isotropic metal plasticity (with linear elastic unloading) conforms to these equations. Another applicable example is a special case of a constitutive theory with microcracking [14], as noted previously [12].

The special microcracking case may be obtained by setting

$$\sigma_{ij}^R = \sigma_{ij}, \quad N = 1, \quad F_{cl} = F_m, \quad \phi_o = F_1, \quad (A.16)$$

$$P_1 = -g(F_m)(F_1 - F_m), \quad g(0) = 0$$

The damage parameter F_m is the maximum value of F_1 , considering the entire deformation history up to the current time. Equation (A.12) yields $h_1(F_1) = -g(F_1)$. Also, we find

$$\phi^C = [1 - g(F_m)][F_1 - F_m] + \int_0^{F_m} [1 - g(F_1')] dF_1' \quad (A.17)$$

and

$$\phi^D = \int_0^{F_1} [1 - g(F_1')] dF_1' \quad (A.18)$$

The stresses for a constant damage process are

$$\sigma_{ij} = [1 - g(F_m)] \partial F_1 / \partial (u_{i,j}^R) \quad (A.19)$$

For a damaging process set $F_m = F_1$ in Eq. (A.19). The function $g(F_1)$ reflects the softening effect of microcracks; for no damage $g = 0$, and for complete damage (uniform failure) $g = 1$. Observe from Eqn. (A.19) that F_1 is the pseudo strain energy density for an undamaged material. It should also be added that g may vanish over an F_1 range, $0 \leq F_1 \leq F_D$. In this case, the "damaging process" would not actually produce damage until the energy F_D is exceeded. According to Eqns. (A.17) and (A.18), $\phi^C = \phi^D = F_1$ for $0 \leq F_1 \leq F_D$, as expected.

A damage parameter which is more general than F_m appears in [14,15]. It is derived from viscoelastic crack growth theory, and may be written in the form of a so-called Lebesgue norm,

$$L_p = \left[\int_0^t F_1^p dt \right]^{1/p} \quad (A.20)$$

If $p = \infty$, Eqn. (A.20) reduces to $L_p = F_m$; this case leads to the previous theory, Eqns. (A.17)-(A.19). On the other hand, if p is not infinite but is at least moderately large ($p \geq 4$), and if the deformation history over a period $0 \leq t \leq t_m$ is one in which $F_m = F_1$, then [15],

$$L_p = A F_1 t^{1/p} \quad (A.21)$$

where A is essentially constant. If Eqn. (A.21) applies up to $t = t_m$, and $F_1 < F_m$ for $t > t_m$, then

$$L_p = A F_m t_m^{1/p} \quad (A.22)$$

at least for a limited period of time beyond t_m . The damage model for which Eqns. (A.21) and (A.22) apply may be used to generalize Eqns. (A.17)-(A.19); viz., replace $g(F_m)$ with $g(F_m t_m^{1/p})$ and $g(F_1)$ with $g(F_1 t^{1/p})$. Hence, microcracking for which p is finite leads to an "aging" elastic material with damage.

The J_V integral: By dividing the continuum into regions of constant and varying damage we may easily extend the theory in the body of the report to allow for damage if the displacement field is sufficiently smooth. In effect, the material may be treated as nonhomogeneous whether the nonhomogeneity is intrinsic or is due to damage. As justification for this extension, consider first the integral δ , Eqn. (8). We will allow for explicit dependence on x_2 , x_3 , and t in the potentials ϕ_0 and P_n in Eqns. (A.7) and (A.8) (besides dependence on $u_{i,j}^R$); but dependence on x_1 , either explicitly or in F_{cn} , is excluded.

At any given time, let $S \equiv S_C$ enclose a region of the body undergoing a constant damage process. Clearly $\delta = 0$ if ϕ^C is used for ϕ . If, for example, we were to use ϕ^C for the special microcracking

model, Eqn. (A.17), it would be necessary for the maximum energy F_m experienced by each material element to be independent of x_1 , although F_m could vary with x_2 (distance from the local crack plane) and x_3 . Now, let $S \equiv S_D$ enclose an adjacent region undergoing a damaging process. Here, $F_{cn} = F_n$, and thus $\delta = 0$ if ϕ^D is used for ϕ ; even though F_{cn} may vary with x_1 , this dependence is through $F_n = F_n(u_{i,j}^R)$ and therefore it causes no problem. Next, take $S = S_C + S_D$, and consider the interface where S_C and S_D are adjoining surfaces. The contribution to δ along the interface from both S_C and S_D vanishes if $\partial u_i^R / \partial x_1$, ϕ , and ϕ_F are continuous across the interface; this follows from the fact that n_1 and T_i^R are continuous in magnitude at the interface but have opposite signs on S_C and S_D . Consequently, if the transition between a damaging process and a constant damage process is sufficiently smooth Eqns. (8) and (10) hold, and surface- independence of J_v , Eqn. (11), and path independence of J_v , Eqn. (12), exists; as an obvious generalization, S may surround an arbitrary number of connected zones with both types of processes.

It is important to recall that $\partial F_{cn} / \partial x_1 = 0$ is required in each constant damage process zone. For example, suppose the body is loaded and a damaging process zone with nonuniform damage is produced. Upon partial unloading, this zone may become a constant (with respect to time) damage process zone; but $\partial F_{cn} / \partial x_1$ and therefore δ for this zone would not in general vanish.

As an illustration of the use of this theory, consider the crack growth problem of Fig. 5 treated in the body of the report. Locally steady-state crack propagation is assumed. We suppose that a given material element in the process zone b undergoes a damaging process as the crack tip P approaches it, which changes to a constant damage

process by the time the left end of the failure zone, $\xi = \alpha$, arrives. Now, by definition, the steady-state condition is one in which each element in the constant damage part of the process zone has damage parameters which are independent of x_1 ; e.g., for the simple microcracking model $\partial F_m / \partial x_1 = 0$. Path independence in the process zone b then permits us to evaluate J_{fa} from J_{vb} (cf. Eqn. (61)) using the contour C_1 in Fig. 5. The result for J_{vb} is in Eqn. (68), where I_α is the line integral of $-\Phi_b$ at $\xi = \alpha$, Eqn. (70). The potential Φ_b is actually Φ_b^C if a constant damage process exists at $\xi = \alpha$ above and below the failure zone. In view of Eqn. (A.15), the integral, $-I_\alpha$, is the net work input to the process zone per unit volume integrated from the bottom to the top of the process zone. If there is no damage in the process zone ($P_n = 0$) and the pseudo strain energy density vanishes at $\xi = \alpha$, then $I_\alpha = 0$. However, dissipation would still exist for a viscoelastic material; it is reflected in the speed-dependent creep compliances which appear in Eqn. (71).

Energy release rate: Equation (17) applies with damage, even if the homogeneity condition in x_1 needed for J_v is not satisfied. This generalization may be shown by retracing the proof without damage, but using Φ^C and Φ^D for Φ where appropriate. Only the virtual work Eqn. (13) needs to be examined as the subsequent steps, Eqns. (14)-(16), are unaffected. Self-similar, virtual crack advancement is imposed through application of appropriate surface tractions to derive Eqn. (17), even though in an actual crack growth process this type of advancement may not occur.

The validity of Eqn. (13) may be established using the same procedure as for Eqn. (8) with damage. Namely, divide the body into

constant damage and damaging process regions. Inasmuch as a change in the displacement field occurs due to δa , thin layers of thickness on the order of δa have to be excluded; these are the layers in which the type of process changes during the crack advancement. However, if ϕ and δu_i are continuous in x_i , the work and pseudo strain energy associated with these layers is of order $(\delta a)^2$, i.e. thickness $\times \delta u_i$, and thus the layers do not affect the result in the limit $\delta a \rightarrow 0$; other contributions to Eqn. (13), including δW^R in Eqn. (16), are of order δa .

Generalization of the damage model: So far we have considered only the case in which all of the damage parameters satisfy $F_{cn} = F_n$ or else all are constant. The model may be easily generalized by adding one or more additional groups of terms to ϕ^C , Eqn. (A.1) or (A.7), with each group possibly representing a different physical mechanism. The regions of constant and varying damage for one group need not be at the same locations as those for another group. All of the results in the Appendix are valid except with this more general formulation the potential ϕ at any given time and location consists of a sum of potentials; some may be for damaging processes and others for constant damage processes.

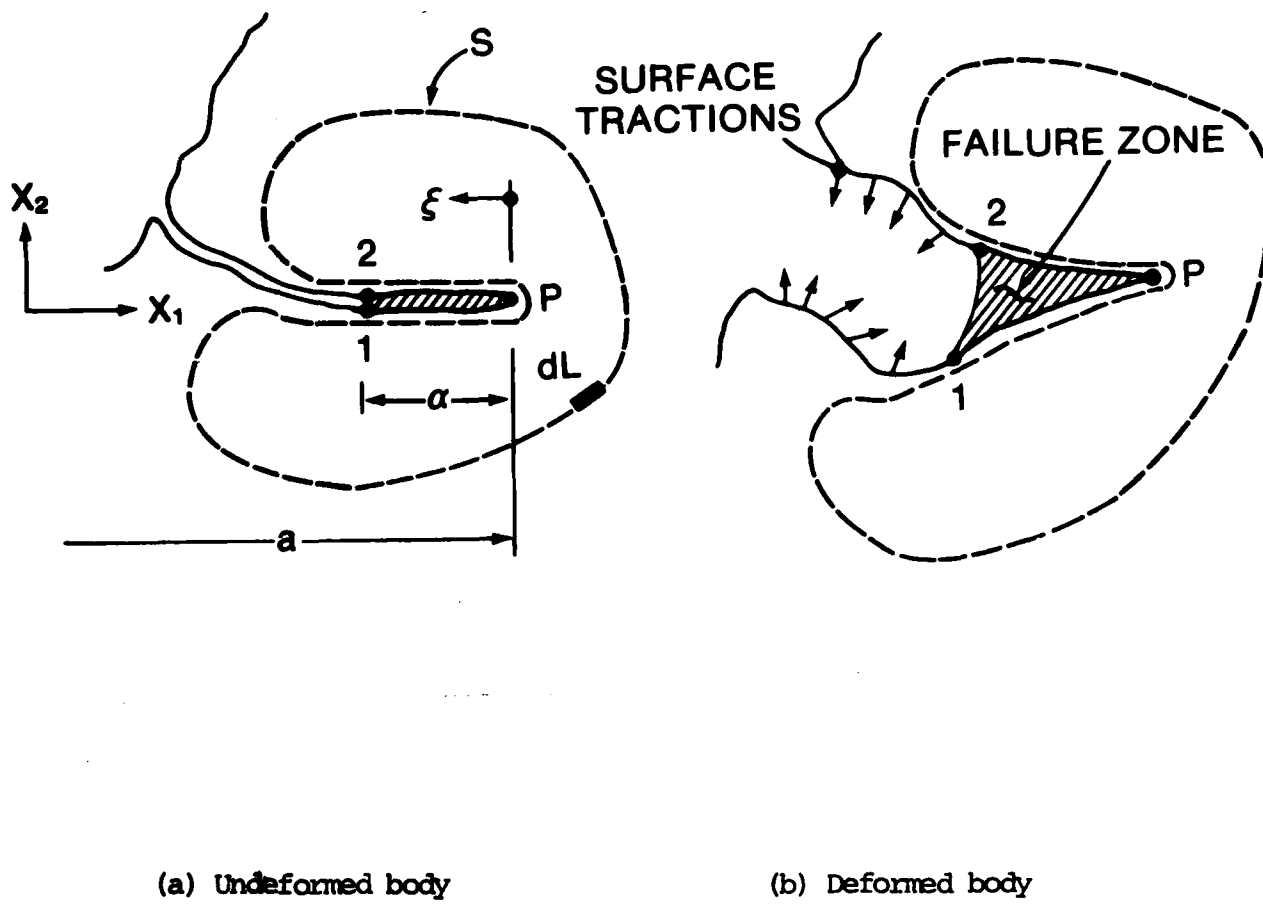


Figure 1. Cross-section of crack in neighborhood of the tip P. The region of intense damage and material separation processes is designated the failure zone, whose length is a in the undefomed body.

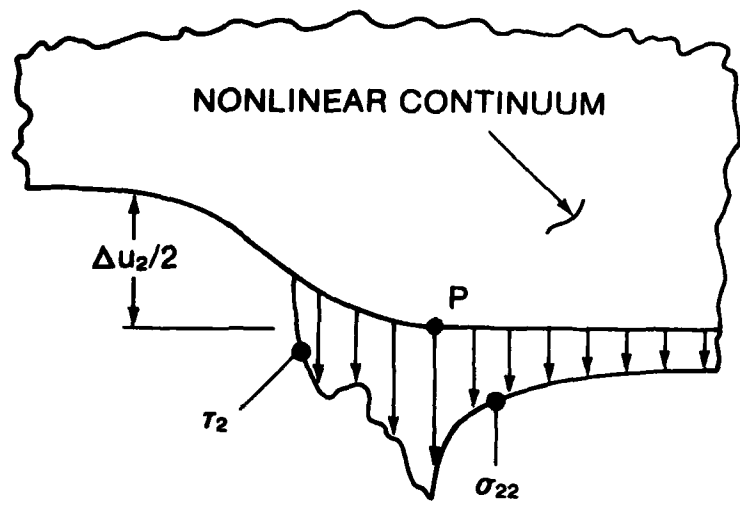


Figure 2. Normal stresses and opening displacement along continuum above local crack plane.

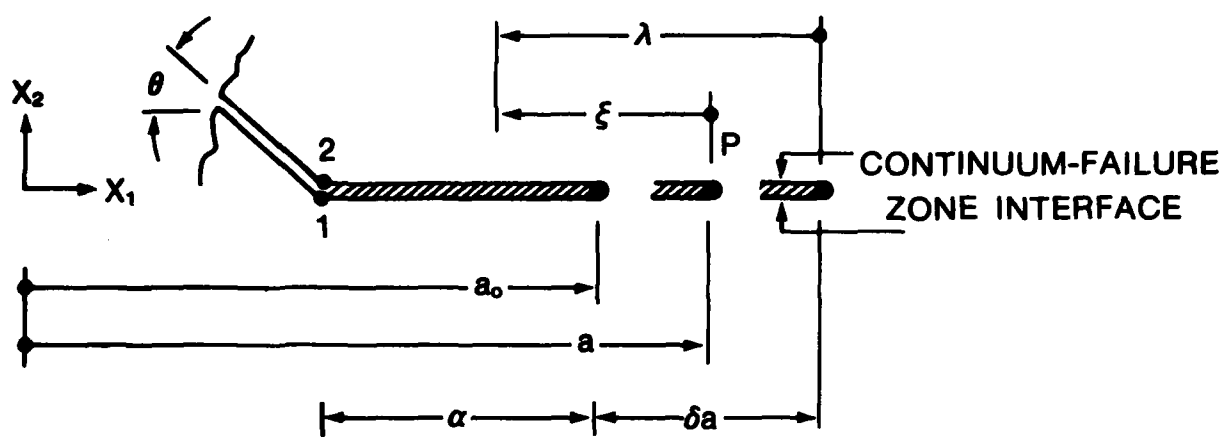


Figure 3. Virtual crack growth referred to undeformed body.

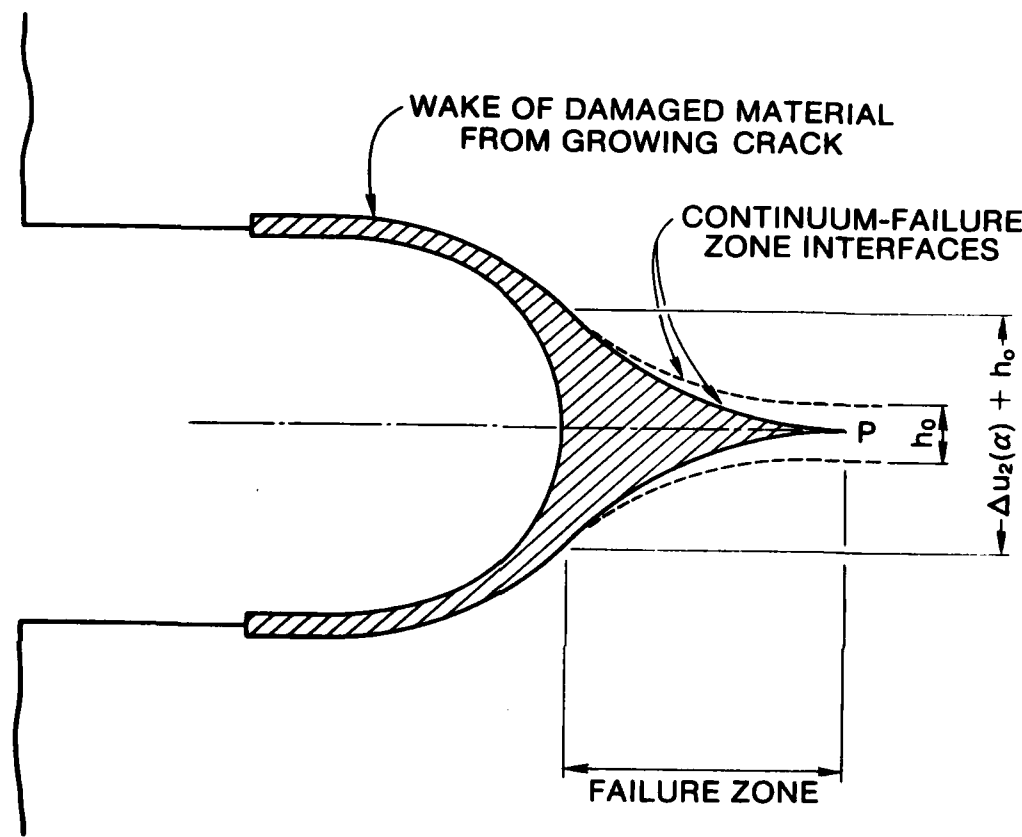


Figure 4. Deformed cross-section of crack in opening mode showing current interface between the continuum and all elements in the failure zone (—), and trajectory of the interface for the element currently at the left edge of this zone (----).

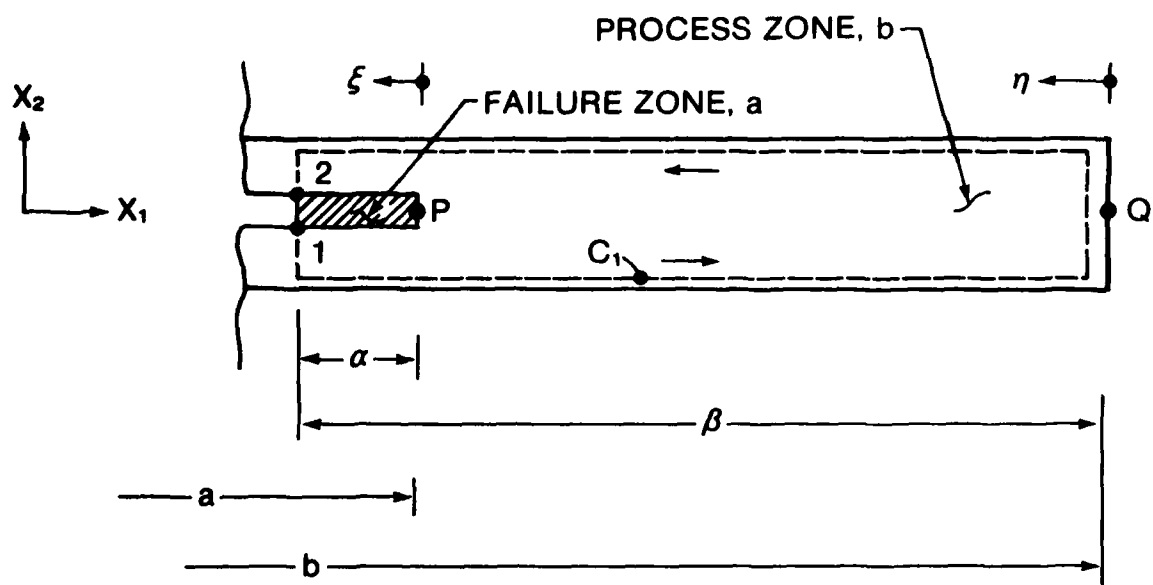


Figure 5. Cross-section of crack in undeformed body with crack tip P embedded in material layer (process zone) having deformation characteristics different from surrounding continuum. The failure zone is not necessarily centered.

Reprinted from CP832, A Bound Collection of Technical Papers

AIAA-83-0799-CP
Assessment of Chemical Cure-Shrinkage
Stresses in Two Technical Resins
B. Harper, D. Peret and Y. Weitsman

AIAA/ASME/ASCE/AHS
24th STRUCTURES, STRUCTURAL DYNAMICS
AND MATERIALS CONFERENCE

Lake Tahoe, Nevada
May 2-4, 1983

ASSESSMENT OF CHEMICAL CURE-SHRINKAGE
STRESSES IN TWO TECHNICAL RESINS

Brian Harper*, Dan Peretz** and Yechiel Weitsman[†]
Mechanics and Materials Center
Texas A&M University
College Station, Texas 77843

Abstract

This paper concerns the effects of chemical cure-shrinkage on the residual stresses which arise in geometrically constrained resins. Results are presented for the FM-73U adhesive, and for the Hercules 3502 resin used in graphite/epoxy composites. It is shown that when cure occurs above the glass transition temperature T_g , like in FM-73U, the stresses are negligible. On the other hand, when cure takes place below T_g , the chemical cure-shrinkage stresses are significant.

Introduction

This paper concerns the residual stresses which arise in geometrically constrained polymeric resins due to chemical shrinkage during cure. In addition, these stresses are compared with stresses at the end of cool-down.

The study involved two materials. The first was the unscrrimmed FM-73U[‡] adhesive, whose glass transition temperature is $T_g \approx 85^\circ\text{C}$ (185°F) and which was cured at $T_c = 120^\circ\text{C}$ (250°F). This material has a glassy modulus $E_g = 2000 \text{ MPa}$ (290 ksi), a rubbery modulus $E_r \approx 5 \text{ MPa}$ (1.5 ksi), and glassy and rubbery coefficients of thermal expansion $\alpha_g = 66 \times 10^{-6} \text{ m/m/}^\circ\text{C}$ and $\alpha_r = 10^{-4} \text{ m/m/}^\circ\text{C}$, respectively. Its chemical cure-shrinkage strain is unknown, but from available information on similar materials^{1, 2} we assumed it to be $\epsilon_{ch} = 5\%$, which is most likely an exaggerated value in the present case.

The second material was the Hercules 3502 resin, which is widely used in graphite/epoxy composites. For this material the glassy modulus has an approximate value of $E_g = 2900 \text{ MPa}$ (425 ksi) and the coefficient of thermal expansion is $\alpha = 30 \times 10^{-6} \text{ m/m/}^\circ\text{C}$. This material is cured at $T_c = 180^\circ\text{C}$ (355°F), which is below its glass transition temperature $T_g \approx 230^\circ\text{C}$ (450°F).

Our approach is basically experimental, with calculations based on simple beam-theory. The main purpose of this investigation is to demonstrate a simple method to assess the significance of chemical cure-shrinkage effects.

Experimental Procedure

The assessment of cure shrinkage effects was provided by strain measurements in a laminated beam formed by pouring the resin on a 2024 T3 aluminum coupon. A narrow dam of soft cork was built around the edges of the aluminum coupon to prevent resin spillage. Two "Micro Measurement" strain gages were attached to both faces of the aluminum coupon and, after placing a resin layer of a predetermined thickness on top of the aluminum, the laminate was placed in a curing oven and heated to the cure temperature T_c . For the 3502 resin $T_c = 180^\circ\text{C}$, while for FM-73U adhesive $T_c = 120^\circ\text{C}$. A sketch of the experimental set-up is shown in Fig. 1.

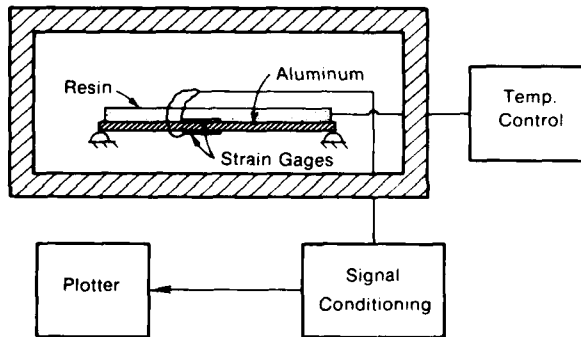


Fig. 1 A schematic drawing of the experimental set-up.

It should be noted that the 3502 resin was first placed in a vacuum oven at 110°C (230°F) for about 30 min. until removal of all visible air bubbles. At that stage the resin was liquid-like and could be poured on top of the aluminum coupon. The cure time was six hours for the 3502 resin and one hour for the FM-73 adhesive.

Upon termination of cure the coupon was cooled down gradually to room temperature of 25°C (77°F). It should be noted that in the case of FM-73U the cooling passed through the glass-transition temperature $T_g = 85^\circ\text{C}$, while for the 3502 resin all temperatures were below its T_g of 230°C .

Fig. 2 (a, b, c) show top, side and bottom views of a typical test specimen after cure and cool-down.

*Graduate Student

**Visiting Scientist, on leave from the Armament Development Authority, Israel

[†]Professor

[‡]The letter U designates an "Unscrrimmed" adhesive



(a)



(b)



(c)

Fig. 2 A laminated polymer/aluminum coupon:
(a) top, (b) side, (c) bottom views.

The readings of both strain gages were recorded throughout the curing and cooling process. Schematic charts are shown in Fig. 3. These "raw data" charts included the effect of aluminum thermal strains as well as the yet uncalibrated thermal effects on the strain gage readings. Those effects were determined by recording strain readings on aluminum coupons undergoing the same temperature excursions as our test specimens, but in the absence of resin. Subtracting "dummy" effects we obtained the stress induced readings.

The dimensions of the aluminum coupons were 8" x 0.8" x 0.038" for the FM-73 adhesive and 8" x 0.8" x 0.0261" for the 3502 resin. The dimensions of the cross-sections of both adhesive and resin varied, as indicated in Figs. 4-6.

Fig. 4 shows the calibrated records of the upper and lower strain-gages vs. temperature during cure and cool-down of laminated aluminum/FM-73U coupons. Figs. 5 and 6 show similar results for aluminum/Hercules 3502 coupons. Fig. 5 relates

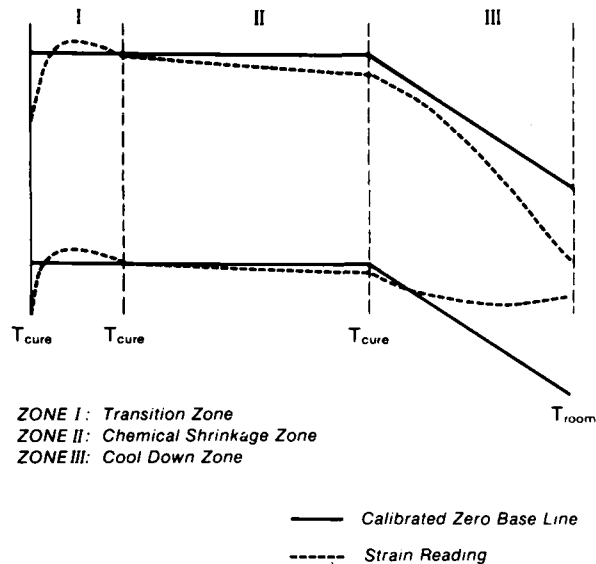


Fig. 3 Typical chart recordings of upper strain-gage (top) and lower strain-gage (bottom) with calibrated lines.

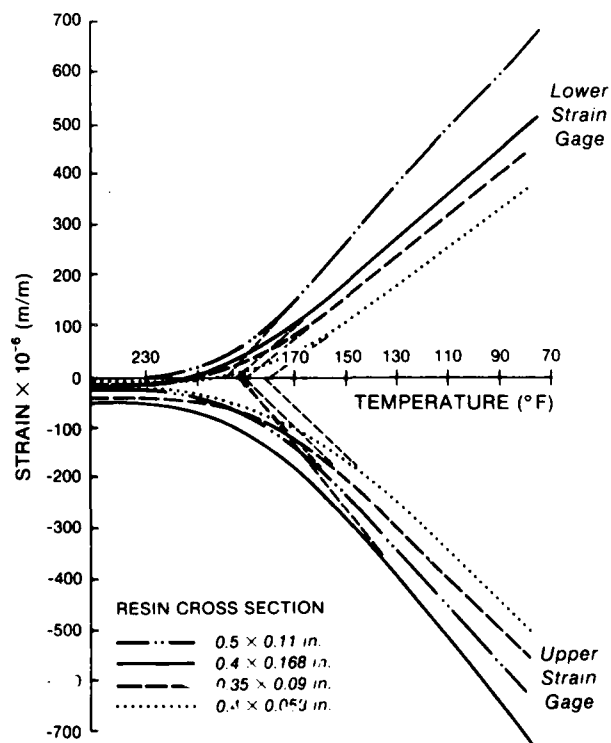


Fig. 4 Cure-shrinkage and thermal cool-down strains vs. temperature for coupons of different cross-sectional areas of FM-73U adhesive. (Areas indicated in figure)

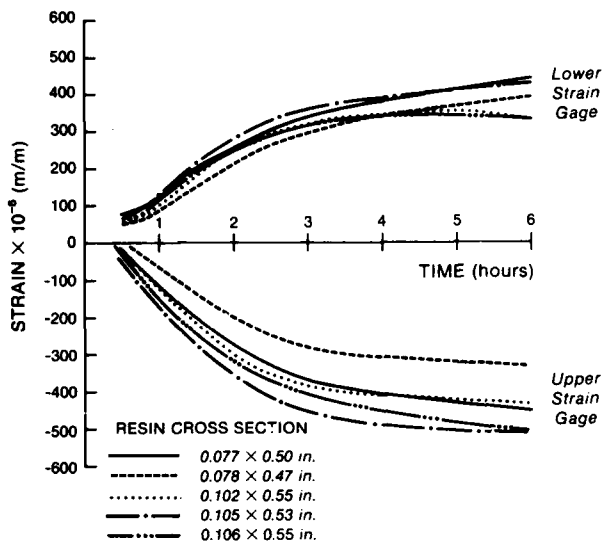


Fig. 5 Cure-shrinkage strains vs. time, measured at $T = 350^{\circ}\text{F}$, for coupons with several cross-sectional areas of the Hercules 3502 resin. (Areas indicated in figure)

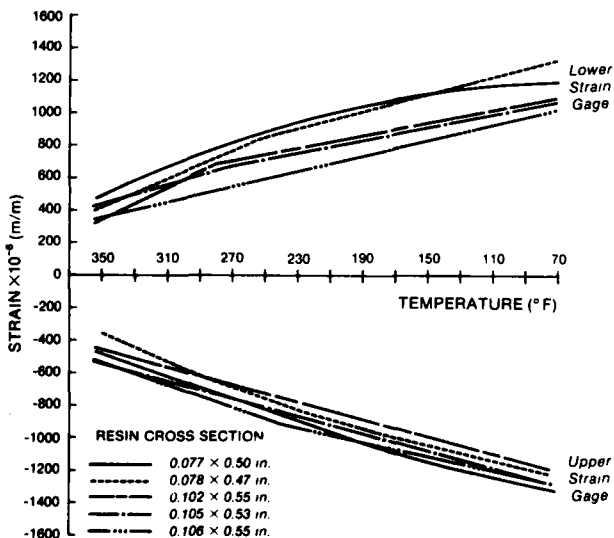


Fig. 6 Thermal cool-down strains vs. temperature for coupons with several cross-sectional areas of the Hercules 3502 resin. (Areas indicated in figure)

the strain records vs. time at the cure temperature of 350°F while Fig. 6 exhibits strains vs. temperature during cool-down. The cross-sectional dimensions of adhesive and resin are listed within Fig. 4-6.

In subsequent tests the temperature was recycled back up to the cure temperature T_c and down to room temperature. Typical calibrated strain-gage readings are shown in Fig. 7 for the FM-73U adhesive and in Fig. 8 for the 3502 resin.

The close reproducibility of the strain reading indicates that, for both materials, cure was practically complete during its original stage and shows that viscoelastic effects during cool down are insignificant.

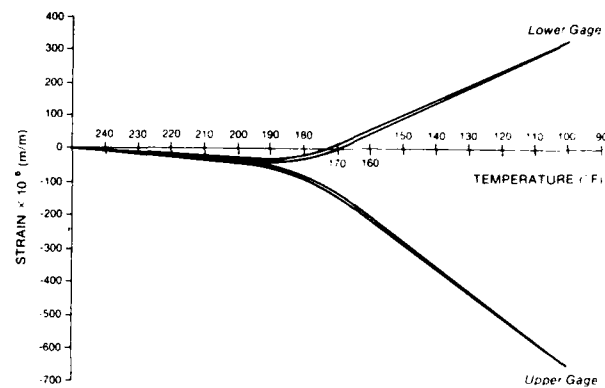


Fig. 7 Cure-shrinkage and thermal strains vs. temperature due to thermal cycling of an FM-73U/Aluminum coupon.

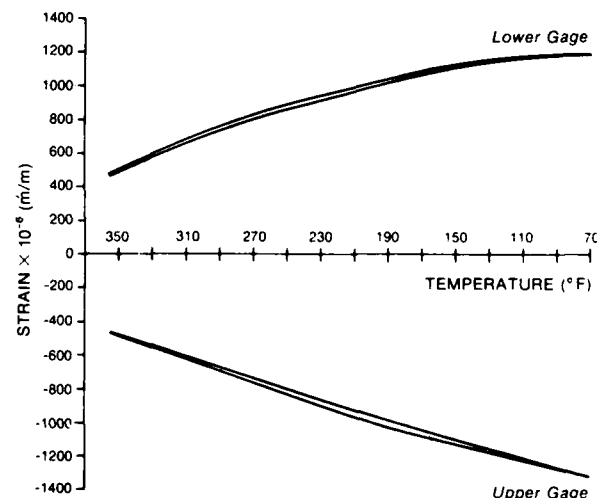


Fig. 8 Cure-shrinkage and thermal strains vs. temperature due to thermal cycling of an Hercules 3502/Aluminum coupon.

An Elastic Laminated Beam Model

Consider the laminated beam shown in Figure 9. Let ϵ denote the shrinkage strain of an unrestricted resin. In the laminated beam the deformation of the resin is constrained by the aluminum. As the resin contracts during cure it induces an eccentric compressive force on the laminated beam, causing both normal and bending strains in the resin and aluminum layers. In keeping with classical beam theory we assume that the bending strains vary linearly across the thickness of the beam, resulting in a piecewise linear stress distribution.

AD-A134 059

RESEARCH ON COMPOSITE MATERIALS FOR STRUCTURAL DESIGN

3/3

(U) TEXAS A AND M UNIV COLLEGE STATION MECHANICS AND
MATERIALS RE. D ALLEN ET AL. APR 83 MM-4665-83-4

UNCLASSIFIED

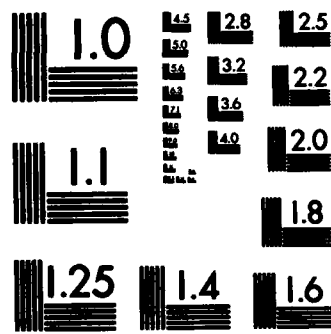
AFOSR-TR-83-0861 F49620-82-C-0057

F/G 11/9

NL

END

FILMED
4/11/83



MICROCOPY RESOLUTION TEST CHART
NATIONAL BUREAU OF STANDARDS-1963-A

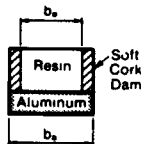
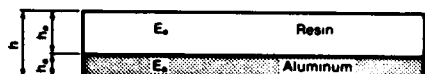


Fig. 9 Geometry of the laminated beam (coupon).

Let E_a and E_e denote aluminum and resin moduli, respectively. Also let ϵ and k be strain and curvature, and σ_a , σ_e designate the aluminum and resin stresses. Finally, let z denote the thickness coordinate, measured from the yet unknown position of the neutral axis of the laminated beam. Elementary calculations then yield

$$\epsilon = -\rho e / (1+\rho) - zk \quad (1)$$

$$\sigma_a = -(\frac{\rho e}{1+\rho} + zk) E_a \quad (2a)$$

$$\sigma_e = (\frac{e}{1+\rho} - zk) E_e \quad (2b)$$

The requirement that the net normal force on the beam vanishes determines the location of the neutral axis. Measured from the bottom face of the beam its value z_b is given by

$$z_b = \frac{1 + (2 + h_e/h_a)\rho}{1+\rho} \frac{h_a}{2} \quad (3)$$

In eqns. (1)-(3)

$$\rho = \frac{E_e h_e b}{E_a h_a b} \quad (4)$$

Furthermore, it can be shown that the moment in the aluminum due to the eccentricity introduced by the shrinkage of the resin is

$$M = \frac{1}{3} kf \quad (5)$$

where

$$k = \frac{3}{2} \frac{E_e h_e b e h}{(1+\rho) f} \quad (6a)$$

and

$$f = E_a h_a b_a \{ h_a^2 + 3z_b^2 - 3h_a z_b + \rho [h_e^2 + (h_a - z_b)^2 + 3h_e (h_a - z_b)] \} \quad (6b)$$

Our purpose now is to relate the shrinkage strain e to the strains recorded by the gages attached to the upper and lower faces of the aluminum coupon, denoted by R_u and R_ℓ , respectively. From eqn. (1) we have

$$R_u = -\rho e / (1+\rho) - k(h_a - z_b) \quad (7)$$

$$R_\ell = -\rho e / (1+\rho) + kz_b \quad (8)$$

Subtracting (7) from (8) we obtain

$$k = (R_\ell - R_u) / h_a \quad (9)$$

Combining eqns. (6) and (9), and expressing z_b in terms of ρ by eqn. (3) we get

$$\rho = \frac{1}{6} (R_\ell - R_u) \frac{h_a}{h} \frac{e}{\rho(1+\rho)} \quad (10)$$

$$\text{In (10), } g = 1 + A\rho + B\rho^2 + C\rho^3$$

$$\text{where } A = 5 + 6n + 4n^2, \quad B = 4 + 6n + 5n^2, \quad C = n^2$$

$$\text{with } n = h_e/h_a.$$

Eqn. (10) thus relates e to ρ .

Note that ρ can be determined by two different methods. If both moduli E_e and E_a are known, then ρ is given directly by eqn. (4). On the other hand, if E_e is unknown then ρ can be evaluated from the upper and lower strain-gage reading R_u and R_ℓ by manipulation of eqns. (7) and (8). In that case we obtain

$$-\frac{R_\ell}{R_u} = \frac{A_0 + A_1\rho + A_2\rho^2 - n^2\rho^3}{B_0 + B_1\rho + B_3\rho^2 + n^2\rho^3} \quad (11)$$

$$\text{where, in (11), } A_0 = 2 + 3n, \quad A_1 = 4 + 6n - n^2,$$

$$A_2 = 2 + 3n - 2n^2, \quad B_0 = 4 + 3n, \quad B_1 = 8 + 6n + n^2,$$

$$B_2 = 4 + 3n + 2n^2 \text{ and } n = h_e/h_a, \text{ as before.}$$

The determination of ρ in eqn. (11), in terms of known R_ℓ/R_u , is accomplished numerically, for instance by Newton's method of tangents. With ρ known, E_e can be determined from eqn. (4) and the shrinkage strain e from eqn. (10).

Significant simplifications occur in eqns. (10) and (11) when $\rho \ll 1$, like in the case of FM-73U (but not for the 3502 resin). In that circumstance eqns. (1) through (11) reduce to

$$z_b = h_a/2 \quad (12a)$$

$$M \approx \frac{1}{12} k E_a b_a h_a^3 \quad (12b)$$

$$k \approx 6h\rho e/h_a^2 \quad (12c)$$

$$R_\ell \approx \rho e (-1 + 3h/h_a) \quad (12d)$$

$$R_u \approx \rho e (-1 - 3h/h_a) \quad (12e)$$

There exists, nevertheless, an inherent difficulty in employing eqns. (12) if E_e (and thus ρ) is not known. This difficulty is due to the fact that in those equations the product (ρe) is lumped together and thus those two unknowns cannot be separated from each other.

Addition and subtraction of (12d) and (12e) yield

$$\rho e = -(R_\ell + R_u)/2 \quad (13a)$$

and

$$\rho e = \frac{h_a}{h} (R_\ell - R_u)/6 \quad (13b)$$

Of the two alternatives, eqn. (13b) is much more reliable. This is due to the fact that R_f and R_u are of opposite signs, so that even small errors in those individual readings can result in a gross mistake when using eqn. (13a). On the other hand, if E_e is not known from an independent experiment then even the use of the more detailed equations (1)-(11) poses a difficulty. This is due to the fact that eqn. (11) employs the ratio R_f/R_u , which may accumulate errors in these individual recordings.

Consequently, we shall resort to independent data on the moduli E_e of the resins and determine ρ from eqn. (4). Equations (10) or (13b) will then be used to evaluate e , while eqns. (11) or (13a) will be employed as a partial check on our results.

Determination of Resin Moduli

As noted in the previous section, the utilization of the strain-gage records R_u and R_f in the context of laminated beam theory may be very sensitive to experimental error if both resin shrinkage e and resin modulus E_e are unknown.

Consequently, the moduli E_e of both the FM-73U adhesive and the Hercules 3502 resin were determined from independent tests. Of these two materials the FM-73U presented a more complicated problem, because the temperature excursion undergone by that adhesive carried it from its liquid and rubbery stages above T_g down to a glassy state below T_g . On the other hand, the Hercules 3502 resin was processed entirely at temperatures below its T_g . For temperatures below T_g , the glassy moduli for both materials were obtained in experimental programs which provided complete viscoelastic characterizations of those polymers.³ These characterization schemes involved creep and recovery tests at several temperature levels, supplemented by sharp temperature-drop tests ("T-Drop" tests). An outline of such generalized characterization schemes appeared recently.⁶

Both materials exhibited time-dependent, viscoelastic behavior. However, in the context of the present work, which aims at providing an assessment of the relative significance of chemical cure-shrinkage on residual stresses, the detailed variations in the relaxation moduli with time are of secondary importance. Consequently, we approximated those moduli by constants, and their reasonable average values were $E_e = 2900$ MPa (425 ksi) for the Hercules 3502 resin and $E_e = 2000$ MPa (290 ksi) for the FM-73U adhesive. The modulus of the aluminum was $E_a = 73,700$ MPa (10,700 ksi). To assess the response of the FM-73U adhesive during cure we conducted several stress-relaxation experiments at 100°C and 120°C. In those tests stresses in "neat" coupons of adhesive material were recorded vs. time due to the sudden application, and subsequent maintainance, of strains ϵ_0 of magnitude 2.5% and 5%. Results are shown in Fig. 10. We observed that, after an abrupt sharp drop, the rubbery modulus approached an equilibrium value of about 5 MPa.

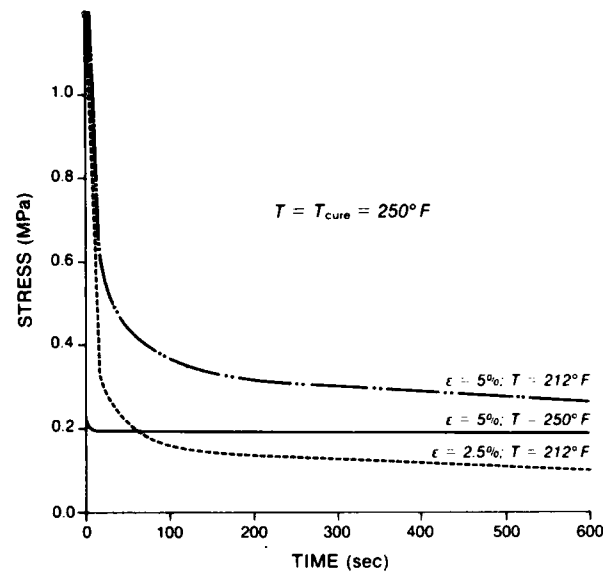


Fig. 10 Stress-relaxation data for a "neat" FM-73U coupon at three temperature and strain levels.

Assessment of Cure-Shrinkage Effects

Consider first the FM-73U adhesive. The process undergone by this material can be viewed as occurring in three stages. In the first stage, whose duration t_{ch} was not clear, the liquid-like material had a relaxation modulus $E_{ch}(t)$ and it underwent chemical changes. In the second stage, the material was above T_g and it had a rubbery modulus $E_r(t)$ like that shown in Fig. 10. This stage lasted until time t_g , when cool-down began and the temperature T_g was encountered. The third stage was the glassy state at temperatures below T_g , characterized by the glassy modulus $E_g(t)$.

A viscoelastic formulation for the viscoelastic stress σ in the adhesive under complete in-plane constraint reads

$$(1-v)\sigma(t) = \int_0^{t_{ch}} E_{ch}(t-\tau) \frac{d\epsilon_{ch}(\tau)}{d\tau} d\tau + \int_{t_{ch}}^{t_g} E_r(t-\tau) \frac{d\epsilon(\tau)}{d\tau} d\tau + \int_{t_g}^t E_g(t-\tau) \frac{d\epsilon(\tau)}{d\tau} d\tau \quad (14)$$

In (14), v designates the Poisson's ratio of the FM-73U adhesive.

Furthermore, under complete in-plane constraint the strains $\epsilon(t)$ for $t > t_{ch}$ are the thermal strains $\epsilon(t) = \alpha T(t)$ where α and T are the coefficient of thermal expansion and temperature difference, respectively. Consider the highly exaggerated circumstance that $\epsilon_{ch} = 5\%$ occurs at the fully developed rubbery modulus E_r and discard all relaxation effects in eqn. (14). Then

$$(1-v)\sigma = E_r[\epsilon_{ch} + \alpha_r(T_{cure} - T_g)] \quad (15)$$

Considering $E_r = 5$ MPa, $\epsilon_{ch} = 5\%$, $\alpha_r = 10^{-4}$ m/m/°C,

$\nu = 0.35$, $T_{\text{cure}} = 120^\circ\text{C}$ and $T_g = 85^\circ\text{C}$ we obtain
 $\sigma = 0.41 \text{ MPa}$.

For purposes of comparison, employ an approximated version of eqn. (14) to evaluate the stress at the end of cool-down, namely

$$(1-\nu)\sigma = E_r[\epsilon_{\text{ch}} + \alpha_r(T_{\text{cure}} - T_g) + E_g \alpha_g (T_g - T_R)] \quad (16)$$

where, in (16) $E_g = 2000 \text{ MPa}$, $\alpha_g = 66 \times 10^{-6} \text{ m/m}^{\circ}\text{C}$, and $T_g - T_R = 60^\circ\text{C}$. Then $\sigma = 12.4 \text{ MPa}$.

It is seen, then even under highly exaggerated assumptions the cure shrinkage effects contribute less than 4% to the total residual stress. A more accurate evaluation of stresses can be obtained by relating the bending moment in the laminated coupon to temperature, through a conversion of the strain-gage readings. Since for the FM-73U adhesive typical value of ρ are $\rho = 0.03$, we can employ the simplified equations (12). This results in a plot shown in Fig. 11*. Comparing the values of moments at 185°F and 77°F we note that the chemical cure shrinkage effects in FM-73U contribute about 3-4% to the residual stress at the end of cool-down, in agreement with our conclusions from eqns. (15) and (16). The chemical effects can thus be neglected.

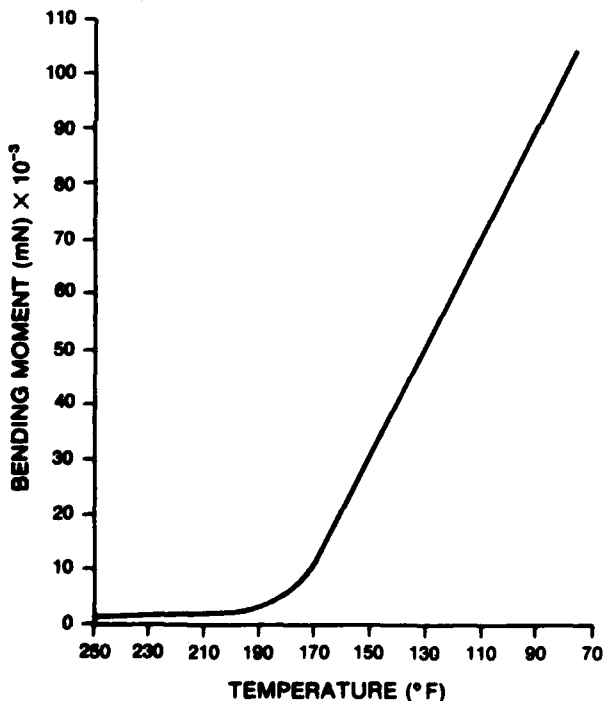


Fig. 11 Computed values of bending moment vs. temperature in an FM-73U/Aluminum coupon. Note the comparatively small values due to cure-shrinkage ($T > T_g = 185^\circ\text{F}$)

Consider now the Hercules 3502 resin. Since in this case $\rho \sim 0.1$ and $h_e/h_a \sim 4$ we refrained from using the approximate equations (12), and employed

the more accurate expressions (1)-(11). As noted earlier we took the modulus of this material to be $E_e = 2900 \text{ MPa}$, thus determining the value of ρ in eqn. (4) for all laminated coupons, whose dimensions are listed within Figs. 5 and 6. With ρ known, the shrinkage strain e at the end of cure can be evaluated from the strain-gage readings according to eqn. (10). Alternately, we employed (10) and (11) simultaneously to determine both E_e and e . Due to the error sensitivity of eqn. (11) we can expect disagreement between both approaches.

Employing the data plotted in Fig. 5 we obtain the values of E_e and e listed in Table 1 below:

Resin Cross Section (in x in)	1st Method		2nd Method	
	$E_e = 2900 \text{ MPa}$ e from eqn. (10)	$e(\text{m/m})$	$E_e(\text{MPa})$	$e(\text{m/m})$
.077 x .5	.00277		4750	.00182
.078 x .47	.00218		9090	.00232
.102 x .55	.00257		3220	.00254
.105 x .53	.00332		940	.00392
.105 x .55	.00298		3450	.00295
Average Values	.00276		4130	.00271
	$\pm .00043$		± 2800	$\pm .00079$

Table 1: Values of cure-shrinkage strain e , from data on five Hercules 3502 coupons, determined by two methods.

Note that in spite of the substantial variations in the calculated values of E_e and e from the individual tests, the predicted average value of the cure shrinkage e is roughly the same in both methods. We took $e = 0.27\%$.

The average stress in the resin is given by

$$\sigma_e^{\text{avg}} = \frac{E_e}{h_e} \int_{\text{resin thickness}} \left(\frac{e}{1+\rho} - kz \right) dz \quad (17)$$

which reduces to

$$\sigma_e^{\text{avg}} = \frac{E_e}{1+\rho} \left(e - \frac{1}{2} kh \right) \quad (18)$$

The average stress in the resin at the end of cure and during subsequent cool-down is shown in Fig. 12. The results were derived for $E_e = 2900 \text{ MPa}$ (assumed known). These calculations indicate that the average stress in the resin due to cure shrinkage is about 30% of the average residual stress at room temperature after termination of cool-down.

*We could, in fact, show four plots in Fig. 11, corresponding to the four coupons and four sets of strain-gage readings shown in Fig. 4. The conclusions would have been the same.

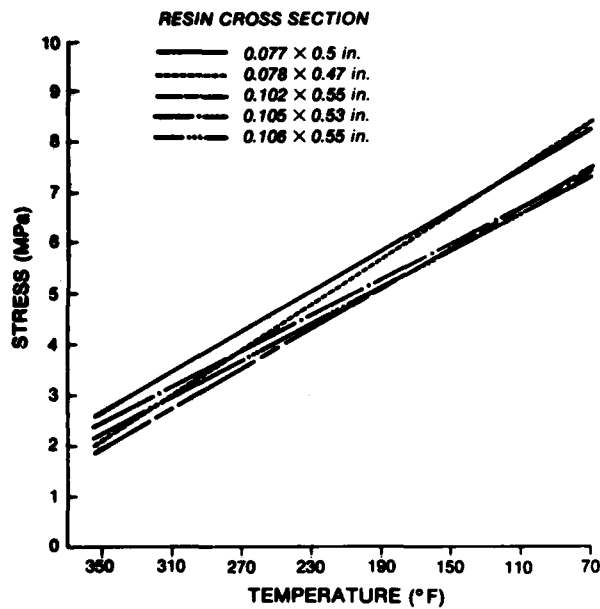


Fig. 12 Computed values of average-stresses in several Hercules 3502/aluminum coupons (with cross-sectional areas given in figure), vs. temperature. Values at $T = 350^{\circ}\text{F}$ are stresses due to cure-shrinkage, subsequent values include effects of thermal cool-down.

References

1. Bolotin, V.V. and Bolotina, K.S.: "Shrinkage of Epoxy Cements During Hardening," Translated From Mekhanika Polymerov, No. 1, pp. 178-181, January-February 1972.
2. Murzakhanov, G. Kh. and Tikhonov, V.A.: "Accumulation of Shrinkage Stresses in Fibrous Composites with Regular Structure," Translated From Mekhanika Polymerov, No. 3, pp. 409-415, May-June 1976.
3. Peretz, D. and Weitsman, Y.: "The Non-Linear Viscoelastic Characterization of FM-73 Adhesive," Journal of Rheology, Vol. 26, No. 3, pp. 245-261 (1982).
4. Peretz, D. and Weitsman, Y.: "The Non-Linear Thermoviscoelastic Characterization of a Structural Adhesive," Journal of Rheology, Forthcoming (1983).
5. Harper, B.D.: Ph.D. Thesis, Texas A&M University, Forthcoming (1983).
6. Weitsman, Y.: "On the Thermoviscoelastic Characterization of Adhesives and Composites," Progress in Science and Engineering of Composites. Proceedings of the 4th International Conference on Composite Materials. Tokyo, Japan. T. Hayashi, Editor. Vol. 1, pp. 771-779 (1982).

Conclusions

An experimental study was conducted to assess the effects of chemical cure-shrinkage on residual stresses in two polymeric adhesives. The experimental results were analyzed by means of a simple, laminated beam theory. In the case of the FM-73U adhesive, which was cured above its glass transition temperature, it was found the chemical cure-shrinkage contributed no more than 3-4% to the residual stresses after cool-down. On the other hand, in the case of the Hercules 3502 resin, which was cured below its glass transition temperature, the effects of chemical shrinkage contributed about 30% to the total residual stress at the termination of cool-down.

It should be noted that our experiments were performed under in-plane geometric constraints, allowing volumetric strains to develop freely in the polymers. Such in-plane constraints seem to apply in composite laminates and some adhesive joints. However, in adhesive joints involving thick adherends the geometric confinement of the polymer may restrict its volumetric deformation. In such circumstances the effects of chemical cure-shrinkage may become significant even in the FM-73U adhesive.

Acknowledgments

This work was supported, in part, by Contract No. F-33615-79-C-5117 from the Materials Laboratory, AFVAL and in part, by Contract F49620-82-C-0057 from the Air Force Office of Scientific Research (AFOSR).

On the Thermoviscoelastic Characterization of Adhesives and Composites

Y. Wallenius

Mechanics & Materials Center, Civil Engineering Department, Texas A&M University, College Station, Tx 77843,
U.S.A.

ABSTRACT

This paper presents a method to characterize the time and temperature behavior of adhesives and polymeric resins within the linear range of stress-strain response.

The method involves an experimental scheme to determine in a non-ambiguous way if the time-dependent behavior is thermoreologically simple or complex and provides suitable analytical expressions to predict the behavior in either case. Some experimental results are discussed and the differences between the predictions of the thermoreologically simple and complex models are assessed for the particular data at hand.

The subject is related to the design of geometrically stable structures.

NOMENCLATURE

$a = a(T)$	Shift factor function
$D = D(c)$	Creep compliance
$D_0 = D_0(T)$	Term in power-law creep
$D_1 = D_1(T)$	Heaviside step function
$h = h(T)$	Horizontal shift function
n	Power term in power-law creep
r	Rate of temperature-rise
s_0, s_1, s_2, s_3	Empirical numerical factors
t	Time
T	Temperature
T_g	Glass transition temperature
T_R	Reference temperature (where $a=h=v_1=v_2=v=1$)
$v_1(T), v_2(T)$	Vertical shift functions ($v_1=v_2=v$)
a	Coefficient of thermal expansion
c	Strain
c_c	Creep strain
$c_r(T, c)$	Recovery strain (after unloading)
J	Time-dependent portion of c
τ, τ_c	Stress
	Reduced times

It is well known that polymeric materials creep under steady loads (1). These recently such behavior was observed for fibrous composites loaded in shear and transversely to the fiber directions (2), (3), (4).

It is commonly recognized that at elevated temperatures the creep is reduced and accelerated. It being generally assumed that the enhancement is due to modulus softening while the acceleration is caused by a reduction in viscosity. At temperatures above the glass-transition temperature, T_g , the thermal effects on deformation are almost exclusively related to reduction in viscosity and can thereby be represented strictly by "telescoping" the time-scale for creep. Mechanically, this means that if at some temperature, $T = T_0 > T_g$, the creep strain is given by $\epsilon = \sigma_0 F(t)$ then at $T = T_0 > T_g$, $\epsilon = \sigma_0 F(T) t$. The empirically determined function $\sigma(t)$ is called the "shift-factor" function because when isothermal creep data are plotted against $\log t$, one obtains $\epsilon(t, \log t) = \epsilon(T_0, \log t + \log \sigma(t))$. Namely, $\epsilon(t, \log t)$ and $\epsilon(T_0, \log t)$ are positioned to the left of $\epsilon(T_0, t)$. Usually, for $T > T_g$, $\epsilon(t, t)$ is in the form of $\log \epsilon$ vs. $\log t$.

The above mentioned type of response is denoted as "thermo-rheologically simple", or alternately referred to as the "time-temperature analogy". It has the appeal of simplicity and also the important advantage that it enables the solution of many boundary-value problems in linear viscoelasticity by direct reference to results from linear elasticity. For thermo-rheologically simple response, the so called "correspondence principle" applies to a wide class of problems.

A vast set of data were collected and reduced by means of the "time-temperature analogy", (1), (5) and employed in solving many boundary value problems (e.g. (6)). Schematically, such data appear in a form shown in Figure 1. At temperatures below T_g , thermal effects on modulus softening cannot always be neglected. This phenomenon is revealed by the fact that isothermal creep data at various temperatures are plainly not relocatable by a horizontal shift factor function $\sigma(T)$ alone. In several cases, it was noted that a relevant vertical shift (7)-(11). Schematically, such data appear in form like shown in Figure 2.

Finally, the creep of many polymers can be represented by the so-called "power law" (12)-(13). It turns out that in this case, isothermal creep data collected at various temperatures can be correlated by either horizontal or vertical shifts, or a combination of both, and it is not a-priori clear which correlation is correct.

The question of the proper form of data representation is of great practical importance for two reasons: (1) the correct form of the vertical and horizontal shift functions is necessary to calculate response under transient stresses and temperatures, (2) the correct expression for the horizontal shift factor is essential for predicting long-time response from short time data taken at elevated temperatures. This is due to the fact that time and temperature may be interchangeable only through the amount of shift which occurs parallel to the $\log t$ axis. The effects of the vertical shift must, of course, be also considered because they scale the stress effects.

This paper outlines an analytical scheme and experimental procedure to sort out the vertical shift, quantify the temperature dependent horizontal and vertical shifts, and determine their appropriate incorporation in a superposition-integral for the case of transient stresses and temperatures.

ANALYSIS

(a) The General Case

Consider isothermal creep data as shown in Figure 2 and assume that these data were fitted to form a continuous "master curve" so that the creep at some reference temperature, T_0 , can be extended and expressed by empirically determined functions $v(T)$ and $h(T)$ as follows:

$$\sigma(t) = \sigma_0 h(t) \quad (1)$$

$$v(t) = T_0 - (T_0 - T_d)h(t - t_1) \quad T_d > T_0 \quad (2)$$

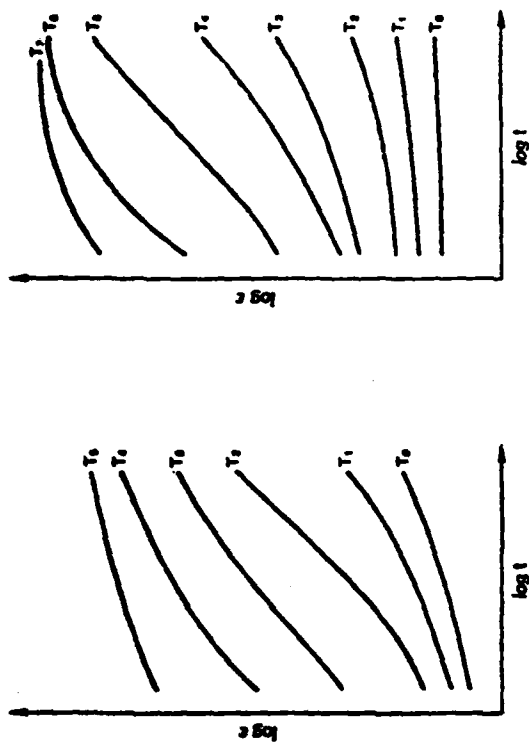


Figure 1. Isothermal data suitable for horizontal shifting alone (schematic).
 $\epsilon(t) = D(t, T) \epsilon_0 = v(T)h(t)t\epsilon_0$, where $D(t; T_0) = F(t)$.
 (1)

In (1), $v(T)$ and $h(T)$ are the vertical and horizontal shift factors, respectively, T is temperature and t is time.

The empirically determined function $h(t)$ can be used to correlate long-time creep at low temperatures from short-time, elevated temperature, isothermal data. However, form (1) is too ambiguous to predict response under transient temperatures. This can be seen by noting that under fluctuating temperatures and stresses, the integral

$$\epsilon(t) = v_1(T(t)) \int_0^t F(t(t) - \xi(\tau)) \frac{d}{dt}(v_2(T(\tau))\sigma(\tau)) d\tau \quad (2)$$

$$+ a[t(t) - T(0)]$$

with $\xi(t) = \int_0^t h(T(s)) ds$ will reduce to (1) in the isothermal case, with $\sigma(t) = \sigma_0 h(t)$, regardless of the functional forms of $v_1(T)$ and $v_2(T)$ as long as

$$v_1(T)v_2(T) = v(T) \quad (3)$$

It is seen that the function $v(T)$ alone does not suffice to characterize the viscoelastic behavior and additional experiments, beyond those of isothermal creep, are required to complete the task. Consider, therefore, creep experiments under constant loads continuing a sudden drop in temperature at time $t = t_1$, namely

Simplifying (4) in (2) we get

$$\epsilon(t) = v_1(T_0) \epsilon_0 (t, T_0) \epsilon_0, \quad 0 < t < t_1 \quad (5)$$

$$\text{and}$$

$$\epsilon(t) = v_1(T_0) \epsilon_0 (t, T_0) \epsilon_0 + \alpha(T_0) (t - t_1) \epsilon_2(T_0) \quad (6)$$

$$- \gamma(T_0) (t - t_1) (v_2(T_0) - v_2(T_0)) \epsilon_0 \quad (7)$$

$$- \alpha(T_0 - T_0) \quad t > t_1 \quad (8)$$

$$\text{Let } T_0 = T_1 \text{ then, by hypothesis } v_1(T_0) = v_2(T_0) = h(T_0) = 1. \text{ Also denote}$$

$$T = T_0 \text{ then (6) reduces to}$$

$$\epsilon(t) = \epsilon_0 \{ [p_0(\epsilon_0) \epsilon_0 + t - t_1] - \gamma(t - t_1) \} \epsilon_0 + \gamma(t - t_1) \quad (9)$$

$$- \alpha(T_0 - T_0) \quad t > t_1 \quad (10)$$

In (6) and (7), α designates the coefficient of thermal expansion.

With $\epsilon(t)$ in (7) measured experimentally, $v_1(T)$ can be determined, since all other quantities in (7) are assumed known from isothermal data. Obviously, we get $v_1(T_0) = v(T_0) / v_2(T_0)$.

The temperature level T_0 can now serve as T_0 in eqn. (6) and thus obtain $v_2(T_0)$, whereby also $v_1(T_0)$, and so on. In such a manner, the form of $v_1(T)$ and $v_2(T)$ can be established.

(b) Power-Law Creep

Many polymeric resins and composites exhibit creep response that can be expressed as follows:

$$\epsilon(t) = [D_0(t) + D_1(\alpha(T)t)] \epsilon_0 \quad (11)$$

$$\alpha(t) = D_1(\alpha(T)t)^n \epsilon_0 \quad (12)$$

In view of (9), we get log-log plots as shown in Figure 3.

Substituting (4) in (2) we get

$\epsilon(t) = v_1(T_0) \epsilon_0 (t, T_0) \epsilon_0 + \alpha(T_0) (t - t_1) \epsilon_2(T_0) \quad 0 < t < t_1$

$\epsilon(t) = v_1(T_0) \epsilon_0 (t, T_0) \epsilon_0 + \alpha(T_0) (t - t_1) \epsilon_2(T_0) \quad t > t_1$

$\epsilon(t) = v_1(T_0) \epsilon_0 (t, T_0) \epsilon_0 - \gamma(T_0) (t - t_1) (v_2(T_0) - v_2(T_0)) \epsilon_0 \quad t > t_1$

Let $T_0 = T_1$ then, by hypothesis $v_1(T_0) = v_2(T_0) = h(T_0) = 1$. Also denote $T = T_0$ then (6) reduces to

$\epsilon(t) = \epsilon_0 \{ [p_0(\epsilon_0) \epsilon_0 + t - t_1] - \gamma(t - t_1) \} \epsilon_0 + \gamma(t - t_1) \quad (10)$

where

$\epsilon_0 = \theta^{1/n} [h(\theta)]^{1/n}$

with

$h(\theta) = \alpha(T) \theta$

Also, $v_1(T) = v_2(T) = h(T) = [a(T)]^{1/(1-n)}$ and we assume that $0 \leq q(T) \leq 1$. It can be readily observed that for $\alpha = \alpha(t)$ and $T = \text{const}$. (10) reduces to $\dot{\epsilon}(t) = D_1(\alpha(t)) \epsilon_0^n$ for \exists v_1, v_2, h and q . Similarly, isothermal behavior under fluctuating stress is insensitive to v_1, v_2, h and q .

As an aside, let us consider the case $\alpha = qh(T)$, but $T = T(t)$. Employing (10) with $q = 1$, i.e. only a horizontal shift, we get

$$\dot{\epsilon}(t) = D_1[\theta^{1/n} a(T(t)) \epsilon_0^n] \epsilon_0 = D_1[a(T(t))] \epsilon_0^n \frac{a(T(t))}{a(T(t)) \epsilon_0^n} \epsilon_0 \quad (12)$$

On the other hand, if we set $q = 0$, i.e. only vertical shift, we get

$\dot{\epsilon}(t) = D_1 v(T(t)) \epsilon_0^n = D_1 [a(v(t))] \epsilon_0^n \quad (13)$

All presently available data indicate that $a(T)$ increases monotonically with T . Therefore, comparing (12) and (13) we note that $\dot{\epsilon}(t) < \dot{\epsilon}(t)$ for all monotonically increasing temperature histories and $\dot{\epsilon}(t) < \dot{\epsilon}(t)$ for all decreasing temperatures.

Returning to our main theme, consider isothermal creep and recovery behavior. Namely, let $T = T_0 = \text{const}$.

$\dot{\epsilon}(t) = \alpha_0 [h(t) - h(t - t_1)] \quad (14)$

In view of (8) and (10) we obtain

$\epsilon_c = [h_0(T_0) + \alpha_0 [a(T_0)t]^n] \epsilon_0 \quad 0 < t < t_1 \quad (15)$

$\epsilon_c = [a(t_0)]^n [t^n - (t - t_1)^n] \epsilon_0 \quad t > t_1 \quad (16)$

From (15) and (16) it is possible to determine $D_0(T_0)$, D_1 , $a(T_0)$ and n according to well established procedures (11), (14), (15), (16).

Consider next creep under constant stress and temperature, followed by recovery after a simultaneous removal of the load and abrupt cool-down. Namely,

$$\alpha = \alpha_0 [h(t_1) - h(t - t_1)] \quad (17)$$

$$T = T_0 - (T_0 - T_R) \ln(t - t_1)$$

By hypothesis, $v_1 = v_2 = 1$ at $T = T_R$, whereby we obtain

$\epsilon_c = \ln \frac{v_2(T_0)}{v_2(T)} \{ [h(T_0)]^{t_1} - [t - t_1]^n - [1 - t_1]^n \} \epsilon_0 = \alpha(T_0 - T_R)$ (18)

Employing curve fitting routines, it is possible to determine $v_2(T)$ and $h(T_0)$ by matching (18) against recovery data. It is, of course, advisable to conduct tests with several time-intervals t_1 . With $a(T_0)$, $h(T_0)$, $v_2(T_0)$ known, it is possible to evaluate $v_1(T_0)$.

Abrupt variations in load and temperature obviously introduce transient effects. However, it appears possible to limit the duration of transients to

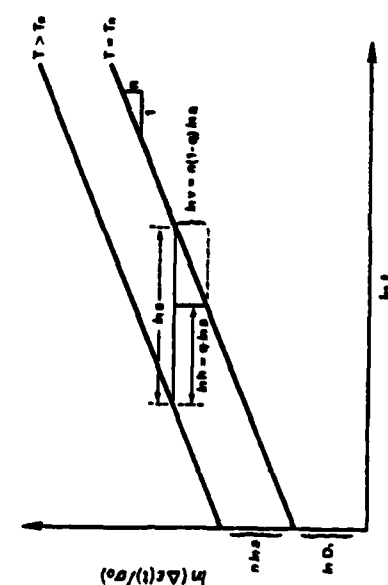


Figure 3. The time-dependent portion $\dot{\epsilon}(t)$ of the creep strain for a "power-law material", with power n , and the various possibilities of vertical and horizontal shifts.

stress 1000 MPa, by selecting sufficiently thin test specimens. With $\tau_1 = \tau_2$, and $\sigma = \sigma_0$, we can replace τ in (17) with $\tau_1 = \tau_2$ and τ_0 in (17) with τ_0 , and so on, to cover the range of temperatures of interest. In some the same manner as for the "general case",

EXPERIMENTAL, NUMERICAL COMPUTATIONS

Creep and recovery data were collected for Figure 3a. This is a rubber-particle reinforced epoxy cured at about 120°C, with $T_c = 150^\circ\text{C}$ and which found to be comonomer, with $a = 6.6 \times 10^{-3} \text{ MPa}^{-1}\text{K}^{-1}$. For stresses up to 20 MPa, the response is linear.

The experiments, which are described in full detail elsewhere, (11), (12) covered temperatures in the range 30°C-60°C. The measurements were recorded for $\tau = 0.45^\circ \times 0.07^\circ$ degrees with the aid of "TTS Series" strain gauges. Isothermal creep and recovery data were collected by means of creep frames at $T = 30^\circ\text{C}$, 40°C, 50°C, and 60°C. Abrupt cool-down tests were performed within an Instron environmental chamber attached to an INSTRON machine. Creep was recorded, typically, for 15 minutes and recovery during 10 additional minutes. The cool-down tests involved temperature drops between various combinations of the above-mentioned temperature levels. Cooling was accomplished by pumping pressurized CO₂ gas into the environmental chamber with concurrent heating of the chamber to counterbalance any over-cooling. The entire process was controlled manually, maintaining good control to within 20.5°C and limiting the transient state of strains to within 100 sec. The minimum amount of transients to such a short time span was accomplished by the judicious selection of 0.07°° stiffnesses for the gauges.

Each and every test was repeated five times to ascertain the reliability of the data. Scatter was limited to about 24%.

The data were reduced by means of a power-law expression and analysed according to the method described above. We obtained:

$$\begin{aligned} D_1 &= 29 \times 10^{-6} \text{ (with time measured in seconds), } a = 0.12 \\ D_0(\tau) &= 360 \times 10^{-6} [1 + 0.91(\tau - \tau_K)/\tau_K] (\text{MPa})^{-1}, \text{ with } \tau \text{ in degrees Kelvin and } \tau_K = 303^\circ\text{K}. \end{aligned}$$

Also, $h = \exp [30(\tau - \tau_K)/\tau_K]$, $v_1 = \exp [-s_1(\tau - \tau_K)/\tau_K]$, $v_2 = \exp [s_2(\tau - \tau_K)/\tau_K]$ with $s_0 = 40$, $s_1 = 8.5$, $s_2 = 12.12$.

Upon completion of the characterisation tests, we measured creep at $\sigma = 10 \text{ MPa}$ with linearly varying temperature $T = T_0 + 0.0083t$. The results are shown by the heavy, solid line in Figure 4.

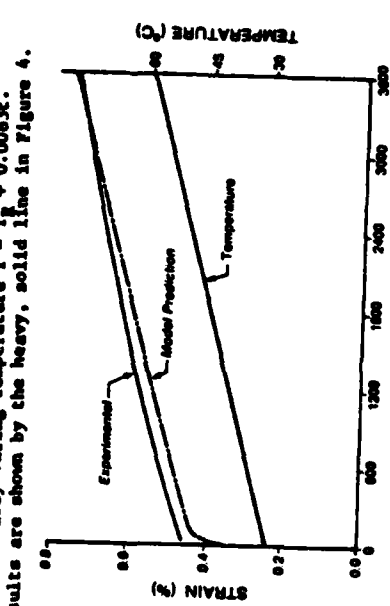


Figure 4. Creep at $\sigma = 10N(t) \text{ (MPa)}$ under linearly varying temperature $T = T_0 + rt$. Experimental results and theoretical predictions (thick and thin lines).

It is interesting to note that if the vertical shifts were erroneously discarded and replaced by an equivalent horizontal shift, namely if one takes $\sigma(\tau) = \exp[s_3(\tau - \tau_K)/\tau_K]$, then

$$v_1(\tau) = v_2(\tau) = 1$$

then the resulting expression for strain is

$$e(\tau) = (D_0(\tau(c)) + D_1(\tau(c))^a) \sigma_0 + a(\tau(c) - \tau_K)$$

yielding values of $e(c)$ almost indistinguishable from (19).

Similar circumstances occur whenever the temperature fluctuations are relatively slow, up to about 1-2°C/min. In all such cases, the errors involved by replacement of eqns. (20) instead of (10) are equivalent in magnitude to the data scatter.

On the other hand, under sharp temperature fluctuations, a deletion of the vertical shifts can lead to discrepancies of 25% - 30% in the predictions of creep strains. Such cases are shown in Figures 5, 7, and 8. In Figure 5, the strain due to $\sigma = \sigma_0 H(t)$ and $T = T_0 H(t) - T_K H(t - t_0)$ is shown vs. time t , $\sigma_0 = 10 \text{ MPa}$, $T_0 = 60^\circ\text{C}$, $T_K = 30^\circ\text{C}$ and $t_0 = 1500 \text{ sec}$. The results shown by solid lines incorporate both vertical and horizontal shifts, while the dotted lines are based on the horizontal shift only as given in (20).

Figure 6 shows a temperature profile T vs. time t used in evaluating the strain in Figure 7 and 8. The strain in Figure 7 is evaluated for one cycle $T(t)$ shown in Figure 6 followed by $T = T_K = 30^\circ\text{C}$ for $t \geq 4000 \text{ sec}$. The strain in Figure 8 corresponds to four cycles of the temperature profile $T(t)$ in Figure 6.

In both Figures 7 and 8, $\sigma = \sigma_0 H(t)$, $\sigma_0 = 10 \text{ MPa}$. The solid lines in Figures 7 and 8 correspond to both vertical and horizontal shifts while the dashed lines are computed on the basis of horizontal shifts only.

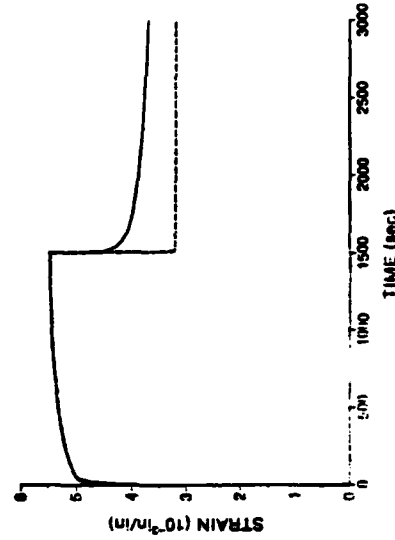


Figure 5. Creep at $\sigma = 10H(t) \text{ (MPa)}$ with temperature $T = T_0 - T_0 H(t) - (T_0 - T_0) H(t - t_0)$. Predictions based on horizontal and vertical shifts (solid line) and on horizontal shift alone (dashed line).

CONCLUDING REMARKS

This work demonstrated that isothermal creep data may be insufficient to characterise the thermo-viscoelastic response of polymers below T_g (unless it is possible to form master curves by horizontal shifts alone). In many cases, additional transient-temperature data are required for the proper formulation of the time-temperature behavior. Illustrations were provided to demonstrate the importance of a complete thermo-viscoelastic characterisation, showing that discrepancies of up to 30% may arise by using an incomplete characterisation. Similar circumstances may occur in polymeric composites.

ACKNOWLEDGEMENT

This work was conducted under AFOSR Contract FA9620-82-C-0057. The author is indebted to Mr. B.D. Harper for obtaining the numerical results presented in this work.

REFERENCES

1. Ferry, J.D., "Viscoelastic Properties of Polymers", J. Wiley & Sons, Inc., 1961.
2. Kibler, R.G., "Time-Dependent Environmental Behavior of Graphite/Epoxy Composites", Technical Report AFMAL-TR-80-4052, Final report for the period August 1, 1977 - January 31, 1980 (May 1980).
3. Ranton, W.J. and Ho, T., "The Effect of Environment on the Mechanical Response of AS/3501-6 Graphite/Epoxy Material", Final Report to the Dept. of the Navy, NSWC, for the period June 1977 - June 1978 (August 1978).
4. Ho, T. and Schapery, R.A., "The Effect of Environment on the Mechanical Behavior of AS/3501-6 Graphite/Epoxy Material", Phase III, Vought Corp., *Ibid.*, (January 1981).
5. Ursuhmasev, Yu. S., "Time-Temperature Analogy. A Review", *Polymer Mechanics*, No. 5, pp. 812-818, September-October 1977.
6. Morland, L.W. and Lee, E.H., "Stress Analysis for Linear Viscoelastic Materials with Temperature Variation", *Trans. Soc. of Rheology*, Vol. IV, 1960, pp. 233-263.
7. Bufford, W.L. and Francis, C.E., "Thermal-Mechanical Interaction Effects in Filled Polymers", In NSF Workshop on a Continuum Approach to Damage and Life Prediction, May 4-7, 1980, pp. 68-75.
8. McCormick, N.G. and Poggeny, G.A., "Time-Temperature Superposition in the a Region of an Epoxy Resin", *J. of Macromol. Sc. - Phys.*, Vol. B4 (1), p. 109 (1970).
9. McCormick, N.G. and Morris, E.L., "On the Measurement of Activation Energy in Creep in Anelastic Solids", *Phil. Mag.*, Vol. 7, pp. 2115-2118 (1962).
10. Dunn, R.N., "Dynamic Mechanical Properties of Crystalline, Linear Polyethylene", *J. of Polymer Science, Part A-2*, Vol. 4, pp. 545-557, (1966).
11. Poretz, D. and Weitman, Y., "The Non-Linear Thermoviscoelastic Characterization of WH-73 Adhesives", Final Report AFMAL-TR-81-4121, pp. 144-172, (October 1981).
12. Mark, R. and Findley, W.N., "Nonlinear Creep of Polyurethane Under Combined Stress and Elevated Temperatures", *Trans. of the Soc. of Rheology*, Vol. 18, (4), pp. 563-582 (1974).
13. Mark, R. and Findley, W.N., "Temperature-History Dependence in Cyclic Tension-Tension Creep of Polyurethane Under Varying Temperature", *Ibid.*, Vol. 19, No. 2, pp. 201-213, 1975.
14. Lai, Y.C. and Schapery, R.A., "Viscoelastic Characterization of a Nonlinear Fiber-Reinforced Plastic", *J. of Comp. Mat.*, Vol. 5, p. 208 (1971).
15. Bocketh, S.W., "Viscoelastic Characterization of a Nonlinear Glass/Epoxy Composite, Including the Effect of Damage", Ph.D. Dissertation, Texas A&M University, December 1974.
16. Poretz, D. and Weitman, Y., "Nonlinear Viscoelastic Characterization of WH-73 Adhesive", to appear in *J. of Rheology*.

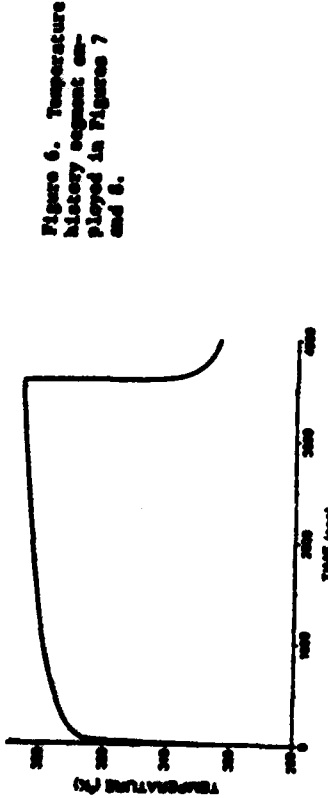


Figure 6. Temperature history sequence displayed in Figures 7 and 8.

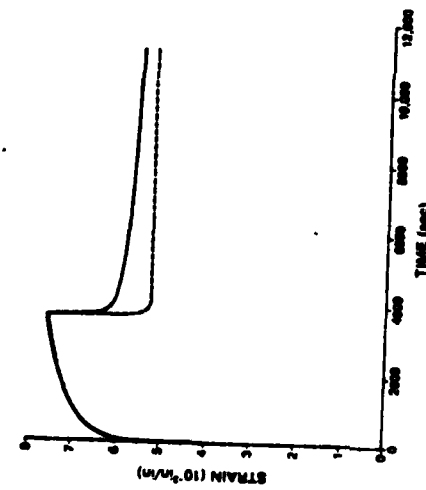


Figure 7. Creep at $\sigma = 10N/cm^2$ (10³ psi) under temperature T as in Figure 6, followed by $T = T_0$ for $t > 4000$ sec solid and dashed lines as in Figure 5.

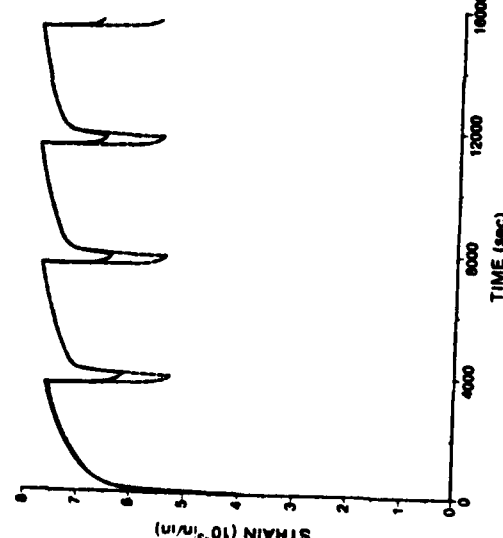


Figure 8. Creep at $\sigma = 10N/cm^2$ (10³ psi) under four sequential cycles of the temperature shown in Figure 6, solid and dashed lines as in Figure 5.

Y. Weitsman
Professor,
Mechanics and Materials Center,
Mem. ASME

B. D. Harper
Graduate Student.

Texas A&M University,
College Station, Texas 77843

Optimal Cooling of Cross-Ply Composite Laminates and Adhesive Joints

This paper concerns the optimal cooling of symmetric, balanced, cross-ply composite laminates and adhesive joints so as to minimize the residual thermal stresses upon termination of the cool-down process. The computations are based on a recently developed analytical scheme and employ up-to-date data on graphite/epoxy laminas. The calculations consider the thermoviscoelastic response of the polymeric resins and incorporate the temperature dependence of the coefficients of thermal expansion. It is shown that the viscoelastic behavior may contribute to a significant reduction of the residual stresses.

Introduction

This paper presents results based on a recently developed optimization scheme [1]¹ and data on viscoelastic response of graphite/epoxy composites [3] whereby specific time-temperature paths are selected during the cool-down stage so as to minimize the residual thermal stresses in cross-ply laminates and in adhesively bonded aluminum/epoxy joints.

The cross-ply laminates under consideration consist of a symmetric and balanced lay-up of 0 and 90 deg plies. When such laminates are cooled from the presumed stress-free cure temperature to room temperature, the stiffer fibers within each ply restrain the transverse shrinkage of the adjacent, perpendicularly directed plies and these mutual geometric constraints introduce substantial residual stresses in the laminate.

Consider a finite cool-down time. During this time interval the temperature introduces two counteracting effects. On one hand, since larger temperature drops induce larger residual stresses it appears that sharp and early temperature drops will generate significant stresses that may undergo relaxation. On the other hand, the relaxation process is retarded at lower temperatures. The optimal time-temperature path achieves the best interplay between the aforementioned competing effects so as to minimize the residual thermal stress at the termination of the cool-down phase.

Elastic Analysis

Consider a symmetric, balanced, cross-ply composite

¹See also [2] for treatment of the same problem.

Contributed by the Applied Mechanics Division and presented at the Winter Annual Meeting, Phoenix, Ariz., November 14-19, 1982 of THE AMERICAN SOCIETY OF MECHANICAL ENGINEERS.

Discussion on this paper should be addressed to the Editorial Department, ASME, United Engineering Center, 345 East 47th Street, New York, N.Y. 10017, and will be accepted until two months after final publication of the paper itself in the JOURNAL OF APPLIED MECHANICS. Manuscripts received by ASME Applied Mechanics Division, April 1983, final version, November, 1983. Paper No. 82-WA/APM-24.

Copyright 1982 by ASME.

laminate, consisting of equal number of 0 and 90 deg plies exposed to fluctuating ambient temperature $T(t)$. In view of the small thicknesses of the composite laminates employed in practice it is permissible to ignore the process of thermal diffusion and employ the approximation that $T = T(t)$ throughout the laminate. A similar circumstance also holds for adhesive joints.

Denoting by subscripts L and T the longitudinal (parallel to fibers) and transverse (perpendicular to fibers) directions, respectively, we have the following stress-strain relations in each individual lamina [4, 5]

$$\begin{aligned}\epsilon_L - \alpha_L \Delta T &= \frac{\sigma_L}{E_L} - \frac{\nu_{TL}}{E_T} \sigma_T \\ \epsilon_T - \alpha_T \Delta T &= - \frac{\nu_{LT}}{E_L} \sigma_L + \frac{\sigma_T}{E_T}\end{aligned}\quad (1)$$

In (1) ϵ and σ designate strain and stress, while α , E , and ν denote coefficient of thermal expansion, modulus, and Poisson's ratio, respectively. ΔT represents temperature difference.

In view of the particular lay-up under consideration we have

$$\sigma_T = -\sigma_L = \sigma, \quad \epsilon_T = \epsilon_L = \epsilon$$

and straightforward manipulations yield

$$\sigma = -\frac{E_T(\alpha_T - \alpha_L)\Delta T}{(1 + \nu_{TL})(1 + \frac{1 + \nu_{LT}}{1 + \nu_{TL}} \frac{E_T}{E_L})} \quad (2)$$

For typical graphite/epoxy laminae we have $E_L \sim 20E_T$ (whereby $\nu_{LT} \sim 20\nu_{TL}$). With $\nu_{LT} \approx 0.28$ we obtain

$$\sigma = -rE_T(\alpha_T - \alpha_L)\Delta T \quad (3)$$

Typically $r \approx 0.90-0.93$.

Alternately, consider two adherend plates, each of thickness h , bonded together by an adhesive layer of thickness

a. Let the joint undergo a spatially uniform temperature excursion ΔT . Elementary calculations then yield

$$\sigma_e = \frac{E_e}{1 - \nu_e} \frac{(\alpha_e - \alpha_A) \Delta T}{1 - \frac{1 - \nu_A}{1 - \nu_e} \frac{E_e}{E_A} \frac{a}{2h}} \quad (4)$$

In (4) subscripts "A" and "e" refer to the adherend and adhesive, respectively. For typical joints $E_A/E_e = 50$ and $h/a = 100$. Consequently (4) can be approximated by

$$\sigma_e \approx \frac{E_e}{1 - \nu_e} (\alpha_e - \alpha_A) \Delta T \quad (5)$$

Viscoelastic Formulation

Data on graphite/epoxy laminas [3] and on "neat" epoxy resins [6] indicate that E_T and E_e are time and temperature dependent.² The time dependence can be approximated by the form

$$E = E_0 (t + t_0)^{-q} \quad (6)$$

while the temperature dependence can be related by means of a shift-factor function $a(T)$, with $a(T_R) = 1$, where customarily T_R is room temperature (293°K). Consequently (6) is extended to read

$$E = E_0 \left\{ t_0 + \left[t/a(T) \right] \right\}^{-q} \quad (7)$$

Available data [3, 6] indicate that $a(T)$ can be expressed by

$$a(T) = \exp \left(-\frac{T}{A} + B \right) \quad (8)$$

Employing the superposition integral, equations (3) and (5) yield [7]

$$\sigma(t) = \alpha E_0 \int_0^t \left[\int_r^t \frac{ds}{a(T(s))} + t_0 \right]^{-q} \frac{d\Delta T(\tau)}{d\tau} d\tau \quad (9)$$

In (9) and the sequel, α represents $(\alpha_T - \alpha_L)$ or $(\alpha_e - \alpha_A)$ and E_0 absorbs the factors r or $1/(1 - \nu_e)$, respectively. It should be noted that in the viscoelastic case the factor r in equation (3) becomes a complicated function of time and its incorporation into the subsequent analysis requires cumbersome details. However, in all the practical cases which we considered $r(t)$ varied at most by 1/2 percent about its average value over the time span of interest. Consequently we employed the approximation $r(t) = r = \text{const.}$ in our work, without sacrificing accuracy. Data on graphite/epoxy [3] indicate that α_T and α_L vary significantly with temperature. This aspect of the material response will be considered later.

Optimal Cooling Paths

Consider now the case of cooling from the initial cure temperature T_I to room temperature T_R in a given time interval t_f . It has been shown [1, 2] that if an optimal path exists then it is possible to obtain a minimal value for $\sigma(t)$ in (9). In such a case this minimal value of $\sigma(t)$ is obtained by following a path $T(t)$ that includes an abrupt initial drop from T_I to T_0 . This initial drop was given by solving the transcendental equation [1]

$$T_0 - T_I = \frac{a(T_0)}{a'(T_0)} \quad (10)$$

In the open interval $0 < t < t_f$ the optimal path $T(t)$ was shown to be smooth and continuous, where it is governed by the nonlinear integrodifferential equation

$$\frac{dT}{dt} = - \frac{E''(t, t_f)}{E'(t, t_f)} \frac{a'(T(t))}{a(T(t)) a''(T(t))} \quad (11)$$

²These data are corroborated by many other sources and publications, which are not listed here.

In (10) and (11) primes indicate derivatives with respect to the argument. Also

$$E(t_1, t_2) = E \left[\int_{t_1}^{t_2} \frac{ds}{a(T(s))} \right]$$

With given $E(t)$, $a(T)$, and T_I , the value of T_0 is determined by (10) and the optimal temperature path can be constructed by iteration through the employment of (11). In most cases the final prescribed temperature T_R is reached through a second abrupt step at time t_f .

A particular simplification occurs for a "power law" response, as expressed in (6) and, in addition, when the shift-factor function is given by (8). In this case it was shown [1] that the optimal path is given by

$$T = \frac{1}{C} \ln \frac{L}{k + Ct} \quad (12)$$

where, in (12)

$$C = \frac{q}{(q+1)A} \quad \text{and} \quad L = K \exp(CT_0)$$

The term K is determined as the root of the transcendental equation

$$Ke^{CT_0} = \left[\frac{e^{Bt_0}(K + Ct_f)^{\frac{1}{q}}}{(q+1)A} \right]^{\frac{q}{q+1}} \quad (13)$$

Under the simplifications that occur in the present circumstances the iterative process alluded to in [1] reduces to the search for the root K of equation (13).

In view of (8), equation (10) yields

$$T_0 = T_I - A \quad (14)$$

With the optimal temperature-path prescribed by (12) the stresses are obtained by direct substitution of (12) into (9). After several manipulations we get

$$\sigma(t) = \alpha E_0 \left\{ \int_0^t Q(\tau, t) d\tau + K(T_I - T_0) Q(0, t) \right\} \quad (15)$$

where

$$Q(\tau, t) = \frac{t_0^{-q} \left\{ \left(\frac{K + Ct_f}{K + Ct} \right)^{\frac{1}{q}} \left[\left(\frac{K + Ct}{K + Ct_f} \right)^{\frac{1}{q}} - 1 \right] + 1 \right\}}{K + Ct}$$

$\sigma(t_f^-)$ is obtained by setting $t = t_f^-$ in (15). At $t = t_f^+$ we get

$$\sigma(t_f^+) = \sigma(t_f^-) + \alpha E_0 t_0^{-q} (T_f - T_R) \quad (16)$$

Temperature-Dependent Coefficients of Thermal Expansion

Recent data on graphite/epoxy composites indicate that the quantity $(\alpha_T - \alpha_L)$ increases monotonically with temperature. Consequently (9) must be modified to read

$$\sigma(t) = E_0 \int_0^t \left[\int_r^t \frac{ds}{\beta(\epsilon_{th}(s))} + t_0 \right]^{-q} \frac{d}{d\tau} [\alpha(T(\tau)) \Delta T(\tau)] d\tau \quad (17)$$

where $\alpha(T(t)) = \alpha_T(T(t)) - \alpha_L(T(t))$.

Consider the thermal strain

$$\epsilon_{th}(t) = \alpha(T(t)) \Delta T(t) \quad (18)$$

In view of the one-to-one correspondence between ϵ_{th} and T we have

$$\alpha(T(t)) = \beta(\epsilon_{th}(t)) \quad (19)$$

Therefore (17) can be rewritten as follows

$$\sigma(t) = E_0 \int_0^t \left[\int_r^t \frac{ds}{\beta(\epsilon_{th}(s))} + t_0 \right]^{-q} \frac{d}{d\tau} (\epsilon_{th}(\tau)) d\tau \quad (20)$$

Table 1 Material parameters

Material system	E_0 (KN/m ²)	r	q	t_0 (min)	α (cm/cm ² K)	A (°K)	B	
graphite/epoxy	AS/3502	$10^{7.055}$	0.9	0.00775	1	$\alpha_L = -0.217 \times 10^{-6}$ $\alpha_T = 24.73 \times 10^{-6}$ (at $T = 372^\circ\text{K}$)	6.258	46.81
	T300/5208	$10^{7.014}$	0.93	0.00717	1	$\alpha_L = -0.593 \times 10^{-6}$ $\alpha_T = 25.65 \times 10^{-6}$ (at $T = 372^\circ\text{K}$)	6.792	43.14
	aluminum epoxy	$10^{6.54}$	1	0.036	0.5	$\alpha_e = 5 \times 10^{-5}$ $\alpha_A = 2.4 \times 10^{-5}$	7.91	37.05

Table 2 The temperature dependence of the thermal expansion coefficients. $\alpha(T) = \alpha_0 + \alpha_1 T$.

Material system	α_L (cm/cm ² /°K)		α_T (cm/cm ² /°K)	
	α_0 (cm/cm ² /°K)	α_1 (cm/cm ² /°K ²)	α_0 (cm/cm ² /°K)	α_1 (cm/cm ² /°K ²)
AS/3502	-0.484×10^{-6}	0.72×10^{-9}	9.5×10^{-6}	0.41×10^{-7}
T300/5208	-0.418×10^{-6}	-0.47×10^{-9}	11.9×10^{-6}	0.37×10^{-7}

Note that (20) is analogous to (9). Accordingly, (10) and (11) yield the following expressions for the optimal path

$$\epsilon_{th}^0 - \epsilon_{th}^f = \frac{\beta(\epsilon_{th})}{\beta'(\epsilon_{th})} \quad (21)$$

and

$$\frac{d\epsilon_{th}(t)}{dt} = - \frac{E''(t, t_f)}{E'(t, t_f)} \frac{\beta'(\epsilon_{th}(t))}{\beta(\epsilon_{th}(t)) \beta''(\epsilon_{th}(t))} \quad (22)$$

$$\text{In (22), } E(t_1, t_2) = E \left[\int_{t_1}^{t_2} \frac{ds}{\beta(\epsilon_{th}(s))} \right].$$

Equations (21) and (22) can be expressed in terms of $a(T)$ and T through the reintroduction of (18) and (19). We obtain

$$T_0 - T_f = \frac{\alpha(T_0)a(T_0)}{\alpha(T_0)a'(T_0) - \alpha'(T_0)a(T_0)} \quad (23)$$

$$\frac{dT}{dt} = - \frac{E''(t, t_f)}{E'(t, t_f)} \frac{a'}{a \left[a'' - a' \frac{2\alpha' + \alpha''(T - T_f)}{\alpha + \alpha'(T - T_f)} \right]} \quad (24)$$

In (24) $a = a(T(t))$ and $\alpha = \alpha(T(t))$.

The solution for the optimal path $T(t)$ can be generated by means of an iterative scheme, as noted in reference [1]. However for the AS/3502 and T300/5208 graphite/epoxy systems the data listed in Tables 1 and 2 indicate that (23) and (24) differ by at most 2 percent from expressions (10) and (11) which assume constant α . Consequently, we shall retain (12) as our solution for the optimal path even for the variable α case at hand. We note however, that although the optimal temperature paths remain unaffected by the variation of α , the thermal stresses do differ significantly.

In the particular circumstance that

$$\alpha(T) = \alpha_0 + \alpha_1 T \quad (25)$$

we obtain

$$\sigma(t) = E_0 \left\{ \int_0^t Q(\tau, t) \left[\alpha_0 + \alpha_1 (2T(\tau) - T_f) \right] d\tau + K \alpha(T_0)(T_f - T_0) Q(0, t) \right\} \quad (26)$$

with the same $Q(\tau, t)$ as in (14). The stress immediately following the initial discontinuity is

$$\sigma(0^+) = E_0 t_0^{-q} \alpha(T_0)(T_f - T_0) \quad (27)$$

After the final discontinuity we have

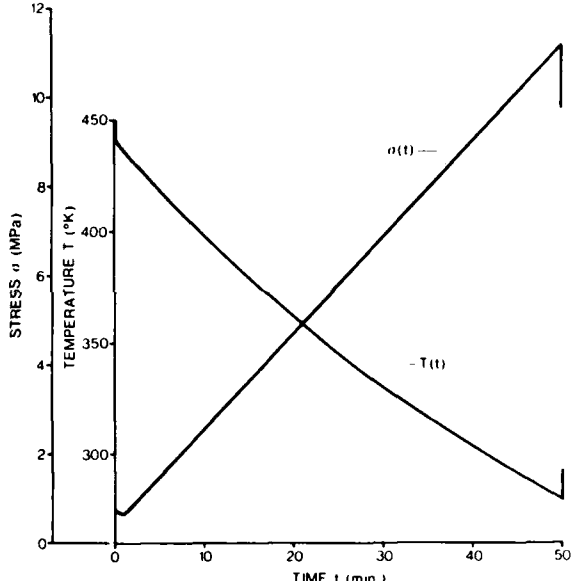


Fig. 1 The optimal cooling path $T(t)$ and the accompanying thermal stress $\sigma(t)$ versus time t for epoxy/aluminum joints and cooling time $t_f = 50$ min

$$\sigma(t_f^+) = \sigma(t_f^-) + E_0 t_0^{-q} \left[\alpha(T_f)(T_f - T_f) - \alpha(T_R)(T_R - T_f) \right] \quad (28)$$

Computations

Calculations were performed for two graphite/epoxy materials and for an epoxy/aluminum joint. The data [3, 6] was reduced to conform with expressions (3), (7), (8), and (25) as shown in Tables 1 and 2.

In our computations we employed $T_f = 450^\circ\text{K}$, $T_R = 293^\circ\text{K}$, and considered cooling times $t_f = 10, 50, 100, 500$, and 1000 minutes.

The integrations (14) and (26) were performed numerically. For this purpose the time interval t_f was divided into n equal subintervals $\Delta t = t_f/n$, resulting in intermediate times $t_i = i \Delta t$ and intermediate temperatures T_i evaluated by means of (12). It was found that sufficient accuracy was obtained with $n = 100$. In order to assess the significance of the variation of

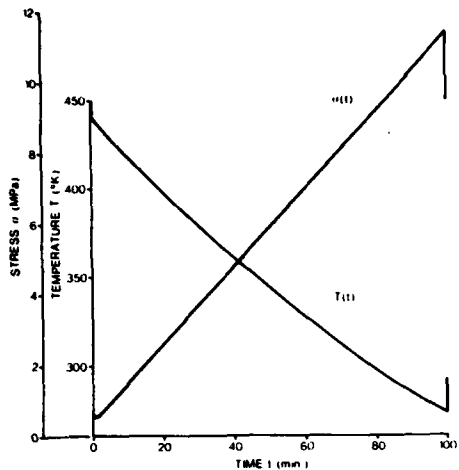


Fig. 2 The optimal cooling path $T(t)$ and the accompanying thermal stress $\sigma(t)$ versus time t for epoxy/aluminum joints and cooling time $t_f = 100$ min

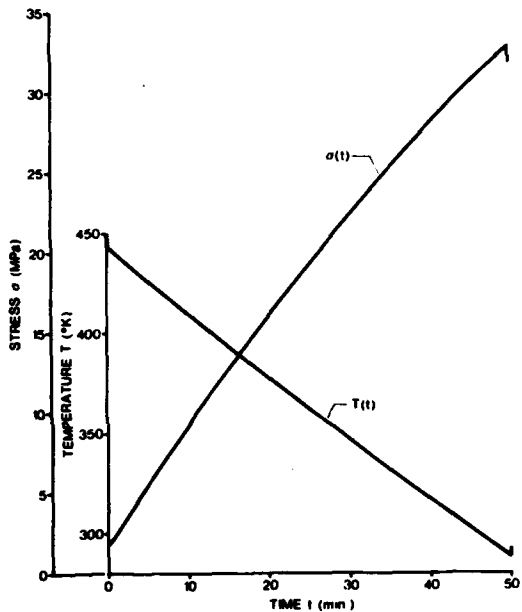


Fig. 3 The optimal cooling path $T(t)$ and the accompanying thermal stress $\sigma(t)$ versus time t for T300/5208 symmetric, balanced 0/90 deg laminates and cooling time $t_f = 50$ min

α with T , we computed (15) with $\alpha_{av} = (\alpha(T_f) + \alpha(T_R))/2$. The results are shown in Figs. 1-9. In all those figures temperature T is in °K, stress is in MPa, and time is in minutes.

Figures 1 and 2 exhibit the optimal cooling paths $T(t)$, with the accompanying residual stress, generated during the cool-down process of typical aluminum/epoxy joints for cooling times $t_f = 50$ and 100 minutes, respectively. Note the jump discontinuities at $t = 0$ and $t = t_f$. Analogous results are shown in Figs. 3 and 4 for the 0/90 deg T300/5208 laminate and in Figs. 5 and 6 for the 0/90 deg AS/3502 laminate.

In all the figures the optimal temperature paths were determined by (12). We note that those paths "undershoot" the level of room temperature (293°K), requiring an upward jump at $t = t_f$. The stresses in Figs. 1 and 2 were computed according to (15) and (16) employing constant α . On the other hand, the curves $\sigma(t)$ in Figs. 3-6 were obtained by employing (26)-(28) considering variable α in accordance with Table 2.

The variation of the residual thermal stress $\sigma(t_f^+)$ with the cooling time t_f is shown in Figs. 7-9. Also shown are the variations of the terminal temperature $T_f = T(t_f^-)$ with t_f . Note that a logarithmic scale is employed for t_f .

For comparison purposes we also exhibit by dashed-dotted

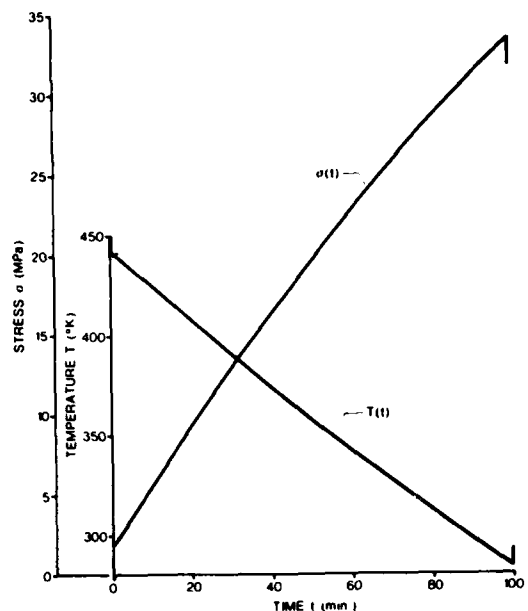


Fig. 4 The optimal cooling path $T(t)$ and the accompanying thermal stress $\sigma(t)$ versus time t for T300/5208 symmetric, balanced 0/90 deg laminates and cooling time $t_f = 100$ min

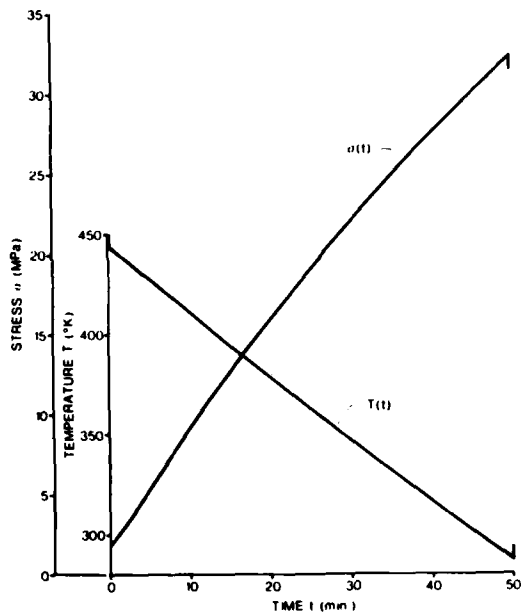


Fig. 5 The optimal cooling path $T(t)$ and the accompanying thermal stress $\sigma(t)$ versus time t for AS/3502 symmetric, balanced 0/90 deg laminates and cooling time $t_f = 50$ min

lines in Figs. 8 and 9 the final residual stresses $\sigma(t_f^+)$ which result from considering a constant, average value of $\alpha_{av} = (\alpha(T_f) + \alpha(T_R))/2$ instead of the actual temperature-dependent $\alpha(T)$. Shown in dashed lines is the elastic value of $\sigma(t_f^+)$, which is computed with $\alpha = \alpha_{av}$.

We observe that by taking appropriate account of viscoelastic effects it is possible to attain reductions of about 25 percent in the residual stresses relative to the linear elastic predictions.

Remarks on Data Reduction

The "power law" representation of relaxation or creep data for polymeric resins or fiber-reinforced composites [3] in the form $E(t) = Et^{-q}$, can be surmised from the fact that the plots of $\log E$ versus $\log t$ are represented by straight lines [3,

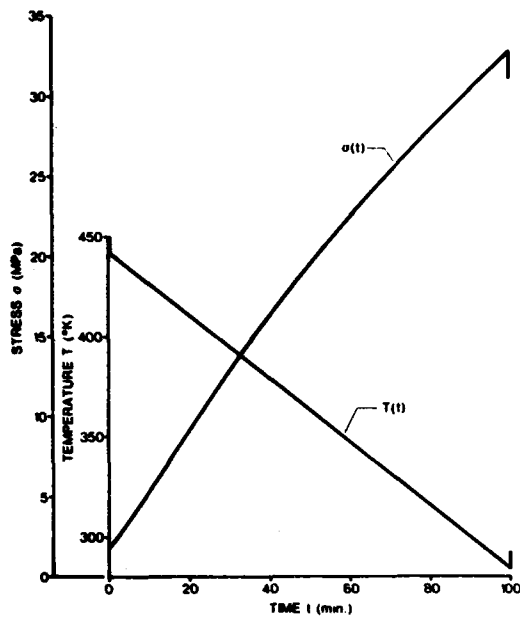


Fig. 6 The optimal cooling path $T(t_f^-)$ and the accompanying thermal stress $\sigma(t)$ versus time t for AS/3502 symmetric, balanced 0/90 deg laminates and cooling time $t_f = 100$ min

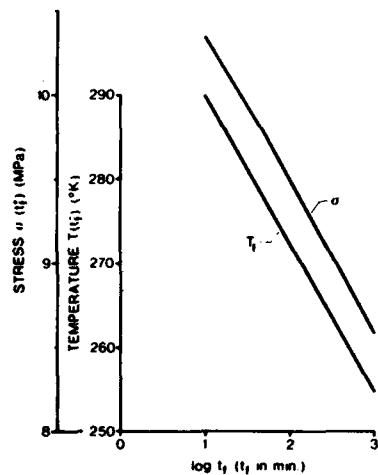


Fig. 7 The variation of $T(t_f^-)$ and the residual thermal stress $\sigma(t_f^+)$ versus $\log t_f$ for epoxy aluminum joints

6). The slopes of those lines determine the power q . Obviously, these plots cannot be extrapolated to time $t = 0$, lest $E(0) = \infty$. Furthermore, creep or relaxation data are unreliable at very short times because of the dynamic effects that are technically unavoidable at the early stages of experiments. Finally, it may also be noted that for $E(t) = ET^{-q}$ the optimization scheme (11) fails because it yields $\lim_{t \rightarrow 0} t'(t) = -\infty$

To overcome the aforementioned artifact, select a certain short time $t = t_0$ at which the data plots are smooth and beyond which $E(t) = Et^{-q}$. The data can then be extrapolated back to $t = 0$ employing Taylor's expansion and the result fitted into the form $E(t) = E_0(t+t_0)^{-q}$ of equation (6). It turns out that by letting $E_0 = E(1+q)$ and $t_0 = t$, we obtain representations in the form of (6) that match all data points indistinguishably from $E(t) = Et^{-q}$.

Acknowledgment

The authors wish to thank Mr. W. Eue of Texas A&M University for his help in obtaining the numerical results presented herein. This work was conducted under Contract

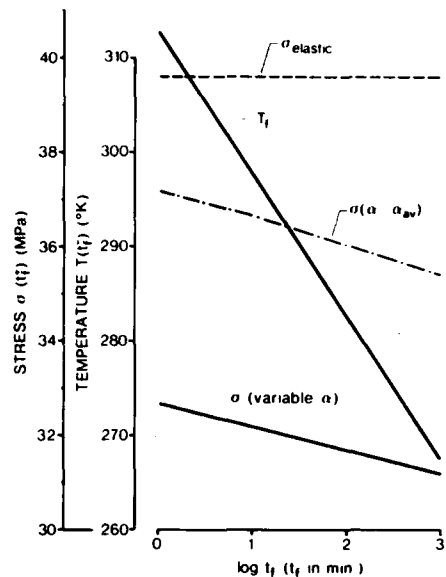


Fig. 8 The variation of $T(t_f^-)$ and the residual thermal stress $\sigma(t_f^+)$ versus $\log t_f$ for the T300/5208 0/90 deg laminates. (The dashed-dotted line corresponds to $\sigma(t_f^+)$ evaluated with $\alpha = \alpha_{av}$.)

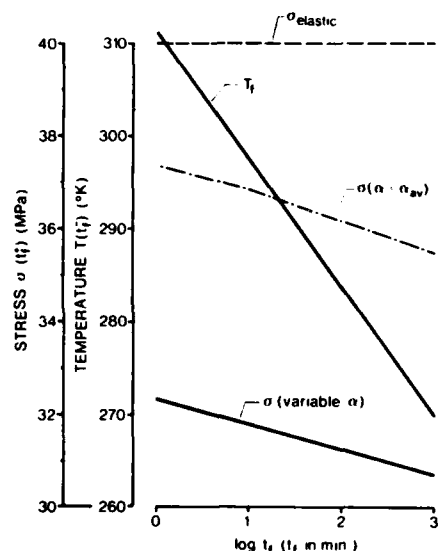


Fig. 9 The variation of $T(t_f^-)$ and the residual thermal stress $\sigma(t_f^+)$ versus $\log t_f$ for the AS/3502 laminates. (The dashed-dotted line corresponds to $\sigma(t_f^+)$ evaluated with $\alpha = \alpha_{av}$.)

F49620-78-C-0034 from the Air Force Office of Scientific Research (AFOSR) whose support is gratefully acknowledged.

References

- 1 Weitsman, Y., "Optimal Cool-Down in Linear Viscoelasticity," *ASME JOURNAL OF APPLIED MECHANICS*, Vol. 47, 1980, pp. 35-39.
- 2 Gurtin, M. E., and Murphy, L. F., "Optimal Temperature Paths for Thermorheologically Simple Viscoelastic Materials," *Quart. App. Math.*, Vol. 38, No. 2, 1980, pp. 179-190.
- 3 Kibler, K. G., "Time-Dependent Environmental Behavior of Graphite/Epoxy Composites," Technical Report AFWAL-TR-80-4052, General Dynamics Corporation, 1980, Fort Worth, Texas.
- 4 Jones, R. M., *Mechanics of Composite Materials*, Scripta Book Co., 1975, pp. 37-41.
- 5 Tsai, S. W., and Hahn, H. T., *Introduction to Composite Materials*, Technomic, 1980, pp. 8-18.
- 6 Beckwith, S. W., "Viscoelastic Characterization of a Nonlinear Glass/Epoxy Composite Including the Effect of Damage," Ph.D. dissertation, 1974, Texas A&M University, College Station, Texas.
- 7 Morland, L. W., and Lee, E. H., "Stress Analysis for Linear Viscoelastic Materials With Temperature Variation," *Transactions of the Society of Rheology*, Vol. 4, 1960, pp. 233-260.

END

FILMED

11-83

DTIC